Volume 18, Number 2

February, 1965

SOVIET ATOMIC ENERGY

АТОМНАЯ ЭНЕРГИЯ
(ATOMNAYA ÉNERGIYA)

TRANSLATED FROM RUSSIAN

CONSULTANTS BUREAU

NEW BOOKS IN PHYSICS

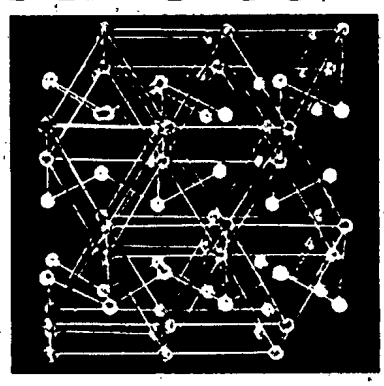

EFFECTS OF RADIATION ON SEMICONDUCTORS

By S. V. Vavilov

Devoted to the effects of electromagnetic and corpuscular radiations on semiconductors, this new volume deals with the processes of absorption of electromagnetic radiation, photoionization and ionization by charged high-energy particles, and the principal types of recombination processes by which an excited crystal returns to its original equilibrium state. Translated from the Russian.

238 pages CB 1965 $15.00

MÖSSBAUER-EFFECT METHODOLOGY

By Irwin J. Gruverman

Reviews applications and describes a methodology permitting scientists in all fields to understand the complexities of equipment required for velocity modulation, measurement of effects, and modification of external environments. Establishes a basis for evaluating the applicability of Mössbauer-effect studies to various areas. The four sections of the book include: Reviews of applications in physics, biology, and chemistry; Three alternative approaches to velocity modulation; Measurement and calibration; and Environmental control with respect to magnetic fields, temperature, and pressure. Excellent as supplementary reading in undergraduate and graduate nuclear physics courses, this volume is also valuable as a text in experimental advanced physics.

Approx. 200 pages PP 1965 $12.50

CERAMIC ACOUSTIC DETECTORS

By A. A. Anan'eva

Deals with the dielectric and piezoelectric properties of barium-titanate ceramics, the methods of determining sound receiver characteristics, and the experimental development of nondirectional wideband sound receivers employing spherical and cylindrical shells of barium-titanate ceramic polarized in various ways. Wideband sound receivers using plane diaphragms and the development of receivers responsive to certain resonance frequencies in the working frequency band — and therefore of high sensitivity — are described in detail. Includes a bibliography on the development of piezoelectric elements for the design and construction of acoustic receivers. A Special Research Report translated from the Russian.

130 pages CB 1965 $22.50

QUANTUM ELECTRON THEORY OF AMORPHOUS CONDUCTORS

By A. I. Gubanov

This is the first monograph to deal with the physics of amorphous electronic conductors. It includes a critical review of the electrical properties and structure of liquid and glassy semiconductors, a separate chapter on the fundamentals of the quantum electron theory of solids, and a consideration of the similarities and differences between the structures of liquid and crystalline substances. Using one-dimensional models, Gubanov deduces the band structure of the electron theory spectrum and extends the theory for three-dimensional models. Also included are discussions of characteristic features of electron scattering in amorphous substances, the mean free path of electrons and the temperature dependence of various galvano-thermomagnetic coefficients of an amorphous substance, and the author's theory of amorphous ferromagnets. Translated from the Russian.

293 pages CB 1965 $17.50

SOVIET RESEARCH IN NEW SEMICONDUCTOR MATERIALS

Edited by D. N. Nasledov *et al.*

Five internationally known Soviet researchers on semiconductor materials — Nasledov, Goryunova, Regel', Lange, and Radautsan — participated in selecting these 18 reports presented at a 1963 Academy of Sciences conference on new semiconductor materials. The editors are themselves authors or co-authors of ten of the reports. The studies include: properties of solid solutions based on materials with a zinc blende type structure, both chain and layer modifications; change of the charge carrier mobility upon melting of semiconductors; anisotropy of the electrical and galvanomagnetic properties of certain semiconductor materials; and the electrical and optical properties of thin semiconductor layers. A Special Research Report translated from the Russian.

127 pages CB 1965 $17.50

CONSULTANTS BUREAU / PLENUM PRESS
227 West 17th Street, New York, New York 10011

Declassified and Approved For Release 2013/09/24 : CIA-RDP10-02196R000700010002-5

SOVIET ATOMIC ENERGY

A translation of **ATOMNAYA ÉNERGIYA**
A publication of the Academy of Sciences of the USSR

Volume 18, Number 2 February, 1965

CONTENTS

	PAGE ENG.	PAGE RUSS.
Penetration of Hydrogen Ions H_1^+ into the Surface of Stainless Steel—E. S. Borovik, N. P. Katrich, and G. T. Nikolaev	113	91
Perturbation of Particle Motion in the Stellarator—A. P. Popryadukhin	118	96
Experiments on the Buildup of Electrons in the Synchrotron—Yu. M. Ado, E. G. Bessonov, and P. A. Cherenkov	129	104
Angular and Energy Characteristics of the Neutrons Emitted in U^{235} Fission—M. V. Blinov, N. M. Kazarinov, and A. N. Protopopov	133	108
Calculation of Average Radiative Capture Cross Sections for Neutrons with Energies of 10^3-10^5 eV—A. G. Dovbenko, S. M. Zakharova, V. E. Kolesov, and A. V. Malyshev	140	114
Asymptotic Formulas for Scattering of Slow Neutrons on Bound Atoms—V. F. Turchin and V. A. Tarasov	146	118
The Attenuation of Reactor Radiation by Means of Serpentine Concrete—G. A. Vasil'ev, A. P. Veselkin, Yu. A. Egorov, V. A. Kucheryaev, and Yu. V. Pankrat'ev	151	121
Study of the Neutron Moderation Process in Beryllium and Beryllium Oxide by a Pulse Method—I. F. Zhezherun	158	127
Experimental Investigations of Shields on the Riz Stand—S. P. Belov, V. A. Dulin, Yu. A. Kazanskii, V. I. Popov, and S. G. Tsypin	167	136
A Whole-Body Counter—Yu. V. Sivintsev, O. M. Arutinov, V. A. Kanareikin, and M. A. Panov	173	141
Variation of the Separation Factor in Isotope Exchange as a Function of the Properties of the Molecules Being Exchanged—A. M. Rozen and A. I. Mikhailichenko	180	147
Prospective Developments and Economics of Nuclear Power Generation—B. B. Baturov and N. M. Sinev	191	157
Chemistry of Nuclear Fuel Reprocessing—V. N. Prusakov and M. F. Pushlenkov	210	171
LETTERS TO THE EDITOR		
Homogeneous Critical Assembly with a Profiled Fuel Charge—A. K. Krasin and E. I. Inyutin	215	175
Angular Distribution of Collimated Radiation—É. F. Fomushkin	219	178
Diffusion of Neutrons in Spin-Orbit Interaction—Yu. N. Kazachenkov and V. V. Orlov	222	179
Characteristics of Asymptotic Spectrum of Neutrons in Uranium—A. A. Malinkin, F. Nasyrov, and V. F. Kolesov	225	181
Excitation Function of Reaction $Cu^{65}(d,2n)Zn^{65}$ and Yield of Isotope Zn^{65}—P. P. Dmitriev and N. N. Krasnov	228	184
Use of Aqueous Glycine Solution for γ-Ray and Fast-Neutron Dosimetry—A. P. Ibragimov and A. V. Tuichiev	231	185

Annual Subscription: $95 **Single Issue: $30** **Single Article: $15**

CONTENTS (continued)

	PAGE ENG.	PAGE RUSS.
Light Output and Amplitude Resolution of Monocrystals—G. V. Miroshnikov and A. I. Kirillov	234	187
Some Data on Equilibria of the Systems $MeS(MeS_2)$-UO_2SO_4-H_2O at Elevated Temperatures and Pressures—B. S. Osipov and R. P. Rafal'skii	237	189
SCIENCE AND ENGINEERING NEWS		
International Betatron Colloquium—A. A. Vorob'ev, V. A. Moskalev, M. F. Filippov, and V. A. Vorob'ev	240	192
Conference on the Physics and Technology of Alkali Halide Scintillators—R. V. Bakradze and Yu. A. Tsirlin	243	193
"Atomic Energy" Pavilion at the 1964 Exhibit of Achievements of the USSR National Economy—L. I. Petrenko	245	194
BIBLIOGRAPHY		
New Books	249	198

The Russian date "Podpisano k pechati" of this issue was 1/21/65. This is equivalent to "approved for printing." Publication did not occur prior to this date, but must be assumed to have taken place reasonably soon thereafter.

Publisher

PENETRATION OF HYDROGEN IONS H_1^+ INTO THE SURFACE OF STAINLESS STEEL

(UDC 533.9)

E. S. Borovik, N. P. Katrich, and G. T. Nikolaev

Translated from Atomnaya Énergiya, Vol. 18, No. 2,
pp. 91-96, February, 1965
Original article submitted July 15, 1963, and in final form June 22, 1964

A system for conducting experiments on the coefficient of penetration is described. The use of hydrogen and helium condensation pumps secures an ultrahigh vacuum in the apparatus. The coefficient of penetration of 35 keV H_1^+ ions is determined. For an ion density in the region of 10^{18} to $2 \cdot 10^{19}$ the coefficient of penetration equals 0.93 and is independent of the number of such ions.

Recently the process of gas ion penetration into various materials has caught the interest of many physicists studying hot plasma. This is because in magnetic traps with the injection of fast particles the maintenance of ultrahigh vacuum depends substantially on the coefficient of penetration. So far this coefficient has been measured in few investigations: for 150 to 2600 eV He^+ ions in [1], and for 7 to 25 keV He^+ and D^+ ions in [2]. Some quantitative characteristics of the penetration process have been given in investigations into the desorption of previously penetrating particles caused by ion bombardment [3-5] and in connection with the development of methods of preparing solid gas targets and the separation of isotopes [6, 7].

None of these investigations, however, was carried out in vacuum conditions ensuring clean surfaces for the bombarded targets. We here present the first measurements of the penetration coefficient of 35 keV H_1^+ into a 1Kh18N9T stainless steel target. The vacuum conditions under which these measurements were made ensured that the target surface bombarded would be quite clean.

Description of Apparatus

The exterior view of the apparatus with which the measurements were made appears in Fig. 1. The arrangement of the main parts of the apparatus as they appear along the direction of motion of the H_1^+ ion beam is shown in Fig. 2. The hydrogen ion beam produced by means of a high frequency ion source 1 was focused by the electrostatic lens 2, accelerated to 35 keV in the accelerator tube 3, and, via the first collimating system 8, 9, fell into the magnetic analyzer chamber 11. In this chamber the H_1^+ hydrogen ions were turned through 60°, and by way of a second collimating system 15, 17 fell into the measuring chamber 18 and on to the target 21. The high frequency ion source with the electrostatic lens made it possible to obtain a well focused beam of H_1^+ ions of up to 120 μA (current density at target up to 160 $\mu A/cm^2$). The consumption of hydrogen in the high frequency ion source, determined by the geometry of the extracting electrode, did not exceed 1.5 cm^3/h. This hydrogen consumption may be regarded as small compared with that in other types of ion source. However, in systems requiring the maintenance of a vacuum of the order of 10^{-7} N/m^2, such gas loadings are very high, since the corresponding pumping rates required must exceed $3 \cdot 10^5$ dm^3/sec.

The pumping rates may be reduced to a few tens of thousands of dm^3/sec if the differential pumping method is employed. However, even these pumping speeds are very difficult to achieve with diffusion pumps, not to mention the contamination of the receiver. In view of this, we used the multistage condensation method of pumping [8], which guaranteed the necessary pumping rate, high vacuum stability, and a fairly clean target. Figure 2 shows the disposition of the helium condensation pumps (HCP) 10, 14, and 16. Each pump comprises a copper vessel of 0.5 dm^3 capacity, with calculated pumping rate $1.2 \cdot 10^4$ dm^3/sec. The limiting HCP vacuum, determined by the hydrogen saturated vapor tension, becomes quite high if the temperature of the pump surface is reduced below the

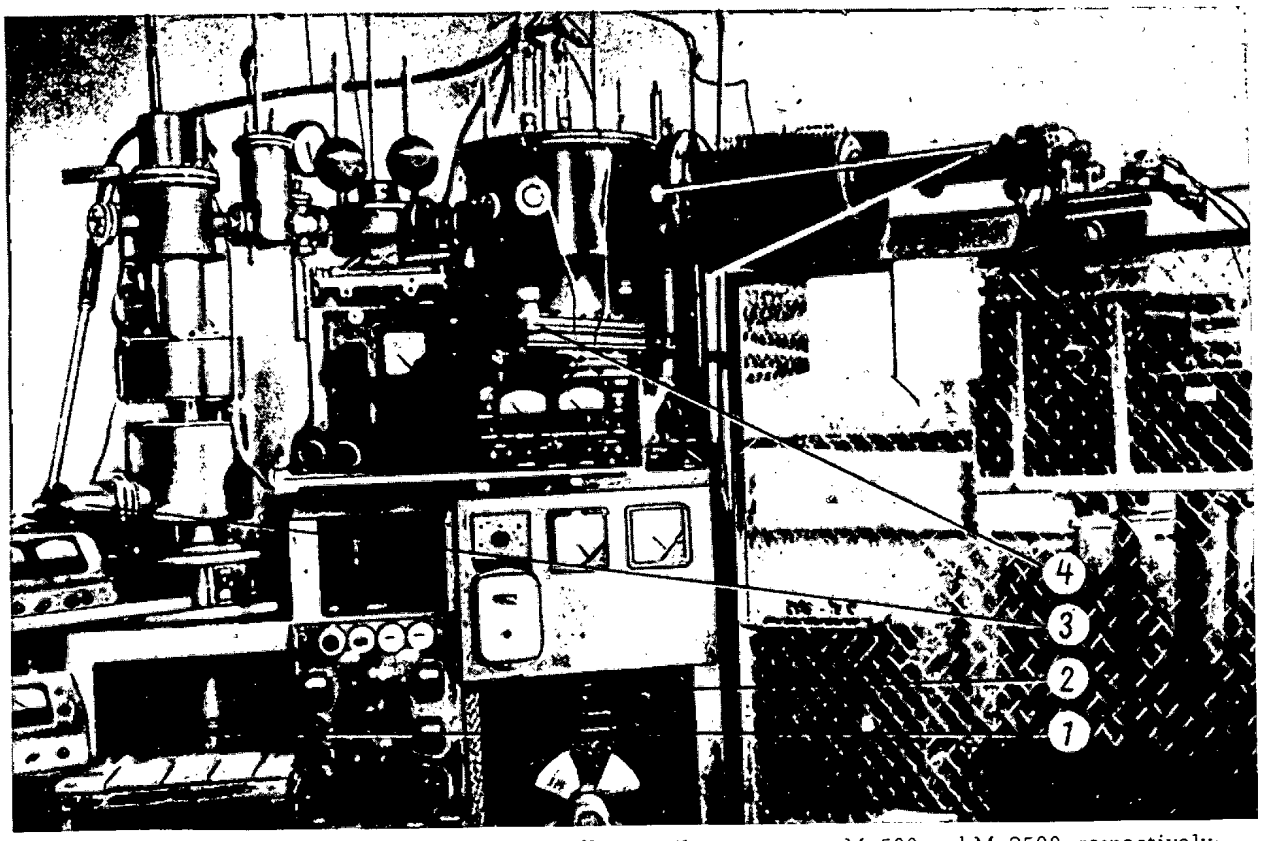

Fig. 1. Exterior view of the apparatus: 1, 2) diffusion oil vapor pumps M-500 and M-2500, respectively; 3, 4) heated and unheated vacuum valves, respectively.

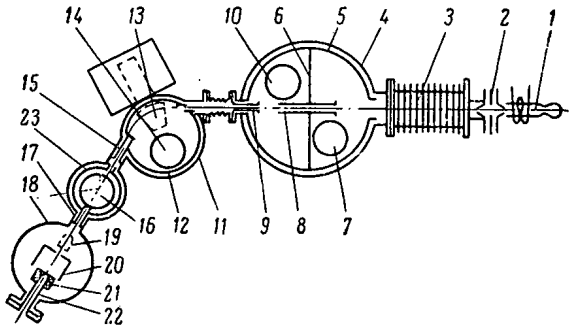

Fig. 2. Arrangement of apparatus.

boiling point of liquid helium. The necessary fall in surface temperature can easily be achieved by pumping out the vapor over the liquid helium. In our pumps the vapor was pumped out to about 18 N/m^2, corresponding to a limiting vacuum of $\sim 1 \cdot 10^{-10}$ N/m^2 [9]. The duration of service of the HCP was determined by the thermal loading and the amount of helium introduced. The priming of the condensation pumps with liquid helium by the ordinary method of pouring over under pressure did not give good results. The amount of helium so introduced was small and hence so was the duration of service.

In view of this, we set up a special arrangement for pouring; this enabled the operation to be effected with continuous pumping of the vapor above the liquid helium. This secured reliable priming for the HCP and a consequent increase in their period of operation (8 to 10 h).

In our apparatus, besides the HCP, we used two hydrogen condensation pumps 7 and 20 with capacity 0.5 dm^3 each, and two oil diffusion pumps M-500 and M-2500 (see Fig. 1). The M-2500 pump was intended for conditioning the vacuum system and for the preliminary evacuation of hydrogen coming from the high frequency ion source into chamber 4 during the experiment. The M-500 pump was intended for conditioning the measuring chamber 18. Both pumps had water and nitrogen shielding, and in case of need could be shut off from the rest of the system by means of the valves shown in Fig. 1. In the lower part of the chamber 4 was placed a nitrogen louver trap; fixed to this was a copper screen 5 separated into two sections by the barrier 6. The right hand side of the screen constituted a chamber communicating with the diffusion pump through the nitrogen trap. Inside this was placed a hydrogen condensation pump 7 intended for pumping out stray gases. The left hand half of the nitrogen screen constitutes a chamber closed on all sides and communicating with the right hand half of the nitrogen screen and with the magnetic

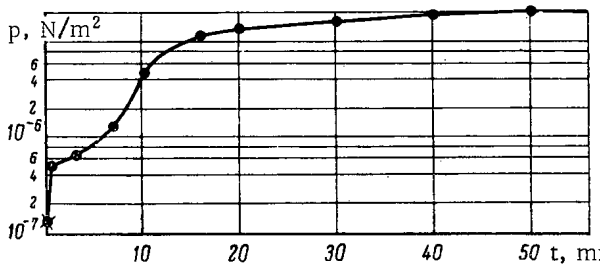

Fig. 3. Measuring chamber pressure as a function of time. ●) Initial pressure.

analyzer chamber by means collimating tubes 8 and 9. Collimator tube 8 (diameter 14 and length 250 mm) had an entrance aperture of diameter 12 mm and was soldered into the partition of the nitrogen screen. Collimating tube 9 (diameter 11 and length 150 mm) with an entrance aperture 9 mm in diameter connected the left hand half of the nitrogen screen to the magnetic analyzer chamber. This geometry of the collimating system ensured a smallish conductivity between the chambers, slightly lowering the hydrogen ion beam current. Within the left hand part of the screen was placed HCP 10 with a hydrogen pumping rate of $1.2 \cdot 10^4$ dm^3/sec. Thus the two condensation pumps bearing the main load during the experiment were located in a comparatively small volume, and the possibility of impurity gases passing into the measuring chamber from the unheated part of the apparatus was almost entirely eliminated. The magnetic analyzer chamber 11 was made of stainless steel 1Kh18N9T and was assembled by means of polyfluorethylene resin gaskets. The pole tips of the magnet 13 were situated inside the chamber, while the rest of the magnet was outside. The magnetic analyzer chamber had a nitrogen screen 12, inside which was HCP 14. The hydrogen ions H_2^+ and H_3^+ and fast neutral particles coming out of the high-frequency ion source and falling into the magnetic analyzer chamber partly passed into the nitrogen screen, while the remaining particles were pumped away by the HCP. The H_1^+ ions passed out of the magnetic analyzer chamber through collimating tube 15, an aperture in the nitrogen screen 23, and tube 17, into the measuring chamber, and on to the target. The nitrogen screen comprised a cylindrical chamber joined to the measuring chamber by a tube 17 of given conductivity. In the upper part of the nitrogen screen, over the path of the beam, was placed HCP 16, intended for pumping out the measuring chamber and protecting it from the onslaught of hydrogen from the magnetic analyzer chamber. Measuring chamber 18 and the components connected to it were made of stainless steel and assembled with copper gaskets compressed between conical surfaces. This construction facilitated heating to temperatures of 400 to 450°C. Below the measuring chamber was placed the heated metal valve (see Fig. 1) separating the measuring chamber from the oil diffusion pump M-500.

The target of the material to be studied was fixed in a copper block, which is turn was fixed to holder tube 22. The open end of the holder tube enabled the target to be cooled during bombardment. The H_1^+ ion beam current was measured by a mobile Faraday cylinder 19. The vacuum in the measuring chamber was measured by an open ionization manometer of the Bayard-Alpert type placed inside the measuring chamber. The hydrogen condensation pump and screen 20 surrounding the target were intended to protect the target from the impact of stray gases.

Preparation of the Apparatus for Measurements

The measuring chamber and valve separating it from the diffusion pump were heated before beginning the experiment to some 400°C for 3 to 4 h. The apparatus was pumped during this heating by the oil diffusion pumps with nitrogen traps and the hydrogen condensation pump 7. When the heating ended, the vacuum in the measuring chamber had reached $1.3 \cdot 10^{-5}$ N/m^2.

After removing the heaters, liquid hydrogen was poured into hydrogen condensation pump 20. The temperature of the measuring chamber and the hydrogen condensation pump at this moment still stayed around 400°C. The total consumption of liquid hydrogen in this was 5 dm^3. Simultaneously the measuring chamber was disconnected from the oil diffusion pump and nitrogen screen by means of the valve. This guarded the measuring chamber from oil decomposition products and reduced the residual gas background to a minimum. The vacuum in the measuring chamber immediately after pouring in the hydrogen reached 4 to $5 \cdot 10^{-7}$ N/m^2. The pouring of liquid helium into the HCP 16 improved the vacuum in the measuring chamber almost instantaneously to $1.3 \cdot 10^{-7}$ N/m^2, and then continued improving more slowly, so that after 1 to 1.5 h it reached $6 \cdot 10^{-8}$ N/m^2 ($5 \cdot 10^{-10}$ torr). The experiments, however, normally began immediately after pouring the liquid helium at a vacuum of $1.3 \cdot 10^{-7}$ N/m^2. Here it was assumed that the main residual gas in the measuring chamber was hydrogen. This assumption was quite legitimate, remembering the presence of the hydrogen condensation pump in the measuring chamber, having a fairly high pumping rate and the capacity of removing all impurity gases except those condensing with difficulty at 20.4°K. This procedure of preparing for experiments ensured a fairly clean target surface and almost entirely excluded the possibility of contaminating this after heating by adsorption from the surrounding medium.

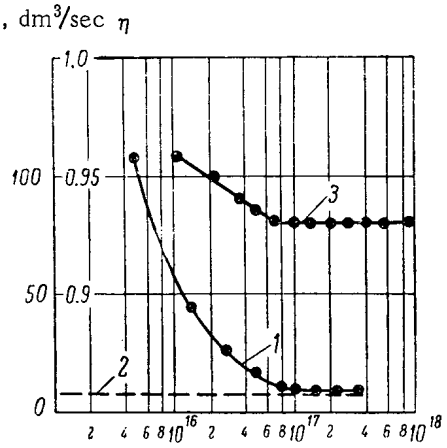

Fig. 4. Pumping rate W and penetration coefficient η as functions of the amount of gaseous hydrogen coming into the measuring chamber. 1) Total rate of pumping hydrogen from the measuring chamber; 2) calculated hydrogen pumping rate for the HCP; 3) penetration coefficient.

Results of Measurements and Discussion

The method of measuring the penetration coefficient was as follows. The beam of H_1^+ ions bombarding the target penetrated into it. The flow of hydrogen from the target due to the nonpenetrating part of the beam as well as hydrogen diffusely emitted from the target altered the vacuum in the measuring chamber. A typical curve relating the vacuum to target bombardment time for a 35 kV, 110 μA H_1^+ ion beam appears in Fig. 3. It should be noted that the change in pressure in the measuring chamber caused by the ion beam passing into the magnetic analyzer chamber is negligibly small. The pressure varies only on bombardment of the target.

Knowing the ion beam current, the vacuum in the measuring chamber, and the rate of pumping hydrogen from the latter, we may determine the pentration coefficient:

$$\eta = 1 - \frac{n(p - p_0)W}{10^5 i^+/e},$$

where n is the number of particles in 1 dm³ under normal conditions, p is the working pressure in N/m², p_0 is the initial pressure in N/m², W is the pumping rate in dm³/sec, i^+ is the ion beam current A, e is the charge on the electron in C, and 10^5 is the atmospheric pressure in N/m².

In the first experiments the penetration coefficient of the H_1^+ ions calculated for a pumping rate of 8 dm³/sec, determined by the conductivity of the tube, was very high, and at the beginning of the bombardment reached a value close to unity (0.99). As the density of penetrated particles rose, the penetration coefficient fell to 0.94 and then remained constant. This was the first time such a high penetration coefficient of ions had been obtained. In view of this the idea arose that extra hydrogen had been extracted by the clean surface of the chamber walls and by the hydrogen condensation pump 20. In order to check this idea, the pumping rate was measured. This was done by using the steady flow of hydrogen through a capillary of known conductivity. The measurements showed that the clean surfaces of stainless steel and copper did not possess any marked extraction rate between room temperature and 78°K.

The clean surface of the hydrogen condensation pump, however, which was made of copper, did extract hydrogen at liquid hydrogen temperature (20.4°K). As the amount of extracted hydrogen rose, the extraction rate rapidly fell, and at concentrations corresponding to approximately 0.01 monolayer practically vanished. This effect had not been observed by anyone before, and was rather unexpected for such low pressures. Figure 4 shows the experimental curve 1 of the pumping rate as a function of the amount of hydrogen coming into the chamber. The calculated hydrogen pumping rate of the HCP 16, determined by the conductivity of tube 17 (see Fig. 2), is shown dotted. The deviation between the experimental (10 dm³/sec) and calculated (8±1.5 dm³/sec) values of pumping rate in the region $N > 10^{17}$ lies within measuring error.

During the bombardment, atomic hydrogen is present in the chamber, and the adsorption of this differs from that of molecular hydrogen. In view of this, we made some experiments to determine the amount of hydrogen adsorbed during bombardment at 20.4 and 78°K, desorbing it by heating the hydrogen pump and screen 20. It was established that the adsorption of atomic and molecular hydrogen took place only at temperatures below 30°K and stopped almost completely for amounts of adsorbed hydrogen roughly equal to 0.01 monolayer. The total amount of desorbed hydrogen agreed with the calculated value. Furthermore these experiments showed that a certain quantity of heavier materials (1 to 2% of the number of incident ions) were evolved by the target during bombardment.

The variation of pumping rate with the amount of hydrogen coming into the chamber causes some difficulty in calculating the penetration coefficient. In fact, in order to determine the penetration coefficient, we must know the pumping rate. But the pumping rate depends on the amount of hydrogen coming into the chamber, i.e., on the penetration coefficient. In view of this, the method of successive approximations was used for calculating η, the zero approximation being a pumping rate of 10 dm³/sec.

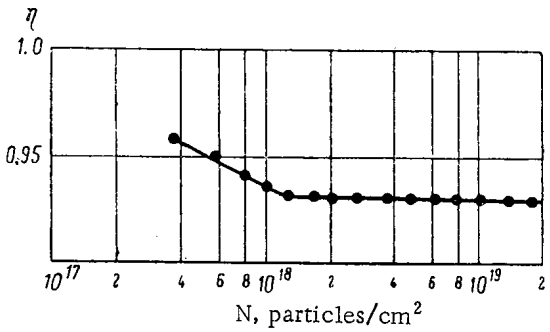

Fig. 5. Variation of η with the number of particles penetrated per unit surface.

The measured values of penetration coefficient for 35 keV, 110 μA (current density 150 $\mu A/cm^2$) H_1^+ ions incident on a stainless steel surface are shown as a function of the penetrated hydrogen concentration in Fig. 5. Figure 4 (curve 3) shows the same results as a function of the amount of hydrogen entering the chamber. It should be noted that a large part of the curve falls in the region where the pumping rate is constant. Hence the penetration coefficient was here calculated without correction for the hydrogen condensation pump extraction rate. As we see from the curves in Fig. 5, as the density of penetrated atoms rises to $N = 10^{18}$ particles/cm^2, the penetration coefficient falls from 0.96 to 0.93. As the concentration of penetrated atoms rises further, the penetration coefficient remains constant right up to $N = 2 \cdot 10^{19}$ particles/cm^2. We may well imagine that it continues steady to much larger concentrations.

In addition to these measurements, we made some experiments to find the amount of penetrated hydrogen by weighing. This showed that the amount of such hydrogen reached $2 \cdot 10^{19}$ particles/cm^2.

These results of ours differ considerably from those of [2]. In [2], the penetration coefficient of D^+ ions for a stainless steel target varied from 0.2 to 0.35 over the energy range 7 to 25 keV. In this range, target saturation occurred, as indicated by the equal flows of deuterium to and from the target. Thus, for example, for 15 keV D^+ ions, saturation occurred for penetrated particle concentrations of $3 \cdot 10^{17}$ cm^{-2}.

The discrepancy between the results of [2] and our own can evidently not be ascribed either to differences in the masses or to differences in the energies of the penetrating particles. It would appear that the vacuum conditions, bearing on the state of the target surface, played some part in this. Although we did not make any specific experiments on the effect of the cleanliness of the target surface on the penetration coefficient, certain results indicated that the value of η fell as the surface became less clean. In [2], the vacuum in the measuring chamber was 1.3 to $4 \cdot 10^{-6}$ N/m^2, in which ~30% constituted impurities. This kind of vacuum is inadequate for maintaining the required clean state of the target. For example, if the partial pressure of active impurities in the measuring chamber exceeds 10^{-7} N/m^2, then up to 0.1 monolayer may form on the target after heating it for 1 min. However, the differences in the state of the vacuum can hardly by itself explain the discrepancy between the results; there must be other sources of error in [2].

We have thus established that the coefficient of penetration of 35 kV H_1^+ ions into a clean 1Kh18N9T stainless steel surface exceeds 93%. This value of η remains unvarying right up to concentration of $2 \cdot 10^{19}$ cm^{-2} penetrated atoms, and no sign of its further fall can be found.

These results suggest that, under magnetic trap conditions, the extraction rate of slow neutral particles may be taken as at least an order less than the value determined by the rate at which fast particles pass out from a plasma region.

LITERATURE CITED

1. L. J. Varnerin and J. H. Carmichael, J. Appl. Phys., 28, 913 (1957).
2. V. A. Simonov, Nuclear Synthesis. Part I [in Russian], Vena, MAGATÉ (1962), p. 325.
3. J. Carmichael and E. Trendelenburg, J. Appl. Phys., 29, 1570 (1958).
4. J. Carmichael and P. Waters, J. Appl. Phys., 33, 1470 (1962).
5. E. Brown and J. H. Leck, Brit. J. Appl. Phys., 6, 161 (1955).
6. J. Koch, Nature, 161, 566 (1948).
7. K. Fiebiger, Z. angew. Phys., 9, 213 (1957).
8. E. S. Borovik, S. F. Grishin, and B. G. Lazarev, "Pribory i tekhnika éksperimenta," No. 1, 115 (1960).
9. E. S. Borovik, S. F. Grishin, and E. Ya. Grishina, ZhTF, 30, 539 (1960).

PERTURBATION OF PARTICLE MOTION IN THE STELLARATOR

(UDC 533.9)

A. P. Popryadukhin

Translated from Atomnaya Énergiya, Vol. 18, No. 2,
pp. 96-104, February, 1965
Original article submitted January 11, 1964, and in final form June 16, 1964

The conditions under which small perturbations do not disrupt the closed surfaces of trajectories of the guiding centers of charged particles in the stellarator are derived. It is shown in the linear approximation that the toroidal stellarator with perturbations of the magnetic field constitutes an absolute trap for individual particles.

It is well known that, in the drift approximation, the ideal stellarator constitutes an absolute trap for individual charged particles. By "ideal stellarator" we mean a trap with a magnetic field possessing helical symmetry [$\mathbf{H} = \mathbf{H}(r, \varphi - \alpha z)$] and constituting the combination of a field created by helical conductors and a homogeneous field parallel to the z axis. The loss of particles through the ends in a system with finite length $2\pi R$ is eliminated, since the ends of the system coincide, i.e., the planes $z_0 + 2\pi R i = \text{const}$ ($i = 0, 1, 2, \ldots$) coincide and form a single plane. We shall call this the image plane.

In an actual stellarator, there are different forms of perturbations to the particle motion: the toroidal aspect, imprecise construction of the magnetic system, currents in the plasma, and electric fields in the plasma. The effect of the toroidal aspect and magnetic field perturbations on the lines of force have been studied in a number of papers [1-6]. In this paper we shall consider typical effects of these perturbations on the motion of the particles.

Motion of Particles in a Helical Magnetic Field

Let us consider the motion of particles in an ideal stellarator field in the drift approximation.

For static fields [7]

$$\frac{d\mathbf{r}}{dt} = \frac{v_{\parallel}}{H}\left[\mathbf{H} + \frac{mc}{e}\operatorname{rot} v_{\parallel}\boldsymbol{\tau} - \frac{mcv_{\parallel}}{e}\boldsymbol{\tau}(\boldsymbol{\tau}\operatorname{rot}\boldsymbol{\tau})\right], \tag{1}$$

where

$$v_{\parallel} = \sqrt{v^2 - J_{\perp}H}, \quad v^2 = v_{\parallel}^2 + v_{\perp}^2 = \text{const}, \quad J_{\perp} = \frac{v_{\perp}^2}{H} = \text{const}, \quad \boldsymbol{\tau} = \frac{\mathbf{H}}{H}. \tag{2}$$

From Eq. (1) we obtain for the trajectory of the guiding center:

$$\frac{dr}{H_r^*} = \frac{r\,d\varphi}{H_\varphi^*} = \frac{dz}{H_z^*}, \tag{3}$$

where in the absence of current in the plasma

$$\mathbf{H}^* = \mathbf{H} + \frac{mc}{e}\operatorname{rot} v_{\parallel}\boldsymbol{\tau}. \tag{4}$$

To Eq. (3) we may add the relations

$$\frac{dz}{H_z^*} = \frac{dl}{H^*} = \frac{v_{\parallel}\,dt}{H}. \tag{3a}$$

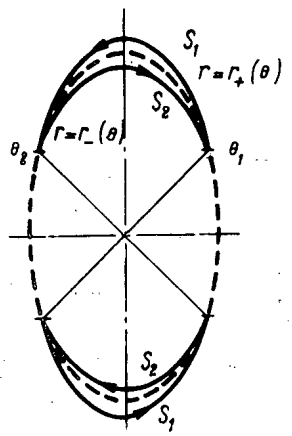

Fig. 1. Surface of guiding centers of blocked particles.

In the case of helical symmetry, $\mathbf{H}=\mathbf{H}(r, \theta)$, $\theta=\varphi-\alpha z$, and system (3) has the integral [7]

$$u_0 = A_z^* + \alpha r A_\varphi^*,$$
$$\mathbf{A}^* = \mathbf{A} + \frac{mcv_\parallel}{eH}\mathbf{H}, \tag{5}$$

where $\mathbf{A}$ is the vector potential of the magnetic field. The trajectory of the guiding center of the particles lies on the surfaces

$$u_0(r, \theta) = C = \text{const}, \tag{6}$$

slightly displaced from the magnetic surfaces determined from Eqs. (5) and (6) for $m=0$. Just as in the case of the magnetic surfaces, for the surfaces of trajectories of the guiding center there is a region bounded by a separatrix in which the surfaces are closed. It is this which determines the absoluteness of the trap. We write the second integral of system (3) in the form

$$w_0(\theta, z) = \int \frac{d\theta}{\frac{H_\varphi^*}{rH_z^*} - \alpha} - z = C_2. \tag{7}$$

The relation $\theta=\theta(z)$ may be found from Eq. (7), but for transitory particles ($v^2 - J_\perp H_{max} > 0$) it may be obtained by using the averaging method [8].

For one harmonic of the helical field

$$H_r = nh_n I_n'(x)\sin n\theta,$$
$$H_\varphi = \frac{n^2}{x} h_n I_n(x)\cos n\theta,$$
$$H_z = H_0 - nh_n I_n(x)\cos n\theta,$$

where $x=n\alpha r$. For $\varepsilon_n=(h_n/H_0)\ll 1$ we may obtain

$$\varphi = \varphi_1 + \alpha\omega^* z + \varepsilon_n \Phi(x)\sin n(1-\omega^*)\alpha z, \tag{8}$$

where

$$\Phi(x) = \frac{n^2}{x}\left[\frac{I_n}{x} - \frac{\alpha\varrho\left(1-\frac{\gamma^2}{2}\right)}{\sqrt{1-\gamma^2}} I_n'\right], \quad \varrho = \frac{mcv}{eH_0}, \quad \gamma = \frac{v_\perp}{v},$$

ω^* is the mean torsional angle of the trajectory, given by the formula

$$\omega^* = \frac{n^4\varepsilon_n^2}{2}\left\{\frac{I_n'^2}{x^2} - \frac{2I_nI_n'}{x^3} + \frac{I_n^2}{x^2}\left(1+\frac{n^2}{x^2}\right) + \frac{\alpha\varrho\left(1-\frac{\gamma^2}{2}\right)}{\sqrt{1-\gamma^2}}\left[\frac{n^2I_n^2}{x^4} + \frac{I_n'^2}{x^2} + \left(1-\frac{2n^2}{x^2}\right)\frac{I_nI_n'}{x}\right]\right.$$
$$\left. - \frac{\alpha\varrho}{x\sqrt{1-\gamma^2}}\cdot\frac{3\gamma^4-12\gamma^2+8}{4(1-\gamma^2)} I_nI_n'\right\}. \tag{9}$$

Considering that the integrand in (7) is a periodic function, it is not difficult to obtain an exact expression for the torsional angle:

$$\int_0^{2\pi} \frac{d\theta}{\frac{H_\varphi^*}{rH_z^*} - \alpha} = \frac{2\pi}{\alpha(\omega^*-1)}. \tag{9a}$$

For $x \ll 1$ expression (9) takes the form

$$\omega^* = \frac{n^3 (n-1) \varepsilon_n^2 x^{2n-4}}{2^{2n} [(n-1)!]^2} \left[1 - \frac{n\alpha\varrho \left(1 - \frac{\gamma^2}{2} \right)}{\sqrt{1-\gamma^2}} \right]. \tag{10}$$

We note that in these formulas $(1-\gamma^2)^{1/2}$ must be taken with the plus sign when the velocity $v_{||}$ is directed along the field H and with the minus sign when $v_{||}$ is opposite to H.

Let us consider the motion of blocked particles. These will be particles the longitudinal velocity $v_{||} = (v^2 - J_\perp H)^{1/2}$ of which may at certain points θ^1 become zero. At these points the particles will be reflected and $v_{||}$ will change sign. Since (5) is an integral of motion for all particles, including the blocked ones, they will move along surfaces $r = r_\pm(\theta)$ [see (6)], oscillating near the field minimum (Fig. 1). Drift of blocked particles will take place in the direction of the z-axis. In fact, from Eq. (7) we may obtain the increment Δz after one reflection:

$$\Delta z = \int_{\theta_1}^{\theta_2} r \, d\theta \left\{ \frac{H^*_{z+}}{H^*_{\varphi+} - \alpha r_+ H^*_{z+}} - \frac{H^*_{z-}}{H^*_{\varphi-} - \alpha r_- H^*_{z-}} \right\}.$$

In expression (4), for H_+^* we take $v_{||}$ with the plus sign and for H_-^* with the minus sign; θ_1 and θ_2 are points of reflection. With an accuracy of the first order in ε_n we obtain

$$\alpha \Delta z = 2n^2 \alpha\varrho \frac{I'_n}{x} \sqrt{\frac{2\varepsilon_n}{nI_n}} [2E(k) - K(k)], \tag{11}$$

where E and K are complete elliptic integrals of argument k, and

$$k^2 = \frac{v^2 - J_\perp H_0 + J_\perp H_0 \varepsilon_n n I_n}{2 J_\perp H_0 \varepsilon_n n I_n}.$$

Analogously calculating the time required for the to-and-fro motion of the particles, we obtain an expression for the drift velocity

$$v_{dr} = \frac{\Delta z}{\Delta t} = \frac{\alpha n^3 \varepsilon_n mc \left(v^2 - \frac{1}{2} J_\perp H_0 \right)}{eH} \cdot \frac{I'_n}{x} \left[1 - \frac{2E(k)}{K(k)} \right]. \tag{12}$$

We note that the direction of drift depends on the direction of H, the sign of the particle charge, and the sign of the expression $1 - [2E(k)]/K(k)$.

Calculation of Image Point Coordinates in the Presence of Perturbation

Let $\mathbf{H}^* = \mathbf{H}^{*0} + \tilde{\mathbf{H}}^*$, where $\mathbf{H}^{*0}$ has helical symmetry and the perturbation $\tilde{\mathbf{H}}^*$ is small. System (3) determines the characteristics for equation

$$\mathbf{H}^* \nabla u = 0, \tag{13}$$

where u is an integral of system (3). Considering that $u = u_0 - \tilde{U}$, in the linear approximation we obtain

$$-\mathbf{H}_0^* \nabla \tilde{U} + \tilde{\mathbf{H}}^* \nabla u_0 = 0. \tag{13a}$$

Since the first term of this expression is a derivative with respect to the direction of vector H_0^*, we obtain a particular solution for $\tilde{U}$:

$$\tilde{U} = \int \frac{\tilde{\mathbf{H}}^* \nabla u_0}{H^{*0}} \, dl = \int_{z_0}^{z} \frac{\tilde{\mathbf{H}}^* \nabla u_0}{H_z^*} \, dz. \tag{14}$$

Integration is carried out over the unperturbed trajectory. This particular solution corresponds to the condition $\tilde{U} = 0$ for $z = z_0$. We note that $\tilde{U}$ is a function of z and also of the coordinates of the initial point of the integration path $\tilde{U} = \tilde{U}(z, C, \theta_0, z_0)$. Considering u_0 as a curvilinear coordinate, we may derive its variation under the influence of the perturbation in the length $z - z_0$. Since u is an integral of (3),

$$u = u_0 - \tilde{U}(z, C, \theta_0, z_0) = C = \text{const},$$

we obtain from (14)

$$u_0 = C + \int_{z_0}^{z} \frac{\tilde{\mathbf{H}}^* \nabla u_0}{H_z^*} dz. \tag{15}$$

The correction $\tilde{\theta}$ to θ caused by the perturbation may be found from the relation $w_0(\theta, z) + \tilde{w}(z, C, \theta_0, z_0) = C_2$; here $\tilde{w}$ is determined by formula (14) if we replace u_0 by w_0 from (7). Carrying out the differentiation, we obtain

$$\tilde{w} = -\int_{z_0}^{z} \left(\frac{\tilde{H}_\varphi^* - ar\tilde{H}_z}{H_{\varphi 0}^* - arH_{z0}^*} - \frac{\tilde{H}_z^*}{H_{z0}^*} \right) dz. \tag{16}$$

Let us now consider the intersection of the image plane by the trajectory of the guiding center. The coordinates of successive image points we obtain by substituting

$$z = z_0 + 2\pi Ri, \quad i = 1, 2, \ldots \tag{17}$$

into formulas (14) to (16) as upper limit of integration. Let us split the integral between the limits $z_0 \leq z \leq z_0 + 2\pi Ri$ into a sum of integrals between limits $z_0 + 2\pi R \times (k-1) \leq z \leq z_0 + 2\pi Rk$ ($k = 1, 2, \ldots, i$). It is easy to see that the integrals obtained will differ only in the initial points of the integration path, coinciding with the successive unperturbed image points (C, θ_k^0). Introducing the notation

$$\tilde{u}(\theta_k^0) = \int_{z_0,\, \theta_k^0}^{z_0 + 2\pi R} \frac{\tilde{\mathbf{H}}^* \nabla u_0}{H_z^{*0}} dz, \tag{18}$$

we obtain for the i-th image point

$$\tilde{U}_i = \sum_{k=1}^{i} \tilde{u}(\theta_{k-1}^0). \tag{19}$$

With the help of Eq. (18) we may determine the change in the coordinate u_0 after one circuit as a function of θ, i.e., $\tilde{u} = \tilde{u}(\theta)$. Then Eq. (19) signifies that the increment in coordinate u_0 after i circuits equals the sum of the increments in the unperturbed image points.

We can use the perturbation method on fulfillment of the conditions

$$\frac{\partial}{\partial u_0}\left(\ln \frac{\tilde{\mathbf{H}}^* \nabla u_0}{H^*}\right) \tilde{U} \ll 1, \quad \frac{\partial}{\partial \theta}\left(\ln \frac{\tilde{\mathbf{H}}^* \nabla u_0}{H^*}\right) \tilde{\theta} \ll 1.$$

The first inequality is fulfilled if, over the whole path of integration, the deviation from the unperturbed surface is small. Apart from this, however, over a long path of integration there may accumulate such a deviation in θ from the true trajectory that the second inequality will not be satisfied.

The convergence of the method may be improved if in formula (19) the value of θ for the unperturbed image points $\theta = \theta_i^0$ is replaced by $\theta = \theta_i = \theta_i^0 + \tilde{\theta}_i$. Then (19) takes the form

$$\tilde{u}_i = \sum_{k=1}^{i} \tilde{u}(\theta_{k-1}). \tag{19a}$$

Condition for the Existence of Continuous Surfaces for the Trajectories of Transitory Particles

We shall suppose that the trajectory forms a closed continuous surface if the imaging points everywhere densely fill up a closed curve on the image plane.

Despite the fact that for a field with helical symmetry the drift equations have integral (5), describing closed surfaces $u_0(r, \theta) = C$, the trajectory of the guiding center of a particle may not form a continuous surface. This will

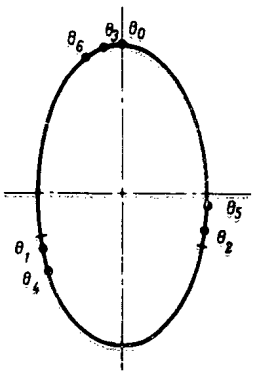

Fig. 2. Position of image points near resonance of the third kind.

be so when the trajectory, after one or any finite number of passages around the system, closes upon itself. Here we obtain individual image points in the image plane. The condition under which the trajectory will have p image points may be obtained by equating the change in the angle after p circuits in formula (8) to a whole number of 2π. This condition, which we shall term resonance, has the form

$$M\omega^* = n + \frac{\nu}{p}, \tag{20}$$

where $M = 2\pi R/L$ is the number of periods of the helical winding in the length of the system.

We see from this that, for the unperturbed trajectory to be described by a continuous surface, $M\omega^*$ must be an irrational number. In this way we shall have a sequence of numbers of passages around the system $p_k \to \infty$ such that image points occur as near as we like to the initial point (C, θ_0), i.e., for

$$p_k \to \infty\ \theta_{p_k} \to \theta_0, \quad \text{and} \quad \tilde{u}_{p_k} = C + \tilde{U}_{pk} \to C. \tag{21}$$

Taking account of Eqs. (19) and (21), we obtain

$$\lim_{p_k \to \infty} \sum_{i=1}^{p_k} \tilde{u}(\theta_{i-1}) = 0. \tag{22}$$

Let us consider the meaning of Eq. (22) in more detail. Introducing the line density $N(\theta) = p_k n(\theta)$ of the image points on the curve $u_0(r, \theta) = C$, we rewrite condition (22) in the form

$$\lim_{p_k \to \infty} \cdot p_k \sum_{i=1}^{p_k} \tilde{u}(\theta_{i-1})\, n(\theta_{i-1})\, \Delta\theta_i = 0,$$

where $\Delta\theta_i = \theta_{i+q_k} - \theta_i$ is the interval between neighboring points out of the p_k image points (Fig. 2), and

$$n(\theta_{i-1}) = \frac{1}{p_k \Delta\theta_i}. \tag{23}$$

Thus (22) is equivalent to the condition

$$Y = \oint_{u_0 = C} \tilde{u}(\theta)\, n(\theta)\, d\theta = 0. \tag{22a}$$

An expression for $\Delta\theta_i$ may be obtained from relations (7) and (9a):

$$|\Delta\theta_i| = \frac{2\pi}{p_k(1-\omega^*)}(1 + \delta p_k q_k)\left(1 - \frac{H_\varphi^*}{\alpha r H_z^*}\right)_{\substack{u_0 = C \\ \theta = \theta_i}},$$

where $\delta = M\omega^* - (\nu_k)/p_k$ (here ν_k/p_k are proper fractions of the expansion of $M\omega^*$ into an infinite continued fraction [9]).

Since for almost all irrational numbers, except a set of degree zero, $\delta < (1)/p_k^2 \ln p_k$ and $q_k < p_k$, passing to the limit for $p_k \to \infty$, we find

$$n_0(\theta) = \frac{1-\omega^*}{2\pi} \cdot \frac{1}{1 - \frac{H_\varphi^*}{\alpha r H_z^*}}. \tag{24}$$

From (14), (22a), and (24), we obtain

$$Y = \frac{1-\omega^*}{2\pi} \int\int \frac{\tilde{\mathbf{H}}^* \nabla u_0\, dl\, d\varphi}{H^{*0}\left(1 - \frac{H_\varphi^*}{\alpha r H_z^*}\right)}.$$

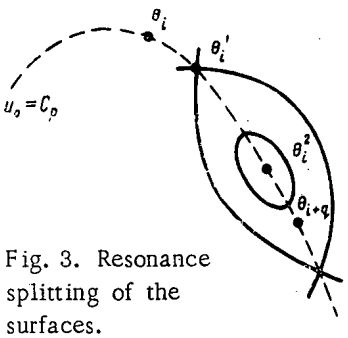

Fig. 3. Resonance splitting of the surfaces.

The integration is carried out over the surface $u_0 = C$. Let us introduce as element of length ds along the curve $u_0 = C$, $z = z_0$:

$$ds = \mathbf{e}_r\, dr + \mathbf{e}_\varphi r d\varphi$$

and calculate the element of area $dS = dl \times ds$ of the surface $u_0 = C$, where $dl = (\mathbf{e}_r H^*_{r0} + \mathbf{e}_\varphi H^*_{\varphi 0} + \mathbf{e}_z H^*_{z0}) \frac{dl}{H^{*0}}$. Using the relation $dr = -\frac{\partial u_0}{\partial \varphi} \Big/ \frac{\partial u_0}{\partial r} d\varphi$ for $z = z_0$ and

$$\frac{\partial u_0}{\partial r} = -H^*_\varphi + \alpha r H^*_z,\ \frac{\partial u_0}{\partial \varphi} = r H^*_r,\ \frac{\partial u_0}{\partial z} = -\alpha r H^*_r, \tag{25}$$

we obtain

$$dS = \frac{\nabla u_0\, dl\, d\varphi}{\alpha H^{*0}\left(1 - \frac{H^*_\varphi}{\alpha r H^*_z}\right)}.$$

Thus

$$Y = \frac{1-\omega^*}{2\pi}\alpha \int\limits_{u_0 = C} \tilde{\mathbf{H}}^*\, dS. \tag{26}$$

Hence, in the presence of perturbation the surface $u_0 = C$ remains closed and continuous if the flux of the perturbing field $\tilde{H}^*$ through this surface is zero and condition (21) is satisfied.

Resonance Action of Perturbations

As already mentioned, when the resonance condition (20) is satisfied, the unperturbed trajectory of the particle does not form a closed surface, but closes upon itself after a certain number of circuits p. Since $\omega^* = \omega^*(u_0)$, resonance of the p-th kind will be observed on the surface $u_0 = C$, corresponding to condition (20). It is clear that, for sufficient proximity to this surface and for sufficient smallness of the perturbation, the image points (u_{0i}, θ_i), where $i = kp$ and $k = 0, 1, 2, \ldots$, will be close to one another, so that by joining them we can obtain the approximate form of the surface of trajectories (Fig. 3). According to formula (19), the increment in coordinate u_0 after p circuits equals

$$u_{0p(k+1)} - u_{0pk} = \sum_{i=1}^{p} \tilde{u}(\theta_{i-1}) = \sum_{i=1}^{p} \tilde{u}(\theta^p_{i-1}) + \sum_{i=1}^{p} \frac{\partial \tilde{u}}{\partial \theta}(\theta_{i-1} - \theta^p_{i-1}), \tag{27}$$

where θ^p_{i-1} are the values of coordinate θ corresponding to exact resonance.

Let us calculate the increment $\delta\theta$ to the coordinate θ after p circuits. If for the resonance surface $\theta_{p(k+1)} - \theta_{pk} = 2\pi n_1$, where the whole number $n_1 = Mp(1-\omega^*_p)$, for the surface $u_0 = C_p + \Delta C$, close to the resonance surface

$$\theta_{p(k+1)} - \theta_{pk} = 2\pi n_1 + \delta\theta$$

and according to (7) we may write

$$\int\limits_{\theta_{pk}}^{\theta_{pk}+2\pi n_1+\delta\theta} \frac{d\theta}{\left(1 - \frac{H^*_\varphi}{\alpha r H^*_z}\right)_{u_0 = C_p + \Delta C}} = -2\pi M p.$$

Expanding the integrand in the neighborhood of $u_0 = C_p$, replacing d/du_0 by $(d\omega^*)/du_0 \cdot (d)/d\omega$, and taking account of (9a) and (24), for small $\delta\theta$ we obtain

$$\delta\theta = \frac{M p \Delta C}{n(\theta)} \cdot \frac{d\omega^*}{du_0},\ \Delta C = \Delta C_0 + \tilde{u}, \tag{27a}$$

where ΔC_0 is the deviation of the unperturbed surface considered from resonance.

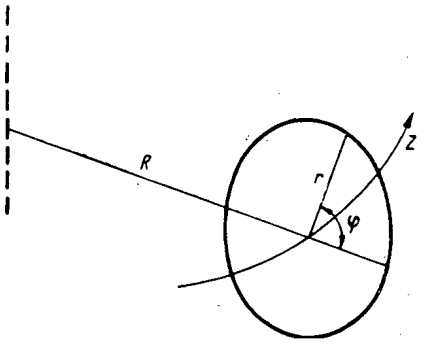

Fig. 4. Toroidal coordinate system.

The condition of sufficient proximity to the resonance surface may be established with the aid of formulas (23) and (27). It is clear that the inequality $\delta\theta \ll \Delta\theta_i$ (see Fig. 2) must be satisfied. Hence we obtain

$$Mp^2 \frac{d\omega^*}{du_0} \Delta C \ll 1. \tag{28}$$

If we take $M\omega^* = M\omega_p^* + \delta$, where $\omega_p^* = \omega^*(C_p)$, then $\delta = M\, d\omega^*/du_0 \Delta C_0$ and inequality (28) gives

$$\delta \ll \frac{1}{p^2}, \quad Mp^2 \frac{d\omega^*}{du_0} \tilde{U} \ll 1. \tag{28a}$$

Selecting the denominators of proper fractions q_k/p_k as p for some value of $M\omega^*$ expressed in the form of a continued fraction, we can satisfy condition (28a) for almost all $M\omega^*$, excluding the set of zero degree. This means that almost all the surfaces are close to resonance.

Let us replace small increments by differentials; then from (27) and (27a) we obtain for the surfaces

$$\frac{d\tilde{U}}{d\theta} = \frac{\tilde{V}_p(\theta) + \sum_{i=1}^{p} \frac{\partial \tilde{u}}{\partial \theta}(\theta_{i-1} - \theta_{i-1}^p)}{\delta + M \frac{d\omega}{du_0} \tilde{U}} \cdot \frac{n(\theta)}{p}, \tag{29}$$

where

$$\tilde{V}_p(\theta) = \sum_{i=1}^{p} \tilde{u}(\theta_{i-1}^p). \tag{30}$$

Let us consider as a particular case of Eq. (29) the behavior of trajectories near resonance of the first kind, when $\delta \gg M\, d\omega/du_0 \tilde{U}$, but at the same time conditions (28a) are satisfied. Equation (29) takes the form

$$\frac{d\tilde{U}}{d\theta} = \frac{1}{\delta} \tilde{u}(\theta)\, n_0(\theta).$$

The surface of trajectories is determined by the expression

$$u_0(\theta) = C + \frac{1}{\delta} \int_{\theta_0}^{\theta} \tilde{u}(\theta)\, n_0(\theta)\, d\theta. \tag{31}$$

We see that the surface is closed if $Y = \int_{\theta_0}^{\theta_0 + 2\pi} \tilde{u}(\theta)\, n_0(\theta)\, d\theta = 0$. If however the integral $Y \neq 0$, the surface winds up (or unwinds) in a spiral, the pitch of which $\Delta u_0 = (1/\delta)\, Y(u_0)$. Let us now consider the resonance case $\delta = 0$. Since the differences $\theta_{i-1} - \theta_{i-1}^p$ in formula (28) are proportional to the perturbation, the second term in the numerator of the right hand side of Eq. (29) will be of a higher degree of smallness than the first. Neglecting this term, we obtain the equation

$$\frac{d\tilde{U}}{d\theta} = \frac{\tilde{V}_p(\theta)\, n_0(\theta)}{pM \frac{d\omega}{du_0} \tilde{U}}, \tag{32}$$

after integrating which we shall have

$$\tilde{U}(\theta) = \left[\frac{2}{pM \frac{d\omega}{du_0}} \int_{\theta_0}^{\theta} \tilde{V}_p(\theta)\, n_0(\theta)\, d\theta \right]^{1/2}. \tag{33}$$

Let us consider the properties of the function $\tilde{V}_p(\theta)$ [see (30)]. By definition we see that $\tilde{V}_p(\theta) = \tilde{V}_p(\theta^p_{i-1})$ for i = 1, 2, ..., since the trajectory emerging from initial point θ^p_{i-1}, forms the same p image points as the trajectory emerging from θ. This indicates that the function $V_p(\theta)$ takes the same values at the ends of the interval (θ_i, θ_{i+q}), where θ_i and θ_{i+q} are neighboring image points. Moreover, if condition (22a) is satisfied,

$$\int_{\theta_i}^{\theta_{i+q}} \tilde{V}_p(\theta)\, d\theta = 0.$$

In fact, as the coordinate θ of the initial point varies over the range (θ_0, θ_q), the coordinates of successive image points will vary over (θ_i, θ_{i+q}) and

$$\int_{\theta_i}^{\theta_{i+q}} \tilde{V}_p(\theta)\, n_0(\theta)\, d\theta = \sum_{i=1}^{p} \int_{\theta_{i-1}}^{\theta_{i-1+q}} \tilde{u}(\theta)\, n_0(\theta)\, d\theta = Y.$$

It follows from these two properties of function $\tilde{V}_p(\theta)$ that it changes sign at least twice in each of the ranges (θ_i, θ_{i+q}), passing through zero at the points denoted by θ^1_i and θ^2_i.

Since at the points θ^1_i and θ^2_i the values of $d\tilde{V}_p/d\theta$ have opposite signs, in each range (θ_i, θ_{i+q}) Eq. (32) has at least one pair of singular points of the "saddle" and "center" type, so that the surface of trajectories of the guiding center in the case of resonance of the p-th kind acquires a rosette structure with p-cells (see Fig. 3). The maximum breadth of the i-th cell is determined by formula (33), in which the integration takes place over the range θ^1_i to θ^2_i. It is seen that this breadth is proportional to $(H^*)^{1/2}$ and $(d\omega/du_0)^{-1/2}$.[1] In the absence of gradient the torsional angle $d\omega/du_0 = 0$ and the topology of the surface becomes unstable with respect to perturbations on satisfying the resonance condition (20).[2] On satisfying condition (20) the rosette structure of the surface may also not be obtained if $\tilde{V}_p(\theta) \equiv 0$.

For the closed stellarator, every perturbation is periodic in z with period $2\pi R$. In the case of a perturbation of the magnetic surfaces (m = 0), the perturbing magnetic field may be represented in the form $\tilde{\mathbf{H}} = \nabla\tilde{\Phi}$, where

$$\tilde{\Phi} = \sum_{k\neq 0} h_{k0} \frac{x^k}{\alpha n k} \sin(k\varphi + \varphi_{k0}) + \sum_{k,\, l\neq 0} \frac{\tilde{h}_{kl}}{|l|} RI_k\left(\frac{|l|x}{Mn}\right) \sin\left(k\varphi - \frac{|l|}{M}\alpha z + \varphi_{kl}\right).$$

After substituting this expression into the formula

$$\tilde{V}_p = \int_{z_0}^{z_0 + 2\pi R p} \frac{\tilde{\mathbf{H}}\nabla u_0}{H^0_z}\, dz,$$

and carrying out some uncomplicated calculations for small ε, we find that $\tilde{V}_p(\theta) \not\equiv 0$, if there is a harmonic of the field for which one of the following relations is satisfied[3]:

$$k\omega - \frac{l}{M} = 0, \quad \pm n(1-\omega) + k\omega - \frac{l}{M} = 0. \tag{34}$$

We note a peculiarity of the resonance action of perturbations on the trajectory of a particle. Since ω^* depends on the mass and velocity of the particle [see formulas (5) and (10)], for one and the same value of u_0 and $\varepsilon_n = h_n/H_0$ there may be resonance and nonresonance particles.

Effect of Perturbations of the Magnetic Field and of the Toroidal State

If the perturbation of the motion is connected with perturbations of the magnetic field $\tilde{\mathbf{H}}$, then

$$\tilde{\mathbf{H}}^* = \tilde{\mathbf{H}} + \frac{mc}{z}\left(\operatorname{rot}\frac{v_\parallel}{H}\mathbf{H} - \operatorname{rot}\frac{v^0_\parallel}{H^0}\mathbf{H}^0\right), \tag{35}$$

[1] An analogous result was obtained in [1].

[2] This result agrees with the results of [4] obtained for magnetic surfaces.

[3] Relations (34) coincide with the resonance conditions obtained in [1].

$$v_{\parallel}^{0} = \sqrt{v^2 - J_{\perp} H^0}.$$

Hence we see that div $\tilde{\mathbf{H}}^* = 0$, and from Eq. (26) it follows that $Y = 0$.

Thus, small perturbations of the magnetic field do not disrupt the closed nature of the trajectory surfaces.

Let us now consider toroidal perturbation. Let us introduce a coordinate system r, φ, z. Here z will signify the arc length of the axial line of a torus with radius R; r and φ will denote the distance to the axial line and the polar angle, respectively (Fig. 4). The metric tensor in these curvilinear coordinates has the form

$$g^{ik} = \begin{vmatrix} 1 & 0 & 0 \\ 0 & \frac{1}{r^2} & 0 \\ 0 & 0 & \frac{1}{\left(1 + \frac{r}{R}\cos\varphi\right)^2} \end{vmatrix}.$$

For $R \to \infty$ the coordinate system so introduced passes over into a cylindrical system. It may be shown that in this case div $\tilde{\mathbf{H}}^* \neq 0$. In fact,

$$\operatorname{div} \mathbf{H}^* = \frac{\partial H_0^{*k}}{\partial x^k} + \Gamma_{ik0} H_0^{*i} \frac{\partial \tilde{H}^{*k}}{\partial x^k} + \Gamma_{ik0}^{k} \tilde{H}^{*i} + \tilde{\Gamma}_{ik}^{k} H_0^{*i} = \operatorname{div}^0 \mathbf{H}^{*0} + \operatorname{div} \tilde{\mathbf{H}}^* + \tilde{\Gamma}_{ik}^{k} H_0^{*i} = 0.$$

Hence

$$\operatorname{div} \tilde{\mathbf{H}}^* = -\tilde{\Gamma}_{ik}^{k} H_0^{*i}.$$

Substituting the values of the Christoffel symbols Γ_{ik}^{k}, corresponding to the metric tensor g^{ik}, we obtain

$$\operatorname{div} \tilde{\mathbf{H}}^* = \frac{1}{R} (H_r^{*0} \cos\varphi - H_{\varphi}^{*0} \sin\varphi). \tag{36}$$

Let us now check the equality of integral Y with zero [see (26)]:

$$Y = \frac{1 - \omega^*}{2\pi} \alpha \int_V \operatorname{div} \tilde{\mathbf{H}}^* \, dV.$$

Going over to variables u_0, θ, z, we find with the help of (25) and (36)

$$Y = \frac{1 - \omega^*}{2\pi M} \alpha^2 \int_0^{2\pi} d\theta \int_0^{C} du_0 \, \frac{H_r^* (u_0, \theta)\, r (u_0, \theta)}{-H_{\varphi}^* (u_0, \theta) + \alpha r (u_0, \theta) H_z^* (u_0, \theta)} \int_{z_0}^{z_0 + 2\pi R} \cos(\theta + \alpha z)\, dz.$$

Carrying out the integration over z and considering that $\alpha R = M$ is a whole number, we convince ourselves that $Y = 0$ and closed surfaces exist.[1] This constitutes a proof of the idealness of the toroidal stellarator as a trap in the drift approximation for transitory particles.[2]

Action of the Perturbation on the Blocked Particles

Making use of expression (14), we obtain the change in the coordinate u_0 after reflection of the particle:

$$\Delta \tilde{U} = \int_{S_1 \theta_1}^{\theta_2} \frac{\tilde{\mathbf{H}}^* \nabla u_0}{H^{*0}} \, dl + \int_{S_2 \theta_2}^{\theta_1} \frac{\tilde{\mathbf{H}}^* \nabla u_0}{H^{*0}} \, dl. \tag{37}$$

The integration is carried out along the unperturbed trajectory corresponding to the to-and-fro motion between the reflection points θ_1, θ_2; these trajectories lie on the surfaces S_1 and S_2 determined from (5) and distinguished by the sign of $v_{\parallel}$.

[1] In [4] the necessity of satisfying condition div $\tilde{\mathbf{H}}^* = 0$ for closed surfaces to exist is indicated, but, despite the fact that this condition is not fulfilled, closed surfaces here exist, since $Y = 0$.

[2] In [10] the proof of this fact is given on the approximation of the conservation of the longitudinal invariant.

As was seen in the first section, the blocked particles drifting along the z axis pass around the system. Let us denote the change in coordinate u_0 after a complete circuit by Y_1. Then the condition for the closed state of the surface of trajectories of the blocked particles will clearly have the form $Y_1 = 0$.

Let us consider the expression $ds \times dl$, where $ds = (\alpha r \mathbf{e}_\varphi + \mathbf{e}_z)dz$ is the element of length of the line $\varphi - \alpha z = \text{const}$; $r = \text{const}$. Using relation (25), it is not hard to confirm that

$$ds \times dl = \nabla u_0 \frac{dz\, dl}{H^{*0}}.$$

Thus

$$Y_1 = \frac{1}{\Delta z}\left(\int\limits_{S_1} \tilde{\mathbf{H}}^* dS + \int\limits_{S_2} \tilde{\mathbf{H}}^* dS\right), \tag{38}$$

where $dS = ds \times dl$ and the direction of the normal to surface S_2 is opposite to ∇u_0.

If $\tilde{\mathbf{H}}^*$ does not depend on $v_\parallel$, then

$$Y_1 = \frac{1}{\Delta z}\oint\limits_S \tilde{\mathbf{H}}^* dS = \frac{1}{\Delta z}\int\limits_V \operatorname{div} \tilde{\mathbf{H}}^* dV.$$

The integration is taken over the region enclosed between surfaces S_1 and S_2.

In the case of perturbation of the magnetic field, we obtain with the aid of formula (35)

$$Y_1 = \frac{1}{\Delta z}\int\limits_V \operatorname{div} \tilde{\mathbf{H}}\, dV + \frac{mc}{e\Delta z}\int\limits_{S_1'} \operatorname{rot} \frac{v_\parallel}{H}\mathbf{H}\, dS - \frac{mc}{e\Delta z}\int\limits_{S_1} \operatorname{rot} \frac{v_\parallel^0}{H^0}\mathbf{H}^0\, dS + \frac{mc}{e\Delta z}\int\limits_{S_2'} \operatorname{rot} \frac{v_\parallel}{H}\mathbf{H}\, dS$$

$$- \frac{mc}{e\Delta z}\int\limits_{S_2} \operatorname{rot} \frac{v_\parallel^0}{H^0}\mathbf{H}^0\, dS = \frac{2mc}{e\Delta z}\oint\limits_{C'} \frac{v_\parallel}{H}\mathbf{H}\, dr - \frac{2mc}{e\Delta z}\oint\limits_{C} \frac{v_\parallel^0}{H^0}\mathbf{H}^0\, dr.$$

The boundaries of the ranges of integration on the surfaces S_1, S_2 and S_1', S_2' are defined as the reflection points of the particles ($S_{1,2}$ and $S_{1,2}'$ do not quite coincide owing to the effect of the perturbation on the reflection points). On the contours C and C' embracing $S_{1,2}$ and $S_{1,2}'$, we have everywhere $v_\parallel = 0$, so that $Y_1 = 0$.

In the case of the toroidal state, the proof that the term containing div $\tilde{\mathbf{H}}^*$ is zero is analogous to that derived for the transitory particles.

Thus, in the drift approximation it is proven that for small perturbations of the magnetic field the toroidal stellarator remains an absolute trap for individual charged particles.

We must comment on the group of resonance blocked particles for which $\Delta z = 0$. Resonance particles are those having such values of $v_\perp/v$ that in formula (11) $2E(k) - K(k) = 0$. For these particles the deviation from the unperturbed surfaces in the linear approximation is unlimitedly large.[1]

Thus the essential condition which the perturbing vector field $\tilde{\mathbf{H}}^*$ must obey so as not to disrupt the closed surface of trajectories of the guiding center of the particles lies in the requirement that $Y = 0$. This condition is satisfied if div $\tilde{\mathbf{H}}^* = 0$. Perturbations for which div $\tilde{\mathbf{H}}^* \neq 0$ are to be suspected. An example of such perturbation is the "toroidalness," but as we saw the condition $Y = 0$ is satisfied for toroidal perturbation. Yet another example of perturbation with div $\tilde{\mathbf{H}}^* \neq 0$ is the perturbation of the magnetic field by plasma currents. In this case, as seen from Eq. (1),

$$\operatorname{div} \tilde{\mathbf{H}}^* = -\frac{4\pi m}{e} \operatorname{div} \frac{v_\parallel}{H^2}(\mathbf{jH})\,\tau \not\equiv 0.$$

We may mention a perturbation for which, apparently, $Y \neq 0$; this is the slow variation of the magnetic field with t time (the field was considered constant).

[1]The existence of resonance blocked particles was noted in [10].

It is also necessary to check perturbation of the motion by the electric field.

LITERATURE CITED

1. L. M. Kovrizhnykh, "Zh. tekhn. fiz.," 32, 517; 526 (1962).
2. L. V. Korablev, A. I. Morozov, and L. S. Solov'ev, Ibid, 31, 10, 1153 (1961).
3. I. M. Gel'fand et al., Ibid, 31, 1164 (1961).
4. G. V. Skornyakov, Ibid., 32, 261; 777; 1494 (1962).
5. L. M. Kovrizhnykh, Ibid., 33, 377 (1963).
6. I. M. Gel'fand et al., "Dokl. AN SSSR," 148, 1286 (1963); 143, 81 (1962).
7. A. I. Morozov and L. S. Solov'ev, "Dokl. AN SSSR," 128, 3 (1959).
8. N. N. Bogolyubov and Yu. A. Mitropol'skii, Asymptotic Methods in the Theory of Nonlinear Oscillations [in Russian], Gostekhteorizdat, Moscow (1955).
9. A. Ya. Khinchin, Proper Fractions [in Russian], Gostekhteorizdat, Moscow (1961).
10. A. I. Morozov and L. S. Solov'ev, "Zh. tekhn. fiz.," 30, 261 (1960).

EXPERIMENTS ON THE BUILDUP OF ELECTRONS IN THE SYNCHROTRON

(UDC 621.384.612)

Yu. M. Ado, E. G. Bessonov, and P. A. Cherenkov

Translated from Atomnaya Énergiya, Vol. 18, No. 2,
pp. 104-107, February, 1965
Original article submitted February 24, 1964

The lifetime of electrons in the synchrotron-accumulator was determined experimentally as a function of residual gas pressure, accelerating voltage, and particle energy. The experiments were carried out in the 280-MeV synchrotron of the Institute of Physics, Academy of Sciences of the USSR, operating in the accumulator condition. It was found that, for small buildup densities, the lifetime of the particles was mainly governed by single events of electron scattering by residual gas atoms.

The possibility of accumulating electrons in the synchrotron by the method proposed in [2] was experimentally verified in [1]. We here present experimental results bearing on the effects of various factors on the lifetime of the particles. The work was carried out in the 280-MeV synchrotron of the Institute of Physics, Academy of Sciences of the USSR [3]. A description of the experimental methods and apparatus may be found in [1].

The number of particles in orbit was measured from the intensity of the synchrotron radiation and recorded on a loop oscillograph. Figure 1 shows one of the oscillograms of the buildup process. The buildup takes place on the rising part of the oscillogram. The falling part characterizes the particle lifetime (microtron switched off). As particle lifetime we take the value of τ for which $\exp[-t/\tau]$ coincides with the envelope of the falling part of the oscillogram. The variation of τ with the following factors was determined: 1) Amplitude of the high-frequency accelerating voltage V; 2) vacuum p; 3) particle energy; 4) peak modulation depth of the high-frequency accelerating voltage $\Delta V/V$ [1, 2]. In the graphs presented, τ is measured either in periods of the variable component of the guiding magnetic field of the synchrotron or else in seconds.

When the synchrotron is operating in the accumulator condition, the particle energy varies according to

$$E = E_{=} + E_0 \cos 2\pi \frac{t}{T}. \quad (1)$$

The particles are periodically accelerated to a maximum energy $E_{max} = E_{=} + E_0$ and retarded to a minimum energy $E_{min} = E_{=} - E_0$. The frequency of the variable component of energy is $1/T = 50$ cps.

1. Variation of τ with V. The following quantities were kept constant: $E_{max} = 180$ MeV, $E_{min} = 7.5$ MeV, $\Delta V/V = 0.2$, $p \approx 3 \cdot 10^{-6}$ torr. The amplitude of the accelerating voltage was varied from 1.5 to 1.0 kV. The relationship found appears in Fig. 2.

2. Variation of τ with Vacuum. This was obtained for the following conditions: $E_{min} = 7.5$ MeV, $E_{max} = 180$ MeV, $V = 1.5$ kV, $\Delta V/V = 0.2$. The vacuum chamber was evacuated with two units operating from diametrically opposite sides. A change in vacuum was effected by shutting off one of these. It turned out that on varying the vacuum by a factor of two τ also changed by the same factor.

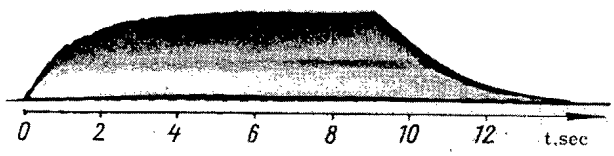

Fig. 1. Oscillogram of the particle buildup process.

3. Variation of τ with Particle Energy. In these experiments the following were the constant quantities: $E_{=} = 94$ MeV, $V = 1.5$ kV, $\Delta V/V = 0.2$, $p \approx 3 \cdot 10^{-6}$ torr. The particle energy was varied by changing the amplitude of the variable component E_0. Particle

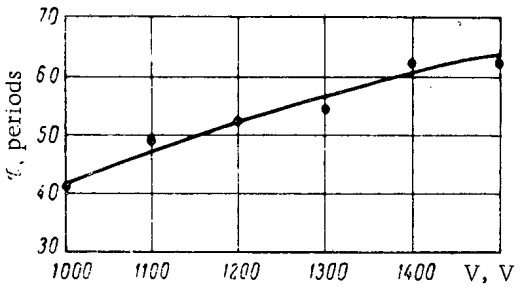

Fig. 2. Variation of τ with accelerating voltage V.

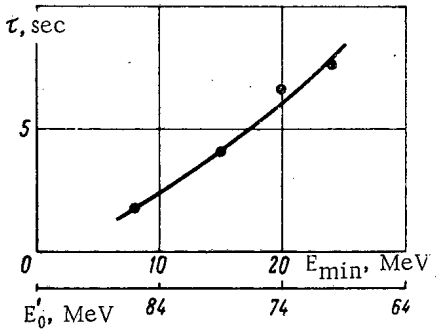

Fig. 4. Variation of τ with the amplitude of the variable component of particle energy E_0'. Continuous curve constructed from formula (2) relative to the experimental value of τ for $E_0' = 86$ MeV.

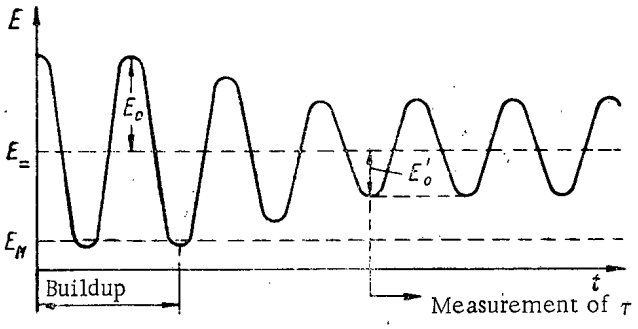

Fig. 3. Illustration of the reduction in amplitude of the variable component of particle energy E_0 to E_0' when measuring the variation of τ with E_0'.

buildup was effected for $E_{min} = 7.5$ MeV. After reaching the limiting number of particles, the value of E_0 was rapidly reduced to some value E_0' (Fig. 3). Injection of particles thereupon ceased. After the establishment of E_0', the particle lifetime was measured. The results of measuring τ for various E_0' (or for various E_{min}, which comes to the same thing) are shown in Fig. 4 by points. In absolute magnitude the calculated values of τ exceed the experimental. This is evidently connected with imprecision in measuring the vacuum.

4. Variation of τ with $\Delta V/V$. The following were kept constant: $E_{min} = 7.5$ MeV, $E_{max} = 180$ MeV, $p \approx 3 \cdot 10^{-6}$ torr, $V = 1.5$ kV. The value of $\Delta V/V$ was varied from 0 to 0.6. The relationship obtained is shown in Fig. 5.

After absolute calibration of the particle recording system, the number of accumulated electrons N was also determined from the intensity of the synchrotron radiation. It was found that $N \approx 5 \cdot 10^8$ for $\tau = 1.7$ sec, microtron pulse current ~8 mA, $\Delta V/V = 0.2$, and growth rate of guiding magnetic field at moment of injection $3 \cdot 10^5$ Oe/sec. As in [1], in place of an inflector system we used a 0.2 mm thick tantalum electron scatterer.

The particle loss mechanism in an accumulator with variable guiding field has a certain peculiarity. Particles whose oscillation amplitude has increased cannot be lost at once, but only when the energy is reduced as a result of an adiabatic increase in the oscillation amplitude.

To the single processes affecting τ belong Coulomb scattering and bremsstrahlung of particles at residual gas atoms. It may be shown that the partial lifetime determined by the Coulomb scattering of particles in the variable energy accumulator is expressed by the formula

$$\tau_p = \frac{\theta_g^2 \gamma_{min} \sqrt{2\gamma_0 \gamma_{min} + \gamma^2_{min}}}{4\pi r_e^2 z^2 N_0 c}, \quad (2)$$

where $r_e = e^2/mc^2$ is the classical radius of the electron, for air $z = 7.2$, the number of residual gas atoms per cm^3 $N_0 = 7.12 \cdot 10^{16}$ p torr, θ_g is the permissible scattering angle for minimum energy, and $\gamma = E/m_0c^2$. For an elliptical cross section of the vacuum chamber with semiaxes r_k and z_k, the value of θ_g is determined by the expression

$$\frac{1}{\theta_g^2} = \frac{1}{8\pi^2}\left(\frac{\lambda_r^2}{r_k^2} + \frac{\lambda_z^2}{z_k^2}\right), \quad (3)$$

where λ_r and λ_z are the wavelengths of the radial and axial free oscillations of the particles.

The partial lifetime for the bremsstrahlung process is practically independent of particle energy, being [4]

$$\tau_T \approx \frac{1.92 \cdot 10^{13}}{N_0}. \quad (4)$$

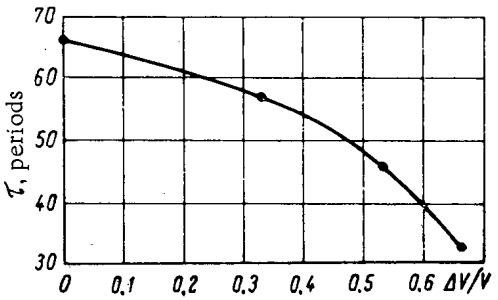

Fig. 5. Variation of τ with modulation depth of accelerating voltage $\Delta V/V$.

Also contributing to particle losses are multiple processes such as quantum fluctuations of the synchrotron radiation and multiple scattering by residual gas atoms. Since the dimensions of the separatrix are always considerably smaller than the radial dimensions of the vacuum chamber cross section, the particle loss will be determined by the setting up of phase oscillations, i.e., in practice by the action of quantum fluctuations [4]. Qualitatively the particle loss mechanism may be represented in the following fashion. Let us separate out an imaginary trajectory which, for particle energies $E \approx E_{min}$, "coincides" with the separatrix in the phase plane. For $E > E_{min}$ the selected trajectory is inside the stable region. Then all the particles which, under the action of the quantum fluctuations, have passed out beyong the limits of this phase trajectory will be lost on subsequent reduction of the energy to $\sim E_{min}$. Here the quantum fluctuations will play a more significant part than in constant magnetic field accumulators.

In order to find an expression for the probability of particle loss in our case, we must solve the Einstein-Fokker equation [5] for the particle distribution function U applicable to a variable guiding magnetic field:

$$\frac{\partial U}{\partial t} = \frac{d\bar{u}}{dt}\frac{\partial}{\partial u}\left[u\frac{\partial U}{\partial u} + \varkappa^2(t)\,uU\right], \tag{5}$$

where u is the square of the true oscillation amplitude, and

$$\frac{d\bar{u}}{dt} = \frac{55\pi}{12\sqrt{3}}\frac{ce\Lambda}{(1-n)R^4V\sin\varphi_s}\gamma^6, \quad \varkappa^2(t) = -\frac{\frac{d\ln D^2}{dt}}{\frac{d\bar{u}}{dt}}.$$

Here $D^2 = e^{-2\int\zeta dt}(\gamma V\sin\varphi_s)^{-0.5}$ describes the adiabatic variation in the amplitude of the phase oscillations and the radiation damping with decrement ζ.

The solution of Eq. (5) for zero conditions at infinity is

$$U_k(u, t) = \frac{1}{\varrho^2(t)}e^{-u/\rho^2(t)}, \tag{6}$$

where $\varrho^2(t)$ obeys the equation

$$\frac{d\varrho^2}{dt} = \frac{d\bar{u}}{dt} + \varrho^2\frac{d\ln D^2}{dt}. \tag{7}$$

For steady dimensions of the particle beam, $\varrho(t+T) = \varrho(t)$. Moreover the periodic solution of Eq. (7) has the form

$$\varrho^2(t) = \frac{D^2(t)\,D^2(t+T)}{D^2(t) - D^2(t+T)}\int_t^{t+T} D^{-2}(t')\frac{d\bar{u}}{dt'}dt'. \tag{8}$$

We can determine the particle loss in each period of the magnetic field after integrating distribution (6) over the limits u_{ex} to ∞. Then the partial lifetime of the particles due to the setting up of phase oscillations by quantum fluctuations of radiation will equal

$$\tau_q = Te^{u_{ex}/\rho^2} = Te^{\alpha V}, \tag{9}$$

since $\varrho^{-2} \sim V$, as $d\bar{u}/dt \sim V^{-1}$. The factor α depends only slightly on V. The ratio u_{ex}/ϱ^2 must be taken for $E \gg E_{min}$, when the distribution (6) is practically contained in the region of linear phase oscillations. The quantity ϱ^2 can be calculated from formula (8), and u_{ex} determined by the method of adiabatic invariants, starting from the u_{ex} for $E \approx E_{min}$.

Let us compare the partial lifetimes τ_p, τ_T and τ_q for a chosen condition of synchrotron accumulation (see relationships 1 to 4). The radius of the synchrotron orbit R = 81 cm, the free space of the vacuum chamber $r_k z_k \approx 4 \times 4$ cm, and n = 0.6. From formulas (2) and (4) it is easy to find that in this case $\tau_T/\tau_p = 23$, i.e., the bremsstrahlung

acts considerably more weakly on the particle lifetime than Coulomb scattering. The quantum fluctuations of the synchrotron radiation markedly affect the particle lifetime, as seen in Figs. 2 and 5 (τ depends on V and $\Delta V/V$). It is difficult to determine τ_p and τ_q from formulas (2) and (9), since the quantities p, V, E_0, and $E_=$ are not known accurately enough. It is however possible to estimate the contribution of the quantum fluctuations and Coulomb scattering to the particle loss on the basis of the experimental relation between τ and V. It follows from Fig. 2 that, for V = 1 kV, $\tau_1 = 0.8$ sec; for V = 1.5 kV, $\tau_2 = 1.2$ sec. Using the difference $(1/\tau_1)-(1/\tau_2)$, formula (9) shows us that $\alpha \approx 4.8$. Substituting this value of α into formula (9), we find $\tau_{q_1} = 2.4$ sec (V = 1 kV), and $\tau_{q_2} = 26$ sec (V = 1.5 kV). From the condition $1/\tau_{1,2} = (1/\tau_p) + (1/\tau_{q_{1,2}})$ we obtain $\tau_p \approx 1.2$ sec. Hence we may consider that, for V = 1.5 kV, τ is completely determined by the Coulomb scattering. This is also indicated by relationship 2 and the agreement between the τ/particle energy relations as found by experiment and calculated from formula (2) (see Fig. 4). Without discussing the relation between τ and $\Delta V/V$ in detail, we can only say that the introduction of amplitude modulation has a weak effect on τ.

In conclusion we note that, on improving the vacuum, the role of quantum fluctuations of the radiation will increase. The particle loss may however be substantially reduced if V is increased. For example, from fromula (9) with $\alpha = 4.8$, the value of τ_q proves to be of the order of a few hours with V = 2.5+ 3 kV.

LITERATURE CITED

1. Yu. M. Ado et al., Transactions of the International Conference on Accelerators [in Russian], Atomizdat, Moscow (1964), p. 355.
2. Yu. M. Ado, "Atomnaya énergiya," 12, 54 (1962).
3. A. Ya. Belyak et al., In the collection "Elementary Particle Accelerators" [in Russian], Supplement No. 4 to "Atomnaya énergiya" for 1957, Atomizdat, Moscow (1957), p. 57.
4. A. I. Alikhanyan, S. A. Kheifets, and S. K. Esin, "Uspekhi fiz. nauk," 81, 7 (1963).
5. A. A. Kolomenskii and A. N. Lebedev, Theory of Cyclical Accelerators [in Russian], Fizmatgiz, Moscow (1962).

ANGULAR AND ENERGY CHARACTERISTICS OF THE NEUTRONS EMITTED IN U^{235} FISSION

(UDC 539.173.84)

M. V. Blinov, N. M. Kazarinov, and A. N. Protopopov

Translated from Atomnaya Énergiya, Vol. 18, No. 2,
pp. 108-113, February, 1965
Original article submitted January 13, 1964; revision submitted March 3, 1964

The velocities of a fission fragment and of a neutron moving in the same direction were measured simultaneously by the time of flight method for the thermal neutron fission of U^{235}. As a result, the emission spectrum of the fission neutrons was obtained. The angular distributions and energy spectra were also measured for the neutrons ejected at different angles to the direction of motion of the fission fragments. These distributions were compared with calculations in which the emission spectrum obtained was used. The comparison showed that the data agree well after excluding small deviations in the angular distribution. It follows from analysis of the results that the emission spectrum agrees with the data calculated by the statistical theory of evaporation and also that not less than 90% of the neutrons from U^{235} fission are emitted in the process of isotropic evaporation of neutrons from the completely accelerated fission fragments.

The energy spectra and angular distribution of neutrons emitted in the thermal and fast neutron fission of U^{235} were measured in [1-3]. The measurements were carried out for angles of flight of 0, 45, and 90° of the neutrons relative to the direction of motion of the fission fragments. It can be seen from the experimental data that in accordance with the hypothesis concerning the emission of neutrons by the moving fission fragments, the neutron spectrum is strongly dependent on the angle of flight. In addition, some information was obtained in these experiments concerning the neutron spectrum in the center of mass system. The results of the experiments show the desirability for additional experiments on the mechanism of fission neutron emission.

The velocities of a fission fragment and of a neutron emitted by this fission fragment in the direction of motion were measured. As a result of the measurements, the neutron emission spectrum was obtained (the spectrum in the center of mass system). Similar measurements were also made of the angular and energy distributions of the neutrons, independently of the type of fission fragment as well as individually for light and heavy fission fragments. The emission spectrum of the neutrons obtained experimentally was used in the spectral and angular distribution calculations.

Measurement Procedure

Figure 1 shows the arrangement of the experiment by means of which the neutron and fission fragment velocities were measured simultaneously by the time of flight method. The uranium target, with a thickness of 100 $\mu g/cm^2$ and containing 97.9% of U^{235} on a thin organic film, was placed in a thin-walled aluminum tube (length 75 cm, diameter 10 cm) which was pumped out to a pressure of $\sim 10^{-3}$ mm Hg. The fissile layer was located at a distance of 1.5 cm from the rim of the tube, where a fission detector was installed—a scintillation film with a diameter of 20 mm in a plastic light guide and connected to a transient photomultiplier. "Zero time" was defined with respect to the instant of impact of a fission fragment on this scintillation film. An additional fragment traversed the entire length of the tube and was recorded by another film detector with a diameter of 80 mm. A correction was introduced for the spread of the time of flight of the fission fragments from the layer to the "zero time" detector. The neutron counter was located at an angle of 15° to the tube axis at a distance of 65 cm from the uranium target. In order to record the neutrons, a stilbene crystal was used with a diameter of 80 mm and a thickness of 40 mm and also an FÉU-33 transient photomultiplier.

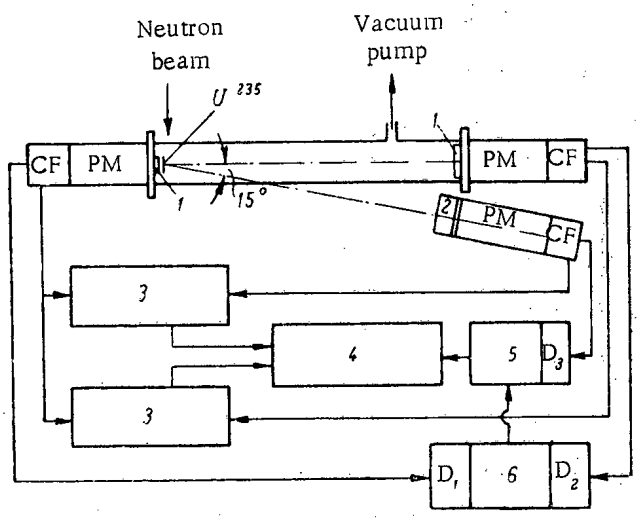

Fig. 1. Diagram of the arrangement for simultaneous measurement of the velocities of a fission fragment and of a neutron, and block diagram of the apparatus: 1) scintillation films; 2) stilbene crystal; CP) cathode followers; 3) time converters; D_1, D_2, D_3) amplitude discriminators; 4) two-dimensional analyzer; 5) transmission block; 6) coincidence circuit.

Two "time into amplitude" converters were used in the equipment: one for measuring the velocity of the fission fragment and the other for measuring the neutron velocity. The pulses from the converters were fed to a two-dimensional analyzer. The characteristics of the time of flight spectrometer used in this project are described in the literature [4]. In the present measurements, the effect of the photomultiplier signal amplitude on the time scale calibration was additionally taken into account which increased the accuracy in determining the neutron energy. The recording efficiency for neutrons with different energies was determined experimentally by means of calibration measurements of the well-known fission neutron spectrum of U^{235}, averaged in the experiment with respect to all fission modes and all angles of flight of the neutrons. The experimental data agreed well with the calculations of the efficiency. The resolving time for recording fission fragment coincidences, measured by means of a chamber in which fission fragment detectors converge up to 2 cm, was found to be equal to 2.5 nsec. The distribution half-width of the prompt γ-radiation, emitted as a result of fission, corresponded to a resolving time for the neutron channel of 4-5 nsec.

In the second part of the project, the angular distributions and energy spectra of the neutrons emitted at different angles to the direction of motion of the fission fragments were measured. For this, the device described in [3] was used; in it the U^{235} fission fragments were recorded in a gas scintillation counter. In order to fix the direction of motion of the fragments, a collimator was located at the uranium layer with a thickness of 2 mg/cm^2, in which the mean angle of deviation from the normal of the fission fragments was 10°. By installing thin layers ($\sim$ 200 μg/cm^2) of uranium in the gas counter, it became possible to separate the fission fragments into two groups—a light and a heavy group, and the neutron spectra are associated with these groups.

The neutron scintillation counter was located at a distance of 65 cm from the fissile layer at various angles to the direction of flight of the fission fragments (0, 15, 30, 45, 60, 75, and 90°). In order to record the neutrons, a thin crystal of stilbene was used (with a diameter of 30 mm and thickness 15 mm) as well as the crystal with a diameter of 80 mm and thickness 40 mm.

Measurements and Results

In all the experiments for measuring the neutron characteristics by the time of flight method, it was assumed that over the time interval 10-100 nsec there are no delayed γ-rays from fission. If the contrary were the case, this would change the experimental results of measurement of the neutron spectrum as well as their number. The relationship between the number and energy of the delayed γ-quanta and the delay time for 50 nsec to 10^{-5} sec was measured in [5] with equipment having a resolving time of $2 \cdot 10^{-8}$ sec. It was found that over this interval, 5.7% of the

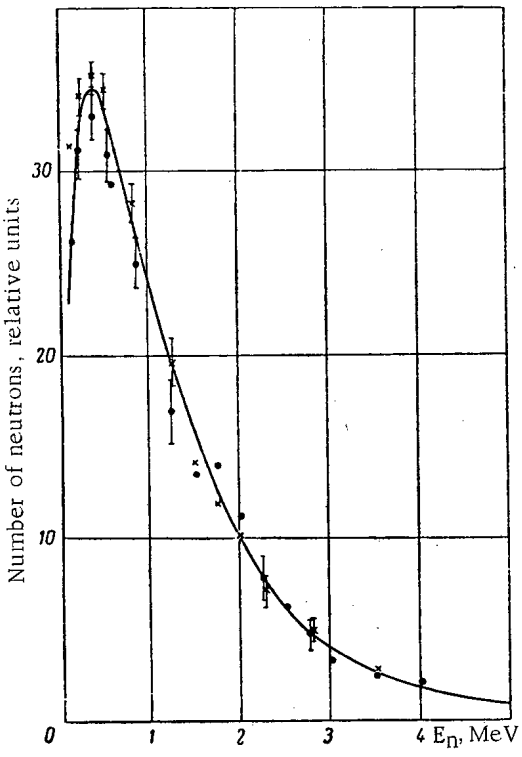

Fig. 2. Neutrum spectrum in the center of mass system measured at an angle of 15° to the direction of motion of light (●) and heavy (×) fission fragments in the laboratory system of coordinates. The continuous line indicates the spectrum used in calculating the neutron spectra and intensities at various angles.

total number of "prompt" quanta is emitted as delayed γ-quanta. In view of the poor resolution and the large range being measured, the interval of time prior to 100 nsec has been inadequately studied.

We measured the number of delayed γ-quanta over the interval 25-80 nsec. For this the neutron counter was located at a distance of 350 cm from the uranium target. Neutrons, on this base line, were almost eliminated from the range of the times of flight being determined. No delayed γ-quanta were recorded within the limits of experimental accuracy. This confirms that even in the case of equilibrium distribution of these γ-quanta, with respect to time their number does not exceed 2% of the total number of "prompt" γ-quanta. Thus, within the stated range of times of flight the delayed γ-quanta, obviously cannot have any significant effect on the determination of the fission neutron spectra.

In the course of the project, measurements were made in which the corrections for scattering of neutrons from the backing and from the collimator in the gas counter were determined, and also for scattering from the shielding. The corrections were introduced into the data for the number as well as for the spectrum of the neutrons. In the case of measurements of the two velocities, about 15,000 pulses from fission neutrons were collected. For the measurements made at an angle of 0°, $50 \cdot 10^3$ neutrons were recorded and two to three times less for measurements at the other angles. The random coincidence background was the same as stated in [3].

Figure 2 shows the neutron spectrum in the center of mass system which was determined from the simultaneous measurements of the velocity of a neutron and of a fission fragment. The neutron velocity in the center of mass system was calculated by the formula

$$v_c^2 = v^2 + v_0^2 - 2vv_0 \cos\varphi.$$

Here v, v_0 and φ are the neutron velocity, the fragment velocity and the angle between the directions of motion of the fragment and neutron in the laboratory system of coordinates respectively. The angle φ was chosen to be the least possible (15°) in order that the neutron contribution from any additional fission fragment would be small. The The average energy of the emission spectrum was $\bar{\varepsilon} = 1.27 \pm 0.03$ MeV and it can be represented numerically by the superposition of three distributions

$$F(\varepsilon) \sim \frac{\alpha_i}{T_i^{3/2}} \sqrt{\varepsilon}\, l^{-\varepsilon/T_i},$$

where $T_1 = 1$ MeV, $\alpha_1 = 0.696$; $T_2 = 0.5$ MeV, $\alpha_2 = 0.310$; $T_3 = 0.1$ MeV, $\alpha_3 = -0.06$.

It should be noted that the spectra of the neutrons emitted by light and heavy fission fragments agree within the limits of experimental accuracy ($\bar{\varepsilon}_l - \bar{\varepsilon}_h < 0.02$ MeV).

The energy spectra of the fission neutrons are shown in Fig. 3 for various angles. For simplicity of comparison of the spectral shifts the maximum probability is reduced to a uniform value for all values of the angles. The relationship between the relative intensity of the fission neutrons and their average energies, and the angle φ for two cases—the registration of all fission fragments and individually for the light fragments[1]—is shown in Fig. 4. It can be

[1]The data refer to the neutron energy region of 0-7 MeV. For energies from 0.3 MeV and above the experimental data are used, and for energies below 0.3 MeV these data are used extrapolated to zero. The error of this extrapolation is small. The distributions for angles 0, 45 and 90° are in good agreement with the results of our measurements carried out previously [3].

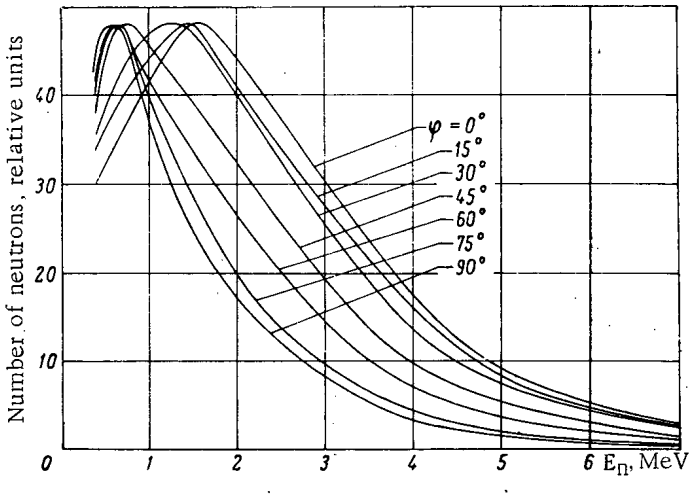

Fig. 3. Energy spectra of neutrons emitted at varous angles φ to the direction of motion of the fission fragments.

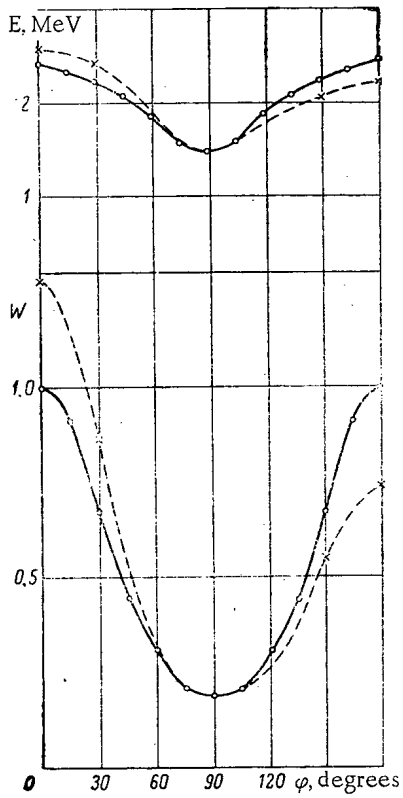

Fig. 4. Relationship between relative fission neutron intensity W and their average energies $\bar{E}$, and the angle of flight φ. ——— all fragments recorded; – – – – only light fragments recorded.

seen that with increase of angle from 0 to 90° and with simultaneous reduction of intensity, a systematic "softening" of the spectra occurs. Qualitatively this is in accordance with the hypothesis of the ejection of neutrons from moving fission fragments.

Discussion of Results

Using the neutron emission spectrum obtained for φ = 15°, the spectra can be calculated in the laboratory system for the various angles and they can be compared with the experimental energy distributions. This calculation was performed on the assumption that the neutron distribution in the center of mass system is isotropic. Instead of the distribution of the fission fragments with respect to velocity, the mean velocities of the light and heavy groups were used. The energy distribution of the fission neutrons emitted at an angle φ to the direction of flight of the light fragments is given by the expression (see for example [6]):

$$N(E)\,dE = \frac{\bar{\nu}_{\text{л}}}{\bar{\nu}_{\text{т}}} \int_{\varphi_1}^{\varphi_2} \sqrt{\frac{E}{\varepsilon}}\, F'(\varepsilon)\, P(\varphi)\, d\varphi\, dE + \int_{180°-\varphi_1}^{180°-\varphi_2} \sqrt{\frac{E}{\varepsilon}}\, F''(\varepsilon)\, P(\varphi)\, d\varphi\, dE.$$

Here, E and ε are the neutron energies in the laboratory and center of mass systems respectively; F'(ε) and F"(ε) are the emission spectra of the neutrons emitted by light and heavy fragments respectively; P(φ) is the distribution with respect to angle of the fission fragments traversing the collimator. The second term of the expression corresponds to the emission of neutrons in the rear hemisphere from an additional fragment. The ratio $\bar{\nu}_l/\bar{\nu}_h$, equal to 1.10, was used for the calculation and satisfied the experimental data best.

Figure 5 shows the ratios of the experimental and calculated values for the average energies and intensities of the nuetrons versus the angle φ, and Fig. 6 shows the ratios of the probabilities for individual parts of the spectra and for various values of φ. The errors in Figs. 5 and 6 include the statistical error as well as the deviation between

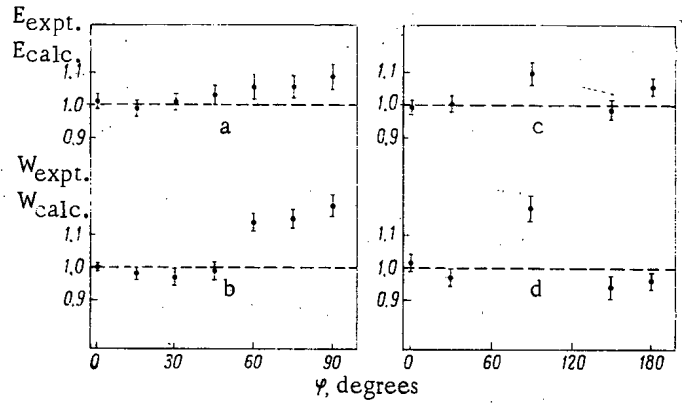

Fig. 5. Experimental and calculated values $\overline{E}_{expt}/E_{calc}$ (a) and W_{expt}/W_{calc} (b) as a function of neutron angle of flight (c and d are the corresponding values for recording only the light fission fragment).

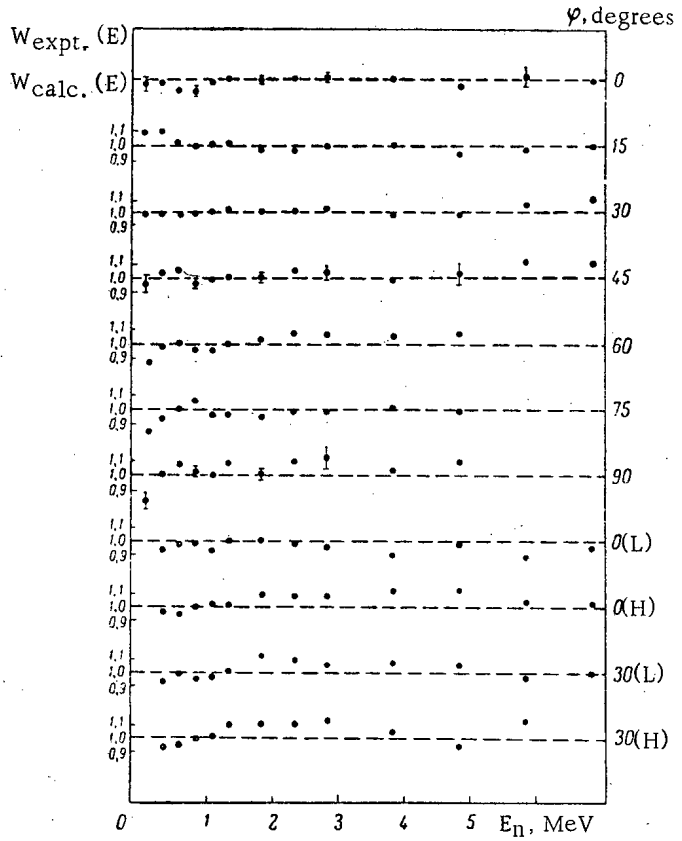

Fig. 6. Ratio of experimental and calculated probabilities W_{expt}/W_{calc} for various parts of the energy spectra and angles of flight φ. The data are normalized for maximum probabilities of the spectra.

series. It can be seen that not only the average energies of the experimental spectra agree satisfactorily with the calculation, but also their shape as a result of changing the spectral intensity by a factor of more than 10. It is possible that there is a small increase of "hardness" of the spectrum relative to calculation at angles close to 90°, although it is found to be within the limits of experimental error. A larger relative intensity can be noticed in the angles of distribution for angles of 60 and 90° and, thus, a less anisotropic distribution in the laboratory system compared with calculation.

An estimate of the effect of velocity distribution of the fission fragments and the dependence of $\overline{\nu}(A)$ on the results of the calculation with respect to angular distribution showed that the error associated with this does not exceed a few percent and thus cannot exert a significant effect.

An attempt was made to completely reconcile the experimental and calculated data on the assumption that the neutrons are emitted by fission fragments having partial velocities. As a result of this the angular distributions are successfully reconciled, but the calculated spectra in this case differ considerably from the experimental spectra.

If it be assumed, as a consequence of [7], that emission of neutrons is possible at the instant of separation of the fission fragments, and if the deviation of W_{expt}/W_{calc} at an angle of 90° be associated with this assumption, then the number of such neutrons in the case of isotropic emission in the laboratory system should not exceed 5-10% of the total number of neutrons.

Yet another reason can be proposed for the appearance of excess neutrons at an angle of 90°. If part of the neutrons is "evaporated" from a fission fragment prior to the establishment of thermal equilibrium by the entire volume of the nucleus, then it is possible that these neutrons are "evaporated" mainly from a local region where the nucleons of the offshoot are situated (the part of the neck joining the fission fragments prior to separation). Ejection of neutrons from this region at small angles to the direction of motion of the fission fragments is unlikely (because of shielding by the mass of the nucleus); thus, a "shadow effect" is created. This same effect, obviously, should be observed also in the case of neutron emission from the neck region prior to or at the instant of separation.

The spectrum, in the center of mass system, which agrees with our experimental data has an average energy $\overline{\varepsilon}$ equal to 1.27 MeV, which is somewhat greater than the value obtained in [8] on the basis of scaling the integral spectra ($\overline{\varepsilon}$ = 1.21 MeV). Here, it is necessary to consider that the deviations at an angle of 60-90° are related to an addition in the low-energy part of the integral spectrum and thus soften it. In order to compute whether the spectrum in the center of mass system has a cascade-evaporative nature it is necessary to take into account in the first instance the energy spread of the excited fission fragments with respect to mass and charge, the relationship between the level density and the characteristics of the fragment and its excitation energy. Over the whole volume this is quite a difficult problem and it has not been considered in this paper. Simplified calculations have been carried out for computing the emission spectrum, in which the change of temperature due to the different excitation energies of the fission fragments and the subsequent emission of neutrons were taken into account. The first calculations, carried out in a similar paper [9], gave as a result a spectrum close to the experimental spectrum but somewhat displaced to the side of low energies ($\overline{\varepsilon}$ = 1.22 MeV). In the second stage of the calculations, for cases of large fragment excitation, when emission of more than one neutron is possible we took account of the relationship obtained in [10] for cascade evaporation of the neutrons. It was found that this calculated spectrum for a = 12 MeV^{-1} agrees well with the experimental spectrum.

Thus, it can be said that despite the small deviations from the calculation, which may be explained by a variety of reasons, the overwhelming portion of the neutrons from the thermal fission of U^{235} is emitted in the process of normal cascade evaporation of neutrons from the completely accelerated nuclei-fission fragments.

It is noteworthy that the emission spectra of the neutrons from light and heavy fission fragments are identical. If the average value of the neutron binding energy is used for the light and heavy fragments, the quantity $\overline{\nu}_l/\overline{\nu}_h$ set equal to 1.1, and the relationship $T \sim (E_b/a)^{1/2}$, then it is found that the average energy of the emission spectrum for a light fission fragment should be considerably greater than for a heavy fission fragment (by $\sim 30\%$). However, the action of shell effects leads to approximate equivalence of the level plane constants, a, for the region of light and heavy fragment masses (in view of the inadequacy of the information in [11, 12] it is difficult to obtain more precise data). The cited effects also affect the values of the average neutron binding energies [13]. By including corrections it can be expected, as the estimates show, that the ratio of the average spectral energies will be equal to 1.0 to 1.1, which agrees with the experimental data.

Calculations of the energy spectra and angular distributions of neutrons for the fission of U^{235} by neutrons with an energy of 14 MeV were carried out by E. I. Sirotinin [6] and for the spontaneous fission of Cf^{252} by Bowman et al. [14]. In the first case of energy production, neutron evaporation from the compound nucleus with subsequent fission is possible. Naturally, these neutrons which are emitted prior to fission make it more difficult to study the mechanism of emission of neutrons associated with the fission process. E. I. Sirotinin came to the conclusion that in this case the division of the neutrons into two components is justified [1] and that the second component is associated with neutron evaporation from the excited fission fragments. In [14], dealing with the investigation of the spontaneous

fission of Cf^{252} it is reported that about 80-90% of the neutrons from the fission of californium are emitted in the process of isotropic neutron emission from the accelerated fission fragments. The authors suggest that 10-20% of the neutrons are ejected at the instant of separation of the fission fragments and that this leads in the experiment to significant ($\sim 30\%$) deviation from calculation at an angle of 90°. It was also observed in the experiment that there was an excess of the measured over the calculated intensity at an angle of 10°.

After completion of the present project two reports were published [15, 16] also devoted to the study of the angular and the energy distribution of the neutrons originating as a result of thermal neutron fission of U^{235}. Measurements are presented in these papers which are similar to those carried out in the second part of this project.

The distributions shown in [16] are close to those obtained by us for the majority of values of the angle φ. Our data were not compared in detail with the experimental data of [15], since they are presented in a form which makes comparison difficult. It should be noted that the two experimental energy spectra of [15] differ significantly from our data. The authors of [15, 16], during the process of analyzing the data, selected an emission spectrum which should satisfy best of all the observed distributions in the laboratory system. As a result, it was found in [16] that the emission spectra of neutrons emitted by light and heavy fission fragments match (the conclusion is drawn in our paper and in [14]). Another result was obtained by the authors of [15]. They stress the considerable difference between these emission spectra (the average energies of the spectra differ by approximately 30%). The difference between certain results of [15] and the three papers mentioned, obviously, is more likely due to a discrepancy in the experimental data than to any incongruity in the calculations. The conclusions cited in [15 and 16] concerning the emission mechanism agree with ours.

The authors express their thanks to Prof. D. M. Kaminker for assitance in mounting the project in the reactor of the Physicotechnical Institute, Academy of Sciences of the USSR, and also to K. A. Konoplev and D. A. Yashin, and to the entire reactor control team for attention to its operation. The authors also thank S. M. S Solov'yev for preparing the uranium targets and V. A. Bogutskii, V. A. Kanin, É. M. Karatayev and V. V. Pikunov for assistance with the measurements and processing of the experimental data.

LITERATURE CITED

1. Yu. A. Vasil'yev et al., Atomnaya Énergiya, 9, 449 (1960).
2. V. N. Nefedov, ZhÉTF, 38, 1657 (1960).
3. M. V. Blinov, N. M. Kazarinov, and A. N. Protopopov, ZhÉTF, 42, 1017 (1962).
4. M. V. Blinov and N. M. Kazarinov, Pribory i tekhnika éksperimenta, No. 1, 40 (1964).
5. F. Maienshtein et al., "Proceedings of the Second International Conference on the Peaceful Uses of Atomic Energy. Selected Reports of Foreign Scientists [in Russian], 2, Moscow, Atomizdat (1959) p. 297.
6. E. I. Sirotinin, Atomnaya Énergiya, 13, 530 (1962).
7. R. Fuller, Phys. Rev., 126, 684 (1962).
8. J. Terrell, Phys. Rev., 127, 880 (1962).
9. J. Terrell, Phys. Rev., 113, 527 (1959).
10. K. LeCouteur and D. Lang, Nucl. Phys., 13, 32 (1959).
11. D. Lang, Nucl. Phys., 26, 434 (1961).
12. D. Thomson, Phys. Rev., 129, 1649 (1963).
13. A. Cameron, Canad. J. Phys., 36, 1040 (1958).
14. H. Bowman et al., Phys. Rev., 126, 2120 (1962).
15. S. Kapoor, R. Ramanna, and P. Rama Rao, Phys. Rev., 131, 283 (1963).
16. K. Scarsvag and K. Bergheim, Nucl. Phys., 45, 72 (1963).

CALCULATION OF AVERAGE RADIATIVE CAPTURE CROSS SECTIONS FOR NEUTRONS WITH ENERGIES OF 10^3-10^5 eV

(UDC 539.17.02)

A. G. Dovbenko, S. M. Zakharova, V. E. Kolesov, and A. V. Malyshev

Translated from Atomnaya Énergiya, Vol. 18, No. 2, pp. 114-118, February, 1965
Original article submitted January 31, 1964

The average radiative-capture neutron cross sections of 30 isotopes of Rb, Zr, Mo, Sn, and Sm are calculated on the basis of the statistical theory of nuclear reactions. The calculation uses penetrability values for the nuclear surface which were obtained from an optical model and level densities corresponding to a Fermi gas model. The results of the calculations are compared with the available experimental data for an energy of 25 keV. It is shown that satisfactory quantitative estimates can be obtained for the average capture cross-sections of isotopes for which experimental data concerning average neutron-resonance parameters are not available.

It was shown in [1-4] that the calculation of the energy dependence of average radiative-capture cross sections, within the limits of statistical theory, with penetrability values of the nuclear surface which correspond to an optical model, is in satisfactory agreement with experimental results. It is also known that the absolute value of the cross section is strongly dependent on the value of the average distance between the levels of the compound nucleus and on the average radiation width. These parameters are usually taken on the basis of experimental data in the low-energy range. If no such data are available, the average parameters are obtained by comparing the results of the calculation of the average radiative-capture cross sections with experimental data. The solution of many questions in the field of reactor construction requires a knowledge of how the average radiative-capture cross sections vary as a function of energy. The experimental data available today were obtained chiefly for isotopes which become activated when a neutron is captured. For most isotopes which are not thus activated and for unstable isotopes there are practically no experimental data. It is therefore of interest to calculate the radiative-capture cross sections on the basis of the average-parameter system mentioned in [5, 6]. For a quantitative comparison of the resulting cross sections, we may use the existing experimental data for an energy of 25-30 keV [7-18]. In addition, by adding the calculated cross sections for the individual isotopes, we can make a comparison with the experimental cross sections for a natural mixture of isotopes, which in many cases are known over a wide range of energies.

Calculations were made for the following isotopes: Rb^{85}; $Zr^{90-92,94,96}$; $Mo^{92,94-98,100}$; $Sn^{112,114-120,122,124}$; and $Sm^{144,147-150,152,154}$.

We used the formula of statistical theory which is generally used for calculating average radiative-capture cross sections [1, 2, 15].

$$\overline{\sigma_{n\gamma}} = \frac{\pi\lambda^2}{2(2I+1)} \sum_l T_l(E) \sum_J \frac{\epsilon^J_{jl}(2J+1)S}{1+\frac{1}{2\pi}\cdot\frac{D(U+E,J)}{\Gamma_\gamma(U+E)}\sum_{l'}\sum_k \epsilon^J_{j_k l'} T_{l'}(E-E_k)}. \quad (1)$$

Here E is the kinetic energy of the impinging neutron; l, l' are the orbital moments of the impinging neutron and the scattered neutron, respectively; J is the total moment of the compound nucleus; $j = I \pm \frac{1}{2}$, $j_k = I_k \pm \frac{1}{2}$ are the spins of the inlet and outlet channels, respectively; I is the spin of the ground state of the target nucleus; I_k

TABLE 1. Parameters Used in the Calculation

Isotope	I^π	a, MeV^{-1}	$\bar{D}$, eV	U, MeV	Γ_γ, eV
Rb^{85} *	$5/2^-$	8.50	750**	8.58	0.410
Zr^{90} *	0^+	9.0	$1.7\cdot10^4$	6.19	0.270
Zr^{91}	$5/2^+$	10.2	$1\cdot10^3$	6.49	0.245
Zr^{92} *	0^+	11.0	$3.7\cdot10^3$	5.79	0.270
Zr^{94} *	0^+	11.6	$6.3\cdot10^3$	5.52	0.220
Zr^{96} *	0^+	14.0	$2.6\cdot10^3$	4.65	0.160
Mo^{92}	0^+	10.2	$2.4\cdot10^3$	6.71	0.270
Mo^{94}	0^+	12.6	$1\cdot10^3$	6.08	0.220
Mo^{95}	$5/2^+$	12.6	220	6.44	0.230
Mo^{96}	0^+	12.9	$1\cdot10^3$	5.49	0.160
Mo^{97}	$5/2^+$	13.2	220**	6.15	0.200
Mo^{98}	0^+	17.6	270	4.99	0.102
Mo^{100}	0^+	18.0	430	4.61	0.090
Sn^{112}	0^+	12.1	850	6.68	0.061
Sn^{114}	0^+	12.2	$1.4\cdot10^3$	6.24	0.063
Sn^{115}	$1/2^+$	16.5	50**	6.85	0.096
Sn^{116} *	0^+	15.5	600	5.39	0.065
Sn^{117}	$1/2^+$	15.5	120**	6.60	0.110
Sn^{118}	0^+	15.0	$1\cdot10^3$	5.00	0.093
Sn^{119}*	$1/2^+$	15.5	180**	6.30	0.106
Sn^{120} *	0^+	15.3	$1.7\cdot10^3$	4.70	0.108
Sn^{122}	0^+	16.2	$1.7\cdot10^3$	4.40	0.106
Sn^{124}	0^+	15.2	$2\cdot10^3$	4.54	0.100
Sm^{144}*	0^+	17.0	325	5.40	0.065
Sm^{147}	$7/2^-$	20.0	14**	5.77	0.059
Sm^{148}*	0^+	22.0	175	4.40	0.063
Sm^{149}	$7/2^-$	23.6	6**	5.27	0.065
Sm^{150}*	0^+	25.0	115	3.98	0.066
Sm^{152}*	0^+	24.0	87	4.25	0.068
Sm^{154}*	0^+	21.0	740	3.80	0.072

*Experimental data on $\bar{D}$ are unreliable or unavailable for these isotopes.

**For these nuclei, D(U, J) was calculated on the basis of $\bar{D}$, with $g_J \approx 1/2$.

is the spin of the k-th excited level of the target nucleus; ϵ^J_{jl} and $\epsilon^J_{j_k l'}$, are factors which take account of the number of open channels and are equal, respectively, to the number of values of j and j_k satisfying the conditions

$$\begin{aligned} |J-l| \leqslant j \leqslant J+l, \\ |J-l'| \leqslant j_k \leqslant J+l, \end{aligned} \tag{2}$$

E_k is the energy of the k-th level of the target nucleus on which the scattering takes place; S is a factor taking account of the distribution of the reduced neutron widths, taken from [2]; $T_l(E)$ and $T_{l'}(E-E_k)$ are the penetrability values of the nuclear surface, calculated for a spherical complex potential

$$V(r) = -V_0 \frac{1+i\xi}{1+\exp\left(\frac{r-R}{d}\right)} \tag{3}$$

where the depth of the potential well is V_0 = 45 MeV, the thickness of the diffusion layer is d = 0.5f, ξ = 0.1, and the radius of the nucleus is $R = r_0 A^{1/3}$, with $r_0 = 1.25f$. The summation with respect to l' includes only the terms which satisfy the law of conservation of parity. In the actual calculation the penetrabilities were chosen on the basis of the condition that the calculated total cross sections and radiative-capture cross sections of neighboring monoisotopic elements must be in optimum agreement with experimental results.

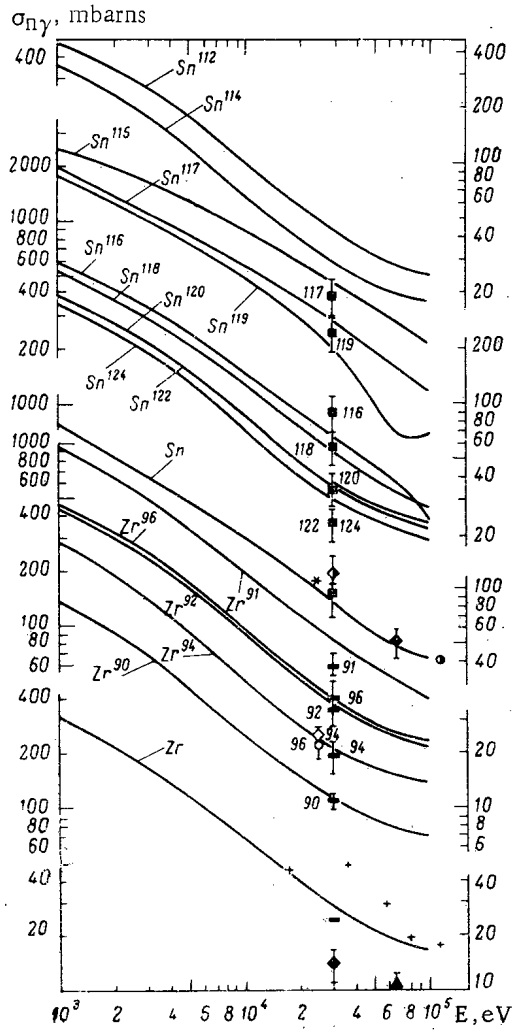

Fig. 1. Variation of the radiative-capture cross sections of Zr and Sn isotopes as a function of the energy of the impinging neutrons. Sources of data: ✳) [11]; ○) [13]; ○, ◆, ◇) [15]; ◇) [16]; ▬) [17]; +) [18];) [21].

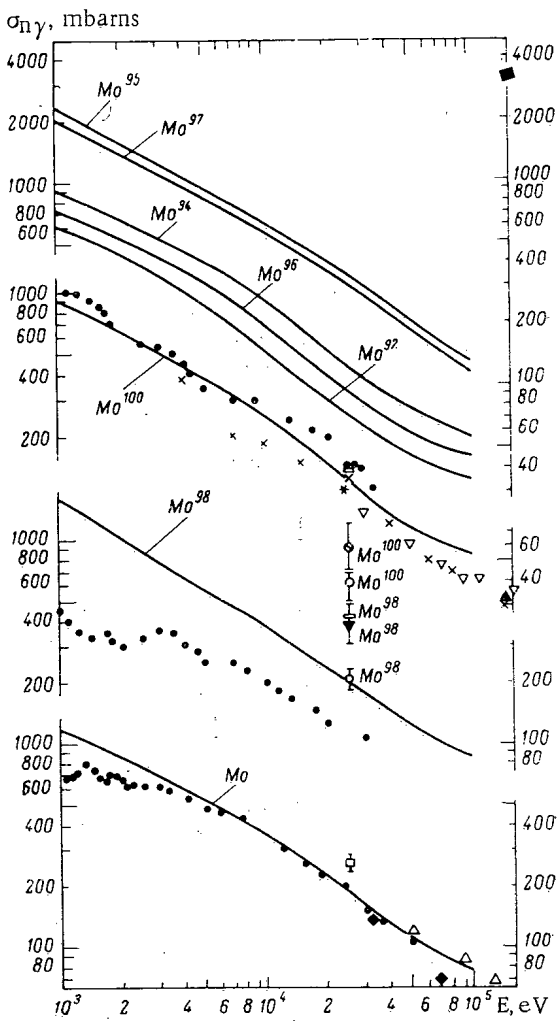

Fig. 2. Variation of the radiative-capture cross sections of Mo isotopes as a function of the energy of the impinging neutrons. Sources of data: ◉) [7]; ×) [9]; ▭) [10]; ○) [12]; ▽) [14]; △, □, ▽, ▲) [15];

The ratio of the average difference D(U + E, J) between levels having a total moment J to the average radiation width $\Gamma_\gamma(U + E)$ at an excitation energy of U + E is of the form

$$\frac{D(U+E,J)}{\Gamma_\gamma(U+E)} = \frac{D(U,J)}{\Gamma_\gamma(U)} \cdot \frac{D(U+E,J)}{D(U,J)} \cdot \frac{\Gamma_\gamma(U)}{\Gamma_\gamma(U+E)} = \frac{D(U,J)}{\Gamma_\gamma(U)} f(E). \tag{4}$$

In calculating the factor $f(E)$, we made the following simplifying assumptions:

$$\varrho(U,J) \equiv \frac{1}{D(U,J)} = \text{const}\,(2J+1)\exp\left[2(aU)^{1/2}\right],$$

$$\Gamma_\gamma(U) = \text{const}\, D(U,J) \int_0^U \varepsilon_\lambda^3\, \varrho(U-\varepsilon_\gamma, J)\, d\varepsilon_\gamma, \tag{5}$$

where ε_γ is the energy of the emitted γ-quantum. We thus have

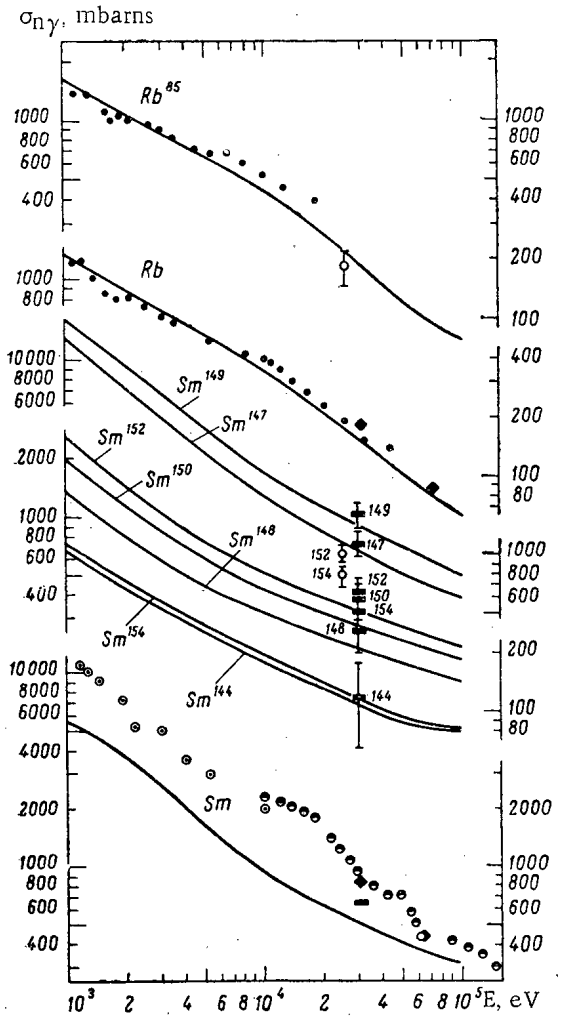

Fig. 3. Variation of the radiative-capture cross sections of Rb and Sm isotopes as a function of the energy of the impinging neutrons. Sources of data: ●)[8]; ⊙, ○) [15].

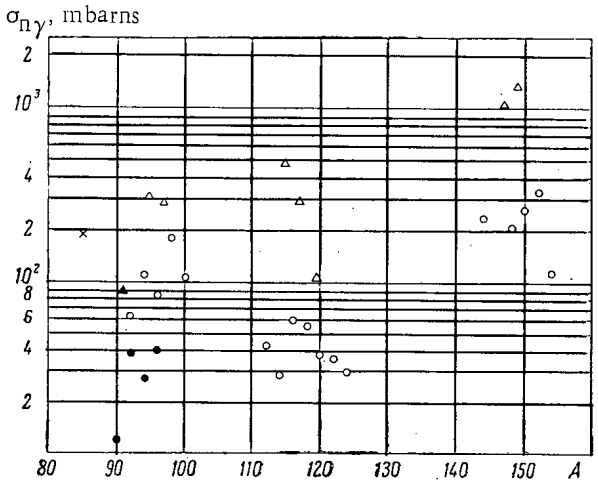

Fig. 4. Variation of the radiative-capture cross sections of isotopes of Rb, Zr, Mo, Sn, and Sm as a function of the mass number A at an energy of ~30 keV. ⊙, ▲) Radiative-capture cross section of Zr isotopes; ▲, △) even-odd nuclei; ●, ○) even-even nuclei; ×) odd-even nuclei.

$$j(E) = \frac{\int_0^U \varepsilon_\gamma^3 \varrho(U-\varepsilon_\gamma, J)\, d\varepsilon_\gamma}{\int_0^{U+E} \varepsilon_\gamma^3 \varrho(U+E-\varepsilon_\gamma, J)\, d\varepsilon_\gamma}. \qquad (6)$$

In the energy range under investigation ($E \ll U$) $f(E) \approx 1$, and consequently the assumptions made above in (5) have little effect on the result of the calculation.

In formulas (1), (4), (5), (6) we have

$$U = B_n - \begin{cases} \delta_p + \delta_n & \text{for even-even compound nuclei;} \\ \delta_p & \text{for even-odd compound nuclei;} \\ \delta_n & \text{for odd-even compound nuclei;} \\ 0 & \text{for odd-odd compound nuclei,} \end{cases}$$

where B_n is the binding energy of the neutron in the nucleus; δ_p and δ_n are the pairing energies of two protons and two neutrons, respectively, as published in [19]. The average distances D(U, J) between levels having a given total moment J and the excitation energy U were calculated by the formulas of a Fermi gas model with the parameters a given in [5]. The values of the average radiation widths were taken on the basis of the function $\Gamma_\gamma(A)$ given in [6].

The $\overline{\sigma_{n\gamma}}$ calculations were made on an electronic computer. The program was based on the method of solving the radial Schrödinger equation with a potential of arbitrary shape which is described in [20].

The table shows the values of the average parameters and characteristics of the ground states of the isotopes which were used in the calculation. As usual [15], for [15], for s-neutrons ($l = 0$) we have $D_J = \overline{D}/2g_J$, where

$\overline{D} = 2D_{obs}$ when $I \neq 0$; $D_J = \overline{D}/g_J$, where $\overline{D} = D_{obs}$ when $I = 0$; $g_J = \frac{2J+1}{2(2I+1)}$.

In calculating $\overline{\sigma_{n\gamma}}$ for Sn^{119} we took into account not only the ground state of the target nucleus but also two excited levels lying below 100 keV: 23.8 keV (3/2+) and 89.0 keV (11/2+). The results of the calculation are shown in Figs. 1-3. For the isotopes Rb^{85}, $Zr^{90,92,94,96}$, Mo^{100}, $Sn^{116-120}$ and $Sm^{144,147-150,152}$ the calculated cross

sections agree with the experimental values[1] within the limits of experimental error. For the isotopes Sn^{122}, Sn^{124}, and Zr^{91} the deviation between the calculated and the experimental cross sections is $\lesssim 50\%$.

In some cases the parameter a obtained from $\overline{D}$ values which had been measured with poor accuracy shows a disagreement with the systematic trend. The theoretical cross sections agree better with the experimental cross sections if the $\overline{D}$ values used in the calculations were calculated with parameters a predicted by the systematic trend.

Rb^{85}. The only experimental result ($\overline{D}$ = 2000 eV) was obtained in [22]. The average capture cross section, calculated with this value of D and Γ_γ = 0.25 eV [15], is about one-third of the experimental value. We obtain agreement with experimental value if we take $\overline{D}$ = 750 eV, calculated on the basis of a = 8.50, and Γ_γ = 0.41 eV,[2] obtained from [6].

Sm^{119}. Calculation using a value of $\overline{D}$ = 300 eV, obtained in [23] from no more than two resonances, yields a cross section about one-half as large as the experimental value. Agreement within the limit of experimental error is obtained if we take $\overline{D}$ = 180 eV, calculated with a = 15.5.

Sm^{154}. This case exhibits the greatest deviation between the calculated and experimental values ($\sigma_{n\gamma exp}$ per $\sigma_{n\gamma calc} \approx 2.7$). The agreement is improved if we take the somewhat high value a = 24. However, the discrepancy still exceeds the experimental error.

In two cases the available experimental data are found to be dispersed. The cross section of Mo^{98} at 25 keV is 415 mbarns according to [10], 390 ± 120 mbarns according to [14], and 120 mbarns according to [7]. The calculation agrees with the results of [13], with a value of 209 ± 21 mbarns. For Mo^{100} the results of earlier studies [12, 13] differ considerably from the results of [7-11]; the calculated cross section agrees with the latter (see Fig. 2).

The cross sections for natural mixtures of isotopes,[3] obtained by adding the calculated cross sections for the individual isotopes, are in good agreement with the experimental values for all the elements investigated, with the exception of Sm. We can obtain agreement with the experimental results if we assume that the cross sections of Sm^{147} and Sm^{149} are 1.5 times as large, but this seems unlikely.

Our calculations showed that the average radiative-capture cross sections of the isotopes are very sensitive to the values of $\overline{D}$ and make it possible to verify the parameters of the Fermi gas model. The reason for this is that the average radiation widths of neighboring nuclei having different parity in the number of their nucleons are about the same, while the average distance between the levels in one of the nuclei may be several times as great as in the other. In all of the elements investigated (Fig. 4) the cross section for even-odd isotopes are considerably larger than those for even-even isotopes. Consequently, even though they constitute only a small percentage of the natural mixture, they make a considerable contribution to its cross section [24].

Thus, the present study shows that it is possible to make theoretical estimates of average radiative-capture cross sections in the 10^3-10^5 eV energy range with an accuracy no worse than 50%, since among the 22 isotopes for which a comparison was made with the experimental values there is no deviation exceeding 50% except in the case of Sm^{154}.

LITERATURE CITED

1. B. Margolis, Phys. Rev., 88, 327 (1952).
2. A. Lane and I. Lynn, Proc. Phys. Soc., A70, 557 (1957).
3. V. A. Tolstikov, V. E. Kolesov, and V. S. Stavinskii, Atomnaya Énergiya, 11, 56 (1961); V. E. Kolesov and V. S. Stavinskii, Atomnaya Énergiya, 13, 371 (1962).
4. P. Nemirovskii and Yu. Yelagin, Nucl. Phys., 45, 156 (1963).
5. A. V. Malyshev, ZhÉTF, 45, 316 (1963).

[1] It should be noted that for most of the isotopes under consideration only one experimental value of $\sigma_{n\gamma}$ is known in each case.

[2] The value Γ_γ = 0.41 eV, taken in accordance with the systematic trend, is in good agreement with the value 0.44 ± 0.15 eV for the resonance E_0 = 230 eV, taken from [7].

[3] The cross section for Rb^{87} is not given, since its contribution to the cross section of the natural mixture is small in comparison with that of Rb^{85}.

6. S. M. Zakharova and A. V. Malyshev, Report delivered at the International Confress on Low- and Intermediate-Energy Nuclear Reactions [in Russian], Paris, (July 1964).
7. S. P. Kapchigashev and Yu. P. Popov, Atomnaya Énergiya, 15, 120 (1963).
8. Yu. P. Popov and F. L. Shapiro, ZhÉTF, 42, 988 (1962).
9. L. Weston et al., Ann. Phys. 10, 477 (1960).
10. I. Vervier, Nucl. Phys., 9, 569 (1959).
11. A. I. Leipunskii et al., In "Proceedings of the Second International Conference on the Peaceful Uses of Atomic Energy, Geneva 1958" [in Russian]. Reports of Soviet Scientists, 1, Moscow, Atomizdat (1959), p. 316.
12. V. Hummel and B. Hammermesh, Phys. Rev., 82, 67 (1951).
13. R. Macklin, N. Lasar, and S. Lyon, Phys. Rev., 107, 504 (1957).
14. R. Booth, W. Ball, and MacGregor, Phys. Rev., 112, 226 (1958).
15. I. V. Gordeev, D. A. Kardashev, and A. V. Malyshev, Handbook of Nuclear-Physics Constants [in Russian], Moscow, Gosatomizdat (1963).
16. R. Macklin, I. Gibbons, and T. Inada, Nucl. Phys., 43, 353 (1963).
17. R. Macklin, I. Gibbons, and T. Inada, Nature, 197, 369 (1963); Bull. Amer. Phys. Soc., 8, 81 (1963).
18. Yu. Ya. Stavisskii and A. V. Shapar', Atomnaya Énergiya, 15, 322 (1963).
19. P. Nemirovskii and Yu. Adamchuk, Nucl. Phys., 39, 553 (1962).
20. S. M. Ermakov, V. E. Kolesov, and G. I. Marchuk, In the collection "Nuetron Physics" [in Russian], Moscow Atomizdat (1961) p. 314.
21. R. Macklin, T. Inada, and I. Gibbons, Nature, 194, 1272 (1962).
22. H. Newson et al., Ann. Phys., 14, 346 (1961).
23. I. Harvey et al., Phys. Rev., 99, 10 (1955).
24. T. S. Belanova and O. D. Kazachkovskii, Atomnaya Énergiya, 14, 185 (1963).

ASYMPTOTIC FORMULAS FOR SCATTERING OF SLOW NEUTRONS ON BOUND ATOMS

(UDC 621.039.512.4)

V. F. Turchin and V. A. Tarasov

Translated from Atomnaya Énergiya, Vol. 18, No. 2,
pp. 118-121, February, 1965
Original article submitted October 3, 1963

The Placzek–Wick approach is employed to derive asymptotic formulas at high neutron energies for the average cosine of the scattering angle, moments of energy losses, and conjugate momenta of energy losses. The latter differ from ordinary momenta in that integration is performed with respect to the initial, rather than the final, neutron energy.

Age approximation methods are used in calculating the spectra of epithermal neutrons, as well as higher-energy neutrons. But the existence of chemical bonds between atoms substantially alters the differential scattering cross sections of epithermal neutrons, as compared to scattering by free atoms, with the result that changes are also brought about in such integrated characteristics as the average energy loss, average cosine of scattering angle, and so forth. These characteristics must be known if the effect of the chemical linkage on the neutron spectra in the epithermal energy range is to be properly taken into account.

Placzek [1] demonstrated that the asymptotic behavior of the scattering cross sections of neutrons on bound atoms may be expressed, in the event of ascending initial neutron energy, in terms of the averages of certain operators characterizing the motion of the scattered atoms, since knowledge of all the parameters affecting the dynamics of the atoms is not mandatory in this case. Placzek derived formulas for the total scattering cross section, the first moment of the neutron energy loss in scattering, and the angular differential cross section $d\sigma/d\Omega$ in the form of expansions in reciprocal powers of the initial neutron energy E_0^{-1}. The expansion coefficients contain the average kinetic energies of the scatterer $K_{av} = \langle K \rangle$, the square of the kinetic energy $\langle K^2 \rangle_{av}$, and of the two operators:

$$B_{av} = \frac{1}{3} \cdot \frac{\hbar^2}{M} \langle \nabla^2 V \rangle,$$

$$C_{av} = \frac{1}{3} \cdot \frac{\hbar^2}{M} \langle (\nabla V)^2 \rangle,$$

where M is the mass of the scatterer and V is the potential of the forces acting on the scattering atom. The Placzek formulas are applicable when the initial neutron energy E_0 exceeds the characteristic energy associated with the motion of the atom. In the case of a single crystal this reduces to the constraint $E_0 > \max(T, \theta)$, where T is the temperature; θ is the Debye temperature of the crystal. In addition, the coefficients of the expansion in powers of E_0^{-1} in Placzek's formulas exhibit the form of an expansion in powers of m/M, i.e., of the reciprocal mass of the atom in units of the mass of the neutron, so that these formulas are valid only when $M \gg m$.

Later on, Wick [2] showed that Placzek's approximation corresponds physically to the case where the scattering time of a neutron scattered by an atom is much shorter than the characteristic time of the atom's motion (low scattering time apprxomation). It became evident in the process just why Placzek's formulas are suited only in the case $M \gg m$. Indeed, the recoil energy of an atom in a scattering process is of the order of $\frac{m}{M} E_0$. The corresponding characteristic time is therefore $\frac{\hbar}{E_0} \cdot \frac{m}{M}$. Considering that this time must be far greater than the characteristic

scattering time of neutrons, i.e., h/E_0, we arrive at the constraint We see then that in order to derive formulas but applicable to light nuclei, we shall have to take proper account of the recoil energy of the atom, and this is in fact done by Wick [2]. In that paper, the formula

$$\sigma_1(E_0) = \sigma_0\left[1 + \frac{1}{3\mu}\cdot\frac{K_{av}}{E_0} - \frac{1}{32\mu}\left(\frac{\mu+1}{\mu}\right)^2\frac{C_{av}}{E_0^3}\right], \tag{1}$$

where σ_0 is the cross section for scattering by a free atom and is derived for the total scattering cross section. Interference between neutron waves scattered by neighboring atoms is ignored here, i.e., Eq. (1) was derived in the incoherent-scattering approximation. We will restrict our treatment to the incoherent approximation, since it suffices entirely for epithermal neutrons.

Designating the mixed differential scattering cross section by the finite energy differential dE and the solid angle differential $d\Omega$ as $(E_0 \to E, \theta)$, where θ is the scattering angle, we find the moments of the energy loss as

$$\sigma_n(E_0) = \int \sigma(E_0 \to E, \theta)(E_0 - E)^n\, dE\, d\Omega.$$

The formula

$$\frac{\sigma_1(E_0)}{E_0} = \sigma_0\left[\frac{2\mu}{(\mu+1)^2} - \frac{8\left(\mu-\frac{1}{2}\right)}{3(\mu+1)^2}\cdot\frac{K_{av}}{E_0} + \frac{\mu+\frac{1}{3}}{4\mu(\mu+1)}\cdot\frac{B_{av}}{E_0^2} - \frac{8}{15}\cdot\frac{\mu+\frac{1}{4}}{\mu(\mu+1)^2}\cdot\frac{\langle K^2\rangle_{av}}{E_0^2}\right] \tag{2}$$

was derived in [3] for the first moment.

Analogously, for the second moment we may obtain

$$\frac{\sigma_2(E_0)}{E_0^2} = \sigma_0\left[\frac{16}{3}\cdot\frac{\mu^2}{(\mu+1)^4} + \frac{8}{3}\cdot\frac{\mu(\mu^2-6\mu+3)}{(\mu+1)^4}\cdot\frac{K_{av}}{E_0} - \right. \\ \left. - \frac{2\mu(\mu-1)}{(\mu+1)^3}\cdot\frac{B_{av}}{E_0^2} + \frac{16\mu\left(\mu-\frac{2}{3}\right)}{(\mu+1)^4}\cdot\frac{\langle K^2\rangle_{av}}{E_0^2}\right] \tag{3}$$

Terms proportional to E_0^{-3} were not computed out in formulas (2) and (3).

The angular differential cross section was derived by Wick in the following form:

$$\frac{d\sigma}{d\Omega} \equiv \int \sigma(E_0 \to E, \theta)\, dE = \frac{\sigma_0}{4\pi}\left(\frac{\mu+1}{\mu}\right)^2\left[\varphi_{0.0}(\theta) + \frac{2}{3\mu}\cdot\frac{K_{av}}{E_0}\varphi_{2.1}(\theta)\right. \\ \left. - \frac{1}{6\mu}\cdot\frac{B_{av}}{E_0^2}\varphi_{3.1}(\theta) + \frac{2}{15\mu^2}\cdot\frac{\langle K^2\rangle_{av}}{E_0^2}\varphi_{4.2}(\theta) + \frac{1}{12\mu}\cdot\frac{C_{av}}{E_0^3}\varphi_{4,1}(\theta)\right]. \tag{4}$$

Here

$$\varphi_{n,m}(\theta) = \left(\frac{\mu}{\mu+1}\right)^{n+1}\left\{\left(\frac{\partial}{\partial x^2}\right)\left[\frac{1}{x}\left(x + \frac{\cos\theta}{\mu+1}\right)^2 V_x^m\right]\right\}_{x=x_0}, \tag{5}$$

where

$$V_x = \left(x - \frac{\mu\cos\theta}{\mu+1}\right)^2 + \sin^2\theta, \tag{6}$$

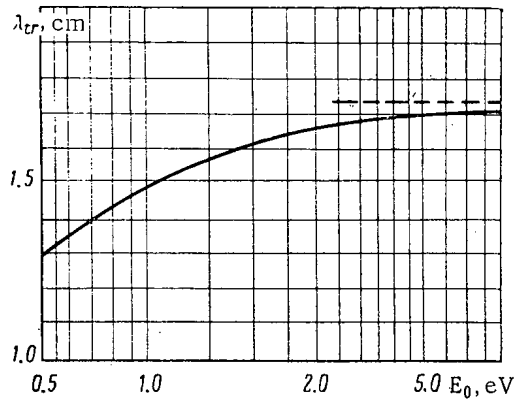

Fig. 1. Transport scattering length λ_{tr} for scattering on water at room temperature plotted versus neutron energy E_0. – – – – – limiting value as $E_0 \to \infty$.

$$x_0 = \frac{(\mu^2 - \sin^2\theta)^{1/2}}{\mu + 1}. \tag{7}$$

The average cosine of the scattering angle

$$\overline{\cos\theta} = \frac{\Phi_1(E_0)}{\sigma_1(E_0)} \tag{8}$$

is an important characteristic of the differential cross section. Here,

$$\Phi_1(E_0) = \int \frac{d\sigma}{d\Omega} \cos\theta \, d\Omega = 2\pi \int_{-1}^{1} \frac{d\sigma}{d\Omega} \cos\theta \, d(\cos\theta) \tag{9}$$

is the first moment of the differential cross section, taken with respect to the solid angle. The value of $\Phi_1(E_0)$, as all other moments of odd order, is computed in a very straightforward manner since, with the exception of $\varphi_{0,0}(\theta)$, all the functions $\varphi_{n,m}(\theta)$ appearing in formula (4) are even functions relative to $\xi \equiv \cos\theta$. This is readily disclosed when the reader notes that V_x is a polynomial of the second degree in x and ξ exhibiting the following properties: the sum of the powers of x and ξ in each term is an even number. This property is retained when V_x is raised to any power of m and when it is multiplied by the function

$$x^2 + \frac{2}{\mu+1} x\xi + \frac{\xi^2}{(\mu+1)^2},$$

appearing in Eq. (5), since this function exhibits the same property. When divided by x, the sum of the powers in each term will change to an odd number. Accordingly, formula (5) may be recast in the form

$$\varphi_{n,m}(\theta) = \left\{ \frac{\partial^n F(x)}{\partial (x^2)^n} \right\}_{x=x_0}, \tag{10}$$

where

$$F(x) \equiv \frac{a_{-1}}{x} + a_0 + a_1 x + \ldots + a_{2m+1} x^{2m+1} \tag{11}$$

possesses the property that the coefficients attached to even powers of x are odd terms in ξ, while the coefficients attached to odd powers of x are even terms in ξ.

Clearly, as formula (7) shows, the value of the variable x substituted into Eq. (10) after differentiation will be an even function of ξ; consequently, the parity of the i-th term is completely specified by the parity of the coefficient a_i. All terms with odd powers of x in formula (11) consequently yield even functions of ξ, and fail to make any contribution to the first moment when integrated with respect to $d\Omega$.

Consider the even terms. The maximum even degree in formula (11) will be $x^{2m} = (x^2)^m$. Accordingly, when formula (10) is differentiated m times, the corresponding term vanishes. Equation (4) clearly shows $n > m$ for all terms excepting the first. The sole term odd in ξ which can be obtained from $\varphi_{0,0}(\theta)$ is then

$$\frac{2\mu}{(\mu+1)^2} \xi.$$

Substitution of this term into Eq. (4) and integration with respect to $d\Omega$ yields

$$\Phi_1(E_0) = \sigma_0 \frac{2}{3\mu}. \tag{12}$$

In the low scattering time approximation, then, the first moment of the differential cross section taken with respect to the angle is energy-independent and equal to its own limiting value corresponding to scattering on a free fixed nucleus. This enables us to calculate the average cosine of the scattering angle and the transport scattering length λ_{tr} in the epithermal energy range, by using only the total scattering cross section which is of course easily measured by the transmission method. From formulas (8) and (12), we have

$$\overline{\cos\theta} = \frac{2}{3\mu} \cdot \frac{\sigma_0}{\sigma_s(E_0)} . \tag{13}$$

The transport scattering length is found by using the formula

$$\lambda_{tr} = \frac{1}{\varrho\sigma_{tr}} = \frac{1}{\varrho\sigma_s(E_0)(1-\overline{\cos\theta})} = \frac{1}{\varrho\left[\sigma_s(E_0) - \frac{2}{3\mu}\sigma_0\right]} , \tag{14}$$

where ρ is the number of atoms populating a unit volume.

On the basis of data reported in [4] on the total scattering cross section of neutrons scattered by water, we computed the λ_{tr} value for water at room temperature as a function of neutron energy over the 0.5 to 10 eV range (see diagram). The transport cross section for scattering by oxygen, which makes a slight contribution to the total transport cross section σ_{tr}, was assumed constant and equal to its value in the case of a free atom. In the range of energies from 1 to 10 eV, the total cross section for scattering $\sigma_s(E_0)$ is extrapolated in accord with formula (1), using the value obtained at 1 eV energy as point of departure.

$$\widetilde{\sigma}_n(E) = \int \sigma(E_0 \to E,\ \theta)(E_0 - E)^n dE_0 d\Omega$$

(where n = 0, 1, 2) are known as conjugate moments of the energy loss, and are used in [5] to calculate the spectra of epithermal neutrons. Computation of the conjugate moments in the Wick approximation assuming low scattering times is a tedious task, and leads to the following results:

$$\widetilde{\sigma}_0(E) = \sigma_0\left[\frac{(\mu+1)^2}{2\mu}\ln\frac{\mu+1}{\mu-1} + \frac{1}{3\mu}\cdot\frac{K_{av}}{E} - \frac{3\mu+1}{12\mu(\mu+1)}\cdot\frac{B_{av}}{E^2} + \frac{2(4\mu+1)}{15\mu(\mu+1)^2}\cdot\frac{\langle K^2\rangle_{av}}{E^2}\right] , \tag{15}$$

$$\frac{\widetilde{\sigma}_1(E)}{E} = \sigma_0\left[\frac{(\mu+1)^2}{(\mu-1)^2} - \frac{(\mu+1)^2}{2\mu}\ln\frac{\mu+1}{\mu-1} + \frac{4}{3(\mu-1)^2}\cdot\frac{K_{av}}{E} + \frac{3\mu+1}{12\mu(\mu+1)}\cdot\frac{B_{av}}{E^2} - \frac{2(4\mu+1)}{15\mu(\mu+1)^2}\cdot\frac{\langle K^2\rangle_{av}}{E^2}\right] , \tag{16}$$

$$\frac{\sigma_2(\widetilde{E})}{E^2} = \sigma_0\left[\frac{(\mu+1)^2}{2\mu}\ln\frac{\mu+1}{\mu-1}\frac{(\mu^2-4\mu+1)(\mu+1)^2}{(\mu-1)^4} + \frac{8\mu(\mu^2+2\mu+3)}{3(\mu-1)^4}\cdot\frac{K_{av}}{E} + \frac{4\mu^2}{2(\mu+1)(\mu-1)^3}\cdot\frac{B_{av}}{E^2} + \frac{16\mu^2(\mu^2+5)}{(\mu-1)^4(\mu+1)^2}\cdot\frac{K_{av}}{E^2}\right] . \tag{17}$$

Formulas are derived in [6] for ordinary and conjugate moments of the energy loss in the case of crystals of cubic symmetry. A method equivalent to the Placzek method in the physical assumptions entertained is used there, since the expansion coefficients attached to reciprocal powers of the energy are in the form of an expansion in powers of $1/\mu$. It is readily seen that if these coefficients can be expanded in powers of $1/\mu$ in formulas (1) to (3) and (15) to (17), then the initial terms of the expansion (up to $1/\mu^3$ inclusive) will be the same as the coefficients obtained in [6].

LITERATURE CITED

1. G. Placzek, Phys. Rev., 86, 377 (1952).
2. G. Wick, Phys. Rev., 94, 1228 (1954).
3. V. F. Turchin, Slow Neutrons [in Russian], Moscow, State Atom Press (1963).
4. E. Melkonian, Phys. Rev., 76, 1750 (1949).
5. V. F. Turchin, Neutron Physics Symposium [in Russian original], Moscow, State Atom Press (1961) p. 66.
6. V. F. Turchin, Ibid, p. 74 [in Russian original].

THE ATTENUATION OF REACTOR RADIATION BY MEANS OF SERPENTINE CONCRETE

(UDC 621.039.538.7)

G. A. Vasil'ev, A. P. Veselkin, Yu. A. Egorov,
V. A. Kucheryaev, and Yu. V. Pankrat'ev

Translated from Atomnaya Énergiya, Vol. 18, No. 2,
pp. 121-127, February, 1965
Original article submitted February 20, 1964
Final revised version submitted May 18, 1964

A description is given of experiments on the study of the shielding properties of concrete that has a serpentine aggregate. It is shown that in comparison with limonite concrete the shielding properties of this type of concrete are slightly better as regards neutrons, and no worse as regards γ-radiation. At the same time, this type of concrete has a much higher capability of withstanding the effect of temperature, and its use in reactor shielding can be recommended at least up to temperature of 450°C.

For a concrete to possess good shielding properties with respect to both neutrons and γ-radiation simultaneously, its composition must include nuclei of both heavy and light elements. The density of the concrete is an important factor in this respect. The effective attenuation of neutrons by a concrete is related, in particular, to the presence in its composition of the hydrogen contained in its chemically combined water and in the water that is part of the makeup of the aggregate. It is, therefore, advisable to increase the water content of the concrete as much as possible and to aim for its retention during the use of the concrete shielding. If the temperature of concrete is increased during use, the water that was combined with the cement during the hardening of the concrete is gradually lost. For example, at a temperature of 100°C ordinary concrete loses more than half of its combined water [1]. At temperature higher than this, the water loss of the concrete is increased. Since the concrete shielding of a reactor

TABLE 1. Characteristics of Serpentine Concrete

Breakdown of materials (kg/m³ of concrete)				Water/cement ratio	Settlement of cone (cm)	Volumetric weight of the freshly prepared concrete (tons/m³)
Cement	Sand	Gravel	Water			
300	786	1000	224	0.75	1.0	2.31

TABLE 2. Chemical Composition of Serpentine Concrete (wt. %)

SiO_2	Al_2O_3	Fe_2O_3	CaO	MgO	H_2O	SO	Other
40	2.73	8.12	10.85	25.7	11.3	0.09	1.21

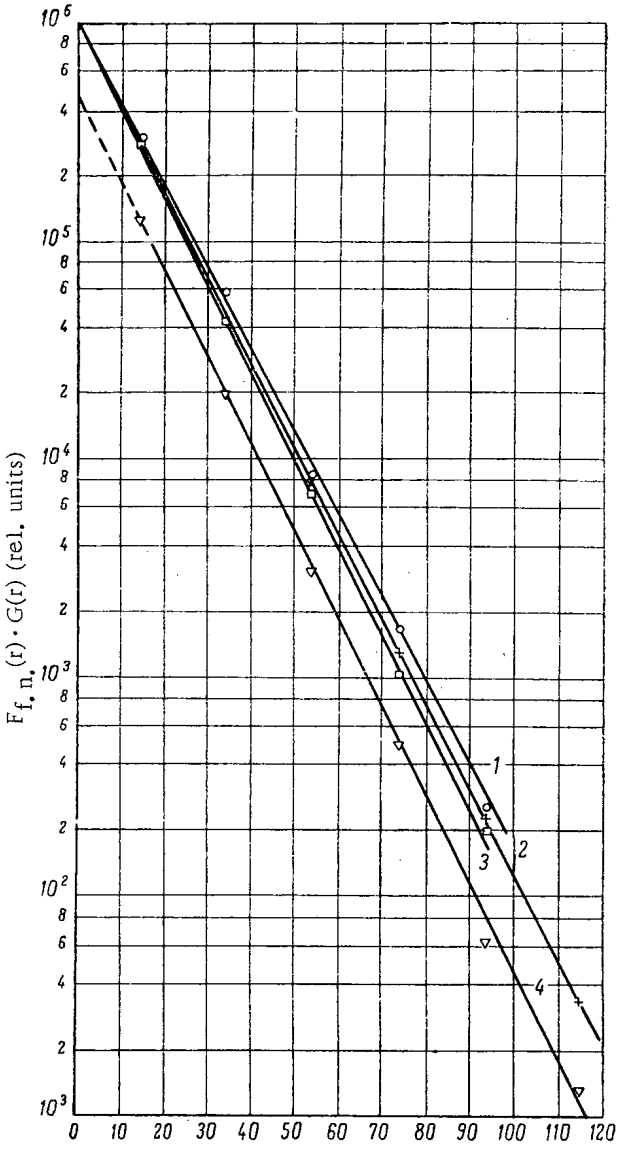

Fig. 1. Attenuation functions of fluxes of fast neutrons in serpentine concrete. 1) Al(n, α); 2) Al(n, p); 3) P(n, p); 4) In(n, n').

TABLE 3. Relaxation Lengths of Fast Neutrons in Serpentine Concrete

Indicator	E_{thresh} (MeV)	E_{eff} (MeV)	λ, cm
In(n, n') In	0.5	1.5	10.9 ± 0.3
P(n, p) Si	0.97	3	10.9 ± 0.3
Al(n, p) Mg	1.96	5	11.2 ± 0.35
Al(n, α) Na	2.44	7	11.6 ± 0.4

is normally subjected to the effect of increased temperatures, in due course its shielding properties deteriorate, and it is, therefore, expedient to introduce into its composition aggregates containing water of crystallization, which is retained at high temperatures.

One aggregate of this type is the mineral serpentine ($3MgO \cdot 2SiO_2 \cdot 2H_2O$), in which the water of crystallization content amounts to approximately 13 wt. %. (The water of crystallization content of serpentine is dependent upon the site of formation of the core; it can vary slightly.) Serpentine loses its water of crystallization when it is heated to a temperature of more than 480°C [2, 3]. According to [3], concrete with a serpentine aggregate can be used in shielding when the temperature of the latter is up to 480°C; at a temperature of 430°C the loss of water of crystallization at the end of 10 y constitutes about 5% of the quantity of water that was contained in the concrete after the first 10 h of heating [3].

The natural source of serpentine is the type of rock known as serpentinite. The specific gravity of serpentine rock is 2.5-2.7 g/cm^3. In addition to magnesium, silicon, oxygen, and water the rock normally contains up to 8-10 wt. % iron, and also very small quantities of calcium and aluminum. In the Soviet Union there are extensive deposites of serpentinite in the Urals, the Caucasus, and in a number of places in Siberia and Kazakhstan. Large quantities of it are accumulated in the refuse ore dumps from asbestos mines. The cost of serpentine ~ 25 rubles/m^3, i. e., slightly higher than that of ordinary building concrete [4].

In the present paper the results are given of an investigation into the shielding properties of a concrete with a volumetric weight of 2.2 tons/m^3 with a serpentine aggregate (the serpentine was added in the form of sand, a fine aggregate, and in the form of gravel, a coarse aggregate). The concrete was prepared from grade M-500 Portland cement. The characteristics of the concrete and its chemical composition are shown in Tables 1 and 2. In calculating the water content of the concrete (see Table 2), only the water of crystallization in the serpentine (10.2 wt. %) and the water combined with the cement during the hardening of the concrete (20% of the weight of the cement in the concrete [1]) were taken into account. The age of the concrete that was investigated was more than 28 days. A detailed description of the physicomechanical properties of this concrete has already been given in [2]. It should be noted that concrete with a limonite aggregate contains approximately the same quantity of water. Its chemical composition differs little from that of serpentine concrete (with the exception of its iron and magnesium contents), and, consequently, it is feasible to expect that the shielding properties of the one must be similar to those of the other. Limonite, however, loses its water almost entirely at 120°C [2], which means that its shielding properties deteriorate sharply, whereas in concrete that has a serpentine aggregate the shielding properties remain unchanged even when it is heated up to 450°C.

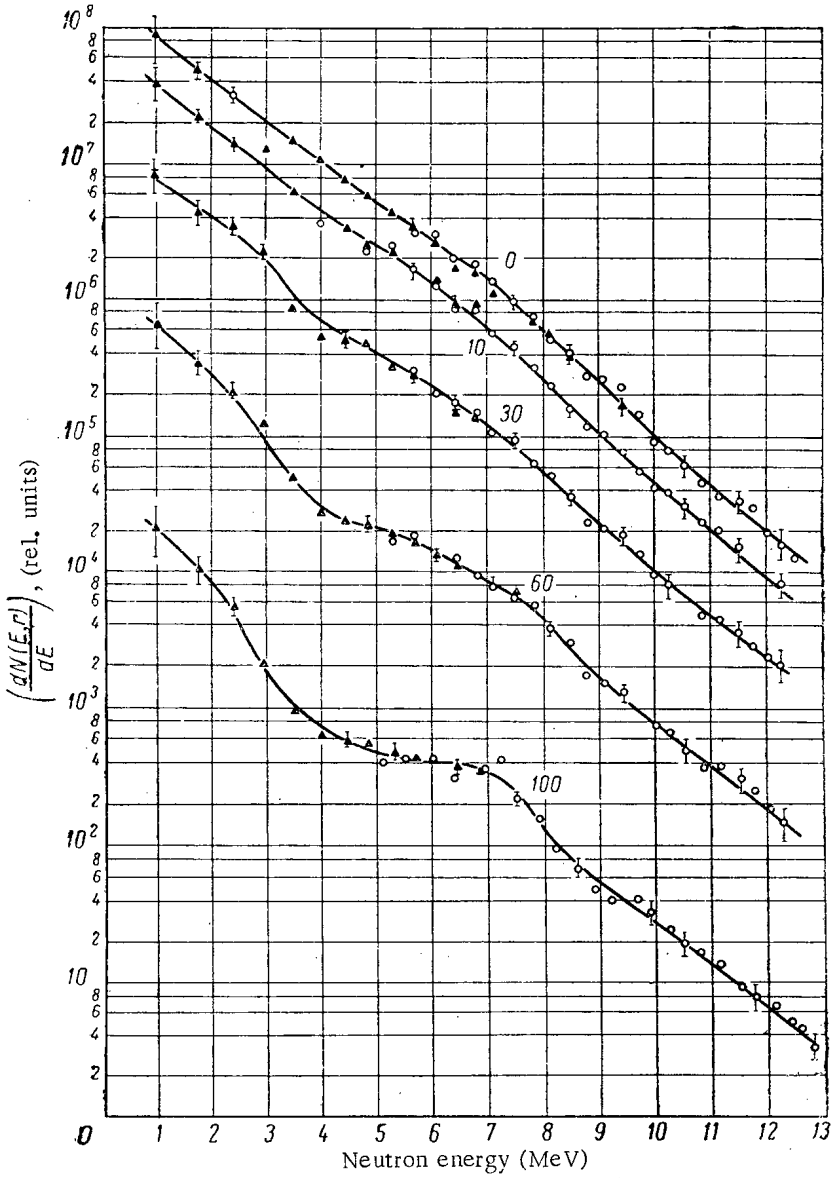

Fig. 2. Spectra of fast neutrons from the reactor after their passage through serpentine concrete barriers of various thicknesses (the figures beside the curves indicate the thickness of the barrier in centimeters). ▲) Energy threshold of the spectrometer E_{thresh} = 0.7 MeV; ○) E_{thresh} = 2.8 MeV.

Experimental Conditions and Equipment

The shielding properties of serpentine concrete were studied on a water-moderated water-cooled research reactor. Slabs of the concrete were installed in special niches cut in the concrete shielding of the reactor; the width of the niches was increased in proportion to the distance from the active zone of the reactor, and so the slabs were made in three sizes: 670 x 670 x 100 mm, 940 x 940 x 100 mm, and 1140 x 1140 x 100 mm.

The spatial distribution of the fluxes of fast neutrons under conditions of semiinfinite geometry was measured with threshold radioactive indicators made of indium, phosphorus, and aluminum [5]. The indicators were irradiated in cadmium borate filters, which made it possible to reduce the activation of the indicators by thermal and epithermal neutrons. The distribution of the fluxes of thermal and epithermal neutrons was investigated with indicators made of dysprosium (Dy^{164}), which were irradiated both in cadmium filters 0.5 mm thick and without filters. The induced activity of the indicators was determined on a scintillation counter which was incorporated in the spectrometer circuit [6].

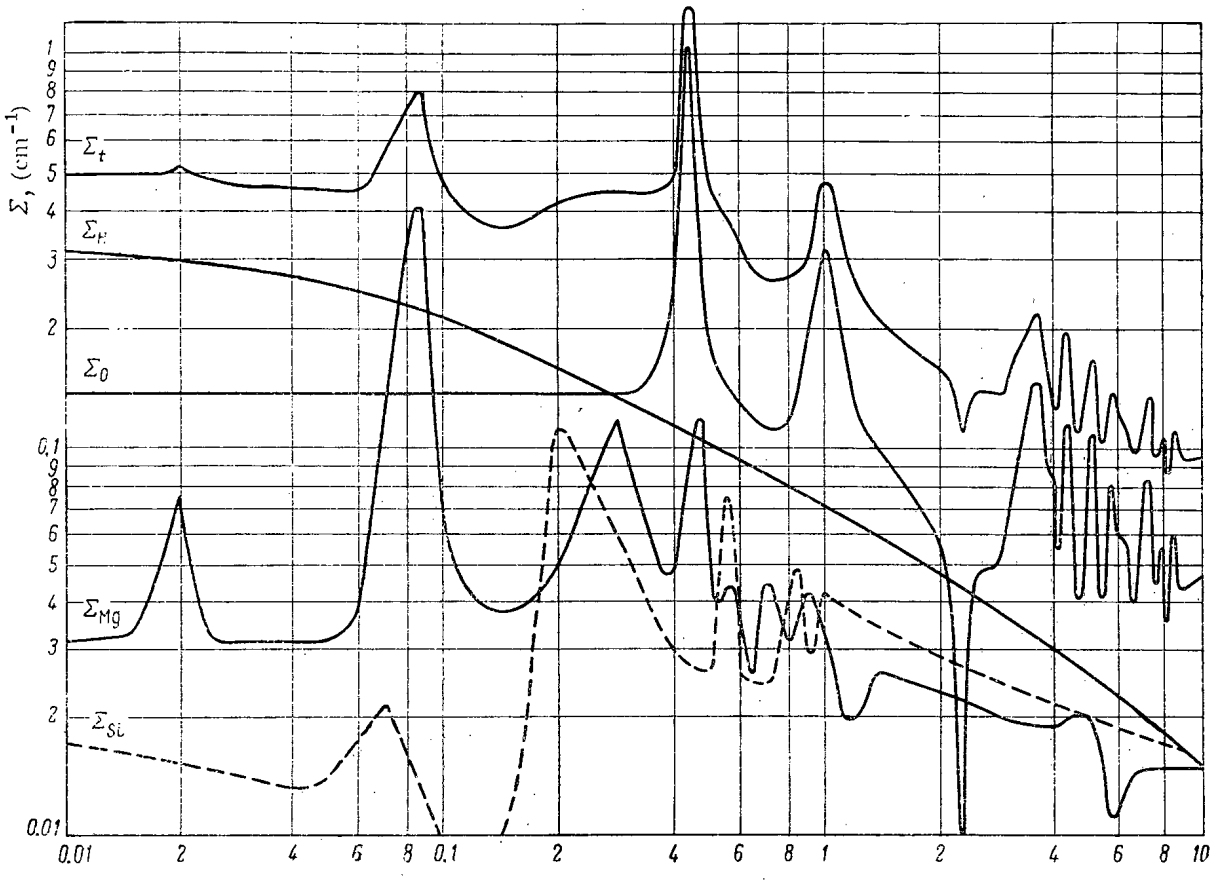

Fig. 3. Total (Σ_t) and partial macroscopic neutron interaction cross sections for serpentine concrete.

To carry out the measurements, the indicators were inserted into holes drilled in the slabs. Since, in the course of the experiment, indicators were placed in several holes at the same time, in order to avoid interaction between the indicators the holes were displaced relative to the axis of the niche. Those holes which were not occupied by indicators were stopped up with plugs.

An investigation was also carried out into the deformation of the fast-neutron spectrum ($E \geq 0.9$ MeV) after the neutrons have passed through concrete barriers of of various thicknesses. For these measurements, a fast-neutron spectrometer was used [7]. The methods of measurement and of processing the results have been described in [8].

In the barrier configuration the attenuation of the neutron dose rate was measured with an isodosic detector [9]. In this experiment, in the same way as in the measurements of spectrum deformation, the thickness of the shielding was imposed in the direction from the source to the detector. The attenuation of the γ-radiation dose rate was studied with a scintillation γ-dosimeter without energy dependence [10] under conditions of semiinfinite geometry.

Attenuation of the Fast-Neutron Flux

Figure 1 shows the attenuation functions of fluxes of fast neutrons in serpentine concrete that were measured with threshold indicators. The attentuation curves that were obtained were corrected to allow for the geometric attenuation of the fast neutron flux along the axis of the niche.

The value of the correction that had to be made was determined by activating these same indicators in a concrete-free niche.

It can be deduced from Fig. 1 that attenuation of the fluxes of fast neutrons of each energy group takes place exponentially with a constant relaxation length. The fluxes of neutrons of energy greater than ~ 1.5 MeV (indium indicator) and ~ 3 MeV (phosphorus indicator) decrease with identical relaxation length in proportion to the increase in the thickness of the concrete layer (Table 3).

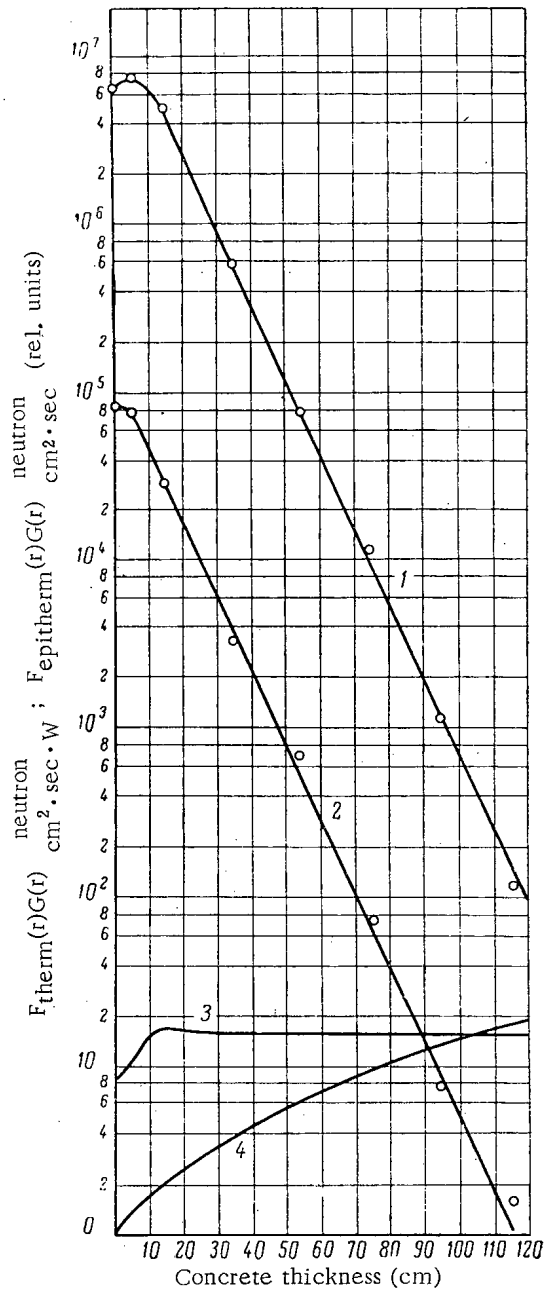

Fig. 4. Spatial distribution of thermal (1) and epithermal (2) neutrons and the cadmium ratio (3) in serpentine concrete [(4) = correction to allow for geometric flux attenuation].

Deformation of the Fast-Neutron Spectrum

The fast-neutron spectra were measured behind concrete barriers 0, 10, 30, 60, and 100 cm thick (Fig. 2). It can be seen from the figure that the greatest spectrum deformation occurs in the energy range 3-8 MeV. Sharp irregularities are observed within this energy range in the total neutron interaction cross-section, calculated for serpentine concrete (Fig. 3). At neutron energies of more than 8 MeV there is hardly any change in the neutron spectrum as the neutrons pass through the concrete, i. e., the slopes of these parts of the spectrum hardly differ at all from the slope of the initial spectrum.

The results obtained from the measurements of the spectral distribution of the neutrons can be used to obtain the data that are required for the multigroup calculation of the spatial distribution of the neutrons in the shielding. In order to obtain these data, four neutrons energy groups were selected (4-10 MeV, 2.5-4 MeV, 1.5-2.5 MeV, and 0.9-1.5 MeV),[1] integration of the spectra within the limits of the boundaries of each group was carried out, and the relaxation lengths of the fluxes of neutrons of each group were determined:

Energy of the neutrons in the group	Relaxation length λ
0.9-1.5	11.8 ± 0.3
1.5-2.5	11.5 ± 0.3
2.5-4	10.2 ± 0.3
4-10	10.8 ± 0.3
≥ 3	10.7 ± 0.3
≥ 5	11.1 ± 0.4
≥ 7	12.0 ± 0.5

In addition, integration was carried out within the energy ranges 3-12 MeV, 5-12 MeV, and 7-12 MeV, i. e., in those energy ranges whose starting values coincide with the effective threshold energies of the indicators P(n, p), Al(n, p), and Al(n, α). A comparison of the results given above with the data cited in Table 3 shows that the values that were obtained for the relaxation lengths by carrying out measurements with indicators are in agreement, within the limits of experimental error, with those obtained by studying the neutron energy distribution.

Attenuation of Thermal and Epithermal Neutrons

Figure 4 shows the spatial distribution of thermal and epithermal neutrons, measured with a dysprosium indicator. It can be seen that some accumulation of both thermal and epithermal neutrons is observed in the case of small concrete thicknesses. As the thickness of the concrete layer increases, the attenuation curves become rectilinear, and within the limits of the thicknesses that were measured their slopes are identical. With a concrete layer more than ~ 10 cm thick the relaxation length is equal to 9.6 ± 0.25 cm.

The cadmium ratio in the concrete was determined for the characteristic of the proportion of fluxes of thermal and epithermal neutrons (see Fig. 4); at thicknesses of more than ~ 20 cm it is constant and equal to 145.

[1] This type of breakdown of the neutron energy scale is used, for example, in the ten-group method of shielding calculation.

It must be mentioned that in the results that were obtained allowance was made for geometric flux attenuation along the axis of the niche, this correction being the same as for fast neutrons. At small distances from the active zone this correction may prove to be not absolutely correct for thermal and epithermal neutrons. At large distances (~ 40 cm) it is quite applicable.

Attenuation of the Neutron and γ-Radiation Dose Rate

With concrete thicknesses of 0-130 cm the neutron dose rate is reduced; in this case the average value of the relaxation length for this thickness is equal to 11.3 ± 0.5 cm.

The spatial distribution of the γ-radiation dose rate was only determined under experimental conditions for thicknesses of more than 35 cm. With thicknesses of 40-100 cm the dose rate is attenuated exponentially with the relaxation length being held constant (λ_γ = 14.7 ± 0.4 cm).

Discussion of the Results

The results obtained from these experiments on serpentine concrete can be compared with those given in [11], in which the relaxation length of neutrons in ordinary building concrete, containing ~ 7.6 wt. % water, was measured with phosphorus indicators. The result obtained in [11] was that $\lambda_{f.n.}$ = 11 cm (E > 3 MeV). In the case of serpentine concrete this value is equal to 10.9 cm. If we take into account the fact that the volumetric weight of ordinary building concrete is 2.4 tons/m^3, while that of serpentine concrete is 2.2 tons/m^3, the shielding properties that are obtained for the latter with respect to fast neutrons are slightly higher. It is also possible to compare the shielding properties of concretes which have serpentine and limonite as their respective aggregates. The results of an investigation on limonite concrete with a volumetric weight of 2.7 tons/m^3 were given in [11]; the relaxation length for fast neutrons was found to be equal to approximately 9 cm. Since the chemical compositions of the two concretes differ little from each other, it can be assumed that the neutron relaxation length is approximately inversely proportional to the density of the concrete; in this case, the shielding properties of the two concretes are identical.

As is known, [12], the removal cross sections for elements with an average atomic weight vary slightly with increase in the neutron energy. Since the serpentine concrete that was investigated consists mainly of elements of this kind, the result that was obtained is in qualitative agreement with the data given in [12]. In actual fact, the main contribution to the magnitude of the removal cross section is made by oxygen (0.036 cm^{-1}), magnesium (0.01 cm^{-1}), and silicon (0.011 cm^{-1})—elements with average atomic weights. The hydrogen and these elements determine the dependence of the cross section upon the neutron energy. Although the hydrogen cross section alters considerably (decreases) in the neutron energy range 1-10 MeV, this is balanced to a large extent by the cross sections of the other constituents of the concrete.

From the point of view of the attenuation of γ-radiation, the composition of serpentine concrete is no different from that of ordinary building concrete. It was reported in [11] that in ordinary concrete the relaxation length of the flux of γ-quanta from the active zone of a water-moderated water-cooled reactor is equal to 13 cm. If we make allowance for the difference between the volumetric weights of the two concretes, the value that was obtained for the relaxation length of the γ-radiation dose rate in serpentine concrete is in good agreement with the data given in [11]. The same can also be said for the result that were obtained by comparing the γ-radiation relaxation lengths in serpentine and limonite concretes, and also in concretes of other compositions [13].

Thus, the results of these experiments show that in comparison with limonite concrete the shielding properties of serpentine concrete with a volumetric weight of 2.2 tons/m^3 are slightly better with respect to neutrons and identical with respect to γ-radiation, and, since the chemical composition of this concrete remains unchanged up to a temperature of 480°C, its use can be recommended in the biological shielding of nuclear power installations at least up to temperatures of 450°C.

The authors would like to thank all the reactor maintenance staff, and also V. P. Zharkov for his help in carrying out the experiments and T. V. Ruch'eva for her help in processing the results; they are also indebted to V. M. Isakov, A. P. Kulaev, V. G. Petrov, and A. T. Pogachev for their assitance in making the measurements.

LITERATURE CITED

1. Instructions for the Design of Concrete and Ferroconcrete Structures Built with Special (Heavy and Hydrated) Concretes [in Russian], Moscow, Scientific Research Institute of Ferroconcrete, ASA, USSR (1959).
2. I. A. Arshinov, In the Collection: Problems of Reactor Shielding Physics [in Russian], State Press for Atomic Energy, Moscow (1963), p. 337.

3. H. Hungerford et al., Nucl. Sci. and Engng., 6, 396 (1959).
4. A. N. Komarovskii, The Construction of Nuclear Installations [in Russian], State Press for Power Engineering, Moscow–Leningrad (1961).
5. V. N. Avaev et al., Atomnaya énergiya, 15, 17 (1963).
6. V. N. Avaev et al., In the Collection: Problems of Reactor Shielding Physics [in Russian], State Press for Atomic Energy, Moscow (1963), p. 270.
7. Yu. A. Egorov and Yu. V. Pankrat'ev, Ibid., p. 304.
8. A. P. Veselkin et al., Atomnaya énergiya, 16, 32 (1964).
9. Kh. D. Androsenko and G. N. Smirenkin, Pribory i tekhnika éksperimenta, No. 5, 64 (1962).
10. Yu. A. Egorov and E. A. Panov, Pribory i tekhnika éksperimenta, No. 4, 57 (1961).
11. V. S. Dikarev et al., Atomnaya énergiya, 1, No. 5, 136 (1956).
12. B. I. Sinitsyn and S. G. Tsypin, Atomnaya énergiya, 12, 306 (1962).
13. V. N. Avaev et al., In the Collection: Problems of Reactor Shielding Physics [in Russian], State Press for Atomic Energy, Moscow (1963), p. 193.

STUDY OF THE NEUTRON MODERATION PROCESS IN BERYLLIUM AND BERYLLIUM OXIDE BY A PULSE METHOD

(UDC 621.039.512.4)

I. F. Zhezherun

Translated from Atomnaya Énergiya, Vol. 18, No. 2,
pp. 127-135, February, 1965
Original article submitted November 30, 1963; Revision submitted February 29, 1964

The moderation time was measured for neutrons up to energies of 1.46, 0.3, 0.178, and 0.0976 eV and also the thermalization time below an energy of ~ 0.1 eV. The time distribution of moderated neutrons was obtained to an energy of 0.3 eV. The measurements made it possible to calculate the correction for moderation of neutrons over the energy range below 1.46 eV and to obtain the square of the moderation length of fission neutrons at various energies close to the thermal region.

The square of the moderation length L_f^2 for the majority of moderators used in nuclear technology has been measured up to an energy of 1.46 eV (indium resonance). A correction for the moderation of neutrons to thermal energy is interpolated by a numerical method and usually contains a significant indeterminacy due primarily to the fact that the average logarithmic energy loss ξ in this region is unknown. The measurement of L_f^2 down to lower energies has been carried out only for beryllium oxide to 0.3 eV (Pu^{239} resonance) [1].

The neutron moderation time and its fluctuations have been studied theoretically in a number of papers [2-6]. Interesting results are given in the paper by I. G. Dyad'kin and É. P. Batalina [7] who considered the time dependence of the space-energy distribution of neutrons N(r, u, t) on a pulsed source having an initial velocity v_0. They found that at distances from the source $r \leq \lambda u\beta$ (where λ is the scattering length, u is the lethargy, and β is a constant of order unity)

$$N(r, u, t) = \frac{\xi v}{\lambda} N_{st}(r, u) N_0(u, t) [1 + \varepsilon(r, u, t)], \quad (1)$$

i. e., the space-energy (stationary) distribution $N_{st}(r, u)$ is derived by the energy-time distribution $N_0(u, t)$, where

$$N_0(u, t) = \frac{\left(1 - \frac{v}{v_0}\right)^{\frac{2}{\xi}-1}}{\xi} \cdot \frac{\left(\frac{vt}{\lambda}\right)^{\frac{2}{\xi}} e^{-\frac{vt}{\lambda}}}{\Gamma\left(1 + \frac{2}{\xi}\right)} \quad (2)$$

for $t > \lambda/(v_0 - v)$.

Thus, the time distribution of neutrons having a velocity v agrees with a Poisson probability for the appearance of $2/\xi$ neutrons after a time t for conditions that the probability of appearance of neutrons at any instant is identical and equal to $(v/\lambda)dt$.

It should be noted that $N_0(u, t)$ is almost independent of the initial neutron velocity v_0 and attains a maximum at the instant

$$t_{max} \approx \frac{2\lambda}{v\xi} \left\{\left(2 - \frac{\beta u}{\sqrt{r^2 + \beta^2 u^2}}\right)\left[1 - \frac{2\alpha}{3}\left(1 - \frac{\beta u}{\sqrt{r^2 + \beta^2 u^2}}\right)\right]^{-1}\right\}, \quad (3)$$

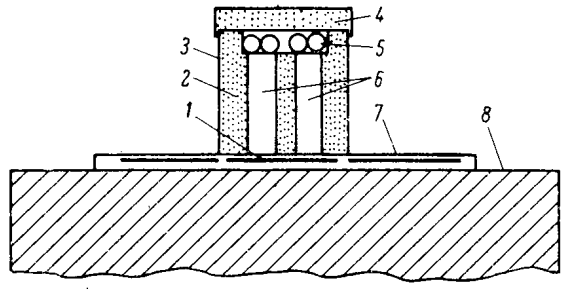

Fig. 1. Geometry of the experiment for measuring the transmissivity of boron filters (transverse section): 1) filter; 2) boron carbide collimator; 3) cadmium sheath; 4) counter shielding screen; 5) BF_3 cpimters; 6) collimator ports; 7) collimator mounting (or support); 8) moderator block. The block shielding (Cd and B_4C) is not shown.

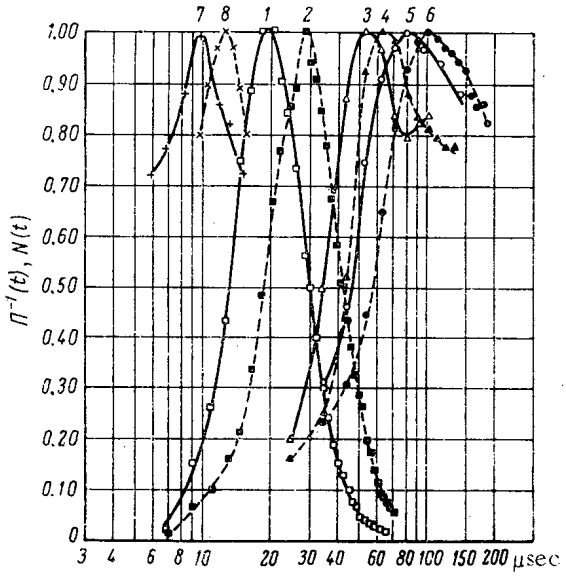

Fig. 2. Moderation time measurement results: 1, 2) count rate N(t) of the 0.3-eV neutron detector in the block of Be and BeO respectively; 3, 4) reciprocal transmissivity $\Pi^{-1}(t)$ of the cadmium filter in Be and BeO; 5, 6) the same for the samarium oxide filter; 7, 8) the same for the indium filter. All curves are normalized to unity at the maximum.

somewhat depending on r (α is a very slowly changing function of u). The additional weak dependence of N(r, u, t) on time is contained in the term $[1 + \varepsilon(r, u, t)]$, which however differs little from unity for $t \approx t_{max} \pm \Delta t$, where Δt is the dispersion of t_{max}; t_{max} is the average moderation time of neutrons having a velocity v. The moderation time at a velocity v, obviously, will be equal to $t_m = t_{max} - \lambda/v$.

One paper [8] and two notes [9, 10] are known in which t_m is measured in water down to thermal energies; in two other papers $t_m \approx 160$ μsec is derived for graphite [11] and $t_m = 230 \pm 30$ μsec for beryllium oxide [12]. The inadequacy of these papers is that it is not defined precisely in them to what energy the stated values for t_m should be related.

Some projects have been devoted to the study of the last stages of moderation—the establishment of the equilibrium spectrum—using a pulsed neutron source. Of the theoretical reports we shall refer only to [13], in which the relationship was found between the coefficient of diffusion cooling C and the thermalization time without using the concept of neutron temperature, and the possibility is shown of determining t_{th} experimentally by measuring the damping decrement of the first harmonic in a similar manner as the diffission coefficient is determined from the damping decrement of the zero harmonic. The experimental reports [12, 14-16] should be mentioned, in which t_{th} was measured in beryllium oxide with a density of 2.96 g/cm^3 by various methods (transmission of a filter of a 1/v absorber, measurement of the coefficient of diffusion cooling, etc.) and a value was obtained of $t_{th} = 165 \pm 10$ μsec. For beryllium (density 1.79 g/cm^3), the approximate value of $t_{th} = 172$ μsec is given in [17], found from measurement of the coefficient of diffusion cooling.

In the present project, the moderation time was measured down to various energies $E \leq 1.46$ eV, and also the thermalization time in beryllium and sintered beryllium oxide. The results of the measurements permitted data to be obtained concerning the moderation length of neutrons in Be and BeO below 1.46 eV.

Measurement Procedure

The neutron moderation time was determined by measuring the transmissivity $\Pi(t)$ of filters with a strong resonance in the absorption cross section as a function of the time t elapsed from the instant of the neutron pulse. One of the beams from the linear accelerator at the I. V. Kurchatov Institute of Atomic Energy [18] was used as a pulsed neutron source. The pulse duration was 0.5-1 μsec and the pulse repetition frequency was 50-100 cps. The filters were in the shape of a cylinder and were attached to a small cylindrical BF_3 counter, inserted in the moderator block. Filters were used of 0.073 g/cm^2 indium, 0.086 g/cm^2 cadmium and 0.047 g/cm^2 samarium oxide, which have resonances at 1.46, 0.178, and 0.0976 eV respectively. In addition to the filters, a pulse detector for neutrons with energy 0.3 eV was used (a plutonium chamber enclosed in a screen of a mixture of samarium and gadolinium oxides) [19], which was shown to be very convenient for measuring not only t_m but also for measuring the time distribution $N_0(u, t)$.

TABLE 1. Measured and Calculated Values of the Moderation Time at Different Energies, μsec

Resonance energy, eV	In beryllium		In beryllium oxide	
	calculation	experiment	calculation	experiment
1.46 (Indium)	7.2	7.5 ± 1	9.3	9.5 ± 1
0.3 (Plutonium)	15.7	17.5 ± 1	19.2	26 ± 2
0.178 (Cadmium)	20.4	40 ± 3	26.3	51 ± 3
0.0976 (Samarium)	27.6	73 ± 5	34.3	88 ± 5

The detectors were positioned on the axis of the moderator block, coincident with the axis of the beam. By changing the position of a detector along the axis, the relationship could also be investigated between t_m and the distance r to the neutron source. The mean density of the material in the beryllium and beryllium oxide blocks was 1.79 g/cm^3 respectively.

The thermalization time was determined by measuring the transmissivity $\Pi(t)$ of plane boron filters containing 0.012 and 0.023 g/cm^2 of boron. The filters, with dimensions 12 x 30 cm, were inserted in slits below the neutron collimator located at the moderator block (Fig. 1). The collimator was made of cadmium and boron carbide and had ports with a diameter of 35 mm and a height of 120 mm. Above the collimator were located four $B^{10}F_3$ counters connected in parallel, with a diameter of 20 mm and length 25 cm. The counters were screened by cadmium, boron carbide and paraffin so that neutrons from the moderator block could only strike them through the ports of the collimator at an angle > 80° to the surface of the block. The distance between the block and the counters was equal to 15 cm.

The moderator blocks were in the shape of a cube or a parallelipiped with dimensions 60 x 60 x 60 and 50 x 50 x 50 cm for beryllium, and 80 x 70 x 75 and 60 x 60 x 60 cm for beryllium oxide; they were covered on all sides by a layer of cadmium (0.86 g/cm^2) and boron carbide (5 g/cm^2). Data concerning the diffusion parameters of these materials are given in [17, 20].

The counting rate of the counters with and without filters as a function of time, from which the transmissivity $\Pi(t)$ was determined, were measured by means of a time analyzer, used in [17, 20] and also a 110-channel analyzer, with a minimum channel width of 1 μsec. The source strength was controlled by two monitors. The background (which did not exceed 1% of the effect) was determined by the count rate at the instant of time immediately prior to the neutron pulse.

Measurement Results and Discussion

Moderation Time. The results of measurement of the moderation time are shown on a semilog scale in Fig. 2. For beryllium these measurements were carried out in the block with dimensions 50 x 50 x 50 cm and for beryllium oxide in the blocks with dimensions 80 x 70 x 75 and 60 x 60 x 60 cm. The time elapsed from the instant of the neutrons pulse is plotted along the x axis and along the y axis is plotted the count rate N(t) of the resonance detector of 0.3-eV neutrons and the reciprocal transmissivity $\Pi^{-1}(t)$ for the resonance filters. The time corresponding to the maximum is equal, obviously, to the moderation time t_m to a given energy plus the time of flight of the neutron from the site of the last collision up to absorption in the detector $t_{fl} = [\lambda(v) + \frac{1}{2}d]/v$ (d is the average cross section of the detector, taking account of the void at the place where it is located) and the time of flight from the accelerator target to the block (~ 0.5 μsec).

The values obtained for t_m are given in Table 1. The errors shown (from 1 to 10 μsec in different measurements) are associated with the finite width of the channel and the inaccuracy in calculating t_{fl}. For comparison, the values are given for t_m obtained in accordance with formula (3) on the assumption that the factor in the curly brackets, which takes into account the relationship between t_{max} and the distance r to the source, is equal to unity. Under our conditions, the sources are obviously the sites of the primary collisions of the neutrons from the beam with the moderator nuclei, which are located in a plane layer of the front face of the moderator block with a thickness of about $2\lambda(v_0) \approx 5$-7 cm. The measurements with the 0.3-eV neutron detector in the blocks at various distances ($r \leq 30$ cm) from this layer did not indicate a dependence of t_m on r, which justifies the assumption made above.

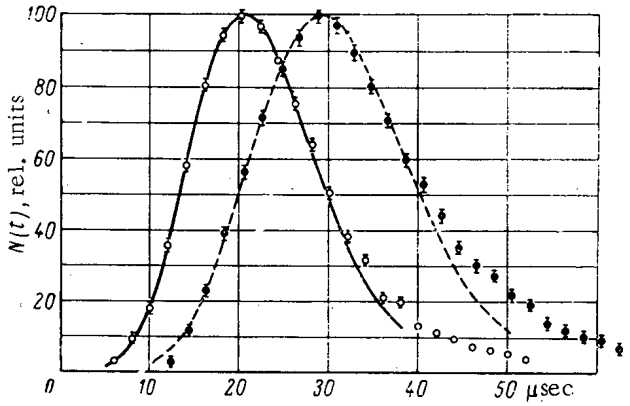

Fig. 3. Comparison of the experimental time distribution of neutrons with energy 0.3 eV with the Poisson distribution: ○) beryllium; ●) beryllium oxide.

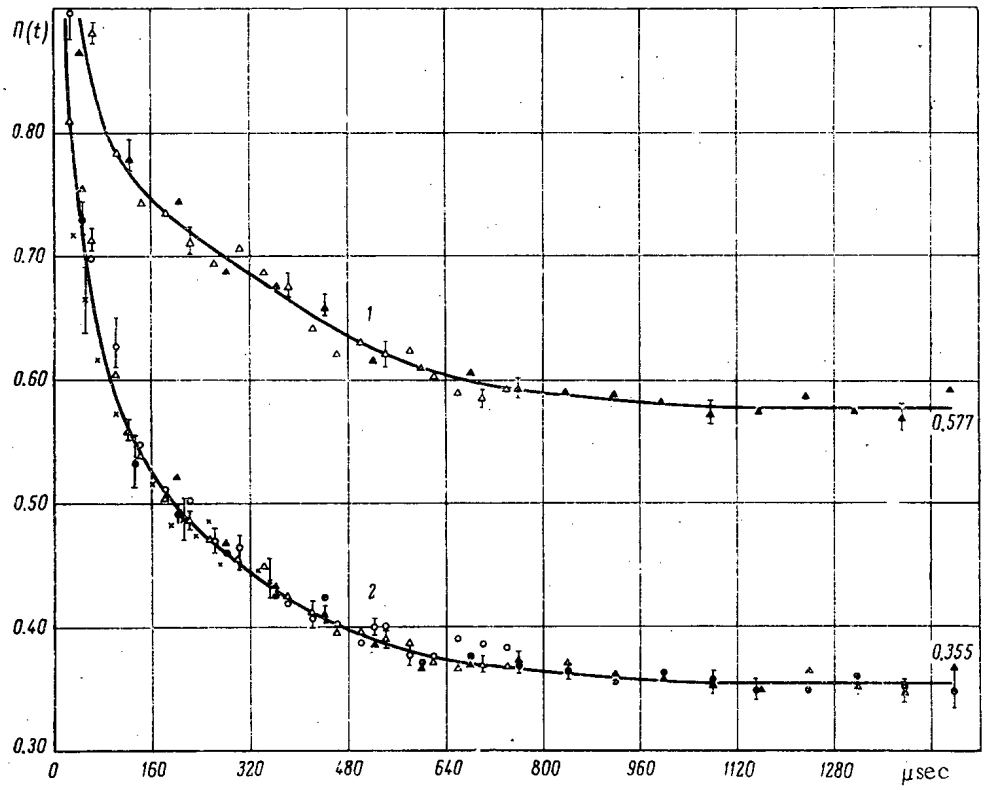

Fig. 4a. Transmissivity of boron filters for blocks of beryllium. The curves are derived visually according to experimental points from different measurement series: 1, 2) for filters containing 0.012 and 0.023 g/cm^2 of boron respectively.

The values for t_m shown in Table 1 will be valid also for fission neutrons, since the spectrum of accelerator neutrons is close to the fission neutron spectrum. It can be seen from the table that for energies less than 1.46 eV the experimental value of t_m is greater than the calculated value. This is obviously associated with the fact that ξ in this region is lower than the value of ξ for collisions with a free atom.

The measurements made with the 0.3 eV neutron detector make it possible to compare the experimental distribution $N_0(u, t)$ with the theoretical distribution [see formula (2)]. Figure 3 shows the experimental data for beryllium and beryllium oxide and the matched (according to experimental data) Poisson distributions for $N_0(u, t) \approx \left(\frac{vt}{\lambda}\right)^{\frac{2}{\xi}} e^{-\frac{vt}{\lambda}}$ with $2/\xi = 12$ for beryllium (continuous line) and $2/\xi = 18$ for beryllium oxide (dashed line).

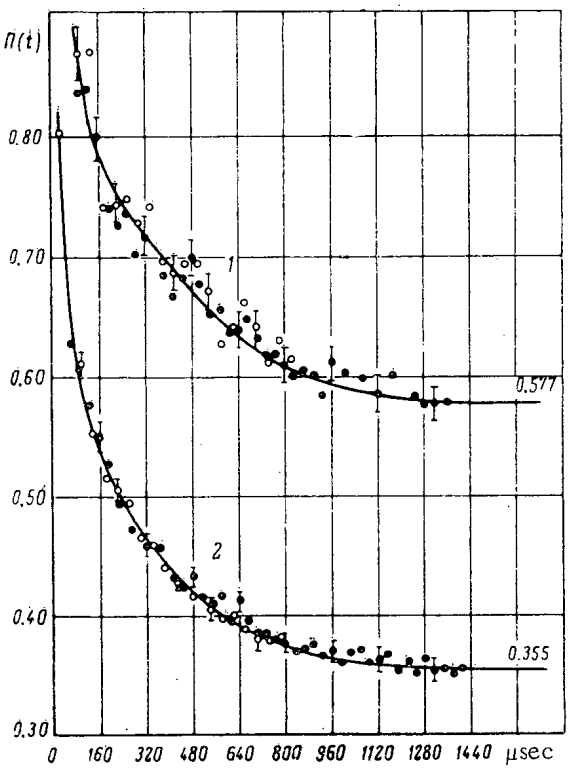

Fig. 4b. Transmissivity of boron filters for blocks of BeO (for legend see Fig. 4a).

It can be seen that they agree well. The divergence is noticeable only at large values of t, which is associated, obviously, with the effect of the term in the square in formula (1) (see [7]). By using the fact that in a Poisson distribution the dispersion is equal to the mean value, it is possiblt to obtain also from the relationships $(vt_{max}/\lambda)_{Be} = 12 = 2/\xi_{Be}$ and $(vt_{max}/\lambda)_{BeO} = 18 = 2/\xi_{BeO}$ the moderation time t_m to an energy of 0.3 eV for beryllium and beryllium oxide. For this it is necessary to subtract from t_{max} the dispersion due to the width of the energy sensitivity region of the detector [19], equal to $\Delta t = 1/2 \cdot (\Delta E/E) t_m$ (2.9 and 4.3 μsec for beryllium and beryllium oxide respectively), and also the time of flight at an energy of 0.3 eV. As a result, we obtain a value for t_m equal to 17.3 μsec for beryllium and 28 μsec for beryllium oxide, which is in agreement with the values found according to the position of the maximum. The average logarithmic energy losses at an energy of 0.3 eV are as follows:

$$\xi_{Be} = 0.19, \quad \xi_{BeO} = 0.12.$$

Thermalization Time. The results of measuring Π(t) for the boron filters are shown in Fig. 4 for blocks of beryllium (60 × 60 × 60 cm) and beryllium oxide (80 × 70 × 75 cm). It follows from the figures that for a time t ≥ 1200 μsec in beryllium and t ≥ 1400 μsec in BeO, the transmissivity attains a minimum asymptotic value corresponding to the established neutron spectrum. The asymptotic values have been measured with a high degree of accuracy and have been shown to be identical for beryllium and beryllium oxide, as would be expected: 0.577 ± 0.003 and 0.355 ± 0.002 for filters containing 0.012 and 0.023 g/cm² of boron respectively.

Similar transmission curves were obtained also for blocks of smaller dimensions with a somewhat smaller asymptotic transmission. Thus, for a beryllium block with dimensions 50 × 50 × 50 cm it was found to be 0.0568 ± 0.008 and 0.346 ± 0.002 respectively.

In order to obtain data concerning the neutron energies from the transmissivity Π(t), it was assumed that the neutron spectrum has a Maxwellian distribution with temperature

$$T(t) = T_e + Ae^{-\gamma t}, \tag{4}$$

where γ^{-1} is the thermalization time in the given moderator block; T_e is the equilibrium temperature under room conditions. Taking into account the spectral deformation due to the flight distance l, we obtain an expression for the transmissivity value

$$\Pi[T(t)] = \frac{\int_0^\infty \frac{E\,dE}{\sigma_{tr}(E)} \left\{T_e + [T(t) - T_e]\, e^{-\frac{a}{\sqrt{E}}}\right\}^{-1} e^{-\frac{E}{T_e + [T(t)-T_e]\, e^{-\frac{a}{\sqrt{E}}}}} \left(1 - e^{-\frac{b}{\sqrt{E}}}\right) e^{-\frac{c}{\sqrt{E}}}}{\int_0^\infty \frac{E\,dE}{\sigma_{tr}(E)} \left\{T_e + [T(t) - T_e]\, e^{-\frac{a}{\sqrt{E}}}\right\}^{-1} e^{-\frac{E}{T_e + [T(t)-T_e]\, e^{-\frac{a}{\sqrt{E}}}}} \left(1 - e^{-\frac{b}{\sqrt{E}}}\right)}. \tag{5}$$

Here $a \equiv \gamma l (KT_0)^{1/2}/v_b$, and v_b is the most probable velocity corresponding to $T_0 = 293°K$; b and c are constants defined by the structure of the detector and by the thickness of boron filter respectively; and $\sigma_{tr}(E)$ is the transport cross section of the moderator material.

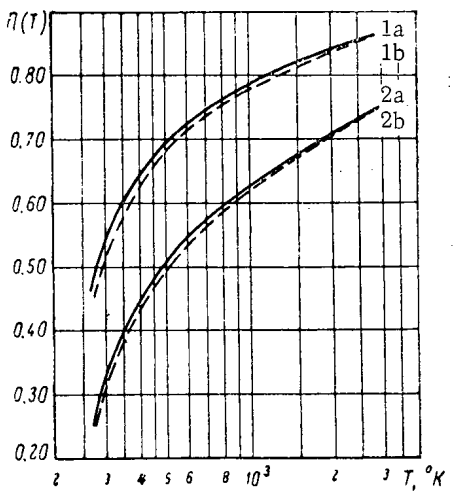

Fig. 5. Relationship between the transmissivity of boron filters and the neutron temperature for beryllium: 1a, 2a) for filters containing respectively 0.012 and 0.023 g/cm^2 boron, using $\sigma_{tr}(E)$ according to the calculated data from [21]; 1b, 2b) by substitution of $\sigma_{tr}(E)$ with the experimental data for $\sigma_s(E)$ [22].

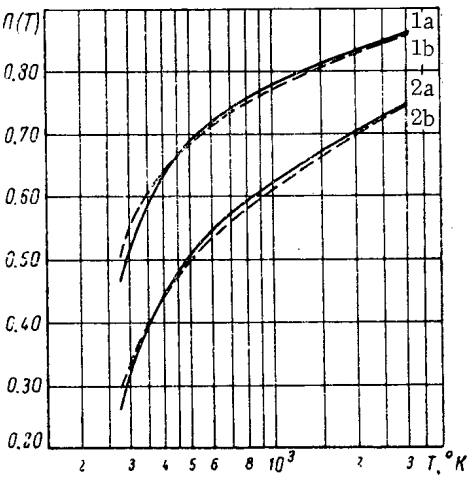

Fig. 6. Relationship between the transmissivity of boron filters and the neutron temperature for beryllium oxide: 1a, 2a) for filters containing respectively 0.012 and 0.023 g/cm^2 boron, using $\sigma_{tr}(E)$ according to the calculated data from [22]; 1b, 2b) by substitution of $\sigma_{tr}(E)$ with the experimental data for $\sigma_s(E)$ for a sample with a crystalline grain size of 13 μ [23].

The function $\Pi(T)$ was evaluated on an electronic computer over the range of temperatures from T_e to 3000°K, for which the value of T_e in the block (taking account of diffusion cooling) was taken equal to 285°K. The thermalization time γ^{-1}, which appears in formula (5) and which was not known previously, was assumed equal to 120 and 170 μsec. The results of a calculation of $\Pi(T)$ are shown in Figs. 5 and 6 for γ^{-1} = 170 μsec using calculated values of $\sigma_{tr}(E)$ [21] and experimental values of $\sigma_s(E)$ from the data in [22, 23]. From the plots of these curves and by the measured values of the transmissivity (the smooth curves of Figs. 4a and 4b), the relationship was obtained between the temperature T(t) and the time elapsed from the instant of the neutron pulse (Figs. 7 and 8). The equilibrium temperature T_e for neutrons emitted from the block was found to be somewhat different, exceeding T_e inside the block by 20-40°K (in accordance, with theoretical predictions [24]). The slope of the linear part of the curves, determining the thermalization time γ^{-1}, are almost independent of whether $\sigma_{tr}(E)$ or $\sigma_s(E)$ is used for the calculation of $\Pi(T)$, and gives γ^{-1} equal to 178 ± 25 and 213 ± 30 μsec respectively for a block of beryllium (60 × 60 × 60 cm) and beryllium oxide (80 × 70 × 75 cm). For blocks of smaller dimensions the values obtained for γ^{-1} were: 170 ± 30 μsec for Be (50 × 50 × 50 cm) and 177 ± 40 μsec for BeO (60 × 60 × 60 cm).

The value of t_m for an infinite medium was calculated by the formula

$$t_{th}^{-1} = \gamma - \frac{1}{3} DB^2, \qquad (6)$$

where D is the diffusion coefficient; B^2 is a geometrical parameter of the block which takes into account the small correction to γ^{-1} in those cases when this value does not agree with that assumed in calculations of $\Pi(T)$. It can be estimated via $\Pi(T)$ for γ^{-1} equal to 120 and 170 μsec. Using D for Be and BeO according to the data from [17, 20] and averaging consistent values of t_{th} with respect to the values measured in blocks of various dimensions, we obtain t_{th} = 185 ± 20 μsec for beryllium and t_{th} = 204 ± 25 μsec for beryllium oxide.

The value of t_{th} for Be agrees with the value obtained from measurements of the diffusion parameters equal to 172 μsec [17]. There is no such agreement for BeO. Having calculated t_{th} for BeO at a density of 2.96 g/cm^2 we obtain 200 ± 25 μsec; according to the measurements in [12, 14, 15], t_{th} = 165 ± 10 μsec. It cannot be excluded that this discrepancy (within the limits of measurement errors) is associated with a difference in the crystal structure of the materials.

The crystal structure of the beryllium and beryllium oxide which we used was not investigated. Therefore it is not clear which of the available data for $\sigma_s(E)$ for various grain sizes should be used for calculating $\Pi(T)$. Calculation variants for a minimum (8 μ) showed, however, that t_{th} may differ by approximately 5% and increases with increase of grain size. Thus, an inaccuracy in calculating $\Pi(T)$ by formula (5) has a weak effect on the value of t_{th}, measured by the transmissivity method, but has a considerable effect on T_e and the quantity A [see formula (4)], i. e., on the maximum temperature $T_{max} = T_e + A$ at which a neutron distribution close to

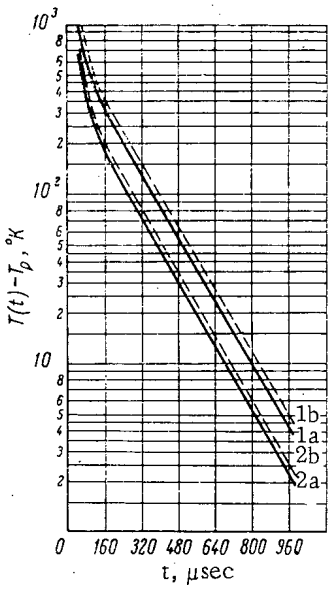

Fig. 7. Relationship between neutron temperature and the time elapsed from the instant of the pulse, for a beryllium block. Curves 1a, 1b, 2a, 2b are obtained by the corresponding curves of Fig. 5.

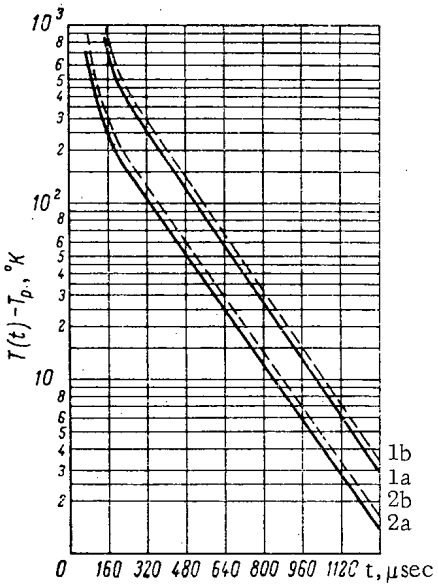

Fig. 8. Relationship between neutron temperature and time for a block of beryllium oxide. Curves 1a, 1b, 2a, 2b are obtained by the corresponding curves of Fig. 6.

Maxwellian is established. It can be seen from Fig. 7 and 8 that the quantity A also depends on the thickness of the boron filter. This may serve as a pointer to the fact that there is indeed no precise Maxwellian distribution. In all the graphs, however, T_{max} does not exceed 700°K. For the curves 2a, and 2b (see Fig. 7 and 8) it can be approximately established that $T_{max} = T_e + A \approx 520$°K ($\sim 0.045$ eV) and that this temperature is attained at 190 μsec for Be and 215 μsec for BeO. By calculating the time of flight of neutrons with an energy of 0.045 eV from the site of the last collision to the detector, equal to 55 μsec, we can obtain approximately t_m up to this energy: 135 μsec for Be and 160 μsec for BeO.

The measured values of t_{th} for Be and BeO are close to the experimental values of t_{th} for other materials: 185 ± 45 μsec [25] and 207 ± 23 μsec [11] for graphite, 130 ± 16 μsec and 194 ± 32 μsec for zirconium hydride (measured by various methods) [26].

The Mean Square Neutron Moderation Length in the Region of Energies Below 1.46 eV. It has already been mentioned earlier that at energies less than 1.46 eV the experimental values of t_m are greater than the calculated values. This, obviously, is due to a reduction of the average logarithmic loss of energy because of the atom bonds within the crystalline lattice. We shall attempt to apply the measured values of t_m in order to estimate ξ and the area of moderation below 1.46 eV.

The moderation time of a neutron from an energy E_1 to E_2, obviously, can be represented as a sum with respect to collisions

$$t_{m2} - t_{m1} = \sum_n \frac{\lambda_i}{v_i}, \qquad (7)$$

where λ_i is the scattering mean free path of a neutron having a velocity v_i. Within the interval 1.46–0.1 eV, the values of λ_i are constant and equal to 1.39 and 1.46 cm respectively for Be and BeO. We shall assume that over the small interval E_1–E_2 is also unchanged, i. e., that $v_{i+1}/v_i = \exp(-\xi/2)$. The formula (7) assumes the form

$$t_{m2} - t_{m1} = \frac{\lambda}{v_2} \cdot \frac{\sqrt{\frac{E_2}{E_1}} - 1}{1 - e^{\xi/2}} \qquad (7')$$

Substituting in this formula the measured values of t_m, we obtain the following values of ξ for moderation below 1.46 eV:

a) within the interval 1.46–0.3 eV: 0.193 ± 0.004 for Be and 0.019 ± 0.012 for BeO;

b) within the interval 0.3–0.178 eV: 0.048 ± 0.008 for Be and 0.047 ± 0.007 for BeO;

c) within the interval 0.178–0.0976 eV: 0.050 ± 0.009 for Be and 0.047 ± 0.007 for BeO;

d) within the interval 0.0976–0.045 eV (approximate estimate): 0.048 for Be and 0.044 for BeO.

Thus, ξ for Be and BeO at energies below 0.3 eV is effectively unchanged. Therefore, within the interval 0.3–0.0976 eV we obtain a more accurate value for ξ: 0.049 ± 0.005 for Be and 0.047 ± 0.005 for BeO. Within the interval 1.46–0.3 eV formula (7') gives only approximate values for ξ, especially for BeO.

TABLE 2. Moderation Time and Neutron Mean Square Moderation Length L_f^2 up to an Energy of $E \leq 1.46$ eV in Beryllium and Beryllium Oxide

Energy interval	Be (density 1.79 g/cm³)		BeO (density 2.79 g/cm³)	
	t_m, μsec	L_f^{2*}, cm²	t_m, μsec	L_f^2, cm²
~2 eV — 1.46 eV	7.5±1	85.8±2.1 [28]	9.5±1	92±1.5 [1]
~2 eV — 0.3 eV	17.5±1	91.5±2.4	27±2	103.4±1.9
~2 eV — 0.078 eV	40±3	98.9±2.6	51±3	112.1±2.1
~2 eV — 0.13 eV	56±5 †	103.4±2.7	69±4 †	117.7±2.4
~2 eV — 0.0976 eV	73±5	107.5±2.9	88±5	122.5±2.9
~2 eV — 0.07—0.045 eV	~135	—	~160	—
~0.07—0.045 eV — 0.025 eV	185±20	—	204±25	—

*The values of L_f^2 are given with the corrections calculated in the present paper.
†Calculated by formula (7) using the values obtained over the range 0.3—0.0976 eV.

In the region where formula (4) is valid, it is easy to obtain that

$$\xi = \frac{\lambda}{v_e t_{th}} \sqrt{\frac{E_e}{E}} \cdot \frac{E - E_e}{E}. \tag{8}$$

Hence it can be seen that as E approximates to E_e, ξ is decreased, and at $E = E_e$ it vanishes. Some authors characterize the last stage of moderation by the quantity $\lambda/(v_e \cdot t_{th})$, which is eaual to 0.034 for Be and 0.031 for BeO (v_e corresponds to an energy $E_e = kT_e$).

Now, by using the values obtained for ξ, the correction can be calculated to the experimentally measured value of L_f^2 up to an energy of 1.46 eV by the well-known relationship

$$L_f^2(E_1 \to E_2) = \int_{E_2}^{E_1} \frac{D}{\xi \Sigma_s} \cdot \frac{dE}{E} = \frac{D}{\xi} \lambda \ln \frac{E_1}{E_2} \tag{9}$$

(D is equal to 0.50 and 0.54 cm for Be and BeO respectively.) Thus, for example, the value ${}_{Be}L_f^2$ (1.46 → 0.3 eV) = 5.7 ± 1.2 cm²; ${}_{BeO}L_f^2$ (1.46 → 0.3 eV) = 11.4 ± 1.2 cm² are in good agreement with the value of 12.5 ± 2.5 cm² obtained for BeO from direct measurements of L_f^2 up to 1.46 and 0.3 eV [1], which indicates that the accuracy of formula (7') is also acceptable over the interval 1.46—0.3 eV; ${}_{Be}L_f^2$ (0.3 → 0.178 eV) = 7.4 ± 0.8 cm²; ${}_{BeO}L_f^2$ (0.3 → 0.178 eV) = 8.7 ± 0.9 cm²; ${}_{Be}L_f^2$ (0.3 → 0.13 eV) = 11.9 ± 1.2 cm²; ${}_{BeO}L_f^2$ (0.3 → 0.13 eV) = 14.3 ± 1.4 cm² etc. In regions where formula (4) is valid, it is easy to obtain, by using formulas (8) and (9), that

$$L_f^2(E_1 \to E_2) = D v_e t_{th} \left\{ 2 \left(\sqrt{\frac{E_1}{E_e}} - \sqrt{\frac{E_2}{E_e}} \right) + \ln \frac{(\sqrt{E_1} - \sqrt{E_e})(\sqrt{E_2} + \sqrt{E_e})}{(\sqrt{E_1} + \sqrt{E_e})(\sqrt{E_2} - \sqrt{E_e})} \right\}, \tag{10}$$

i. e., for $E_2 \to E_e$, $L_f^2 \to \infty$. The latter result, as already repeatedly mentioned (see, for example [27]), confirms the fact that it is incorrect to assume the value of $E = kT_e$ as the lower limit of the integral in Eq. (9) for calculating the moderation length down to thermal energy.

Conclusions

The measurements carried out indicate that the moderation process for neutrons in beryllium and beryllium oxide up to an energy of 1.46 eV takes place in collisions with free atoms and lasts for a relatively short time, not exceeding 10 μsec (Table 2). Over the interval 1.46-0.3 eV the effect of the atomic bonds in the crystal lattice is already noticeable, especially for BeO. The logarithmic energy loss ξ is reduced on the average by 10% with Be and by 60% with BeO relative to its value for the free atom. The moderation time over this interval is 1 ½ to 2

times greater than t_m up to 1.46 eV. Over the interval from 0.3 to ~ 0.07-0.08 eV (below which a spectrum is established which is close to Maxwellian), ξ for Be and BeO is reduced to ~ 25% of its value for a free atom. The moderation time over this interval is six-seven times greater than t_m up to 1.46 eV. The energy-time distribution of neutrons in the region prior to ~ 0.07 eV can be obtained by formula (2), if the values of ξ given above are substituted in it. Below ~ 0.07-0.045 eV the moderation proceeds very slowly and lasts on an average for 185 ± 20 μsec for beryllium and 204 ± 25 μsec for beryllium oxide.

The value of L_f^2 up to 0.13 eV (5.2 kT_0) given in Table 2 for beryllium is somewhat greater (for scaling at a density of 1.84 g/cm^3) than the value of the Fermi age given in [29], in which the lower limit in the integral of Eq. (9), in accordance with thermalization theory, is assumed equal to 5.2 kT_0. The value of L_f^2 up to 0.3 eV for BeO is in good agreement with the value of 104.5 ± 2 cm^2, obtained by direct measurements of L_f^2 up to an energy of 0.3 eV for the same for beryllium oxide.

In conclusion, the authors express their thanks to the operating personnel of the accelerator in the beam of which the measurements were carried out, to M. P. Shustov for the numerical calculations, to A. A. Osochnikov and G. V. Yakovlev for assistance in maintaining the analyzers and to Yu. D. Kurdyumov and G. P. Perov for assitance with the measurements.

LITERATURE CITED

1. I. F. Zhezherun et al., Atomnaya énergiya, 13, 258 (1962).
2. J. Sykes, J. Nucl. Energy, 2, 31 (1955).
3. G. Hayneman and M. Crouch, Nucl. Sci. and Engng., 2, 626 (1957).
4. J. Waller, Proc. of the Second. Intern. Conf. on the Peaceful Uses of Atomic Energy, Geneva, Unit. Nat., Vol. 16 (1958), p. 450.
5. L. Pol and G. Nemeth, Nucleonik, 1, 165 (1959).
6. G. Kosaly and G. Nemeth, Ditto, p. 225.
7. I. G. Dyad'kin and E. P. Batalina, Atomnaya énergiya, 10, 5 (1961).
8. M. F. Krouch, Nucl. Sci. and Engng., 2, 631 (1957).
9. J. De Juner, Nucl. Sci. and Engng., 9, 408 (1961).
10. E. Moller and N. Sjostrend, Nucl. Sci. and Engng., 15, 2 (1963).
11. A. V. Antonov, Trudy fizicheskogo instituta im. Lebedava, 14, 147 (1962).
12. S. Iyenger et al., Proc. Indian Acad. Sci. A, 45, 215 (1957).
13. S. N. Purohit, Nucl. Sci. and Engng., 9, 157 (1961).
14. R. Ramanna, Cf. [4], p. 315.
15. V. A. Couhall et al., Ditto, p. 319.
16. S. Iyenger et al., Proc. Indian Acad. Sci. A, 45, 224 (1957).
17. I. F. Zhezherun, Atomnaya énergiya, 16, 224 (1964).
18. R. M. Voronkov et al., Atomnaya énergiya, 13, 327 (1962).
19. I. F. Zhezherun, I. P. Sadikov, and A. A. Chernyshov, Pribory i tekhnika eksperimenta, No. 3, 43 (1962).
20. I. F. Zhezherun, Atomnaya énergiya, 14, 193 (1963).
21. K. Singvi and L. Kokhari, In the book: "Proceedings of the Second International Conference on the Peaceful Uses of Atomic Energy, Geneva, 1958," Collected Reports of Foreign Scientists, Vol. 2, Moscow, Atomizdat [in Russian] (1959), p. 675.
22. J. Yuz and R. Schwartz, Atlas of Neutron Cross Sections, Izd. IL, Moscow, Atomizdat [Russian translation] (1959).
23. I. F. Zhezherun, I. P. Sadikov, and A. A. Chernyshov, Atomnaya énergiya, 13, 250 (1962).
24. K. Singwi, Arkov fys., 16, 385 (1959).
25. K. Beckurst, Nucl. Sci. and Engng., 2, 516 (1957).
26. J. Meadows and J. Whalen, Nucl. Sci. and Engng., 13, 230 (1961).
27. E. Cohen, In the book: "Experimental Reactors and Reactor Physics," (Reports of Foreign Scientists at the International Conference on the Peaceful Uses of Atomic Energy, Geneva, 1955), Moscow, Gostekhteorizdat [in Russian] (1956), p. 257.
28. J. Yuz, Neutron Research on Nuclear Reactors [Russian translation], Izd. IL (1954), p. 161.
29. L. Weinberg and E. Wigner, Physical Theory of Nuclear Reactors [Russian translation], Moscow, Izd. IL (1961), p. 310.

EXPERIMENTAL INVESTIGATIONS OF SHIELDS ON THE RIZ STAND

(UDC 621.039.538.7)

S. P. Belov, V. A. Dulin, Yu. A. Kazanskii,
V. I. Popov, and S. G. Tsypin

Translated from Atomnaya Énergiya, Vol. 18, No. 2,
pp. 136-140, February, 1965
Original article submitted April 2, 1964

The present article describes a stand with a zero-power reactor designed for investigating the processes occurring in that part of the shield which is in close contact with the reactor core. If the processes occurring in this part of the shield (formation of the neutron spectrum and generation of strong γ-radiation) are known, the dimensions and the weight of the reactor's entire shield can be properly calculated.

The results obtained in measuring neutron spectra and investigating shielding materials (iron, nickel, and borated nickel) on the stand are given.

Studies of the processes occurring in that part of the shield which is in direct contact with the reactor core are very important, since the neutron spectrum and powerful capture γ-radiation are generated in this part of the shield. These processes basically determine the dimensions and the weight of the entire shield. It is most convenient to investigate experimentally these rather complex problems by means of a zero-power reactor, where the shield under investigation can readily be mounted or dismantled.

The use of a zero-power reactor for investigating secondary γ-radiation is also convenient with regard to the possibility of quickly changing the power level in a wide range, securing good ratios of the background to the effect to be measured, and varying the dimensions and design of the shields under investigation.

For experimental investigations of shielding, we constructed the RIZ stand with a zero-power water-moderated reactor.

In designing the stand, we considered the possibility of varying the emerging neutron spectrum, convenient arrangement of the shielding materials to be investigated, and the performance of experiments. Since the main purpose of the RIZ stand was to investigate the yield of capture γ-radiation and the neutron spectrum, attention was mostly paid to the possibility of securing the optimum ratio of the neutron flux to the γ-radiation at the stand's operating surface.

Description of the Core, the Shielding Screens, and the Control System

The zero-power water-moderated uranium reactor which we use (the prototype of this reactor was developed under the direction of V. A. Kuznetsov) has a cylindrical core with a diameter of 335 mm and a height of 275 mm. The core is filled with distilled water, into which the lattice with the fuel elements is immersed. The fuel elements consist of 90%-enriched uranium dioxide, which is packed in hermetically sealed stainless-steel tubes. Each rod contains 10.5 g U^{235}; the over-all core charge with respect to U^{235} amounts to 3.5 kg.

The lateral shield of the core consists of iron, water, and concrete layers with an over-all thickness of about 130 cm (Fig. 1). The lower shield consists of a mixture of iron and water (60% iron by volume) with an over-all thickness of 35 cm. A shield consisting of a boron carbide layer with a thickness of 4.5 g/cm^2 and a bismuth layer with a thickness of 8.5 cm is provided at the upper end-face of the core; the diameter of this shield is 110 cm; beyond the shield is a ring with a width of 35 cm, which consists of boron carbide (7 g/cm^2) and lead (6.5 cm) (see Fig. 1).

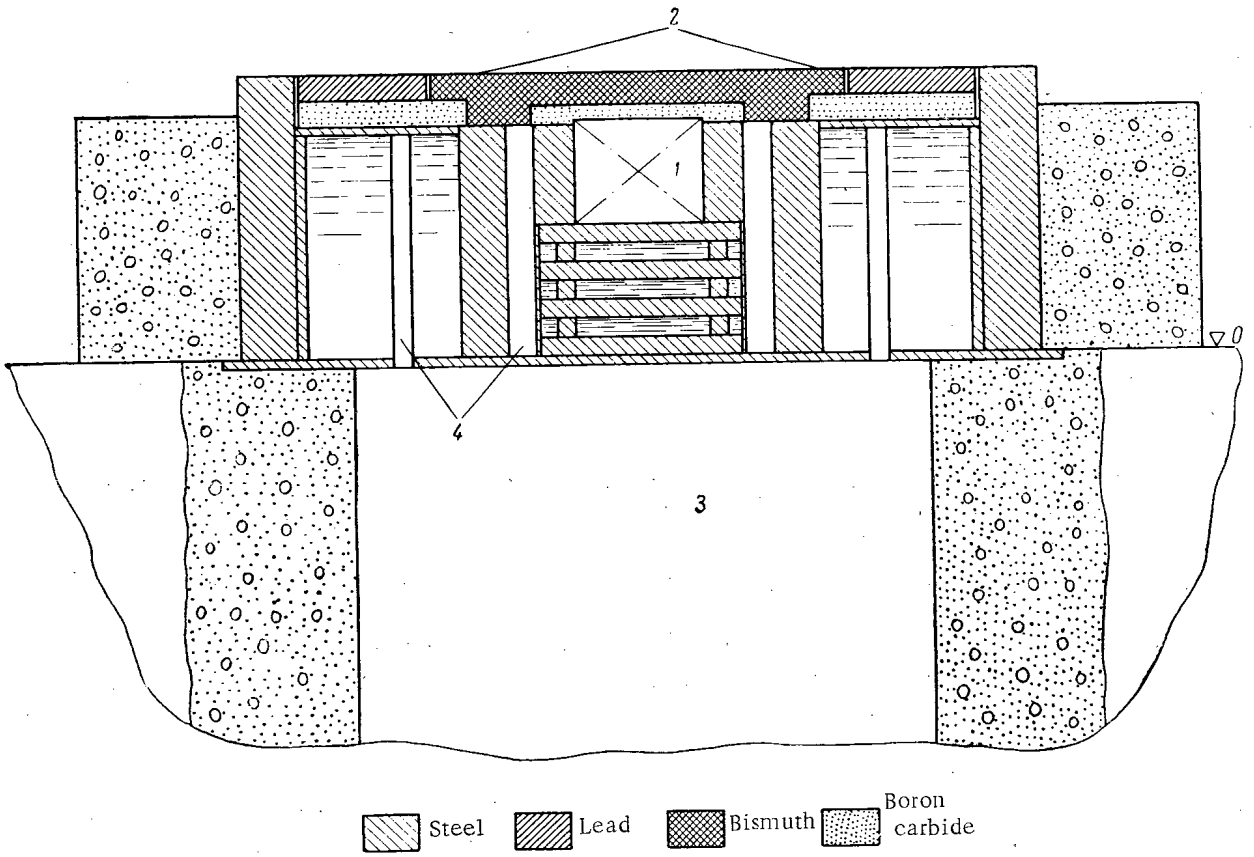

Fig. 1. Schematic diagram of the core and the shielding screens of the RIZ stand reactor. 1) Core; 2) operating surface; 3) room for the control system and shielding; 4) channels for the control equipment detectors.

The purpose of the shield at the upper end-face of the core is:

1) to reduce materially the yield of hard γ-radiation from the core, the structure, and the lateral reflectors and shields;

2) to attenuate the soft portion of the spectrum of neutrons emerging from the core; this task is fulfilled by boron carbide that is located directly at the end-face of the core;

3) to reduce the effect of the shields under investigation on the reactor's reactivity.

Figure 2 shows the external view of the shield and the operating surface of the stand at the reactor's upper end-face.

The reactor is controlled from a room located under the iron-water shield. Boron rods, which are arranged in the core along a diameter of 215 mm, serve as the regulating and emergency rods. Quick draining of water from the core is also provided for the emergency shutdown of the reactor.

The detectors of the control and the emergency equipment (boron-coated chambers and counters filled with boron trifluoride) are located in the water layers of the lateral shield at radii of 32 and 62 cm from the core center. The instruments of the control equipment and of the emergency protection channels are mounted in the control panel room (Fig. 3).

The reactor is equipped with an automatic device for raising the power from the zero level and maintaining it at the assigned level, which is achieved (from the control panel) by means of a remote control system for filling the core with water.

A fission chamber with Th^{232}, which can be moved inside a special channel along the generatrix of the core by means of a remote control device, serves as the monitor of the reactor's power level. This makes it possible to extend the range of counting rate measurements by a factor of 15-20.

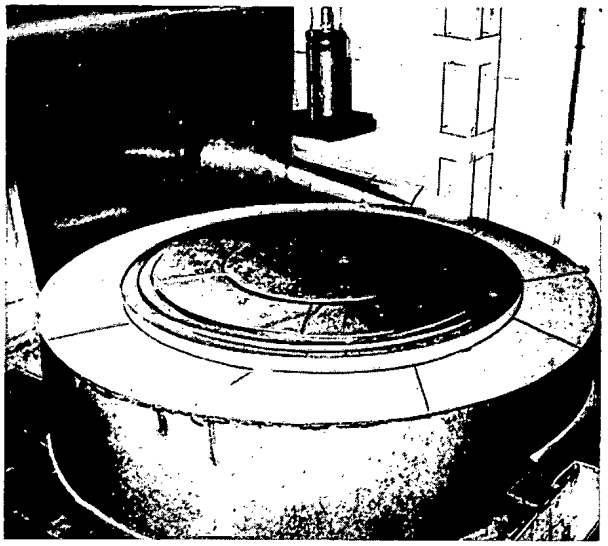

Fig. 2. External view of the shield and the operating surface of the RIZ stand reactor (top view).

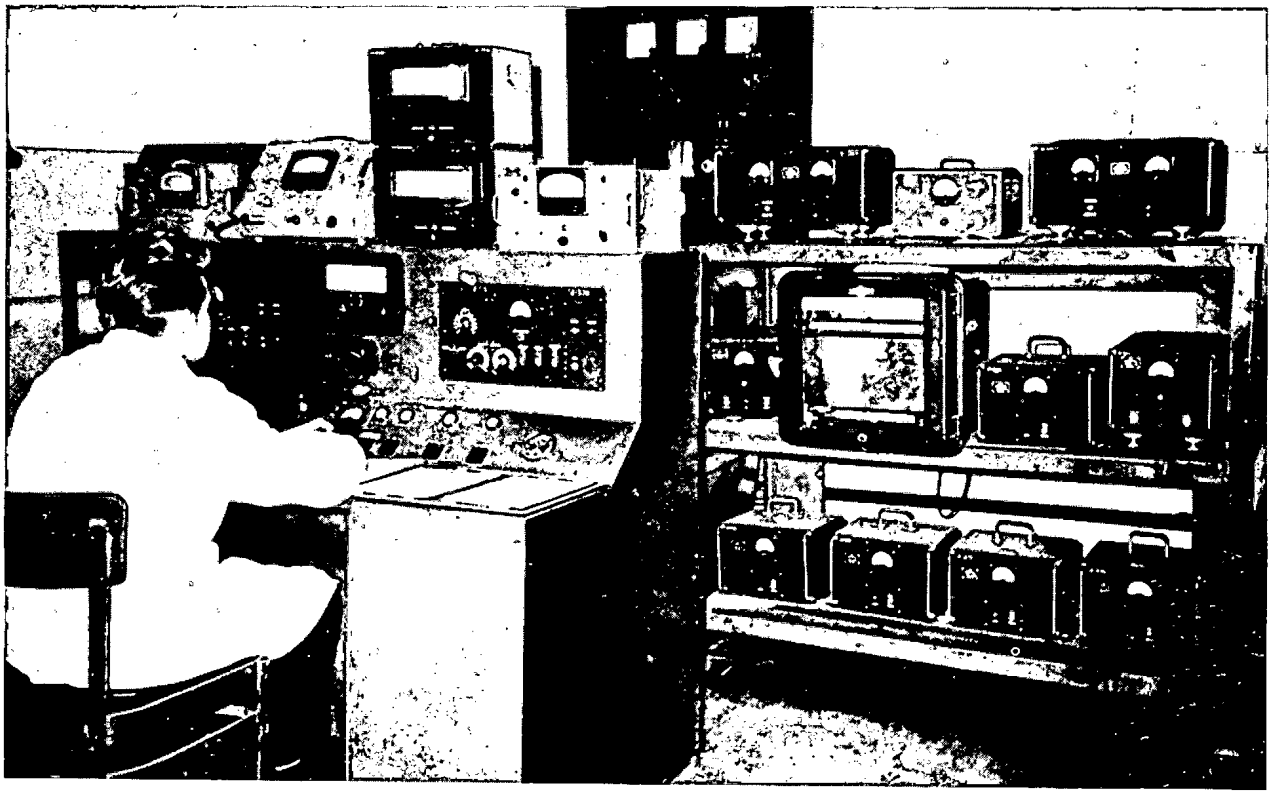

Fig. 3. Control panel of the RIZ stand reactor.

Since the stand is basically used as a source of reactor-spectrum neutrons, and changes in the reactor's physical parameters are connected only with variations in its reactivity as a result of addition of the materials under investigation at the upper end-face, the core is constructed so that excess reactivity does not exceed 0.3% if the core is completely filled with water and the material under investigation is absent. This considerably simplifies the control reactor and enhances its safety.

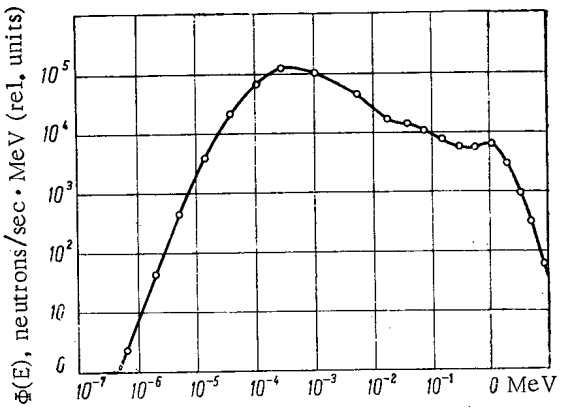

Fig. 4. Calculated spectrum of neutrons emerging from the upper reflector of the RIZ stand reactor.

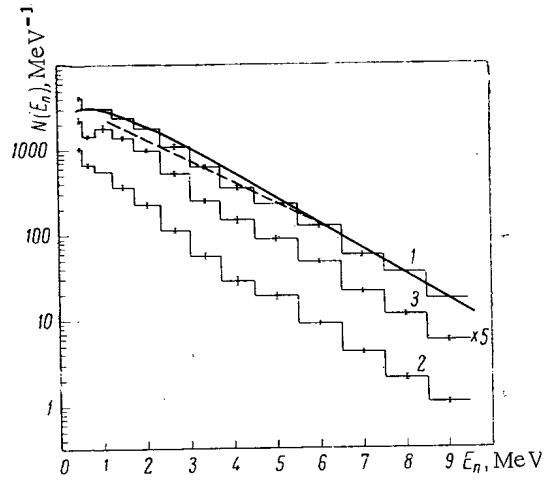

Fig. 5. Fast neutron spectra measured by means of a scintillation spectrometer. 1) At the center of the stand's operating surface; 2) and 3) at distances of 40 cm and 1 m from the center of the stand's operating surface, respectively.

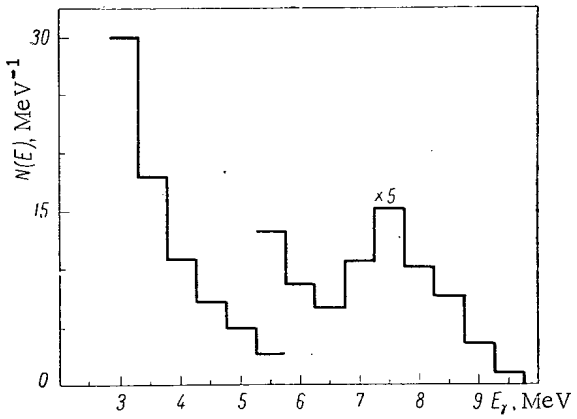

Fig. 6. γ-radiation spectrum measured by means of a scintillation γ-spectrometer at a height of 1 m above the center of the operating surface of the RIZ stand reactor.

The upper reflector, which consists of boron carbide and bismuth, reduces the effect of the material under investigation on the reactivity by not more than 0.1%.

1. Characteristics of the Stand as a Radiation Source

Figure 4 shows the spectrum of neutrons emerging from the upper reflector, which was calculated by V. P. Kochergin. Due to filtration by boron that is contained in the reflector, the neutron spectrum is much harder than the neutron spectrum of a thermal reactor. By varying the boron thickness in the reflector, it is possible to change the neutron spectrum in the energy range below 10 keV and thus simulate the neutron spectra of different thermal and intermediate reactors. The fast neutron spectrum was measured by means of a single-crystal scintillation neutron spectrometer [1]. The measurement results are given in Fig. 5. The solid curve indicates the U^{235} fission spectrum, while the dashed curve shows the same spectrum with an allowance for the attenuation by bismuth in the extraction cross section.

Figure 6 shows the spectrum of γ-radiation emerging from the surface of the bismuth shield, which was measured by means of a single-crystal scintillation spectrometer for energies above 3 MeV. The hard portion of the spectrum is obviously due to the capture γ-radiation in iron (in the structure, the reflector, etc.).

The neutron and γ-radiation spectra were measured in the same geometry and were reduced to the same reactor power level. This made it possible to estimate the ratio of the neutron flux to the γ-radiation above the operating surface of the stand. The ratio of the number of neutrons with an energy above 0.5 MeV to the number of γ-quanta with an energy above 3 MeV was equal to ~ 20. The ratio of the total number of neutrons to γ-radiation with an energy above 1 MeV, which was estimated with an allowance for the calculated spectrum on the basis of measurements with a stilbene crystal (in the 1-3 MeV range), was equal to ~ 7.

The fairly good ratios of neutron fluxes to γ-radiation that we obtained made it possible to measure neutron spectra and even the angular distribution of neutrons, to measure the yield of secondary γ-radiation from different materials, and to compare spectra of capture γ-radiation. As an example of the latter measurements, we can cite [2], where considerable distortions of the γ-radiation spectrum for such important structural materials as nickel, iron, and copper were detected. The described stand was used for many experiments in investigations of the yield of capture γ-radiation for a number of structural and shielding materials by means of the method described in [3].

The measurement results for iron and nickel are given below.

Results of Measurements on the RIZ Stand

Iron				Nickel				Borated nickel (2% boron by weight)			
thickness, cm	relative yield of γ-radiation	ratio of γ-radiation fluxes	β, %	thickness, cm	relative yield of γ-radiation	ratio of γ-radiation fluxes	β, %	thickness, cm	relative yield of γ-radiation	ratio of γ-radiation fluxes	β, %
5.5	0.88	14.1	0.80	4.8	0.81	15.4	1.06	4.7	0.54	–	–
10	1	10.3	1.03	9.6	1	9.5	1.47	9.4	0.43	1.6	1.07
20	0.78	8.2	1.21	20	0.69	6.4	2.12	13.1	0.32	–	–
40	0.36	7.6	1.17	30	0.36	7.3	1.82	20.3	0.20	2.0	1.0
								28	0.10	–	0.96

Investigation of the Yield of Capture Radiation from Iron and Nickel

Prisms with different thicknesses, which were made up of 900 x 1000 x 9 mm iron sheets, 800 x 800 x 8 mm nickel sheets, and borated-nickel sheets with 2% boron by weight, which had a diameter of 900 mm and a thickness of 15-20 mm, were placed on the operating surface of the stand.

Shields made of boron carbide, paraffin, and mixtures of boron carbide, paraffin, and water were used for reducing the neutron radiation background. These shields, which surrounded the prism on all sides, were placed on the surface of the shield under investigation.

The γ-radiation detector was also surrounded with boron-paraffin and bismuth shields. It was mounted at distances of more than 100 cm from the surface of the shield under investigation. For measuring the background, the solid angle formed by the detector and the prism surface was cut off by a bismuth shield with a thickness of 8-9 cm. In the γ-radiation energy range from 3 to 6 MeV, the effect-to-background ratio was equal to unity even for iron with a thickness of 40 cm.

As in [3], the end result of the experiments was the determination of the secondary radiation coefficients β—the ratios of the total number of γ-quanta with an energy exceeding a certain threshold E_{thr} that emerge from the shield surface to the total number of neutrons emerging from the same surface.

The table provides the secondary radiation coefficients and the relative yields of capture γ-radiation from nickel, borated nickel, and iron as functions of the shield thickness. For iron, E_{thr} = 5 MeV, while, for nickel and borated nickel, E_{thr} = 7.5 MeV.

The secondary radiation coefficients for a Po—α—Be-source placed inside a flat iron layer were given in [3]. Comparing our results with the data for iron from [3], we see that, for thicknesses exceeding 20 cm, the secondary radiation coefficients are in agreement within the limits of measurement accuracy (the errors in our results are equal to 10-13%) in spite of the difference between the neutron spectra of such sources as a Po—α—Be-source and the RIZ reactor. Considerable discrepancies are likely to be observed for smaller thicknesses due to the fact that the influence of the iron layer under the neutron source is manifested in measurements with a Po—α—Be-source.

In the case of a two-component shield consisting of a heavy and a hydrogenous medium, the capture γ-radiation considerably increases, since the neutrons reflected by the hydrogenous medium are absorbed in the heavy shield. The table also provides the ratios of γ-radiation fluxes for the case where the heavy shield is in contact with water and the neutrons reflected by boron carbide are blocked (a B_4C thickness equal to 0.5 g/cm^2 is sufficient for this purpose). It should be mentioned that these ratios depend on the thickness of the next shield because of the different angular distributions of the γ-radiation produced by reflected and transmitted neutrons. This problem was discussed in detail in [4, 5].

In conclusion, the authors consider it their pleasant duty to express their deep gratitude to A. I. Leipunskii and I. I. Bondarenko[1] for their continued interest in the experiments performed on the RIZ stand, to V. A. Kuznetsov

[1]Deceased.

for his valuable assistance in constructing the stand, and to A. F. Popov and A. F. Sotnikov for their work on the construction and adjustment of the control and safety equipment for the stand.

LITERATURE CITED

1. V. A. Dulin et al., Pribory i Tekhnika Éksperimenta, No. 2, 39 (1961).
2. A. T. Bakov et al., ZhÉTF, 44, 3 (1963).
3. A. T. Bakov et al., Atomnaya Énergiya, 13, 31 (1962).
4. D. L Broader et al., Problems in the Physics of Reactor Shielding [in Russian], Moscow, Gosatomizdat (1963), p. 112.
5. B. F. Gromov et al., Atomnaya Énergiya, 18, 69 (1965).

A WHOLE-BODY COUNTER

(UDC 539.107)

Yu. V. Sivintsev, O. M. Arutinov, V. A. Kanareikin, and M. A. Panov

Translated from Atomnaya Énergiya, Vol. 18, No. 2, pp. 141-147, February, 1965
Original article submitted June 24, 1964

A description is given of a whole-body counter using NaI(Tl) crystals which was constructed at the I. V. Kurchatov Atomic Energy Institute in 1961. Results of work on improvement of instrument parameters are presented. As a result of this work, a background count rate per kilogram of scintillator equal to 7800 cts/h was obtained for the energy range 150-2100 keV. From calibrations performed with water solutions of K^{40} and Cs^{137} in a phantom, it was determined that the sensitivity for a γ-emitting isotope in the human body was $1.4 \cdot 10^{-11}$ Ci/kg. The mean potassium content in males of middle age was 1.96 ± 0.08 g K/kg body weight, and for females of the same age, it was 1.53 ± 0.04 g K/kg weight. A sharp increase in the specific activity of Cs^{137} in the human body appeared during the period from September, 1962 to August, 1963 (from 35 to 135 nCi/g K) resulting from contamination of the biosphere by the products of nuclear explosions.

The comparatively great hazard from internal radiation, the negligibly small permissible level of isotopes in the human body (fractions of a microcurie in the entire body), and the associated need for reliable identification and measurement of quantities of radioactive materials led to the construction of a whole-body counter. Similar equipment has been built in recent years in the United States, England, France, and other countries [1]. The high sensitivity of such spectrometers makes it possible not only to determine the type and absolute amount of radioactive isotopes which have entered the human body, but also to solve other problems, for example, such as the determination of the potassium content in vivo, the measurement of absorbed dose for neutron irradiation, the study of the distribution and elimination of radioactive isotopes introduced into the human body, the inspection of foodstuffs for radioactive contamination, etc.

In this paper, a whole-body counter constructed at the I. V. Kurchatov Atomic Energy Institute is described.

Description of the Whole-Body Counter

The spectrometer is located in the basement of a four-story building with brick exterior. The spectrometer detectors and the subject to be measured are placed inside a steel chamber with internal dimensions 2 × 2 × 2 m. The walls, floor, and ceiling of the chamber, which are covered on the inside by plastic sheeting, are 20 cm thick, and are made of steel plates. The rolling door of the chamber is put into motion by an electric deive. Four detectors with scintillation counters (Fig. 1) are set up in the chamber; a canvas litter, on which an individual or phantom is placed for measurement, is centered vertically in the chamber. Two detectors are located above the litter and two below it. A suspension system assures independent manual shifting and securing of each detector both in the horizontal and vertical directions. If necessary, the litter can be moved away from the detectors, or moved to a vertical position on a wall of the chamber.

The chamber is ventilated by an inflow of heated air (actual flow, 300 m^3/h). The air is kept free of naturally radioactive aerosols by means of high-efficiency, fine-fiber filters. Auxiliary rooms (Fig. 2) are located close to the chamber which make it possible to eliminate the chance of accumulating within the chamber accidental radioactive contamination brought in on clothing or on the body. The subject being studied, after registration and medical examination, goes through a health control point, undergoes radiometric checking for cleanliness of the body surfaces, dresses in a cotton suit, and enters the chamber for measurement. The main electronic equipment (pulse

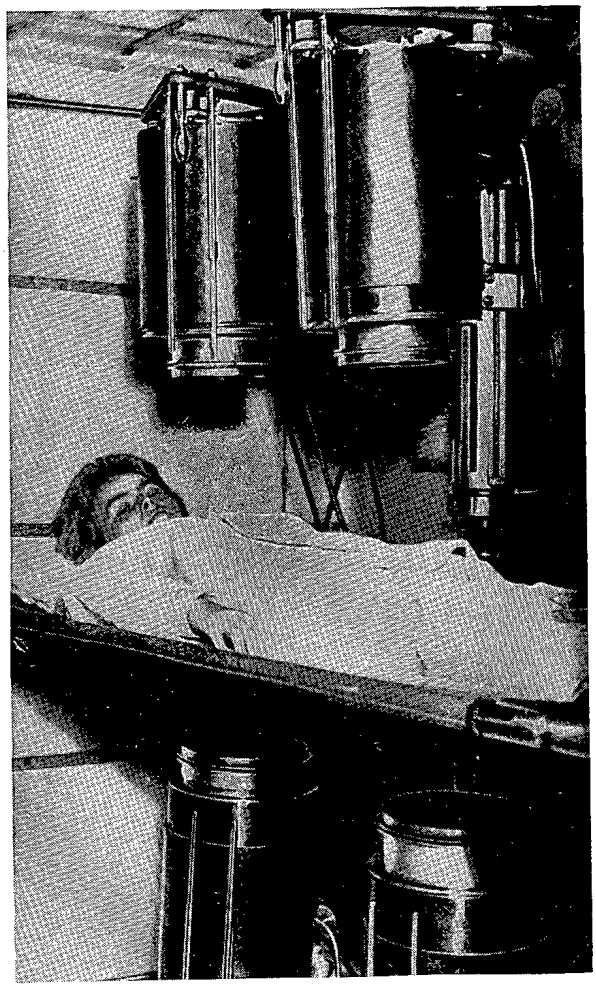

Fig. 1. Inside view of chamber with the four scintillation detectors of the whole-body counter.

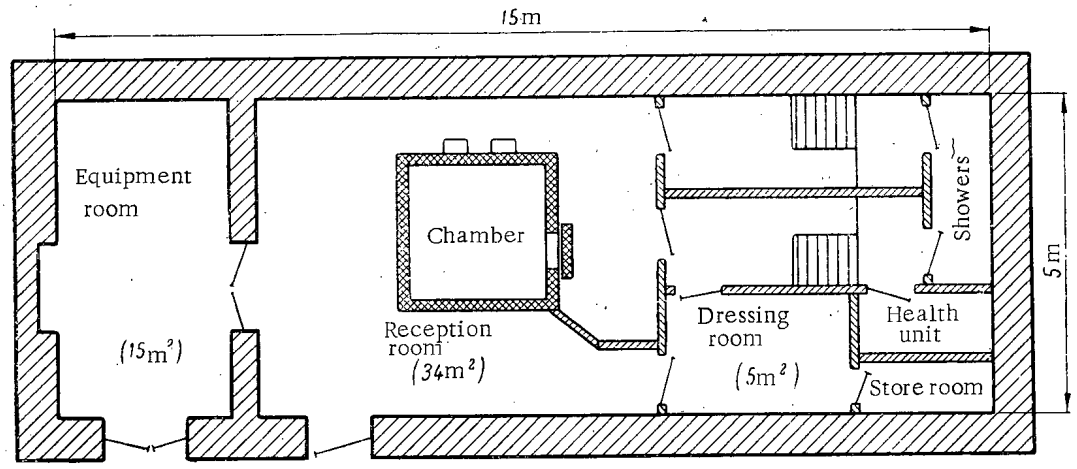

Fig. 2. Plan of spectrometer arragement and associated auxiliary rooms.

Crystal Dimensions and Can and Window Materials Used in the Detectors

Crystal dimensions, mm		Can material	Window material
diameter	height		
200	60	Aluminum	Quartz
200	50	"	"
140	50	1Kh18N9T stainless steel	Type TK-16 potassium-free glass
140	50	"	"

height analyzer, distribution unit, plate-filament power supply, electromagnetic stabilizers) and instruments for checking and adjustment are located in a neighboring room.

Each of the four detectors contains a scintillation counter consisting of a NaI(Tl) single crystal and an FÉU-44 photomultiplier with an envelope of type S49-1 (3S-5-Na) potassium-free glass. The crystal cans are made of stainless steel or aluminum; the windows are of quartz or potassium-free glass. The table gives the dimensions of the crystals installed in each detector and the materials used in cans and windows.

The construction of the detectors assures minimum absorption of recorded γ-radiation in the entrance window because the aluminum container which fastens the crystal to the detector covers only the lateral surfaces of the crystal can and has a minimal thickness of 1.5 mm. The materials from which structural elements of the detectors are made (aluminum, St. 3, Armco iron, SAV aluminum alloy) were previously investigated with respect to radioactive contamination in order to select materials with minimum specific activity.

A cathode follower with 6N6P dual triodes is mounted in each detector.

Signals from the output of the cathode follower, as well as high voltage for the photomultiplier and the plate-filament supply of the preamplifier, are fed by cables coming out of the ceiling of the chamber through the labarynthine entrance of the ventilation duct.

Pulses from all detectors are summed in the distribution unit. At the same point, regulators are provided with which one can vary the high voltage supplied to the photomultipliers of each detector in order to couple them. The high voltage is taken from two VS-22 high-voltage rectifiers fed by SNE 220/0.5 electromagnetic stabilizers. VS-12 rectifiers are used for the plate-filament supply of the detector preamplifiers.

The pulse height analysis is carried out with ADA-50 or AMA-3S analyzers. As a rule, the latter is kept in reserve.

Studies to Improve Spectrometer Parameters

The particular conditions under which a whole-body counter is used are, as already mentioned, the small amount of radioactive materials requiring identification and quantitative determination, and the large dimensions and complex geometric shape of the volume source and of the absorbing and scattering media. Thus there arises the necessity for ensuring low background and high detection efficiency for low-intensity γ-radiation.

It is necessary to change the location of the detectors from measurement to measurement because of the large dimensions of the human body and the possibility of a concentration of activity in individual organs. Consequently, an additional requirement is the stability of detector readings under constant conditions of irradiation. It is therefore necessary to eliminate the effect of a magnetic field on photomultiplier operation. For the same reason, localized sources of increased background are not permissible in the chamber equipment or in the detectors.

The complexity of the geometric shape of the subjects measured that has been mentioned makes it necessary to give up the use of point sources of known activity for calibrating the spectrometer and to calibrate either with

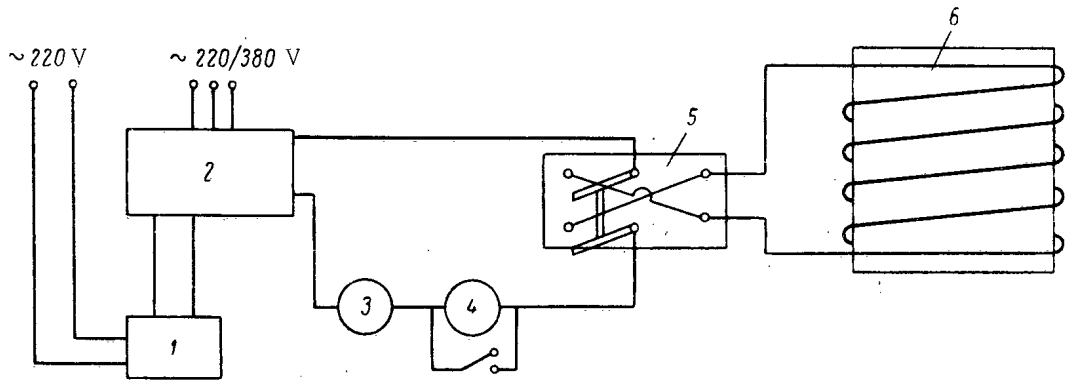

Fig. 3. Electrical circuit used for demagnetization of the chamber: 1) VSA-5 rectifier; 2) type PS-500 welding unit; 3) 600 A ammeter; 4) 30 A ammeter; 5) current-reversing switch; 6) steel shielding.

phantoms or with humans in whose bodies there are known amounts of radioactive materials. Because spectrometer calibration for many isotopes with a phantom is an extremely time-consuming process, instrumental stability and constancy of background counts over a period of several months are desirable. In turn, this places rigid requirements on such parameters as constancy of gain, invariance of the calibration curve for dependence of spectrometer sensitivity on radiation energy, steady background, etc.

In order to reduce the inherent detector background, studies were made of the potassium contamination in glasses and in canning materials, as well as in the raw materials for the manufacture of NaI(Tl) single crystals at various stages in processing and production, and in the finished scintillators. As a result, a strong fluctuation of potassium content from batch to batch (of an order of magnitude) came to light. It was further established that, during the course of the process adopted for growing single crystals of NaI(Tl), potassium from the ceramic forms migrated into the sodium iodide melt. A satisfactory solution for the problem of reducing potassium content in finished crystals (down to $5 \cdot 10^{-4}$%) was obtained by using quartz ampoules for growing crystals from selected raw materials.

The work on growing potassium-free crystals was carried out by members of the single-crystal scintillator laboratory of the All-Union Instrument Research Institute, and the spectral analysis of potassium content in raw materials and at various stages of the crystal production process was performed by members of the State Rare Metals Research Institute and of the Geochemical Institute, both in Moscow, to all of whom the authors take this opportunity to express their gratitude.

A significant source of potassium background was detected in the glasses used in several types of photomultipliers and scintillators. For example, the use of a type FÉU-44 photomultiplier, whose envelope is made of 3S-5-Na potassium-free glass, instead of the previously used FÉU-24, in a detector with a commercial NaI(Tl) scintillator 70 x 50 mm in size (potassium content ~ $2 \cdot 10^{-2}$%) reduced the background counting rate by approximately 1.8 times. At the same time, the total counting rate for measured activity in the glass of the FÉU-24 photocathode and in the window of the can of the single crystal mentioned was approximately 9500 and 5000 cts/h, respectively, the photopeak for K^{40} radiation being clearly visible in both spectra. A significant admixture of potassium is also found in the FÉU-11A, FÉU-13, and particularly the FÉU-23 photomultipliers.

In order to select materials for scintillator windows, studies were made of plastic (Plexiglas),[1] quartz, and 3S-5-Na and TK-16 potassium-free glass. In none of the materials was any noticeable activity whatever detected with the exception of TK-16 glass. Measurements of the latter revealed an insignificant rise in counts, mainly in the 0.6-MeV region. Apparently, this is explained by the contamination with isotopes of the radium and barium families found in TK-16 glass.

The measurements also showed that slightly active materials suitable for use inside crystal and detector cans are manganese oxide, polystyrene cement, 1Kh18N9T stainless steel, copper, aluminum, St. 3 carbon steel, Armco iron, Permalloy-78, and various synthetic materials. These materials were used in the manufacture of scintillator cans and detector components.

[1]NaI(Tl) crystals sealed in cans with Plexiglas windows were short-lived.

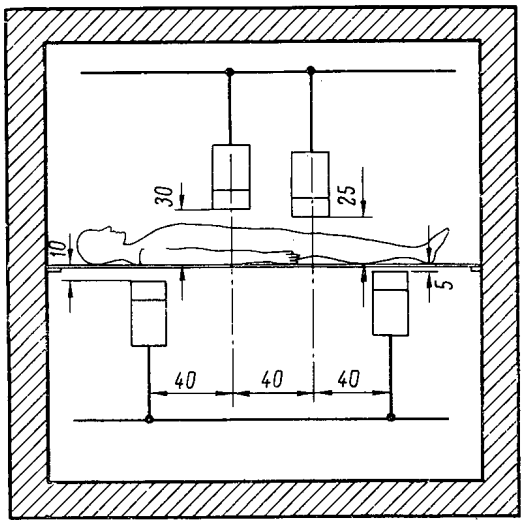

Fig. 4. Location of detectors for whole-body counting.

The most suitable photomuliplier turned out to be the FÉU-44 with an envelope of 3S-5-Na potassium-free glass. As a result, the total background counting rate in the 150-2100 keV energy range per kg of scintillator was reduced to 7800 cts/h [2]. This made it possible to achieve a sensitivity of 10^{-9} Ci of a γ-emitting isotope in the body of an individual ($1.4 \cdot 10^{-11}$ Ci/kg) for a counting period of 300 sec. The resolution for the 661 keV γ-quanta of Cs^{137} was 17-21% for individual detectors and 19% for measurements with the four detectors.

During tests of the electronic equipment, it was observed that the main source of unstable operation was the photomultiplier. A batch (15 samples) of type FÉU-44 photomultipliers was checked by testing each sample for 24 h. After a four-hour warmup, variations in pulse height (for pulses corresponding to the Cs^{137} photopeak) did not exceed 1% for four of the FÉU-44, were no more than 6% for four others, and were greater than 6% for the rest. Subsequent measurements were made on selected samples of stable photomultipliers during 24-h operation of the equipment.

When using the FÉU-44 photomultipliers, it became apparent that the pulse heights at the photomultipliers, output varied with shifts or changes in the positions of the detectors in the chamber though irradiation conditions remained the same. The same sort of an effect, although to a lesser degree, was observed with the use of FÉU-24 photomultipliers. By shielding a detector with several layers of Armco iron or Permalloy, it was established that the variations in pulse height were associated with the existence of a magnetic field in the chamber which distorted the electron trajectories in the focussing region of the FÉU-44 photomultiplier (in the FÉU-24 photomultiplier, this effect was smaller because the electron trajectories in it are considerably shorter). Therefore, the magnetic shielding of the photomultipliers (Armco iron, 2 mm thick) proved to be unsatisfactory.

Direct measurements with a magnetometer verified the existence of strongly inhomogeneous magnetic field inside the chamber whose instensity in particular areas exceeded values typical of the Earth's magnetic field. The maximum value of the horizontal component of the magnetic field inside the chamber was 0.8 Oe. Evidently, the existence of such a field was connected with the fact that the chamber was constructed of steel plates which very likely had previously undergone magnetization.

To reduce the effect of the field on the operation of the detectors, it was decided to demagnetize the chamber with alternating current. To accomplish this, the multilayer steel shielding was wrapped with 20 turns of copper conductor 150 mm^2 in cross section. The current supply was a PS-500 welding machine to whose excitation winding a VSA-5 rectifier was connected to provide current regulation (Fig. 3). The current during a single cycle was varied manually in such a way that its time variation was approximately sinusoidal. The length of a cycle was chosen to be 1 min on the basis of the reaction to the skin effect. After each cycle, the current direction was reversed by means of a switch. The maximum current amplitude in the first cycle was 600 A; the reduction in amplitude from cycle to cycle was 20 A.

As a result of this demagnetization, the field in the chamber became uniform; the average value of the horizontal component of magnetic field intensity was reduced to 0.06 Oe. When a detector with an FÉU-44 without magnetic shielding was moved around the chamber, the pulse height at the photomultiplier output underwent no variation.

Spectrometer Calibration

There are several methods, differing in accuracy and principles, for calibrating the spectrometer. The first of these consists of the introduction of a known amount of radioactive isotope into the body of a control subject and the measurement of the resulting radiation. This method is the most accurate since it takes into account self-absorption and scattering of the γ-radiation in the body of the particular individual. However, the introduction of radioactivity into the body is accompanied by the acquisition of an additional dose of internal radiation, which is undesirable despite its negligibly small amount. A second, less exact method of calibration is based on a comparison of γ-ray

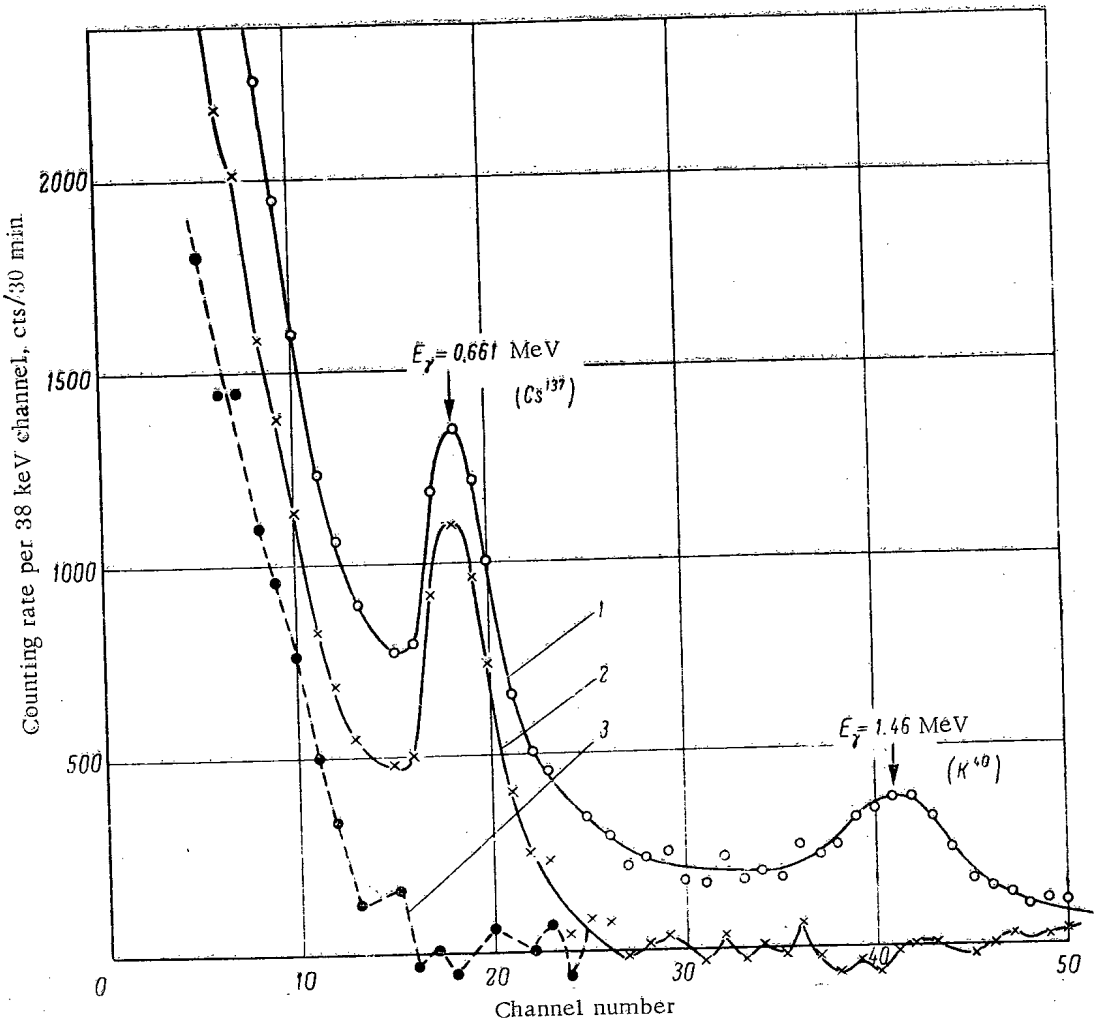

Fig. 5. Analysis of a radiation spectrum for an individual containing 127 g potassium and 15.7 nCi Cs^{137} (subject 121, female): 1) spectrum of radiation from the individual; 2) difference spectrum for radiation from the individual and from a phantom containing KCl; 3) difference spectrum for radiation from the individual and from a phantom containing KCl and Cs^{137}.

spectra from a person and from a phantom filled with a solution of one or another radioactive material of known activity. In our investigations, we used the second method, which is not accompanied by the drawback mentioned above. The phantom, made of plastic, had the dimensions of the so-called standard man (176 cm in height, 70 kg in weight). Two isotopes, K^{40} and Cs^{137}, which are most widely distributed in people's bodies, were chosen for calibration. The long-lived radioactive isotope K^{40} is contained as a contaminant in the natural potassium in the muscle tissue of all people, and its content in the body depends on the sex, weight, and age of the individual. After 1955, Cs^{137} showed up in people because of systematic contamination of the atmosphere by the products of nuclear explosions.

For calibration with K^{40} γ-radiation, the phantom was filled with a solution of KCl in distilled water. Experiments that were performed showed that the distribution of the isotope and the scattering and absorption conditions for γ-quanta were the same in the phantom and in the human body. In order to reduce the dependence of detector counting rate on the height of an indivudal, the detectors were positioned with a 40 cm spacing along the control subject (Fig. 4) as had been done previously [3]. Studies with phantoms of varying lengths (155-186 cm), made to determine a height correction, showed that the counting rate at the K^{40} γ-ray photopeak, for K^{40} uniformly distributed throughout the phantom, was practically independent of the length of the phantom.

A phantom of constant thickness was used for calibration while the mass of the control subjects varied over a rather wide range. However, for fixed distances from the crystals to the litter, the increase in self-absorption in the

more massive subjects compensated for the effect of the reduced effective distance from radiator to detector [3]. These facts made it possible to use the K^{40} γ-ray spectrum, averaged over many phantom measurements, to calculate the content of this element in the body of any individual regardless of anthropometric data. The statistical standard error of a measurement of the average amount of potassium in a human (from the area under the photopeak) is ± 2% for our equipment.

The method we used for calibrating with Cs^{137}, like the calibration with potassium, involved the use of a phantom filled with a water solution of Cs^{137} Cl of known activity. The statistical error of a measurement of the average amount of Cs^{137} in a human by means of the spectrometer being described is ± 4%. To this must be added the error in the determination of the activity of a standard source, ± 3%, which increases the total error to ± 5%.

Analysis of Spectra

After amplification, pulses from the four detectors are sent to a 128-channel pulse height analyzer with an electrostatic memory. The analyzer can also be switched to 64 channels. To accelerate data taking, and also because of the inadequate resolution of the NaI(Tl) crystals, the latter mode is mainly used, for which the width of each channel is 38 keV in the 38-2100 keV energy range. After the completion of each measurement, curves for the pulse height spectrum are constructed on the basis of the instrumental data obtained (number of pulses in each channel per time of measurement). To obtain a reference point on the energy axis, brief measurements of a Cs^{137} source are made before and after recording the spectrum to be analyzed. An example of an energy spectrum recorded with our equipment for radiation from an individual having no occupational contact with radioactive isotopes is given in Fig. 5.

The method of successive subtraction is used to determine the amount of radioactive material in the body. First the background obtained in the chamber with a phantom filled with distilled water is subtracted from the total instrumental spectrum. This procedure is necessary in order to take into account the contribution of multiple γ-quantum scattering to the total background spectrum. Then, by comparing the areas under the K^{40} photopeaks for measurements of the individual and of the phantom, the amount of K^{40} in the body of the subject is determined, and a normalized γ-ray spectrum of K^{40} is subtracted from the spectrum being analyzed (curve 2, Fig. 5). Next, the Cs^{137} content is subtracted by a similar method. If radioactive materials other than Cs^{137} and K^{40} are observed in the primary γ-ray spectrum of the individual, the difference spectrum (curve 3, Fig. 5) is compared with tabulated data for the γ-ray spectra of isotopes.

Finally, we present data on natural activity from a survey carried out during the period September, 1962-August, 1963 on 150 subjects having no occupational contact with radioactive isotopes. According to these measurements, the average potassium content in males of middle age was (1.96 ± 0.08) g K/kg weight; for females, the corresponding quantity was (1.53 ± 0.04) g K/kg weight. The error given is the root-mean-square error. In the bodies of people during the period mentioned, a sharp increase was observed in the specific activity of Cs^{137}: from 20-50 nCi/g K (average value, 35 nCi/g K) at the end of 1962 to 100-150 nCi/g K (average value, 135 nCi/g K) in August, 1963. This increase is explained by contamination of the biosphere by the products of earlier nuclear explosions.

In conclusion, the authors consider it their pleasant task to express their deep appreciation to Acad. A. P. Aleksandrov for suggesting the problem and for his continuing interest in these studies.

LITERATURE CITED

1. Whole-Body Counting, Proc. Symposium, IAEA, Vienna (1962).
2. Yu. V. Sivintsev et al., Proceedings of the V Scientific and Technical Conference on Nuclear Electronics, Vol. 3, Moscow, Gosatomizdat (1963).
3. Rudno, in Proceedings of the Second International Conference on the Peaceful Use of Atomic Energy, Geneva, 1958. Izbr. dokl. inostrannykh uchenykh. Vol. 9, Moscow, Atomizdat (1959), p. 212.

VARIATION OF THE SEPARATION FACTOR IN ISOTOPE EXCHANGE AS A FUNCTION OF THE PROPERTIES OF THE MOLECULES BEING EXCHANGED

(UDC 621.039.3)

A. M. Rozen and A. I. Mikhailichenko

Translated from Atomnaya Énergiya, Vol. 18, No. 2,
pp. 147-156, February, 1965
Original article submitted March 28, 1963

The article considers the variation of the equilibrium constant in isotope exchange in diatomic compounds as a function of properties of the atoms and molecules being exchanged: the force constant, the dissociation energy, the electronegativity, the structure of the electron cloud, the internuclear distance, the mass of the isotopic atom, and the mass of the complementary atom. Semiempirical formulas are used to obtain analytical equations which describe the influence of these factors on the value of the equilibrium constant. Suitable correlation methods are found for predicting how the β factors will vary in series of analogous compounds. Recommendations are given for the choice of isotope separation systems. An attempt is made to extend some of the resulting conclusions to isotope exchange in polyatomic compounds.

Various isotope-exchange reactions have been widely used for separating isotopes of many elements [1-8]. Research is currently in progess to find systems which provide a high separation factor, thereby making the technological process more economical. However, such research must be carried on in a purely empirical fashion; the choice of the systems is still random to a very large extent.

It is important to be able to predict what systems will provide a maximum separation factor. For this purpose it is necessary to explain how the separation factor varies as a function of the properties of the molecules being exchanged. In the present article we develop further the principles and conclusions obtained in [9, 10] for the case of isotope exchange in diatomic molecules.

The equilibrium constant and the separation factor in isotope exchange can be calculated which sufficient accuracy from the oscillation frequencies of the isotope molecules [1-4, 7]. Let us consider the isotope-exchange reaction

$$mAG_n + nBG_m^* \rightleftarrows mAG_n^* + nBG_m, \tag{1}$$

where G is the isotopic atom; the asterisk identifies the molecule containing the heavier isotope.

The separation factor α and the isotope exchange constant K for the reaction (1) are related by the formula

$$\alpha = \left(\frac{K}{K_\infty}\right)^{1/mn}, \tag{2}$$

where K_∞ is the value of the equilibrium constant for the case of equally probable distribution of the isotopes. In statistical calculations it is somewhat more convenient to calculate, for each pair of molecules participating in the reaction, the so-called β factors (the ratio of sums according to state, from which the symmetry numbers have been eliminated [11-13]):

$$\alpha = \frac{\beta_{A^*-A}}{\beta_{B^*-B}}. \tag{3}$$

TABLE 1. Values of β Factors and Oscillation Frequencies ω_e for Diatomic Compounds of the Alkali Metals

Complementary atom	Isotopic atom										
	Li^{6-7}		Li^{6-8}	Na^{22-24}		K^{39-41}		Rb^{85-87}		$Cs^{133-135}$	
	β	ω	β	β	ω	β	ω	β	ω	β	ω
F	1.0697	930	1.1202	1.0079	477	1.0024	405	1.0006	390	1.0003	385
Cl	1.0490	705	1.0839	1.0068	380	1.0020	305	1.0005	270	1.0002	240
Br	1.0419	576	1.0714	1.0062	315	1.0016	230	1.0004	181	1.0002	171
J	1.0335	501	1.0569	1.0056	286	1.0014	200	1.0003	147	1.0001	120
Li	1.0097	361	1.0167	—	—	1.0003	—	1.0001	—	1.0000	—
Na	—	—	—	1.0010	159	1.0003	—	1.0000	—	1.0000	—
K	1.0055	207	1.0094	1.0008	123	1.0002	92.6	—	—	—	—
Rb	1.0048	185	1.0081	1.0007	107	—	—	1.0000	56,8	1.0000	—
Cs	1.0040	167	1.0068	1.0007	97	—	—	1.0000	49,4	1.0000	42

TABLE 2. Values of β Factors and Oscillation Frequencies ω of a Number of Diatomic Compounds

Molecule	β	ω	Molecule	β	ω	Molecule	β	ω
$Mg^{24-26}Cl$	1.0089	466	$Tl^{203-205}Cl$	1.0001	288	$Br^{79-81}Cl$	1.0014	456
$Ca^{40-42}Cl$	1.0027	364	$C^{12-14}Cl$	1.0585	844	$J^{127-129}Cl$	1.0005	384
$Sr^{86-88}Cl$	1.0006	301	$Si^{28-30}Cl$	1.0093	535	$O^{16-18}O$	1.0786	1580
$Ba^{136-138}Cl$	1.0002	279	$Ge^{72-74}Cl$	1.0014	408	$S^{32-34}O$	1.0170	1124
$B^{10-12}Cl$	1.0728	830	$Sn^{118-120}Cl$	1.0004	352	$Se^{78-80}O$	1.0027	909
$Al^{27-29}Cl$	1.0080	481	$Pb^{206-208}Cl$	1.0001	304	$Te^{126-128}O$	1.0009	796
$Ga^{69-71}Cl$	1.0012	365	$F^{17-19}Cl$	1.0374	791			
$In^{113-115}Cl$	1.0004	317	$Cl^{35-37}Cl$	1.0075	565			

The value of the β factor for a diatomic molecule is determined by the frequencies of oscillation of the isotopic molecules (see, for example, [7]):

$$\beta = \left(\frac{u^*}{u} e^{-\frac{u^*-u}{2}} \frac{1-e^{-u}}{1-e^{-u^*}} \right)^{1/n}. \quad (4)$$

Here $u = hc\omega_e/kT$, where ω_e is the frequency of oscillation of the isotopic molecule, **c** is the velocity light, **h** is Planck's constant, **k** is the Boltzmann constant, and T is the temperature in °K.

In order to solve this problem, we must find the relationship between the β factors (or the ratios of sums according to states) and the force constants of the potential energy, which depend, in turn, on the structure of the molecules.

The frequencies of oscillation of the isotopic molecules depend on two factors: the strength of the bond in the molecule and the mass of the oscillating atoms. Consequently it is expedient to consider how the β factors vary as a function of a number of parameters: the binding energy of the molecules (the value of the force constant, the dissociation energy, the electronegativity of the atoms); the mass of the isotopic and complementary (non-isotopic) atoms; the structural factors of the molecule (the structure of the electron cloud, the value of the internuclear distance).

Relationship Between the β Factor and the Force Constant

The frequency of the oscillations, ω_e, is related to the force constant by the formula

$$\omega_e = \frac{1}{2\pi c} \sqrt{k_e/\mu}. \quad (5)$$

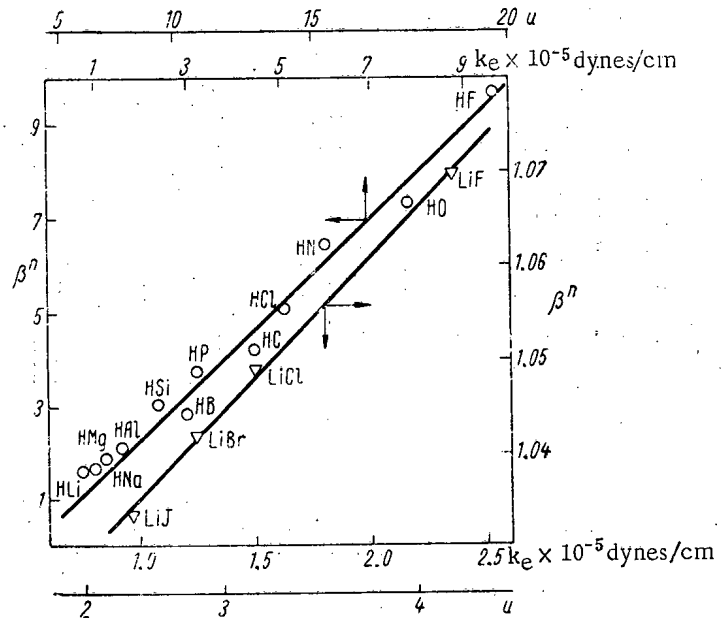

Fig. 1. Variation of β factors as functions of the force constants k_e: ○) diatomic hydrides of the first and second periods of the periodic table; ▽) lithium halides.

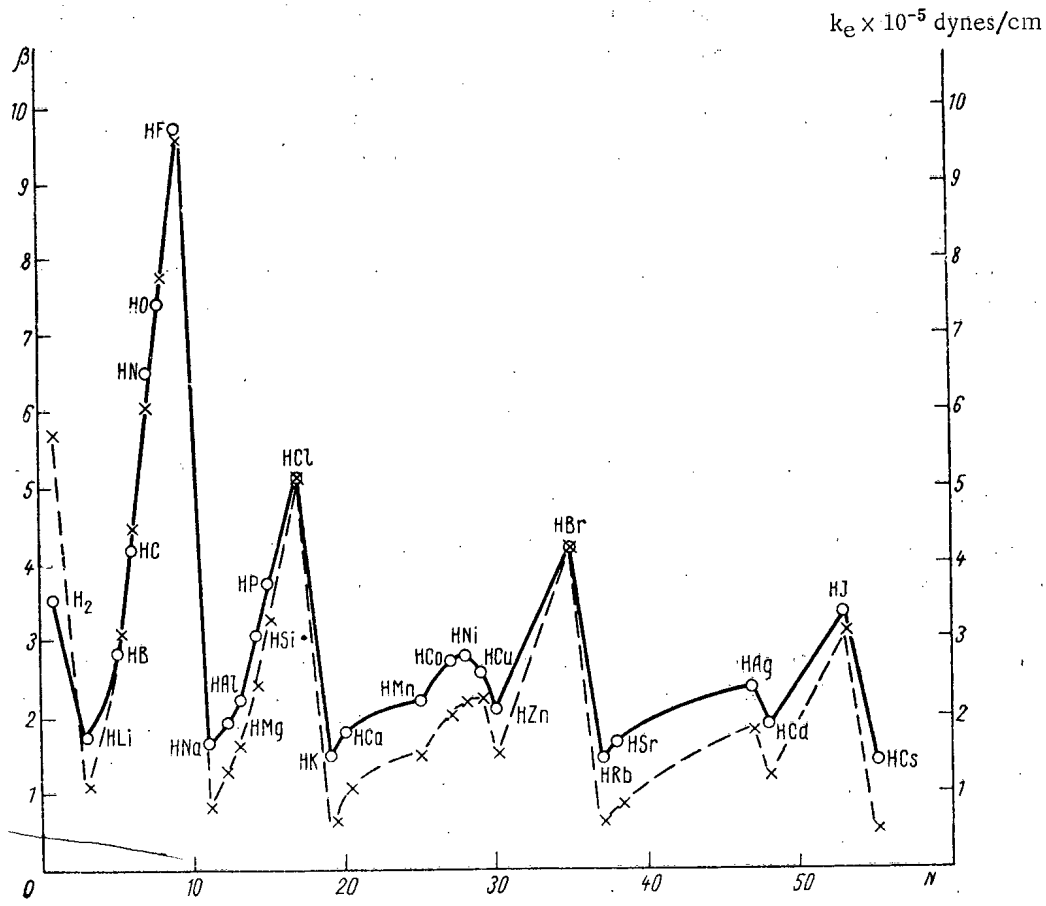

Fig. 2. Variation of the β factors and of the force constants k_e (————) of diatomic hydrides as functions of the atomic number N of the element bound to hydrogen. (The letters on the figure refer to points on the solid curve.)

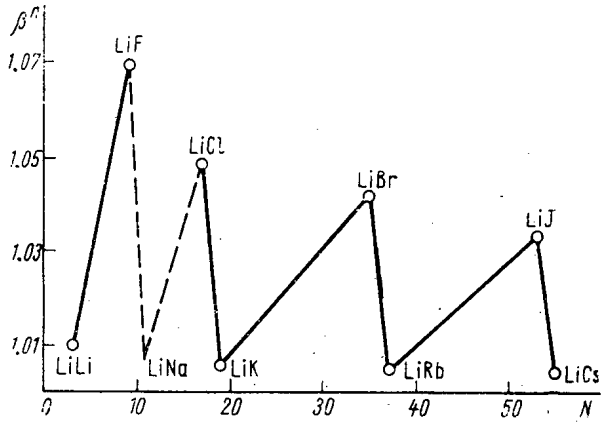

Fig. 3. Variation of the β-factors of diatomic compounds of lithium ($Li^{6-7}R$) as a function of the atomic number of the element R combined with the lithium. (The curves connecting the maximum and minimum points are drawn tentatively as straight lines.)

Here μ is the reduced mass of the molecule: $\mu = \frac{mm_0}{(m+m_0)}$, where m and m_0 are the masses of the isotopic and complementary atom, respectively. Using Eq. (4), we can find the relationship between the β-factors and the force constants. For the region of low quantum effects (the region of sufficiently high temperatures or low frequencies of oscillation) when $u < 2$, we have, in accordance with [9],

$$\beta = \left(1 + \frac{\bar{u}\Delta u}{12}\right)^{1/n}, \qquad (6)$$

where $\bar{u} = \frac{u+u^*}{2}$, $\Delta u = u - u^*$. If the values of u and, correspondingly, the frequency of oscillation from (5) are substituted into (6), we obtain

$$\beta^n|_{u<2} = 1 + \frac{1}{96\pi^2}\left(\frac{h}{kT}\right)^2\left(\frac{1}{\mu} - \frac{1}{\mu^*}\right)k_e = 1 + \frac{1}{96\pi^2}\left(\frac{h}{kT}\right)^2\frac{\Delta m}{\bar{m}^2}k_e, \qquad (7)$$

where $\Delta m = m^* - m$; $\bar{m} = \sqrt{m^* m}$. In the case $u > 5$ (sufficiently low temperatures or high frequencies, when the oscillations still have not become excited and the correction factor $\frac{1-e^{-u}}{1-e^{-u^*}}$ in Eq. (4) can be neglected), we find [9]

$$\beta^n|_{u>5} = \sqrt{\mu/\mu^*}\, e^{b\sqrt{k_e}}, \qquad (8)$$

where

$$b = \frac{1}{4\pi}\cdot\frac{h}{kT}\left(\sqrt{1/\mu} - \sqrt{1/\mu^*}\right).^1$$

Starting with Eqs. (7) and (8), which give the relationship between the β-factors and the force constants, we can draw the following conclusion: the higher the force constant, the greater will be the β-factor, i.e., the more strongly marked will be the difference between the isotopes. In the intermediate range ($2 < u < 5$) the variation of β as a function of k_e is expressed by more complicated formulas, but even in this case, as can be seen in Fig. 1, β varies directly with k_e. The values of the β-factors of isotope exchange in diatomic molecules derived in this article were calculated by the method of [3], except in the case of deuterium-protium exchange in hydrides, for which the data are taken from [11]. The corresponding values are given in Tables 1 and 2. The oscillation frequencies required for the calculation were taken from [14, 15], except in the cases of the molecules KF, KCl [16], LiCl [17], and FCl, for which the frequency was calculated from the value of the force constant [17]. In the present study we neglected the anharmonic terms in calculating the oscillation frequencies.

The Periodic Law of Variation of β-Factors in Isotope Exchange

It is known that when there is a change in the atomic number of the element bound to hydrogen, the force constant changes periodically [14]. By virtue of this fact, we can use Eqs. (7) and (8) for predicting how the β-factors of a

[1] For small values of $\frac{\Delta m}{m}$ we find $b \approx \frac{h}{8\pi kT}\cdot\frac{\Delta m}{m^2}\sqrt{\mu}$; for $m \gg m_0$, we have $b \approx \frac{h}{8\pi kT}\cdot\frac{\Delta m}{m^2}\sqrt{m_0}$, and for $m \ll m_0$, we have $b \approx \frac{h}{8\pi kT}\cdot\frac{\Delta m}{m^{3/2}}$.

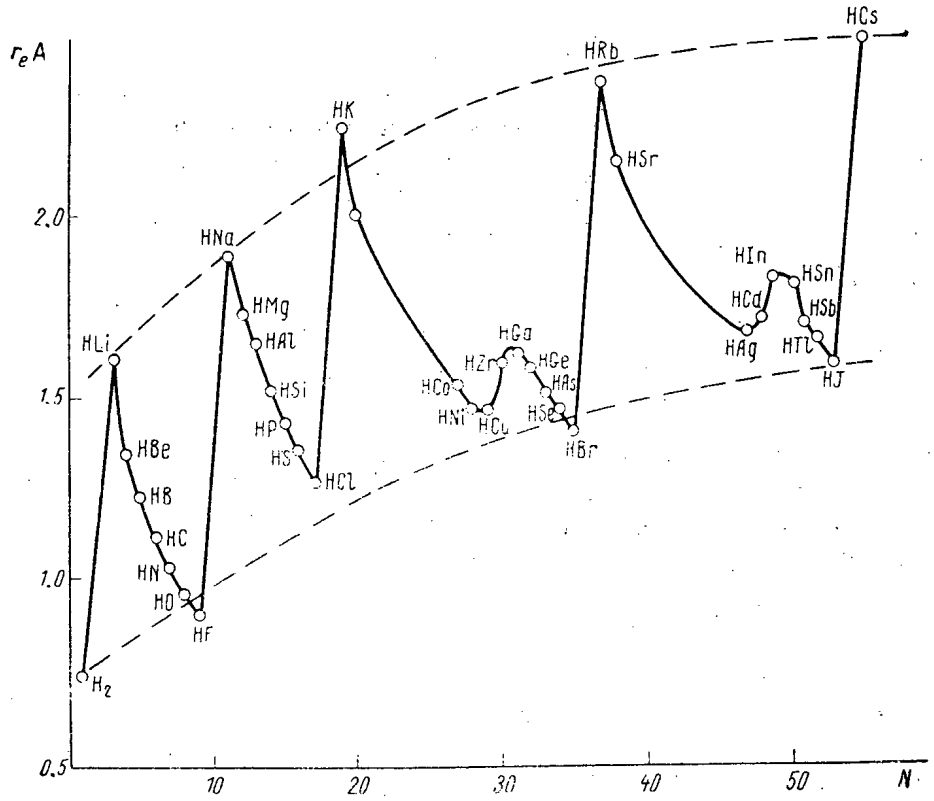

Fig. 4. Variation of the equilibrium internuclear distances r_e of the diatomic hydrides as functions of the atomic number N of the element combined with the hydrogen.

univalent element in diatomic molecules will vary as functions of the atomic member of the complementary (non-isotopic) element bound to the isotopic element. Since the force constant varies periodically (for example, in the case of hydrides) while the reduced mass varies monotonically, it follows that the β-factors will also vary periodically; this was, in fact, observed in [11-13]. In order to verify this conclusion, we have plotted in Fig. 2 the values of the β-factors and the force constant k_e of diatomic hydrides as functions of atomic number of the element bound to hydrogen (the values of k_e were calculated from Eq. (5) or were taken from [18]). It can be seen from Fig. 2 that the values of β and k_e are approximately proportional. Thus, we may assume that the periodic variation of the β factors is due to the analogous variation of the force constants.

Since (7) and (8) are general formulas, the observed rules for the variation of the β-factors are valid not only for hydrogen but also for any univalent element. In order to plot a curve for the periodic variations of the β-factors of other elements we need more than spectral data. However, the available information on the frequencies of oscillation enables us to find the extremum points for some elements (for example, lithium), as is shown in Fig. 3.

Influence of the Molecular Structure

In order to determine how the β-factor varies as a function of the structure of the molecule in isotope exchange, we must relate the force constant k_e to the quantities which determine it. Since a quantum-mechanical calculation of the potential energy of the molecules is not yet possible, we are like-wise unable to calculate k_e (the hydrogen molecule is an exception). However, it is known that the force constant depends to a large extent on the properties of the atoms forming the molecule, the structure of its electron cloud, and the nature of the electrons forming the bond [19]. A number of known semiempirical formulas can be used for quantitative calculations. In particular, it is convenient to use Guggenheimer's empirical formula [15].

$$\omega_e = c_1 (z_1 z_2)^{1/4} \mu^{-1/2} r_e^{-c_2}, \tag{9}$$

where z_1 and z_2 are the numbers of electrons in the outer shells of the two atoms forming the molecule; r_e is the equilibrium internuclear distance between the molecules; $c_1 = (2.065\text{-}2.976) \cdot 10^3$ and $c_2 = (0.92\text{-}1.23)$ are constants found by analyzing the experimental data on the frequencies of oscillation of 150 diatomic molecules.

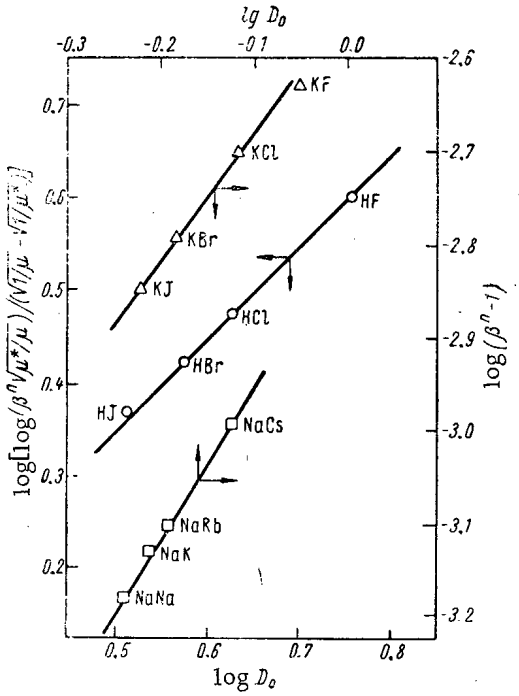

Fig. 5. Variation of $\log_{10}(\beta^n-1)$ and $\log[\log(\beta^n\sqrt{\mu^*/\mu})/(\sqrt{1/\mu}-\sqrt{1/\mu^*})]$ as functions of the dissociation energy of the molecules. The values of the β factors in isotope exchange for sodium and potassium were calculated for a difference of Δm = 2 between the isotope masses: ○) tan α = 1.0; △) tan α = 1.4; □) tan α = 1.7.

From Eqs. (5) and (9) we obtain

$$k_e = 4\pi^2 c^2 c_1^2 (z_1 z_2)^{1/2} r_e^{-2c_2}. \tag{10}$$

Evidently the periodicity of variation of the force constants of the diatomic molecules (in particular, hydrides)—and consequently of the β-factors—is due to the periodic nature of the filling of the electron shells of the second atom z_2 and the equilibrium internuclear distance of molecule r_e.

A number of qualitative considerations explaining the proportionality of the force constant to the geometric mean of the numbers of electrons in the outer shells of the atoms are given in [15].

By solving Eqs. (7), (10) and Eqs. (8), (10) simultaneously, we find

$$\beta^n|_{u<2} = 1 + \frac{1}{24}\left(\frac{hc}{kT}\right)^2 c_1^2 (z_1 z_2)^{1/2} r_e^{-2c_2} \frac{\Delta m}{m^2}, \tag{11}$$

$$\beta^n|_{u>5} = \sqrt{\mu/\mu^*}\exp\left[\frac{c_1}{2}\cdot\frac{hc}{kT}\left(\sqrt{1/\mu}-\sqrt{1/\mu^*}\right)\times (z_1 z_2)^{1/4} r_e^{-c_2}\right]. \tag{12}$$

Equations (1) and (12) are the quantitative expression of the periodic law governing the variation of the factors: (11) applies to the region of low quantum effects, when u < 2, and (12) applies to the region of large quantum effects, when u > 5 (for example, in the case of hydrides). These equations relate the β-factor to the filling of the electron shells, and, in addition, indicate that the β-factors depend not only on the filling of the electron shells but also on r_e.

As is known, the internuclear distance of diatomic hydrides also varies periodically (see Fig. 4, plotted on the basis of data from [14, 15]); within one period, r_e decreases as z_2 increases, while r_e increases when z_2 remains constant (dotted curves in Fig. 4). The increase in r_e with increasing values of the atomic number N of the element combined with hydrogen leads to a decrease of the β-factors (for z_2 = const), which can be seen in Fig. 2. On the other hand, a decrease of r_e within one period leads to a stronger dependence of the β-factor on the atomic number of the second (non-isotopic) atom.

From Eqs. (11) and (12) we may draw the following conclusions concerning the relationship of the β-factor to the structure of the electron cloud of the molecule. The value of the β-factor is determined primarily by the electrons in the outer shells of the atoms, i.e., the valence electrons, which participate in the formation of the chemical bond. The inner shells affect the β-factor through the increase of r_e, which varies symbatically with the number of completed shells.

Influence of the Binding Energy

Qualitatively, the variation of the β-factors as a function of the binding energy of the molecules can be determined by means of Morse's formula [14], which is used for describing the potential curve:

$$V = D_e\left[1 - e^{a(r-r_e)}\right], \tag{13}$$

where V is the potential energy of the molecule; D_e is the dissociation energy, referred to the minimum of the potential curve; $r-r_e$ is the deviation from the equilibrium position; a is a constant for the molecule in question, depending on the structure of the electron cloud.

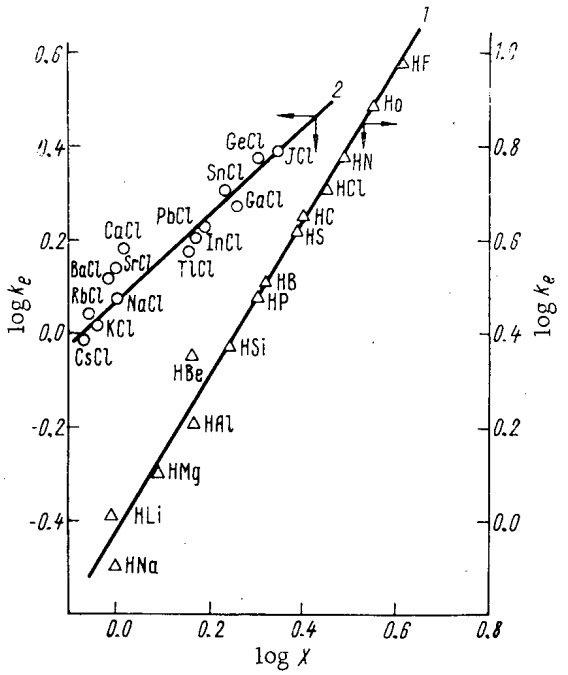

Fig. 6. Variation of the force constants k_e of diatomic molecules as functions of the electronegativity of the second atom: 1) hydrides of the first and second periods of the periodic table of the elements; 2) chlorides for which u < 2.

From Eq. (13) it follows that

$$k_e = 2D_e a^2. \tag{14}$$

Thus, the force constant is proportional to the binding energy. Taking Eqs. (7) and (8) into account, we may conclude that the β-factor will vary symbatically with the binding energy. Thus, the greater the energy of the bond with the non-isotopic atom, the greater will be the β-factor, i.e., the more strongly the difference between the isotopes will be manifested.

For quantitative calculations we can also use an empirical formula [18]:

$$k_e = \frac{c_3 D_0}{r_e}, \tag{15}$$

where c_3 is a constant for the series of similar molecules in question; D_0 is the dissociation energy, referred to 0°K.

It follows from Eqs. (10) and (15) that the internuclear distance is approximately inversely proportional to the binding energy:

$$r_e = \left[\frac{4\pi^2 c^2 c_1^2 (z_1 z_2)^{1/2}}{c_3 D_0}\right]^{\frac{1}{2c_2-1}} \sim D_0^{-\frac{1}{2c_2-1}} \approx \frac{1}{D_0}, \tag{16}$$

where $\sim$ is the sign of proportionality. Substituting (16) into Eq. (10), we find that within one subgroup of the periodic system, when $z_1 z_2$ = const, the force constant is approximately proportional to the square of the binding energy [and not to its first power, as indicated by (14)]:

$$k_e = c_1' (z_1 z_2)^{-\frac{c_4-1}{2}} D_0^{c_4} \sim \approx \frac{D_0^2}{\sqrt{z_1 z_2}}, \tag{17}$$

where $c_1' = (4\pi^2 c^2 c_1^2)^{-(c_4-1)} c_3^{c_4}$, $c_4 = 2c_2/(2c_2-1) = 1.68 - 2.2 \approx 2$.

It should be noted that the formula (16) we have used is identical with the formula proposed by Pauling [20]. In other studies it is assumed that for a series of similar bonds the binding energy is inversely proportional not to r_e but to its square [21] or its cube [22]. If we use the latter formula, we obtain a weaker dependence of the force constant, and hence of the β-factors, on the binding energy.

Substituting (17) into Eqs. (7) and (8), we find:

for u < 2

$$\beta^n|_{u<2} - 1 = \frac{c_1'}{96\pi^2}\left(\frac{h}{kT}\right)^2 (z_1 z_2)^{-\frac{c_4-1}{2}} D_0^{c_4}\left(\frac{1}{\mu} - \frac{1}{\mu^*}\right) \sim D_0^{c_4} \approx D_0^2, \tag{18}$$

for u > 5

$$\beta^n|_{u>5} = \sqrt{\mu/\mu^*}\exp\left[5\sqrt{c_1'}(z_1 z_2)^{-\frac{c_4-1}{4}} D_0^{\frac{c_4}{2}}\right] \sim \exp\left(dD_0^{\frac{c_4}{2}}\right) \approx \exp(dD_0). \tag{19}$$

Formulas Eqs. (18) and (19) express the desired law of variation of the β-factors as functions of the energy of the bond between the isotope and the non-isotopic atom. If we were to use formula (14), we would find a weaker dependence: $(\beta^n - 1) \sim D_e$ and $\beta^n \sim \exp(d\sqrt{D_e})$. The reason for this result is that we took account of the decrease in the internuclear distance as the binding energy increases [see Eqs. (15) and (16)].

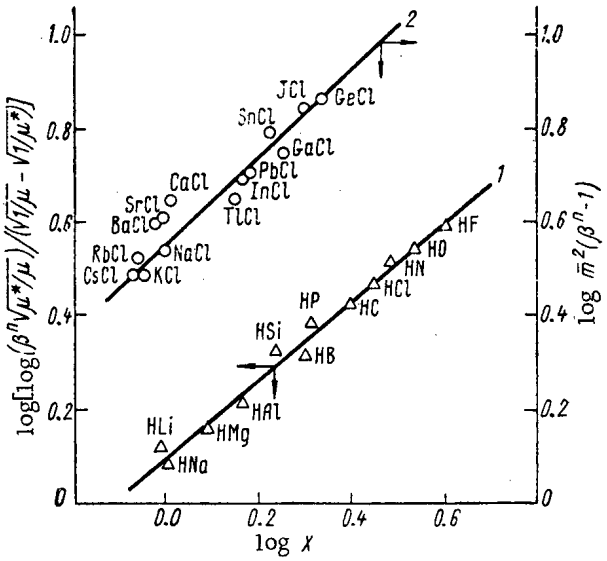

Fig. 7. Variation of $\log_{10}[m^2(\beta^n-1)$ and $\log[\log(\beta^n\sqrt{\mu^*/\mu})/(\sqrt{1/\mu}-\sqrt{1/\mu^*})$ for diatomic molecules as a function of the electronegativity of the second atom: 1) hydrides of the first and second periods of the periodic table; 2) chlorides for which u < 2.

To verify formulas Eqs. (18) and (19), we have plotted three graphs in Fig. 5; for the molecules NaNa, NaK, NaRb, NaCs, and KF, KCl, KBr, KI (u < 2) the coordinates are $\log_{10}(\beta^n-1)$ and $\log_{10}D_0$, while for the hydrides HF, HCl, HBr, HI (u > 5) the coordinates are $\log[\log(\beta^n\sqrt{\mu^*/\mu})/(\sqrt{1/\mu^*})]$ and $\log_{10}D_0$. As can be seen from the figure, formulas Eqs. (18) and (19) are qualitatively satisfied to a satisfactory extent; however, the values of the exponent agree with the calculated values only for sodium and hydrogen exchange: the value of c_4^{Na} calculated from Eq. (17) is 1.68, and the exponent of tan α found from Fig. 5, is 1.7; similarly, for $c_4^H/2 = 1.09$ we find the value $\tan\alpha = 1.0$. On the other hand, for potassium, $c_4^K = 2.19$, whereas the value we found was $\tan\alpha = 1.4$, i.e., the dependence on the binding energy is intermediate between (18) and (19). The reason for this is that Guggenheimer's formula [15] is not satisfied. It is important to observe that even in those cases in which the isotope exchange is not described by formulas (18) and (19), we find a symbatic variation of the β-factors and the dissociation energy (for example, in the case of potassium halides).

On the basis of the formulas so obtained, we can recommend a choice of the pairs of substances to be used in isotope exchange. The separation factor in isotope exchange is equal to the ratio of the two β-factors.

From the relationship between the β-factor and the binding energy we may conclude that the isotope separation factor is greatest when the isotope exchange takes place between the two compounds of the isotopic element which have the greatest difference between their binding energies. On the other hand, when the exchange takes place between compounds which are in two different phases, it is advisable to have a strong bond in one phase and a weak bond in the other. It should be noted that these recommendations are valid only when we are considering series of similar compounds. In the general case, larger force constants will not correspond quite strictly to higher dissociation energies [23].

Influence of Electronegativity

In many cases no information is available on force constants (frequencies of oscillation) and dissociation energy, and therefore it is desirable to find a quantity more easily available for the correlations and suitable for qualitatively predicting the variation of the β-factors in series of similar compounds. Such a quantity is the electronegativity of the atoms forming the molecule [24, 25].

As can be seen from Fig. 6, which we plotted from the data of [15, 18] for the force constants and from the data of [26] for the electronegativity X, the logarithm of the force constant of a diatomic hydride in the first or second period is a linear function of the electronegativity of the element combined with the hydrogen. This relationship is described by the equation

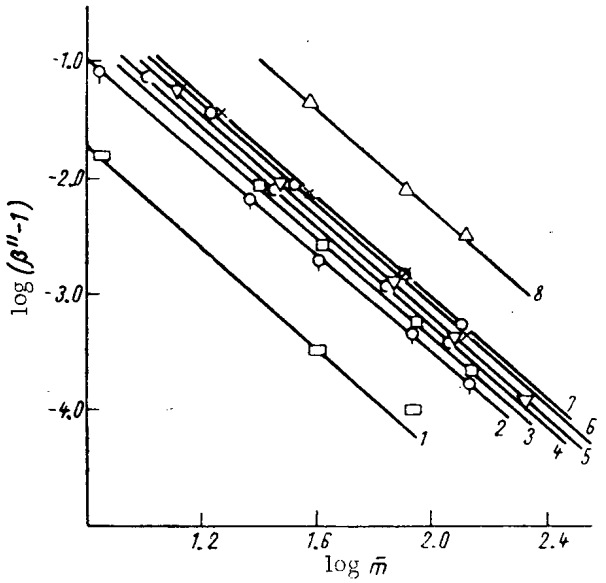

Fig. 8. Variation of $\log_{10}(\beta^n - 1)$ as a function of $\log_{10} \bar{m}$. In all the series shown, the isotopic element is written first in the formula. The values of the β-factors were calculated for a difference of $\Delta m = 2$ between the isotopic masses: 1) LiLi, KLi, RbLi, $\Delta = 0.22$; 2) LiCl, NaCl, KCl, RbCl, CsCl, $\Delta = 0.14$; 3) MgCl, CaCl, SrCl, BaCl, $\Delta = 0.10$; 4) BCl, AlCl, GaCl, InCl, TlCl, $\Delta = 0.10$; 5) CCl, SiCl, GeCl, SnCl, PbCl, $\Delta = 0.15$; 6) O_2, SO, SeO, TeO, $\Delta = 0.14$; 7) FCl, Cl_2, BrCl, ICl, $\Delta = 0.14$; 8) ClO_3^-, BrO_3^-, IO_3^-, $\Delta = 0.16$.

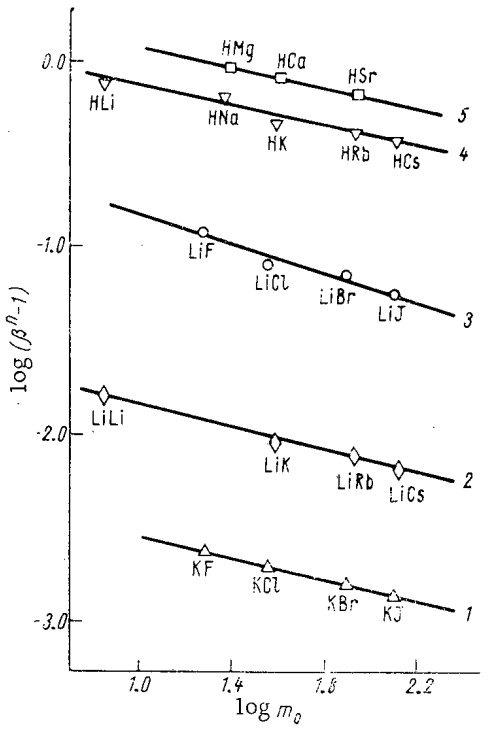

Fig. 9. Variation of $\log_{10}(\beta^n - 1)$ as a function of $\log_{10} m_0$. In all the series shown, the isotopic element is written first in the formula. The values of the β-factors were calculated for $\Delta m = 2$, except in the case of hydrogen isotopes, where $\Delta m = 1$. The values of δ are: 1) 0.27; 2) 0.30; 3) 0.38; 4) 0.31; 5) 0.25.

$$k_e = pX^l. \tag{20}$$

where p and l are constants (for hydrides, p = 0.92 and l = 1.67). The resulting formula enables us to express the β-factor of the isotope exchange in terms of the electronegativity. Substituting the value of the force constant into Eq. (8), we obtain

$$\beta^n|_{u>5} = \sqrt{\mu/\mu^*} \exp\left[\frac{1}{4\pi} \cdot \frac{hc}{kT} \left(\sqrt{1/\mu} - \sqrt{1/\mu^*}\right) \sqrt{p} X^{l/2}\right]. \tag{21}$$

It follows from this that the quantity $\log[\log(\beta^n \sqrt{\mu^*/\mu})/(\sqrt{1/\mu} - \sqrt{1/\mu^*})]$ must vary linearly with $\log_{10} X$. The correctness of this conclusion is evident from Fig. 7 (line 1). It is interesting that the correlation between Eqs. (20) and (21) covers several periods, whereas the above-mentioned correlations with respect to energy were found only within the limits of a group.

A similar rule may be expected for the case of isotopes of different elements combined with the same complementary atom. Figure 6 shows the variation of the force constant of diatomic chlorides as a function of the electronegativity of the isotopic atom for $u < 2$ (line 2). Equation (21) is applicable in this case as well (the constants are $p_1 = 1.15$ and $l_1 = 0.94$), but the degree of approximation is more crude. On substituting the value of k_e into (7), we obtain

$$\beta^n|_{u<2} = 1 + \frac{1}{96\pi^2} \left(\frac{hc}{kT}\right)^2 \frac{\Delta m}{\bar{m}^2} p_1 X^{l_1}. \tag{22}$$

from which it follows that $\log_{10}[\bar{m}^2(\beta^n - 1)]$ will vary linearly with $\log_{10} X$; this is, in fact, seen in Fig. 7 (line 2).

Thus, we have found that the β-factor increases as the electronegativity of the complementary element increases [Eq. (21)] and also as the electronegativity of the isotopic element itself increases [Eq. (22)]. However, this conclusion and the resulting linear variations are subject to certain limitations. The correlations of Eqs. (21) and (22) are valid only when the isotopic or complementary atom is an element of the first or seventh group of the periodic table or when it is hydrogen (the case we have considered). In the general case, however, the force constant varies nonlinearly with the electronegativity. For example, it was found in [27] that

$$k_{AB} = \sqrt{k_{AA}k_{BB}} + (X_A - X_B)^2, \tag{23}$$

where K_{AB}, K_{AA}, and K_{BB} are the force constants of the bonds AB, AA, and BB. The last term may be reduced to a nonlinear variation of K_{AB} as a function of X_B. On the other hand, in the vertical groups of the periodic table the symbatic relationship between the β-factors and the electronegativity is usually satisfied.

Influence of Atomic Masses

For small values of u the variation of the β-factors as functions of the masses of the elements being separated can be derived from Eq. (11). If r_e is independent of the atomic masses, then it follows from Eq. (11) that for a series of similar compounds M_iR the value of $(\beta^n - 1)$ is inversely proportional to the square of the average mass of the isotopic element, $\overline{m} = \sqrt{m^* m}$ (M_i are isotopic elements of the same subgroup; R is the complementary atom, which is identical for all i molecules). Figure 8 shows the variation of $\log_{10}(\beta^n - 1)$ as a function of the logarithm of the mass of the isotopic element for diatomic halides of the first, fourth, and seventh groups of the periodic table, as well as for molecules of the alkali metals and oxides of the fifth group. The figure shows that for all the groups $\log_{10}(\beta^n - 1)$ varies linearly with $\log_{10}\overline{m}$ and the slopes of the lines are very close to one another. The average value of the tangent of the angle of inclination is 2.15. The deviation from a quadratic relationship can be explained by the fact that r_e also depends on the mass of the isotopic element. This produces the additional amount $\Delta = 0.15$ in the expression for $\log_{10}(\beta^n - 1)$ as a function of the mass. It is interesting to note that the relationship we have just found has also proved valid in the $u > 2$ region (see Fig. 8, lines 4-7), although the analytical expression in this case is more complicated.

From the linear variation of $\log_{10}(\beta^n - 1)$ as a function of the logarithm of the mass of the isotopic atom we obtain the formula

$$(\beta_1^n - 1)/(\beta_2^n - 1) = (m_2/m_1)^{2+\Delta}, \tag{24}$$

where the subscripts 1 and 2 refer, respectively, to the two different isotopic elements (and molecules). Formula (24) makes it possible, starting from the values of the β-factors of two molecules, to calculate the β-factors for a series of similar molecules G_iR. For approximate calculations it is sufficient to know the β-factor of one molecule alone, since, as was mentioned earlier, the slopes of all the lines are approximately equal and $\Delta = 0.15$.

Let us now consider how the separation factor varies as a function of the mass of the second (non-isotopic) atom m_0. The theoretical formulas of [28] lead to the conclusion that in the region of small quantum effects ($u < 2$) the β-factors are independent of m_0. As can be seen from formula (11), this would be valid if r_e were independent of m_0. However, since r_e increases as m_0 increases, we may expect that the β-factor will decrease as the mass of the second atom increases. Figure 9 shows that this is indeed the case, although the dependence is relatively weak: $(\beta^n - 1) \sim m_0^{-\delta}$, where $\delta = 0.25$-0.38. This effect explains the decrease in the β-factors of hydrides when the atomic number of the element combined with the hydrogen increases (within one group of the periodic table).

Polyatomic Molecules

For the simplest types of polyatomic molecules the values of the β-factors are determined by the corresponding force constants [3]. This enables us to extend some of the above derived conclusions to the case of polyatomic molecules.

The monotonic variation of the β-factors as functions of dissociation energy in series of analogous compounds is confirmed by a large amount of calculated and experimental data not only for diatomic but also for polyatomic molecules. For example, for deuterium-protium exchange in molecules of H_2O, H_2S, and H_2Se the values of the β-factors at 20°C are equal, respectively, to 11.62, 5.46, and 4.42 [11]. The energy of separation of the first hydrogen

atom in these compounds is 116, 90, and 66 kcal/mole,[1] respectively [23]. The quantitative relationship between the β-factors and the dissociation energies in this case is more complicated, but qualitatively the picture is the same. A similar picture, it appears, will be found in the case of complex compounds as well.[2]

The approximately quadratic variation of the β-factor as a function of the mass of the isotopic element in similar series for symmetric polyatomic molecules of the type XY_p (where X is the central atom surrounded symmetrically by p atoms of Y) might have been expected from the formula [3]

$$\beta^n = 1 + \frac{\Delta M m}{24M^2} u^2 p, \qquad (25)$$

where M and ΔM are, respectively, the mass of the central atom and the difference between its two isotopes; m is the mass of the Y atom; u corresponds to a completely symmetric frequency.

Figure 8 (line 7) shows the data for the polyatomic ions ClO_3^-, BrO_3^-, and JO_3^- [4]. As can be seen from the figure, β varies as a function of M in the same way as in the case of diatomic molecules. Equation (24) was found to be valid in this case also.

LITERATURE CITED

1. H. Urey and Rittenberg, J. Chem. Phys., 1, 137 (1933).
2. H. Urey and L. Greiff, J. Amer. Chem. Soc., 57, 321 (1935).
3. J. Bigeleisen and M. Mayer, J. Chem. Phys., 15, 26 (1947).
4. H. Urey, In the collection "The Chemistry of Isotopes" [Russian translation], Moscow, Izd-vo inostr. lit. (1948) p. 86.
5. A. I. Brodskii, The Chemistry of Isotopes [in Russian], Moscow, Izd-vo AN SSSR (1952).
6. M. Benedict and T. H. Pigford, Nuclear Chemical Engineering [Russian translation], Moscow, Gosatomizdat (1960).
7. A. M. Rozen, Theory of Isotope Separation in Columns [in Russian], Moscow, Gosatomizdat (1960).
8. E. M. Kuznetsova et al., Dokl. AN SSSR, 148, 144 (1963).
9. A. M. Rozen and A. I. Mikhailichenko, Dokl. AN SSSR, 148, 1133 (1963).
10. A. M. Rozen and A. I. Mikhailichenko, Ibid., p. 1354.
11. Ya. M. Varshavskii and S. É. Vaisberg, Dokl. AN SSSR, 100, 97 (1955).
12. Ya. M. Varshavskii and S. É. Vaisberg, Zh. fiz. khim., 29, 523 (1955).
13. Ya. M. Varshavskii and S. É. Vaisberg, Usp. khimii, 26, 1434 (1957).
14. G. Hertzberg, Spectra and Structures of Diatomic Molecules [Russian translation], Moscow, Izd-vo AN SSSR (1949).
15. K. Guggenheimer, Proc. Phys. Soc., 58, 456 (1946).
16. K. S. Krasnov and V. G. Antoshkin, Zh. neorganich. khim., 3, 1490 (1958).
17. T. Moran and J. Trishka, J. Chem. Phys., 34, 923 (1961).
18. G. Somayajulu, J. Chem. Phys., 33, 1541 (1960).
19. M. V. Vol'kenshtein et al., Oscillations of Molecules [in Russian] 2, Moscow-Leningrad, Gostekhteorizdat (1949).
20. L. Pauling, J. Phys. Chem., 58, 662 (1954).
21. H. Jenkins, Trans. Faraday Soc., 51, 1042 (1955).
22. H. Feilchenfeld, J. Phys. Chem., 63, 1346 (1959).
23. T. Cottrell, The Strength of Chemical Bonds [Russian translation], Moscow, Izd.-vo inostr. lit. (1956).
24. L. Pauling, The Nature of the Chemical Bond [Russian translation], Moscow, Goskhimizdat (1947).
25. S. S. Batsanov, The Electronegativity of Elements and Chemical Bonding [in Russian], Novosibirsk, Izd-vo SO AN SSSR (1962).
26. E. Little and M. Jones, Chem. Educ., 37, 231 (1960).
27. G. Somayajulu, J. Chem. Phys., 28, 814 (1958).
28. J. Bigeleisen, Phys. Rev., 99, 638 (1955); J. Chem. Phys., 23, 2264 (1955).

[2] For H_2Se we list the average binding energy, which is close in absolute value to the dissociation energy.
[3] It is assumed that the strength of a complex varies symbatically with its dissociation energy.

PROSPECTIVE DEVELOPMENTS AND ECONOMICS OF NUCLEAR POWER GENERATION

B. B. Baturov and N. M. Sinev

Translated from Atomnaya Énergiya, Vol. 18, No. 2,
pp. 157-171, February, 1965

The principal item at the Third International Conference on the Peaceful Uses of Atomic Energy (Geneva, 1964) was the question concerning the prospects and development routes for the economical generation of nuclear power in the various countries of the world. More than 50 reports[1] were devoted to the discussion and investigation of this problem and there were communications from more than 20 countries. Moreover, in almost all the reports devoted to basic construction and materials, to the fuel cycle, raw materials and other problems, the problem concerning the prospects for the development of nuclear power generation was touched upon to some degree or other.

The discussion showed that nuclear power generation has emerged from the period of experiments and demonstration of the possibilities into a period of extensive industrial development. Even at the present time, thermal reactors are entering into a new phase of yearly increasing economically sound construction; fast reactors will enter into this phase somewhat later, probably in the next 6-10 years. This was one of the most important conclusions of the conference.

According to forecast, the installed output from nuclear power stations in the capitalist countries may amount by 1980 to 14-20% of the total installed capacity (Table 1). It should be remembered that at the time of the First Geneva Conference (1955) the output from nuclear power stations amounted to a total of only 5000 kW, at the time of the Second Conference (1958) it was 185,000 kW and in 1964 it had already reached ~5000 MW. Forecast estimates of the total nuclear power station capacities after 1980 are less reliable. Here, the discrepancies attain considerable magnitudes, depending on the assumptions made concerning the increase of population and of the over-all level of power production. It is acknowledged, however, that the fraction of nuclear energy generation within the coverage of energy requirements towards the year 2000 may amount to about 50%.

This figure represents the probable situation, despite the fact that according to the estimates in Report 256, the world reserves of conventional fuel may suffice, on the average, up to the middle of the next century. The substitution of conventional fuel by nuclear fuel will be commenced well in advance of exhaustion of (conventional fuel) reserves. Obviously, this process will involve a long period of time,[2] estimated at decades (256).[3]

The conditions for competitive capability of nuclear power stations with thermal power stations differ sharply in different countries and also in different regions of one and the same country, depending on the reliability of the energy resources and on the scale of energy requirement. There is no universal index for the level of competitive capability of nuclear power stations which is independent of actual geographical, industrial and raw material conditions. In individual cases construction of relatively low-capacity (~50-100 MW) nuclear power stations is considered to be economically justified: for example, for certain regions of Pakistan and other developing countries[1].

[1]The list of papers from Soviet scientists is published in Atomnaya Énergiya, 17, No. 3, 235 (1964), and the list of papers by foreign scientists in Atomnoi tekhnike za rubezhom, No. 9, 27 (1964).

[2]It should be borne in mind that in the next decade industrial development may increase and produce new sources of energy and new routes for the development of energy generation: thermonuclear fusion, magnetohydrodynamic generators, direct transformation of thermal energy into electrical energy, etc. However, at the present time it is not possible to clearly represent the effect of these new factors on the future development of nuclear power generation.

[3]The numbers of the reports are given in brackets.

TABLE 1. Rated Power of all Electric Power Stations, Millions of kW (192, 256, 294)

Country or group of countries	1964		1970		1975		1980	
	total	NPS	total	NPS	total	NPS	total	NPS
USA	–	0.94	257	6-7	354	21-37	472	60-90
Other capitalist countries	–	3.25	117	14-15	171	35-50	240	80-110
USSR	102.4	0.9	180-200	Several million kW	–	–	500-600	Several tens of millions of kW

The general tendency to improve the efficiency indexes of nuclear power stations consists in the exploitation of power stations with a unit output of 500-600 MW, and in individual cases even higher, with increased average fuel burnup: up to 4000 MWD/t of U in gas-graphite reactors; 10,000 MWD/t of U in heavy water reactors and 20,000 MWD/t of U in water-cooled/water-moderated reactors. Attainment of these technological indexes enables a competitively feasible cost to be obtained for electrical energy from nuclear power stations in developed industrial countries, and for many other regions a lower cost relative to the cost of electrical energy generated by conventional power stations (1, 10, 31, 37, 192, 216, 247, 559, 561).

A brief review will be given below of the over-all concepts of development and the conditions for achieving competitively feasible nuclear power generation according to the leading foreign countries.[4]

USA

The output from nuclear power stations in the USA may amount to 60-90 million kW towards 1980 (192).

At the conference of the Nuclear Industrial Forum in San Francisco on December 1, 1964 the Chairman of the AEC, Dr. Glenn Seaborg, reported that the Federal Commission on power generation in the USA assumes that the output from nuclear power stations in 1980 should amount to about 70 million kW and the output from all power stations to 550 million kW. Thus, the fraction from nuclear power stations will reach 13-14% [2]. Water-cooled per water-moderated reactors will be used in the majority of nuclear power stations. After 1970, the whole of the increasing fraction of the installed capacity will consist of nuclear power stations with advanced thermal reactor-converters, which should ensure more efficient consumption of uranium because of the increased breeding factor (plutonium factor). These projects will be undertaken mainly by private commercial firms.

According to Dr. Glenn Seaborg's statement, towards this time (prior to 1980) "The AEC will concentrate its effort exclusively on the construction of breeder reactors with a large breeding factor. Our present-day program of constructing advanced reactor-converters is approaching the time of commercial production." "... Towards 1970 the principal consideration of the AEC will be given to fuel, materials and other components essential for breeder reactors. The majority of the possibilities and limitations concerning materials, fuel, technology, processing, etc., will be studied and mastered by 1980, so that when the improved breeder reactors, with a capacity of 1000 to 1500 MW, are ready for use by power generation companies, precise data on costs will be available for almost the entire planned nuclear power station installation."[5]

After 1985, with the faster tempo everywhere, breeder reactors will begin to enter into commercial operation. As a result of this, the operation of light water reactors and of advanced breeder reactors will be extended. The proportion of each type of reactor in the over-all output of electrical energy from nuclear power stations will depend on the relative efficiency, the rate of increase of nuclear power station capacity, fuel breeding in fast reactors and uranium costs.

[4] A similar review by the USSR is published in the journal "Atomnaya Énergiya" 17, No. 4, 243 (1964).

[5] The firm of General Electric (Nucleonics, 22, No. 11, 18, 1964) has stated that towards 1974 it is proposing an efficient reactor-breeder for commercial use, taking into account the necessity for accelerating development of this type of nuclear power station and for justifying the large expenditure put into their development.

TABLE 2. Natural Uranium Requirements (256), Tons U_3O_8*

Country or group of countries	1970		1975		1980	
	annual	cumulative†	annual	cumulative†	annual	cumulative†
USA	1450-3800	8150-12,700	8100-12,700	33,500-58,000	17,200-24,400	100,000-154,000
Other capitalist countries	5450-8150	25,400-30,000	12,700-17,200	72,500-100,000	21,800-29,000	163,000-218,000

*For development of nuclear power generation according to Table 1 data, using PWR and BWR type reactors and taking into account fuel recycling, and using uranium tailing enriched to 0.253% U-235.
†Cumulative requirement beginning with 1965.

The AEC plans to carry out the production of five types of advanced thermal breeder reactors: 1) high-temperature gas(helium) cooled; 2) heavy water, organic-cooled (high power for a dual-purpose nuclear power station with distillation unit); 3) a reactor with a seed- and breeding-zone (for a uranium-thorium cycle); 4) a reactor with spectral shift; 5) graphite-sodium. From 1964, the first three types will be given a great deal of consideration, since they have the maximum potential for achieving economic competitive capability and for the prospective use of the Th^{233} cycle almost in the "breeding" regime.

The program of study and construction of advanced reactor-converters is recognized by the AEC as guaranteeing the time necessary for developing high-efficiency breeder reactors. It is considered that the USA's program cannot be based on the assumption that these breeder reactors will be developed and introduced into industry over a short period and to an adequate extent.

The development of the technology of advanced breeder reactors is represented in the USA as the more simple problem, the solution of which will permit the accomplishment of a wide program of construction of economical nuclear power stations and will prevent the rapid exhaustion of relatively inexpensive uranium resources as a result of the development of nuclear power generation, based only on thermal reactors of the PWR and BWR type. It is emphasized that the development of breeder reactors should be achieved at the proper time, in order that the proportion of reactor-converters and breeder reactors constructed after this time would enable the generation of cheap electrical power to be guaranteed (192).

This observation reflects the fear that because of increasing uranium demands and the processing of increasingly lower-grade ores, uranium prices may be increased and, consequently, the cost of electric power from reactor-converters (which is more sensitive to uranium costs than the cost of electrical power from breeder reactors) will increase to values which will necessitate the limitation of the number of reactor-converters under construction and possibly in operation. Nevertheless, it is emphasized (192) that serious limitations are not expected in the development of nuclear power generation and that natural uranium, as a result of efficient utilization, will remain at a reasonable price. Natural uranium requirements for nuclear power generation developed with the predominant use of water-cooled/water-moderated (PWR type) and boiling (BWR type) reactors are shown in Table 2 (256). Although at the present time it can be seen that there is an overproduction of natural uranium and it is expected (256) that world uranium production will be reduced (from ~20,000 tons in 1964 to ~14,000 tons of U_3O_8 in 1970), this is an apparent surplus of uranium.

It follows from Table 2 that the world uranium requirement for 15 years and the annual requirement at the 1980 level is extremely large. These requirements cannot be guaranteed by reserves of prospected uranium which can be produced at an acceptable price, assumed to be 17.6 per kg (256). Because of this, despite the apparent overproduction of uranium, it will be necessary even now to extend uranium prospecting and to discover new deposits in order to ensure the rapid growth of nuclear energy generation in the period after 1975. Only in this way can a stable market be ensured for natural uranium, with respect to volume and price, on which will depend the stability of the efficiency indexes of the reactors installed.

The natural dependable uranium reserves of the USA, from which uranium can be extracted at a cost of $11 to $22 per kg, are estimated at 50-100 thousand tons. The possible supplementary reserves are estimated at 250 thousand tons. It is emphasized that at the time of exhaustion of the natural uranium reserves, advanced reactor-converters should be widely distributed and breeder reactors should be widely installed, which will reduce significantly

TABLE 3. Efficiency Indexes of Nuclear Power Stations in the USA (216, 247) [3]

Name of NPS	Year of startup	Electrical capacity, MW	Efficiency, %	Fuel rating, MW/t U	Average fuel burnup, MWD/t U	Specific cost, $/kW	Cost of electrical energy, cent/kWh
PWR type reactor							
Yankee	1960	185	29.0	8.40	8000-12,000	220	0.950
Indian Point	1962	255	26.0	15.60	17,000	350	0.731
San Onofre	1966	395-430	31.0	6.80-7.40	20,000	190-208	0.639
Malibu	1967	460	31.4	6.86	20,000	174-187	0.470
Connecticut Yankee	1967	460-490	31.0	6.85-7.25	20,000	174-184	
BWR type reactor							
Dresden	1959	200	30.6	3.88	8600	183-245	
Bodega Bay	1966	313	31.0	4.67	16,000	190-212	0.582
Nine Mile Point	1968	500	32.0	5.26	16,000	180	0.667
Oyster Creek	1968	515-640	32.0	5.42-6.53	16,000	110-140	0.350-0.405

the natural uranium requirements after 1980. By the further use of nuclear power stations with water-cooled/water-moderated reactors in the USA and by taking account of recycling and recovery of fuel, the requirement should be (256): 135,000 tons in 1980-1985 (installed capacity of nuclear power stations 150,000 million kW), 380,000 tons in 1980-1990 (nuclear power station capacity 280,000 million kW) and 900,000 tons in 1980-2000 (nuclear power station capacity 730,000 million kW).

In the final report [4] summarizing the work of the Conference, Dr. Glenn Seaborg stated: "Some delegates feel that at present no effort should be spared on breeder reactor installation, since the reactors existing at the present time and also the advanced reactor-converters will be able to generate energy over many decades. This opinion will be strengthened considerably if it proves feasible to extract uranium from sea water at a cost not exceeding $ 44 per kg."

Thus, from the point of view of raw materials and economics, alternatives for the widespread development of nuclear energy generation are as follows: either to develop nuclear power generation using thermal reactors with a definite time-preference in the extent of the processing and ever increasing size of the output of dispersed uranium for relatively low-grade ores (possibly even from rocks and sea water) on a large scale and, as a consequence, increasing the dependence of the cost of electric power on the cost of uranium extraction from low-grade rocks; or, to develop a technology, at present inadequately proved, using predominantly fast reactors, with limited natural uranium requirements and almost total independence of the cost of electric power on the cost of extraction and the cost of uranium.

Intermediate solutions are also possible, in which the transition period from thermal to fast reactors is determined by the quantity of available inexpensive uranium, and by the demands and planned scales of development of nuclear power generation. However, this solution is palliative if there is a proven fast breeder reactor-converter, but in the absence of such a reactor it is essential to accelerate in every possible way its development and to solve the technological problems associated with the fuel cycle, provided that it is not directed by the processing of rocks or sea water.

In the ten years which have elapsed since the day of startup of the first nuclear power station, thermal reactors have been sufficiently developed to enable a wide program of nuclear power station installation to be undertaken. Consequently, there are no grounds for assuming that processing of the entire complex of problems associated with the installation of economical breeder reactors for large-scale nuclear power generation will require a great deal of time, energy and investment. The next five or six years will probably permit a more accurate estimate (it may be even at the Fourth Geneva Conference) as to which route for the development of nuclear power generation should predominate during the following decade.

A certain discrepancy should be noted in the forecasts of the relative trends of price change in natural uranium as reported by Dr. Glenn Seaborg, R. Faulkner, and V. McVey (256). Dr. Glenn Seaborg, at the conclusion of

the report, noted [4] that "...The universally-used figure of $13.2 per kg U is probably the upper limit at present... An increase in the quantity of uranium mined will lead also to a reduction in its price." At the same time, it is shown (256) that "...It would be unrealistic to assume that uranium prices should be extended to remain at this low level for more than a few years. Higher prices can be expected soon after 1970. There is a strong possibility that prices will hold out at the level of $17.6 per kg or less during this decade, but this will depend to a great extent on when large-scale exploration will be undertaken and what will be the results of this exploration."

The impression is created that in the USA intense efforts are being made to inform interested countries and domestic firms that the future of nuclear power generation based on water-cooled thermal reactors is ensured by natural uranium (conditioned by widespread exploration and the opening of new deposits) and also by enriched uranium (for conditions applicable to the USA, where 150 tons of U^{235} are reserved for foreign reactors). For this, the assurance is given (192) "...To enrich all uranium which is required in foreseeable quantities for domestic power production as well as for the external market, possibly arising in Europe and in other parts of the world."

The efficiency indexes of large-scale nuclear power stations in the USA are shown in Table 3. Particular emphasis should be laid on the offer by American firms to install reactors at a cost of $140 per kW, and possibly even lower, with a guaranteed cost of electrical energy generation. The conclusion of an agreement between the Jersey Central Power and Light Company and the General Electric Company on the construction at Oyster Creek of a nuclear power station with a 515-620 MW capacity at a total cost of $68 million, including all expenses, should be noted as a significant achievement in the area of producing competitive electric power. The cost of the electrical energy generated is guaranteed at 0.4 cent/kWh for a station load factor of 88%. The term "all expenses" is obviously, in this case, of a somewhat legal nature and implies that the Jersey Central Power and Light Company does not "hand out" expenses to any large extent. However, this does indicate what actual cost of the nuclear power station is contained in the stated sum. This cost of 0.4 cent/kWh for electric power should be considered, more precisely, as rather optimistic especially as it assumes—in addition to relatively low investments—a high load factor for the nuclear power station, which is difficult to achieve with the fuel recharging conditions and power requirements. In a recent publication by the General Electric Company, the price list of costs for boiling water reactors [5], it is pointed out that these costs are approximately 12% higher than given in the contract for installing the Oyster Creek nuclear power station.

If it be assumed, however, that the cost of the land plot, the interest on capital over the construction period and contingency expenses amounting to an average of 15% of those given in the contract are not included in the price list, then the actual cost of the Oyster Creek nuclear power station will be ~27% greater than that stated in the contract. Consequently, it can hardly be reconciled with the attempt to represent closure of the contract as a kind of "economic breakthrough" in the realm of production of competitive nuclear electric power, perfected by means of water-cooled/water-moderated boiling reactors, taking account of the degree of validity in the published information. Moreover, it is not possible to reconcile it with the attemp to attribute to this "breakthrough" the nature of a result which is applicable to the majority of countries in the world, as is suggested in the General Electric Company's report (205).

The efficiency characteristics presented for the Oyster Creek nuclear power station were the subject of a discussion in material published at the conference and in its lobbies. This question, in particular, was discussed in [6]; an economic comparison was undertaken of such American reactors as Oyster Creek and Nine Mile Point with Canadian reactors of the CANDU type. The results of this comparison are presented in Table 4. It follows from the table that if the comparison were made under comparable conditions, with identical initial assumptions and by a single method for taking into account expenditure on fuel, then the cost of the Oyster Creek nuclear power station increases considerably in comparison with the sum stated by General Electric, although the cost of electric power is somewhat reduced. As a result of this, the cost of electric power from a reactor of the CANDU type is found to be comparable with the cost of generation in the Oyster Creek reactor and significantly lower in comparison with the cost of energy generated by the Nine Mile Point nuclear power station. The increase of capital expenditure on the Oyster Creek nuclear power station is explained mainly by the addition of fuel costs to the extent of ~$15 million, which, in the Canadian version of the calculation, are considered as capital investments.

It is emphasized, in particular, that the cost of electric power in the two nuclear power stations with boiling water reactors of capacity ~600 MW at Oyster Creek and Nine Mile Point differs by approximately 20%, although the expenditure on the reactor, equipment, etc., should be approximately the same since the reactors are constructed by one firm and at one and the same time. The conclusion can be drawn from the difference as stated that the

TABLE 4. Comparison of Nuclear Power Stations in the USA and Canada [6]

Characteristics	Oyster Creek type			Nine Mile Point type		CANDU type		
Electrical capacity (net), MW	515	565	620	500	600	500	600	750
Total capital expenditure, $M	82.95	83.45	83.45	96.7	97.1	116.5	128.8	139.8
Capital costs, cent/kWh (interest on capital 5.5%; lifetime 30 years; load factor 85%)	0.158	0.144	0.132	0.190	0.159	0.228	0.212	0.196
Fuel costs, cent/kWh	0.132	0.131	0.130	0.170	0.170	0.060	0.059	0.057
Operating costs, cent/kWh	0.061	0.056	0.053	0.059	0.051	0.065	0.059	0.053
Cost of power, cent/kWh	0.351	0.331	0.315	0.419	0.380	0.353	0.330	0.306

efficiency data for the Oyster Creek reactor obviously reflect a certain optimism, while the Nine Mile Point reactor data are more realistic. In connection with this, a reactor of the CANDU type is estimated to be the most promising and most economical plan in any case for Canadian conditions.

The results of the analysis undertaken in Canada confirm the point of view expressed at the Conference which, obviously, is universally accepted at present; it consists in the fact that as a result of the efficiency analysis, carried out in conformity with the conditions applicable to one country, and taking account of the singularities of its judicial legislation (land, insurance, defining the ownership rights for nuclear fuel, etc.) industrial and financial conditions of this country (interest rate on capital guaranteed by the government for the price of recovered plutonium, payment for enrichment and further enrichmentof fuel), it is not possible to draw conclusions about the economic prospects of the use of comparable reactors for other countries, where legal, industrial and financial conditions may differ sharply from the conditions set as the basis of the analysis.

The factors which affect significantly the cost of electric power are the method of determining fuel costs, including the first fuel charge, and the value of the capital interest. For example, in the USA the capital interest assumed in calculations fluctuates from 3 to 14%; in Great Britain the capital interest from 1955 to 1964 rose from 4 to 7.5%; in Canada up to ~7% and in France a figure of 7% is used for the EDF-3 and EDF-4 reactors. For the nuclear power station at Wylfa (Great Britain) the change of capital interest from 4 to 7.5% leads to an increased cost of electrical power from 0.56 to 0.67 d/kWh (10, 37, 216, 559).

As a rule, increased capital expenditure in the installation of nuclear power stations is associated with relatively low capital interest. This circumstance enables a moderate capital component of the cost of power to be obtained for relatively high capital investments. It is difficult, however, to say to what extent the choice of capital interest rate and the station lifetime reflects the objective economic conditions in different countries and the technological possibilities of the various types of reactors.

Even so, the methods of calculating fuel costs, including the first charge, are different. In Great Britain, in estimating the cost of electrical energy in nuclear power stations (559) the cost of the first charge is included in the capital costs and the cost of replacement fuel is included in the running expenses. There is no full credit on the plutonium, which can be accepted as a variable in calculating the cost of power, but which hardly represents the practical side of the problem, taking account of the fact that the accumulated plutonium is assumed to be usable. In Canada, in estimating the cost of power, only the cost of one-half of the first charge is related to the capital expenditure, the remaining fuel supplies being related to the running costs. There is also no credit on the plutonium, which is quite natural, taking into account the Canadian concept of the once-only use of fuel in reactors with very high burnups. In the USA, economy estimates are based on different assumptions concerning the procedure for fuel ownership (rented by the AEC or private ownership) and, correspondingly, on different types of calculations. With fuel rental by the AEC, an annual rental fee is levied to the extent of 4.75% of the fuel costs borne by the cost of power. With private ownership of fuel, the cost of the first charge in power cost calculations is related to the capital costs and the cost of replacement fuel is related to the running costs. However, in the stated

costs for nuclear power stations, the cost of the first charge is sometimes not included, as was done for the Oyster Creek nuclear power station. In the calculations, a plutonium credit is used to a total of $10 per g over the period prior to 1970 and $8 per g in the period after 1970. According to a law passed by the Congress of the USA a transition period has been established prior to July 1, 1973 during which nuclear fuel for power production requirements would be transferred completely to private ownership. The granting of nuclear fuel for rental will be discontinued from 1971 [7].

In connection with the comparisons which have been discussed, only such power cost estimates can be taken into account which are made for the conditions of a single country and by a single procedure.

In our opinion, the concept of the development of nuclear power generation in the USA, based on the predominant installation over the next 20 years of nuclear power stations with advanced and nonadvanced thermal reactors with a capacity of 70-100 million kW, has certain distinctive features which give one the impression of its not being entirely satisfactory:

1) the extremely inefficient use of stocks of available cheap uranium, which involves the necessity for developing methods of extraction and production of uranium from ores containing small concentrations, or from sea water;

2) the dependence of the cost of electric power on the successes achieved in the technology of extraction and refining of low-grade uranium ores in ever-increasing quantities, proportional to the scale of development of nuclear power generation;

3) reduction of the breeding factor with burnup, associated with which the most economical reactor of the PWR or BWR type—operating with maximum fuel burnup—is a poor converter and does not create the conditions for efficient and timely transition to the widespread use of breeder reactors.

The program for the extensive use of water (including boiling) reactors in the USA over the period prior to 1980 is determined by specific characteristics of the American economy based on private enterprise and also on the politics of the AEC in the realm of fissile materials (of guarantees in the granting of enriched uranium and of enrichment facilities, guarantees in relation to the acquisition and price of plutonium, etc.). Therefore, it can hardly be assumed that the stated economical preference for reactors of the PWR and BWR type will be maintained also beyond the territorial limits and economic conditions of the USA unless some other country creates for itself the appropriate conditions or agrees to establishing its nuclear power generation as a function of the economic and legal conditions existing within the USA. Consequently, in the Canadian paper [6] it is shown directly that "...The boiling water reactor attracts low capital costs, but it depends on an enriched uranium fuel cycle with the entire resultant political and economic indeterminacy."

An extremely important factor is that the economical prospects for nuclear power generation in the USA are based on cost estimates for the production of electric power for individual nuclear power stations and not on an analysis of the development of nuclear power generation as reflected entirely by industry, including proportional development of the fuel cycle plant. One of the sources of additional indeterminacy in the efficiency indexes of reactors is the taking account of fuel cycle costs based on prices laid down by the AEC on the rental of nuclear fuel (and in individual cases arising from the conditions of private ownership). In this case the additional capital costs of the fuel cycle installation are not taken into account, and should be built additionally into the standards necessary for developing nuclear power generation. An analysis carried out by the USSR (294) showed that the capital costs of the fuel cycle installation (extraction and enrichment of uranium, manufacture and chemical processing of fuel elements) for the development of nuclear power generation based on the use of slightly enriched uranium are considerable and may reach one-half of the capital costs incurred in construction of the nuclear power stations themselves (especially with water-cooled/water-moderated reactors). This situation is quite explicable and, with a large degree of certainty, is invariant relative to the conditions existing in the USSR and the USA since it is governed by the physical characteristics of reactors operating on slightly enriched uranium: for low initial fuel enrichments, the quantities subjected to processing in the cycle and the costs associated with this processing are very considerable. At the same time, recovery of the regenerated uranium and plutonium for secondary use is small: consequently, the amount of fuel necessary for makeup of the cycle and the costs determined by these quantities are also considerable.

If the capital costs incurred in construction of the fuel cycle plant are taken into account for nuclear power generation developed, for example, by the use of Oyster Creek type of reactors, then to the $68 million constituting

the capital costs inherent in the construction of the station it is necessary to add further costs to the extent of $34 million (0.5 · $68 million) incurred in development of the fuel cycle plant, which has either been done previously or which should be done additionally if the existing capacity of fuel cycle plant is inadequate for the planned scale of development of nuclear power generation.

In any case, in considering the prospects for the development of power generation on national scales for a country which is planning to set up an independent nuclear power program based on water-cooled/water-moderated and boiling water reactors with slightly enriched uranium, the costs incurred by construction of the fuel cycle plant and by loading them with fuel are very considerable.

Taking account of what has been stated, the total capital expenditure on the construction of a nuclear power station with a capacity of 620 MW at Oyster Creek and ensuring its normal operation should amount to $102 million, i.e., $165 per kW without costs incurred by the fuel charge.

Of course, as a result of these figures the relative economical prospect for reactors of this class for the extensive development of nuclear power generation may be considerably altered if nuclear power generation is considered as a branch of industry on a national scale and not as an individual nuclear power station for which all the related installations must be developed.

At the same time, there is no cause for doubting the possibility of producing economical power from water-cooled/water-moderated reactors, even taking account of the fuel cycle costs. It can also be assumed that the Geneva Conference has once again confirmed the necessity for an accelerated development and construction of economical fast breeder reactors, since the problem of the most complete and efficient utilization of cheap nuclear fuel reserves can only be solved reliably by their use.

The fact that the taking into account of the fuel cycle plant costs, the development of nuclear power generation with the predominant use of fast reactors is found to be economically satisfactory and that by way of the sole alternative to this development route it was proposed at the Geneva Conference to investigate an inexpensive technology for processing low-grade ores, confirms the future of large-scale nuclear energy generation beyond fast reactors.

The question concerning the period when an economical fast reactor will be completed and many of the problems associated with its construction are solved successfully (acceleration of processing and recovery in the fuel cycle, manufacture of special plant, etc.)—this is a problem concerning the rates of operation and the scale of conditions which will be applied for this. Even the scale of effort, in its turn, is determined by the capacities for nuclear energy generation which must be introduced in the immediate future.

The over-all situation which is building up in different countries, just as in the rapidly-developing world as a whole, requires that no effort be spared and that the problem of economical fast breeder reactors be solved rapidly.

GREAT BRITAIN

In 1960, the installed capacity of power stations in Great Britain amounted to 27 million kW (561), of which 88% operated on coal and 12% on liquid fuel. The increase in the demands for electrical power made the addition necessary of up to 34 million kW of installed capacities towards the end of 1965. The installed capacities of the nuclear power stations, according to the situation in September, 1964 amounted to 1.25 million kW; the nuclear power stations produced 5% of the country's electrical power (559). It is postulated that towards 1970 the total capacity of power stations will amount to 67 million kW, comprising 76% coal-fired, 15% liquid fuel and 7.5% (or 5 million kW) nuclear-fuelled. These nuclear power stations should cover 12% of the electrical power requirement, since it is planned to use them in the basic operating regime (with a load factor of 0.75-0.85).

The over-all expenditure on the first installation program for nuclear power stations in Great Britain, including the costs of the first reactor fuel charges, will exceed £600 million ($1680 million), which amounts on the average to about £120 per kW net ($336 per kW net), taking account of the capital investment in the fuel cycle undertaking (Table 5).

For the construction of thermal power stations with a capacity of 100-275 MW, introduced in 1962, the specific cost amounted to £50 per kW net. In the period 1965-1970 it is anticipated that these costs will be considerably lower than the specific cost of the most modern nuclear power station at Wylfa, with two Magnox reactors of capacity

TABLE 5. Capital Costs and Initial Characteristics of Nuclear Power Stations in Great Britain (559)

NPS	Year of startup of first reactor	Guaranteed output, MW(e)	Thermal efficiency, %	Fuel rating, MW(e)/t U	Capital cost	
					£/kW	$/kW
Berkeley	1962	275	24.4	0.59	186	516
Bradwell	1962	300	28.2	0.63	176	488
Hunterston. . .	1964	300	28.3	0.60	*	*
Hinkley Point.	1964	500	26.4	0.72	150	416
Trawsfynydd . .	1964	500	29.4	0.85	137	380
Dungeness . . .	1965	550	32.9	0.92	114	311
Sizewell	1965	580	30.5	0.91	107	297
Oldbury.	1966	600	33.6	1.02	108	299
Wylfa.	1968	1180	31.5	1.00	100	278

*Under negotiation.

TABLE 6. Cost of Electrical Power from Nuclear Power Stations in Great Britain, d/kWh (559)

NPS	For lifetime 20 years, load factor 75% and fuel burnup 3000 MWD/t U			For lifetime 25 years, load factor 85% and fuel burnup 4000 MWD/t U		
	capital charge*	running cost†	generating costs	capital charge*	running cost†	generating costs
Berkeley	0.83	0.38	1.21	0.68	0.30	0.98
Bradwell	0.77	0.30	1.07	0.62	0.24	0.86
Hinkley Point .	0.69	0.35	1.04	0.56	0.27	0.83
Trawsfynydd . .	0.63	0.33	0.96	0.50	0.27	0.77
Dungeness . . .	0.50	0.24	0.74	0.40	0.20	0.60
Sizewell	0.47	0.26	0.73	0.38	0.21	0.59
Oldbury.	0.47	0.23	0.70	0.38	0.19	0.57
Wylfa	0.44	0.23	0.67	0.35	0.19	0.54

*The capital charge includes the interest on capital (including during the construction period), amortization deduction and initial fuel charge.
†Running costs include replacement fuel, interest on its use, manufacture of fuel elements, costs incurred by other operations, and also insurance, indirect expenditure and taxation.
Footnote. 1d (penny) = 1.6 American cent.

590 MW each (£100 per kW net). The fuel component cost of energy from nuclear power stations is assumed to be reduced from 0.25 to 0.15 d/kWh (Table 6). The fuel component cost of energy from conventional power stations over the period 1965-1970 is expected to be 0.35-0.50 d/kWh, depending on the source of fuel and the transportation distance.

It is noted (561) that the indexes for conventional power generation are less "dramatic" than for nuclear power generation but the gap between them is being reduced continuously, although at a lesser rate than was postulated in 1955.

The data presented in Table 5 characterize the progress of the technological and economic indexes of nuclear power stations with Magnox reactors. The cost of electrical power from these nuclear power stations is quite high (see Table 6), but it is given in the report to illustrate the effect of reactor characteristics on the cost of power, in the assumed absence of credit on the plutonium.

Over the period 1970-1975, according to the plan of the Central Electricity Generating Board (CEGB), an increase is contemplated of 5 million kW of power generation capacity. However, in the UKAEA report (559) it is pointed out that this program "... if we really desire to make nuclear energy attractive is small." "Even conservative assumptions show that nuclear energy during the period will be economical."

The type of reactor for the second program has not yet been selected. It is noted that each type of reactor can display its advantage for defined economic conditions. From the point of view of the UKAEA, the gas-graphite reactor operating on enriched uranium (AGR) is the most advantageous for British conditions; however, before making the final choice, it is proposed to study carefully the possibilities of water reactors. It should be noted that in the development program a heavy water reactor is included with nuclear steam superheat and with a capacity of 100 MW, which is planned for startup in 1968. It is presumed that this reactor will be competitive over a large range of capacities.

A considerable fraction of the costs is expended on fast reactor development (559), since on this depends the widespread development of nuclear power generation which will ensure cheap electric power. The problem is to achieve burnups of 5% and to study the engineering problems of large-scale reactors. In order to obtain results which will enable the type of fuel and the reactor design to be chosen, it is proposed to construct a prototype reactor which would demonstrate the operating characteristics of commercial fast reactors with a capacity of 1000 MW. In the event of successful achievement of this program the prototype will be commissioned soon after 1970. The first commercial nuclear power station with a fast reactor may come into service towards the end of the 1970's.

The well-known indeterminacy of the British route for developing nuclear power generation was mentioned at the Conference and it was the subject of questions and discussions, in the course of which the British specialists were forced eventually to defend themselves by the thesis that "There is no more economical reactor than that which will accept mass production." This hypothesis is only relatively valid, although in specific economic conditions (by the availability of established specialized branches of industry for the production of reactor plant and materials) it can be resolved by argument as a result of choosing a reactor type for the extension of the development program for nuclear energy generation. In this sense the future development is presented logically for Magnox reactors in the direction of increased coolant temperatures (with the object of increasing efficiency) and increased enrichment (with the object of reducing the reactor dimensions and decreasing the capital costs).

The reasoning appears to be somewhat unexpected that "Possibly 30-40 years will elapse before, in the absence of fast reactors, the necessity for conserving uranium resources proves to be a significant factor (559)." This remark, to a positive degree, is contradictory to the conclusions which can be drawn from the reports, where the magnitudes are compared of the positive cheap uranium reserves with the scales of demand for it to meet the needs of nuclear power generation, if it is to be developed in relation to attainable efficiency indexes. In particular, it is stated (164) that the proved estimated uranium stocks are low and in order to ensure increasing nuclear energy generation with uranium after 1975 it is essential to apply serious efforts also to ensuring a reliable estimate of the known deposits and exhaustive exploration of new deposits, which will be capable of providing inexpensive uranium ($22 per kg). This is all the more important and should be undertaken immediately since "... It can be supposed that new important deposits will be discovered in the next five years and a further five years will be required in order to initiate production."

The stated requirements for fast reactors, relative to the onset period, is obviously characteristic for British conditions and, possibly, for conditions in certain other countries, since it is possible to represent the scales of construction of nuclear power stations by the relatively small scales of development of conventional power generation in Great Britain and for which the requirement in the use of U^{238} as fuel also in the construction of fast reactors may not be so critical over the next period. However, if (as can be expected) the technological and economic indexes of breeder reactors is to be better than the advanced thermal reactors, then this will also stimulate countries with a relatively low level of power generation development to accelerate the construction of nuclear power stations with fast reactors.

TABLE 7. Manufacturing, Transportation and Chemical Reprocessing Costs of Fuel Elements for Magnox and AGR Type Reactors

Fuel elements	Uranium enrichment, %	Unirradiated fuel elements, $/kg		Burnup, MWD/t	Reprocessed fuel elements, $/kg	
		manufacture	transportation		transportation	chemical processing
Magnox reactors	Natural	16.8	0.14	4000	0.70	5.6-8.4
AGR type reactors	2	64.4	0.70	20,000	2.80	16.8

Certain data are noteworthy regarding the fuel cycle costs for Magnox type reactors, AGR and SGHW and the effect of the scale of the nuclear power station installation program on the fuel cycle costs (159a, 159b).

These data are interesting because firstly, they are given with reference to experiment and industrial capacity, for example in comparing the cost of fuel element manufacture from plutonium and uranium; secondly, they are related, in particular, to fuel elements for the AGR of uranium dioxide for a mixture of uranium and plutonium dioxides clad in stainless steel (dimensions 15 × 4 mm), i.e., to the type of composition and construction of fuel elements most widely distributed in the various reactors; thirdly, and finally, the irradiation level of the spent AGR fuel elements, considered for economical analysis, is equal to 12,000-20,000 MWD/t (i.e., it is quite high) and is also representative for investigations applicable to the energy generation operating regime of nuclear power stations.

It is pointed out in particular, that for the fuel cycle installations (diffusion plant, fuel element manufacturing equipment, plant for chemical reprocessing of spent fuel) they are the minimal, economically-justified ratings. As applied to the AGR type construction program (in which uranium is used with an enrichment of 2%), the minimum output of the diffusion plant is defined as 400 tons per annum, which corresponds to a minimum program for installation of AGR type reactors with a total capacity of 10 million kW. It is emphasized that this plant will require 2-3% of the electric power generated by the reactors, and the value of the separation costs will amount to £15-20 per t of U ($42-56 per t U). With a natural uranium cost for this plant equal to $19.6 per t of U, the ore charges will be about 50% of the price of the enriched uranium. Capital costs incurred in construction of the plant, according to estimates, amount to about 5% of the capital cost of installing the nuclear power station.

The capital costs incurred in uranium metallurgy and production of fuel elements for this same scale of development of nuclear energy generation are estimated to be in the range of 2-4% of the capital expenditure for construction of the nuclear power station. The provisional cost of the fuel element chemical reprocessing plant, for natural uranium fuel elements, with an output of 3000 tons per annum, and the same plant with additional facilities in the technological circuit for reprocessing AGR type reactor fuel elements of 2% enriched uranium oxide with an output of 500 tons per annum is fixed within the total of $42 and $48 million respectively (£15 and £17 million). Because of maintenance difficulties in the process, the operating lifetime of such a plant is fixed only at 10 years. Consequently, the capital charges for reprocessing may exceed 90%. Table 7 shows also the costs incurred in manufacture, transportation and chemical reprocessing of fuel elements for Magnox and AGR type reactors.

In connection with the possible use of plutonium in thermal reactors a comparison is given of the costs incurred in the manufacture of AGR type fuel elements in uranium and uranium-plutonium versions for a plant with a capacity of 250 tons per annum (159c). The capital costs in installing the fuel element manufacturing plant for a mixture of uranium and plutonium dioxides exceed by approximately $2.8 million (£1 million) the capital costs for installing a plant for manufacturing the same fuel elements from UO_2 with 2% enrichment. The manufacturing costs of $OU_2 + PuO_2$ fuel elements, on the assumption of full and uniform loading of the plant, exceed the cost of their manufacture from UO_2 by $14-28 per kg U (£5-10 per kg U). It is emphasized that these figures are corroborated by experience in plutonium production at Windscale. It is noted that the rise in costs of fuel element production (associated with the use of plutonium) when converted to electric power gives 0.1 d/kWh, and for the expected total value of the fuel costs of 0.10 to 0.15 d/kWh it does not exceed 10%. Consequently, it may not be a deciding factor in the choice of the enrichment method.

It follows from the British reports on the fuel cycle that:

1) The capital costs in the installation of plant for chemical reprocessing and manufacture of fuel elements are comparable in size ($42-48 and $36-64 million for specific capital investments in constructing AGR type reactors of $180 per kW), which differs to a certain extent from our concepts;

2) The rise in costs of electric power associated with additional expenditure on construction and operation of a plutonium fuel element manufacturing plant is quite trivial. This may serve as additional confirmation of the satisfactory efficiency of the uranium-plutonium cycle;

3) The total capital costs in the fuel cycle, without taking account of the capital costs invested in the ore industry, may amount to 11-13% of the capital costs of the nuclear power station.

FRANCE

The installed capacities of all power stations in France in 1963 amounted to 24 million kW (Table 8).

More than 70% of the energy was generated by hydro-electric stations (43) [8]. It is noted that in 1966-1967, the nuclear power station capacity will be 850 MW. This will permit about 5% of the national demands for electric power to be met. In 1970-1971 the proportion of nuclear power generation to cover requirements should increase to 7.5-8%.

In the period after 1965 a significant increase is expected in power requirements, which must be covered either by importing fuel or by nuclear power generation (Table 9).

In order to meet these demands it is essential to introduce the following capacities for thermal power stations: in 1965-1970—6.9 million kW; in 1970-1975—10 million kW; in 1975-1985—35 million kW. It is assumed that the situation reveals the enormous possibilities ahead for nuclear power generation; this, in the future, will permit a significant increase in the fraction of the energy requirements which can be met by means of natural resources (31).

At the present time there are three nuclear power stations operating in France—G-1, G-2 and EDF-1, with a total capacity of 150 MW. Future construction of nuclear power stations with a capacity of 200 to 500 MW (EDF-2, EDF-3 and EDF-4) will permit an approach to be made towards obtaining competitive electric power. Certain technological and economic characteristics of large-scale French nuclear power stations are shown in Table 10.

TABLE 8. Power Generation of Certain Foreign Countries in 1963 [8, 10]

Country	Electric power output, milliard kWh/y	Installed capacities		
		total, million kW	by thermal power stations, %	by hydro-electric stations, %
USA	900	220	80	20
Great Britain	150	41	90	10
Canada	140	28	10	90
Japan	125	30	50	50
Federal German Republic	95	31	80	20
France	80	24	50	50
Italy	79	21	39	61
Sweden	48	10	10	90
Norway	40	8.4	—	~100
Switzerland	24	6	—	~100
India	23	7	60	40
Spain	18	7.5	30	70

TABLE 9. Requirement and Capacity of Electric Power in France (milliard kWh)

	1965	1970	1975	1985
Requirement	103	150	205	410
Possible capacity:				
by hydrostations. . .	43.5	51	59	70
by thermal stations.	26.1	28.4	29	30
Deficit	31.4	68.6	116	310

The program of nuclear power development in France is based on natural uranium, gas-graphite reactors. It is emphasized that the equipment for them can be organized from many countries, while the enriched uranium plant requires control from a unique source, since enrichment plants in Great Britain and France have a small output and consequently cannot compete with the price and scale of production in the world market. Large requirements are noted in foreign currency for the creation of enriched uranium stocks.

The construction of gas-graphite reactors over the next period by France is appraised as "an excellent starting platform for the widespread development of nuclear power generation, capable of satisfying the requirements of the country." Since reactors of the EDF type, with a capacity of 500 MW, are acknowledged to be competitive for French conditions, it is proposed to supplement the existing program of construction of gas-graphite reactors (see Table 10) over the period prior to 1970 by three reactors with a total capacity of 1500 MW (31). The installed capacities of nuclear power stations towards 1980 may amount to 8.5-16.0 MW and will meet 15-30% of the country's requirements for electric power. The requirement in natural uranium in this case will amount to (72): 1400-1800 tons per annum in 1975; 2600-4800 tons per annum in 1980 and 6600-8600 tons per annum in 1985.

Such a high demand for uranium is due to the fact that in the next period no provision is made for reprocessing of spent fuel, but it is proposed to increase the fuel burnup in the reactor. Since natural resources are estimated at approximately 50,000 tons of natural uranium (with an annual requirement of about 1200 tons, this quantity is sufficient for 30-50 years) France is forced to search for supplementary foreign sources of uranium (72). This explains the development of projects in France for a heavy water reactor with gas cooling and for breeder reactors. Heavy water reactors are considered to be very suitable for an intermediate stage of development of nuclear energy generation, and their development is a logical extension of the development of gas-graphite reactors, since it is easy to obtain in them: a fuel rating which is five times greater and a volume density of energy release in the core which is eight times greater than in the EDF-4 reactor; a lower fuel consumption per kWh of generated energy; moreover, the U^{235} loaded into them is almost completely used and the energy generation per unit weight of U^{235} loaded is almost doubled because of burnup of the accumulated plutonium. They assume (39) that heavy water reactors may have the lowest fuel costs relative to any other reactors and their efficiency indexes depend to a lesser degree on the price of natural uranium.

Commissioning of breeder reactors is considered to be less than for heavy water reactors, associated with which their commercial utilization is considered possible in the third stage of development of nuclear power generation in France. They propose (31) that "For the present there is no possibility of predicting accurately the time when other reactor types will be of significant commercial importance (in particular, heavy water and breeder reactors)."

Despite the point of view expressed concerning plans for the prolonged storage of spent fuel from gas-graphite reactors, several French reports were presented at the Conference on the chemical processing of irradiated fuel and the possible economics of this process (64, 98). This confirms that in France there is obviously divided opinion that the rejection of chemical reprocessing and recovery of fuel in the cycle is economically inadequately justified as applied to gas-graphite reactors, which use the accumulated plutonium associated with low burnup only relatively feebly. This may be, of course, only as a temporary measure prior to the construction of a chemical plant for a small development program. It is hardly possible also to assume the trend to metallic fuel for operation of reactors in the power generating cycle to be justifiable in the long term plan, taking into account the prospects for further increasing the fuel burnup in them.

CANADA

In 1961, the entire installed electric power capacity in Canada amounted to 24.9 million kW, including 20.0 million kW from hydroelectric stations and 4.9 million kW from thermal power stations. According to forecasts, the increase in power demands prior to 1980 will amount to about 6.4% per annum. It is proposed that the installed electric power in 1981 will be 70-80 million kW, including 50-58 million kW from hydroelectric stations and 15-17 million kW from thermal power stations. The nuclear power station capacity, according to estimates (1) should amount to: 0.7 to 1.2 million kW in 1971; 2.0 to 3.0 million kW in 1976 and 5.0 to 7.0 million kW in 1981.

TABLE 10. Technological-Economic Indexes of Canadian and French Nuclear Power Stations (1, 10, 31, 37-39) [9]

NPS	Year of reactor startup	Capacity, MW	Thermal efficiency, %	Fuel rating, MW/t U	Average fuel burnup, MWD/t U	Specific cost, $/kW†	Cost of electric power, cent/kWh
Heavy water reactors (Canada)							
Douglas Point	1964	203	29.1	4.88	8800	349	0.509-0.550
Ontario Hydro	1970	457 × 2	29.7	5.21	10,500	238	0.357-0.373
Gas-graphite reactors (France)							
EDF-2	1964	200	25.0	0.80-0.85			
EDF-3	1966	480	31.8	1.14-1.17	3500	248	0.592-0.663
EDF-4	1967	480	30.0	1.08-1.17	3500	235	0.59-0.66
Heavy water reactors (France)							
EL-4 (modernization)		500*	35.0	6.25	8700-15,000	240	0.34

*It is possible that the capacity will be adjusted to 300 MW.
†1 Canadian dollar = 0.933 American dollar.

TABLE 11. Cost of Electrical Power (Canadian cents/kWh) from a Nuclear Power Station with a CANDU Type Reactor of 457 MW (net) Capacity, Operating on Uranium Dioxide

Component of power cost	Coolant			
	pressurized D_2O	boiling D_2O	boiling H_2O	organic*
Capital costs . . .	0.250	0.241	0.242	0.233
Operating costs (including maintenance). .	0.060	0.057	0.059	0.039
Fuel costs	0.073	0.073	0.068	0.086
Total cost of power.	0.383	0.371	0.369	0.358

*Uranium carbide fuel (10).

The basic type of reactor, on which it is proposed to base the development of nuclear power generation is the heavy water reactor operating on natural uranium, using heavy water (pressurized) as coolant in the first period and then, possibly, boiling heavy or light water or an organic liquid coolant. Chemical reprocessing of nuclear fuel over the next period is not proposed. The reactor will be designed for operation on a deep once-through fuel burnup cycle in which the accumulated plutonium is used quite intensely. In calculating the cost of electrical power, credit on the plutonium and on the depleted fuel is not taken into account. The efficiency indexes of the nuclear power stations are shown in Table 9. It should be noted that in the operating regime "at peak," the fuel component cost of power is ~20%. The price structure of electrical power for a specific nuclear power station cost of ~$250 (Canadian)/kW is shown in Table 11.

The cost of heavy water has been taken as $45.2 (Canadian)/kg, which amounts to 20-25% of the capital expenditure on construction of the assembly, i.e., it is relatively small. It is proposed to adjust the production of heavy water to this price by commissioning a Canadian heavy water plant with an output of up to 400 tons per annum. Startup of this plant is planned for 1966 (1, 11).

Canada is one of the principal suppliers of natural uranium and will remain so for a long time, at least up to 1980 (24, 164). Stocks of cheap uranium will enable not only a relatively small-scale development of national nuclear power generation to be ensured, but also will ensure a very considerable export of natural uranium which, according to forecasts, should satisfy up to 75% of the requirements of the capitalist and developing countries in natural uranium for nuclear energy generation (24, 164). Thus, the Canadian route for the development of nuclear power generation is entirely substantiated and is applicable to conditions in Canada but is, in our opinion, unacceptable for countries where these conditions are absent.

ITALY

The installed capacity of power stations in Italy in 1963 was 21 million kW, including 61% from hydroelectric stations. Towards 1973 it is proposed to increase the installed capacities to 36.24 million kW of which 3.19 million kW, or 8.8%, would consist of the installed capacities from nuclear power stations [10]. Commencing in 1958 from almost nothing, Italy has constructed under contract with the USA and Great Britain and has put into operation three large-scale nuclear power stations with three types of reactors: boiling water, pressurized water and gas-graphite. The total capacity of the nuclear power stations amounts to 525 MW.

In 1965 the capacity of these power stations will be increased to ~600 MW with an annual generation of electrical power of 4.2 milliard kWh. This is equivalent to 4.8% of the total Italian requirements for electric power which, in 1965, will amount to 87 milliard kWh (24).

With the introduction of these nuclear power station capacities Italy now occupies fourth place in the world and is ahead of Canada and France.

We note that in a report from Great Britain (131), devoted to the problem of international cooperation, recommendations on the program of development for national nuclear energy generation and to the choice of reactor types, a typical graph is presented which defines the period of development and construction of a nuclear power station. According to this graph, the period of construction of a nuclear power station prior to startup at full power is determined at 4 years, which is confirmed by the Italian experiment (550). By shortening the construction periods, the cost of nuclear power stations is additionally reduced and their efficiency indexes are improved, and also to a certain degree the competitive struggle for the power reactor market is reflected on the part of the supplier firms.

The experiment for operating different types of reactors in Italy will enable the main type of reactor to be selected for the generation of national nuclear power.

OTHER COUNTRIES

The increasing interest towards nuclear energy generation is observed in many countries of the world. Large-scale nuclear power stations are being constructed in the Czechoslovakian SR, the German Democratic Republic, Federal German Republic, Japan, and Sweden. It is planned to construct nuclear power stations in India, Pakistan and Spain (Table 12). The types of reactors contemplated for use are essentially the same in all the countries being considered. The following may be mentioned as characteristic special features of national programs: a) the undertaking, in collaboration with the Soviet Union, of the development and construction of nuclear power stations in the German Democratic Republic and in the Czechoslovakian SR; b) the construction, with the assistance of foreign contractors, of nuclear power stations with one or several different types of reactors in Japan, Pakistan and Spain; c) directing Sweden to heavy water reactors, including boiling and nuclear steam superheat; d) widespread commercial testing of nuclear power stations with reactors of several different types in the Federal German Republic.

There is a distinctive interest appearing towards nuclear power generation from the direction of Belgium, the United Arab Republic, the Scandinavian and Latin-American countries. The general point of view consists, as a rule, in the fact that even in countries with adequately ensured fuel and hydroresources there are regions where it is difficult to supply fuel and energy and where it is precisely in nuclear power generation that it is possible to see the most economically desirable solution to the problem of power supplies.

The underdeveloped countries, whose populations comprise more than 70% of the entire terrestrial population, require a total of 14.8% of the world's generated electrical power. According to forecasts (741), the primary source of energy in these countries will be fossil fuel, the reserves of which (as a result of an increase of energy requirements, anticipated at 8-9% per annum) will be exhausted in the next few decades. Consequently, in the underdeveloped

TABLE 12. Nuclear Power Stations in Operation, Under Construction and Being Planned in Certain Countries (550, 577, 603, 606, 741) [1, 8, 11, 12, 13, 14]

Country	Site location of nuclear power station	Reactor type	Electrical capacity, MW	Remarks
		Operating		
Italy	Garigliano (SENN Project)	BWR	150-200	Constructed with participation of USA (General Electric Corp.)
Italy	Trino (SELNI Project)	PWR	176-240	Constructed with participation of USA (Westinghouse)
Italy	Latina (SIMEA Project)	Magnox	200	Constructed with participation of Great Britain
		Under construction		
Belgium, France	Chooz (SENA Project)	PWR	240	Constructed with participation of USA (Westinghouse)
Czechoslovakian SR	Bogunitse	Gas-cooled, heavy water	150	Constructed with participation of the USSR
German Democratic Republic.	Rheinsberg	Pressurized water	70	Constructed with participation of the USSR
Federal German Republic	Karlsruhe	Heavy water	57	Constructed by Siemens-Schuckertwerke
Federal German Republic	Gundremmingen	BWR	237	Constructed with participation of USA (General Electric Corp.)
Japan	Tokai Mura	Magnox	149	Constructed with participation of Great Britain
Sweden	Marviken	Heavy water, with nuclear steam superheat	138-200	
		Planned		
India	Taranpur	BWR	380	Planned with participation of USA (General Electric)
India	Rana-Pratar-Sagar	CANDU	400	Planned with participation of Canada
India	Kalpakkam	Heavy water, boiling	400	Planned with participation of Sweden
Pakistan	Karachi region	CANDU	132	Planned with participation of Canada
Federal German Republic	Obrigheim	PWR	280	Planned by Siemens-Schuckertwerke
Federal German Republic	Lingen	Boiling, with boiler superheat	160-250	Planned by AEG
Federal German Republic	Bayern (Bavaria)	Gas-cooled, heavy water	100	Planned by Siemens-Schuckertwerke
Spain	Zorita	PWR	140	Planned with participation of USA (Westinghouse)
Sweden	Simpvarp	BWR	60	
Japan	No information	PWR	300	Planned with participation of USA

TABLE 13. Development of Nuclear Energy Generation in India

Year	Nuclear power station capacity, million kW	Total capacity, million kW
1966	–	12
1971	1.2	24
1976	3.0	38
1981	8-10	60
1986	18-20	~90

countries a large-scale investigation is being undertaken to determine the essential national scales for developing nuclear power generation. For example, an important role is assigned to nuclear power generation in India (Table 13).

The study showed that in India, nuclear power stations with a capacity of 400 MW can compete even now with conventional thermal stations operating on fuel transported from long distances. The nuclear power stations in India will be constructed mainly in the western and southern parts of the country. Stocks of natural uranium are adequate for ensuring nuclear power generation to the stated scale up to 1975-1976. Further development of nuclear energy generation will require the use of thorium resources. This is considered possible under conditions of plutonium utilization, which it is proposed to obtain from natural uranium reactors. Of the total nuclear power station capacity of 1.2 million kW towards 1971, 800 MW will be ensured by natural uranium heavy water reactors. The plutonium which is extracted from the spent fuel will be used in a mixture with uranium or thorium in newly commissioned reactors.

In order to attain the levels of energy supply which exist in the industrial countries, the underdeveloped countries must give sufficient consideration to the development of nuclear energy generation. The actual routes for its development in each country are defined by the specific local conditions.

CONCLUSIONS

1. Nuclear energy generation is entering the stage of technological and economic maturity. In the next 10-15 years it will occupy an important place in meeting the demands for electrical power in many countries.

2. The types of reactors on which it is proposed to base the program of development of nuclear energy generation are different in different countries.

The scales of demands for nuclear energy generation have a significant influence on the choice of reactor type, and on the period when its development becomes urgently necessary, the prehistory of the establishment in a country of an industry for producing enriched uranium and plutonium, the degree of technological operation of the reactors, the economic situation in the country and also the system of government assurances concerning nuclear fuel estimates, in particular for processing.

The development of nuclear power generation in the next 15-20 years is considered to be founded:

In the USA – on water-cooled/water-moderated reactors, operating on slightly-enriched uranium of the PWR and BWR type with gradual transition through advanced thermal reactor-converters to fast breeder reactors;

In the USSR – predominantly on fast reactor-converters with gradual transition to the operating cycle of breeder reactors by the limited construction during the forthcoming period of Novo-Voronezh and Beloyarsk type of nuclear power station reactors (thermal neutron reactors) in regions where this is economically justified;

In Great Britain – on gas-graphite reactors, operating on natural uranium, of the Magnox type, then on gas-graphite reactors of the AGR type operating on enriched uranium, or water-cooled/water-moderated reactors of the PWR or BWR type with gradual transition to fast breeder reactors;

In France – on EDF type of reactors, with gradual transition to fast breeder reactors or to heavy water reactors;

In Canada – on reactors of the CANDU type.

3. The concept of development of large-scale nuclear power generation with fast breeder reactors is acknowledged as the principal prospective route by the seven main highly industrialized countries. Deviations from this concept are concerned only with estimates of time and scale of effort necessary for solving the whole complex problem associated with the creation of economical nuclear power generation with these reactors.

In the long-term view of the majority of countries – excluding Canada – it is directed to transition to the construction of fast breeder reactors.

The time when the transition to breeder reactors is acknowledged to be necessary is determined by the scales of development of nuclear power generation and by the available resources of cheap uranium for thermal reactors. This time in various countries is estimated at from 10 to 40 years.

The time when the transition to breeder reactors is acknowledged to be possible, resulting from the extent of the engineering development of the problem, is determined by scientific and technological circumstances and by material means directed towards the solution of this problem which, in their turn, depend on how much this problem is considered paramount and on what kind of planned scales of construction for nuclear power stations. The accomplishment of the engineering development of reactors and the startup of large-scale economical prototypes with a capacity of up to 1 million kW can be expected towards 1970-1972.

The possibility of using a fast reactor as a converter in the transition period will enable this period to be shortened somewhat and to make it independent of the time necessary for accumulating plutonium in thermal reactors.

In the period of development of nuclear power stations and of the fuel cycle for energy generation with breeder reactors in regions where, according to economic reports, this is necessary, it is advantageous to install a certain number of competitive (relative to coal-fired power stations) nuclear power stations with thermal neutron reactors having, possibly, higher fuel burnups, high reliability and higher efficiency.

4. It is not possible to compare directly the efficiency indexes of nuclear power stations (in particular the cost of electric power) produced in different countries, since they are calculated by different national procedures and they are based on particular characteristics of the economics of the various countries. It is possible to consider representatively only comparison of the various reactor types on the basis of a unified procedure which is applicable to the conditions of the country for which the possibilities are being considered for the development of nuclear power generation. Such a comparison must take account of the economics of the fuel cycle plant and the planned dynamics of nuclear power station introduction, since by taking these factors into account the degree of competitiveness of the various reactor types may be changed.

5. In the immediate future (approximately towards 1967-1968), it will be possible to produce competitive electric power from water-cooled/water-moderated (including boiling water) gas-graphite and heavy water reactors. This possibility, for the majority of countries, is based especially on credit allowance for the plutonium and the depleted fuel. The exception is the Canadian heavy water reactor which is calculated on a once-through high fuel burnup and which includes a significant fraction of the plutonium formed.

In connection with the passing in the USA of a law in 1964 concerning the transfer of nuclear fuel to private ownership, a finite correction should be introduced into the efficiency indexes of nuclear power stations if they were obtained on the assumption of using fuel rented by the AEC.

6. The following tendencies, directed at the production of higher efficiency indexes, in the development of an energy-generating reactor installation and fuel cycle are noteworthy:

a) Increase of the unit power of the reactor up to 500-600 MW, increase in the number of reactors installed at nuclear power stations to two-four and increase of efficiency to 35-40%;

b) Increase of nuclear fuel burnup to 10,000-30,000 MWD/t U and transition in the majority of newly designed reactors to oxide fuel;

c) A trend to provide for a possible rapid increase of recycled uranium and plutonium in the reactor by setting up a mixed uranium-plutonium cycle;

d) Shortening of the construction periods for nuclear power stations, which will lead to an improvement of their efficiency indexes.

7. The unit capacities for the various reactor types which, at present, are evaluated as technologically justified and economically profitable amount to 500-600 MW.

In isolated regions (in particular, in undeveloped countries) economically-profitable unit capacities may be 50-100 MW.

8. The fuel burnup essential for competitive power generation depends on the reactor type. However, quite clearly a tendency is appearing towards the use, in various types of reactors which must operate in the energy generating regimes (BWR, PWR, AGR, CANDU, VVER, BN-350), of uranium dioxide fuel clad in stainless steel or zirconium

alloys. Uranium dioxide is becoming an universal nuclear fuel, capable of operating over a wide range of temperatures and burnups in various types of reactors. This situation creates the possibility of establishing a unified fuel cycle technology, including the creation of a mixed uranium-plutonium fuel technology, which will be of considerable importance in the development of power generation and in fuel cycle plants on industrial scales.

9. The use of a mixed fuel cycle with reenrichment of the recycled nuclear fuel by plutonium does not, according to published data, lead to a significant increase in fuel costs and to an increase in the cost of electric power. This testifies to the adequate efficiency of this cycle on industrial scales.

LITERATURE CITED

1. Address by the Pakistan representative at plenary session "B" [in Russian], (Third International Conference on the Peaceful Uses of Atomic Energy, Geneva, 1964).
2. Address by the representative of the USA Atomic Energy Commission, Dr. Glenn Seaborg at the session of the Atomic Industrial Forum on December 1, 1964 in San Francisco—"The Forthcoming Decades: Possibility and Challenge" (Preprint) [Russian Translation].
3. Nucleonics, 22, No. 7, 54 (1964).
4. G. Seaborg, Concluding report at the Third International Conference on the Peaceful Uses of Atomic Energy, [Russian Translation], Geneva (1964).
5. Nucleonics, 22, No. 11, 20 (1964).
6. Canad. Nucl. Technology, 3, No. 3, 45 (1964).
7. Nuclear Industry (The Forum Memo to Member), 11, No. 8, 50 (1964).
8. Nucl. Engng., 9, No. 100, 319 (1964).
9. AECL-1950, p. 25, 29, 31 (1964).
10. Atomo e Industria, No. 3, 8 (1964).
11. Address by the representative of the Czechoslovakian SSSR at plenary session "B" (Third International Conference on the Peaceful Uses of Atomic Energy [Russian Translation], Geneva (1964).
12. Nucleonics Week, 5, No. 10, 3 (1964).
13. W. Zinn, F. Pittman, and J. Hogerton, Nuclear Power USA, McGraw-Hill Publication, New York (1964).
14. Atomwirtschaft, 9, H.8/9, 433 (1964).

CHEMISTRY OF NUCLEAR FUEL REPROCESSING

V. N. Prusakov and M. F. Pushlenkov

Translated from Atomnaya Énergiya, Vol. 18, No. 2,
pp. 171-174, February, 1965

With the increase in the number of reactors for diverse purposes (power generation, desalinization, research, etc.) the quantity of depleted fuel which must be reprocessed in chemical plants will increase with every year. The radiochemical separation process is an important component of the fuel cycle and has a considerable influence on its economy. The solution of the fuel reprocessing problem is complicated by the different types of fuel elements, although nowadays a tendency can be seen toward their unification (associated with the preferential circulation of uranium dioxide fuel and stainless steel and zirconium for cladding). The main interest of the chemical sections of the Conference centered on the technological aspects of the results achieved in the chemical reprocessing of fuel elements. More than 40 reports [1] were presented on this subject.

In the last few years, two approaches have been formulated in the technological sphere of reprocessing spent nuclear fuel elements. One of these is based on the use of an aqueous medium and of organic solvents for separating the fissible materials. The other is based on the use of nonaqueous volatilization processes of the heavy metal halides, pyrometallurgy and pyrochemistry. The sessions of Sections 2.6 and 2.7 at the Conference were devoted to the problem of nuclear fuel reprocessing.

In the reports presented in Section 2.6, general results were given of 5-10 y of operating experience with radiochemical plants in Great Britain (160),[2] USA (249), France (67, 65) and Belgium (773). Experimental installations were also described which are being planned and under construction in Norway (761), Yugoslavia (704), Sweden (418), India (786) and USA (281). In addition, the results were reported of experimental projects concerned with the study of extraction processes, carried out in the USSR (345, 346, 347, 348), Czechoslovakia (760), Poland (804), the Netherlands (758) and other countries.

The extraction method for reprocessing irradiated fuel, using tributylphosphate (TBP) as solvent, has now become classical. Extraction technology is sufficiently well established and proved on industrial scales (USA, Great Britain, France, and Belgium). Operating plants usually contain three uranium and two plutonium extraction cycles designed for the extraction and separation of these elements, and also for purifying them from fission product elements.

However, despite the successes achieved in extraction, research projects in many countries are being extended to improve existing technology and to discover more economical methods for carrying out the processes. A tendency can be observed toward shortening the number of extraction cycles because of improved separation facilities and the use of more efficient reagents in oxidation-reduction processes for separating plutonium, and also because of the use of selective complex-forming reagents for combining the fission product elements. Selective distillation of ruthenium is being used. At the present time particularly great importance is being attached to the purity of the extraction agents used, to the study of the effect of various impurities in them and to radiolysis products in the extraction mixture. In the Hanford plant (249), the process which previously comprised three cycles has been cut to two cycles because of the use of ion exchangers for the final plutonium purification. Meanwhole, USA scientists have stated that the national laboratories of the USA have almost shut down research projects dealing with extraction, which are given to branch institutes and plant laboratories.

As a result of the possible increase of the degree of enrichment, fuel burnup and also shortening of the fuel cooling periods due to the development of nuclear power generation, there is emerging an urgent need for considerable modernization of extraction technology. Unfortunately, these problems were not found to be reflected in the Conference reports.

---

[1] A list of the reports from Soviet scientists is published in Atomnaya Énergiya, 17, No. 3, 235 (1964), and a list of reports from foreign scientists in Atomnoi tekhnike za rubezhom, No. 8, 27 (1964).

[2] The report numbers are given in brackets.

One of the approaches for modernizing existing technology may be the improvement of extraction equipment, enabling the phase contact time to be shortened with the object of reducing radiation effects on the extraction mixture and decreasing the extractor volumes, thus increasing the criticality safety of the process, etc. This may be found feasible by using centrifugal extraction equipment. In the USA report (249) it is stated that at Savannah River and also at Oakridge National Laboratory extremely efficient centrifugal devices of small volume are used, thus permitting a considerable shortening of the contact phase time.

In the reports presented to the meeting, a wide range of problems was discussed—from opening and dissolution of the fuel elements to utilization of valuable components. In cost and complexity, the carrying out of these operations may be close to or even surpass the basic extraction operations. Thus, for example, it is very difficult to remove fuel element cladding of stainless steel or zirconium alloy (Zircalloy). They are usually dissolved out in sulphuric or nitric acid with the addition of hydrofluoric acid. There are indications that a more satisfactory method will be the mechanical opening of the fuel elements by special machines. However, these machines are quite complex because of the necessity of remotely controlling them. In the USA report (249) a description is given of a large experimental installation for cutting open fuel elements, but up to now it has been tested only on experimental fuel assemblies. A description is also given of a successfully-used noncontact electrolytic plant for dissolving fuel elements. Such a unit is being constructed at Savannah River with a production capacity of up to 400 kg/day for dissolving fuel clad in stainless steel.

The new Windscale plant (160, 161), a model of which was demonstrated at the Geneva Exhibition, serves as an example of the thoroughness of study of extraction technology which takes into account the costs. The plant is designed for reprocessing irradiated fuel elements of natural or slightly enriched uranium with magnesium (Magnox alloy) cans. The output of the plant will be 1500 t/year, fuel burnup 3000 MWD/t and cooling period 130 days. The decontamination factors from fission products are assumed to be $1 \cdot 10^7$ for uranium and $3 \cdot 10^7$ for plutonium. The separation factors are Pu/U: U—$3 \cdot 10^5$ and Pu—$1 \cdot 10^7$. In contrast from the old plant, in which extraction columns were used, mixer-settling tanks with a turbine mixing unit are used in the new plant. The technological layout of the plant consists of three consecutive extraction cycles, separation and purification of valuable components being carried out in the last two. A mixture of TBP with kerosene (80%) is used as the extraction agent. Each cycle of the extraction has 20 stages. In planning this plant, the abundant experience of extraction technology was taken into consideration, as a result of which a number of original solutions were decided upon with the aim of reducing the cost of the plant. The so-called "steamless" version is used, in which the re-extracts are subjected to no evaporative operations between cycles; this makes it possible to reduce a certain number of units and, correspondingly, the volume of the plant. Individual shielding of the remote control units is replaced by group shielding. The technological and design solutions have made it possible to reduce significantly the over-all cost of the plant. According to statements by the specialists who designed the plant, its cost is 40% less than that of the old plant, relative to the unit of productivity.

There was mention in the reports of the use of uranium-IV as a plutonium reducing agent in the extraction process. This, obviously, is conditioned by the general tendency to maximum reduction of the volumes of active waste solutions and reduction of their salt content. In this respect there is interest in the tests of catalytic reduction of uranyl nitrate to quadrivalent uranium by hydrogen; this process was demonstrated at the Italian stand of the Geneva Exhibition.

A complex and hitherto unsolved problem is the development of methods for regenerating the extraction mixture after contact with highly active solutions. These problems are interpreted differently in different reports. At present there are no unified regeneration methods and also methods for removing or preventing interphase formations (of films).

Interpretations were given at the Conference of certain methods for intensifying radiochemical production processes. Attention was drawn to a model of a plant for producing plutonium oxalate directly, shown in the Belgian exhibit; the Federal German Republic demonstrated a model of a plant for the direct crystallization of salts from solution which hitherto has not emerged outside laboratory practise, but which is intended for industrial use. Interest was created in a sol-gel process for the remote preparation of secondary thorium fuel (239), the processing of which is complicated by the γ-active Th^{232} and U^{233} decay products. It involves essentially four operations: 1) denitration (to produce the oxides, 185-475°C); 3) water evaporation (to produce a gel, 80-85°C); 4) condensation of the gel by calcining. As a result of these operations ceramic particles are obtained of an almost theoretical density. The sol-gel process, and also the subsequent remotely-controlled manufacture of tubular fuel elements by vibracompression of the powders obtained have been tested on a pilot-plant scale with a favorable result. The packing density

reached 70-80% of theoretical. This process is well adapted to remote control conditions and makes it possible to control the size and shape of the particles. It was found possible by this same method to obtain microspheres of a uranium and plutonium dioxide mixture and also of a carbide fuel. In the latter case dispersion is effected in an organic solvent, for example in 2-ethylhexanol.

In order to better evaluate the potential possibilities and technological significance of "dry" methods, which previously have been relatively little reported in scientific literature, it will be of advantage to describe in detail the reports discussed in Section 2.7. The chemistry of dry processes was presented to the Conference in five reports from the USA (250, 251), Japan (798), Belgium (771) and France (66). Hitherto, there have been no large-scale plants in the foreign atomic industry operating on the technology of dry (nonaqueous) fuel reprocessing. However, in the countries mentioned—first and foremost in the USA—research directed towards the study of dry processes has been undertaken very resourcefully and very intensively. This is due to the fact that the development of nuclear power generation has promoted specific demands on the technology of chemical recovery of nuclear fuel and which have not been successfully solved or which it is impossible to solve by the extraction method. The small duration of the chemical cycle and the capability to process fuel elements highly enriched in plutonium or uranium-235 with low holding time are related to these problems. Dry methods of fuel processing potentially satisfy these requirements and permit the development of an economically favorable fuel cycle.

At the present time, the following basic qualities are stressed for "dry" processes for reprocessing fuel elements of various types:

a) technological compactness of the radiochemical process;

b) the feasibility of obtaining waste products directly in solid form;

c) the radiation stability of the reagents used in the process;

d) simplification of the conditions for criticality safety of the process.

In developing dry methods of fuel element recovery, two routes have been contemplated. One of these has the objective of incomplete separation of the fuel from radioactive fission products, which is feasible only for fast reactors and assumes remotely controlled repetitive manufacture of the fuel elements; the other is the complete purification of the fuel and manufacture of the fuel elements by the normal method. The first route is based on the use of pyrometallurgical and pyrochemical methods; these are: dissolution and fusion extraction of the metals and salts, high temperature oxidation-reduction attack on ceramic fuel, electrolysis in the fused salts, etc. The second route is based on the volatilization of volatile halides of uranium and plutonium and their fractionation. It is considered that the fluoride method will permit the reprocessing of different forms of fuel: metals, oxides, carbides, after a small cooling time. In the concept of the "fluoride method," which is based essentially on volatility of the fluorides, certain processes are included which differ in the initial state: the purely gaseous process of fluorination of the fuel, fused salt fluorination and the nitrofluorine process. It is proposed to discriminate between the uses of each of them.

It should be noted that the halides enable the problem of reprocessing fuel elements without removing the cladding to be solved completely, especially if it concerns aluminium or zirconium cladding. In order to remove the cladding, dissolution in fused salts is used or the fuel elements are treated with chlorine, hydrogen chloride, during which $AlCl_3$ or $ZrCl_4$ volatilization takes place, and other methods.

The French, Belgian, and, especially, the USA reports confirm that the study of dry processes in these countries has reached a high level and large-scale plants are already in operation there. In Idaho (USA), as from August 1964 a pyrometallurgical plant has been operating which has been serving the fuel cycle of the experimental fast reactor EBR-II. The fuel assembly from the core, containing 6 kg of enriched (46%) uranium alloy with an activity of $2.5 \cdot 10^5$ Ci, is fed to the separation plant after a minimum of 15 days cooling. The steel cladding of the fuel elements is removed mechanically. The fuel, in 10 kg batches, is subjected to only partial purification by means of oxidizing slag (of a pure fused salt) in a zirconium oxide crucible. As a result of this, the majority of the fission products is either volatilized (mainly Cs, I) or, having been selectively oxidized, they (Ba, Sr, rare earths) are concentrated at the surface of the crucible in the molten uranium oxides. The noble metals (Mo, Nb, Zr, Ru, Pd) remain in the fuel and are returned to the reactor. Fuel elements from repetitive manufacture have an activity of $6 \cdot 10^4$ Ci. Part of the uranium (about 5-10% of the original) remains, having undergone oxidation, and it is then extracted with liquid metallic zinc and magnesium for complete removal of the noble metals, in order to maintain

their concentration in the core approximately at a constant level. Reduction of the oxides is accomplished in a zinc-magnesium melt. These operations are carried out in a tungsten crucible and are generally similar to those used for extracting plutonium from breeder cores: dissolution of the uranium in a mixture of zinc and magnesium (800°C), settling at a reduced temperature (400°C), decantation and evaporation of the zinc and magnesium. The chemical processing costs in the EBR-II fuel cycle amount to 20%.

At Oak Ridge (USA), there is an experimental unit in operation for reprocessing highly-enriched uranium-zirconium and uranium-aluminum fuel elements. The technological process consists in dissolution of the fuel element assemblies in a fluoride salt melt ($NaF-LiF-ZrF_4$) by means of hydrogen fluoride, with subsequent treatment of the uranium and plutonium fluorides with gaseous fluorine. Dissolution and fluorination can be carried out in one and the same apparatus, made out of nickel alloy. The uranium is separated from the solution in the form of UF_6 and is then subjected to sorption scrubbing from the fluorine compounds of fission fragment elements, which volatilize along with it, by granulated sodium fluoride. The purification efficiency of uranium hexafluoride is extremely high (10^9-10^{10}). As stated (250), such a high factor has previously been unattainable in a radiochemical process, even with the inclusion of three water extraction cycles. Hitherto there has been the problem in this interesting process of separating the plutonium but efforts have been made to resolve it. It is noteworthy that there is a relatively high corrosion rate of the primary units (~ 10 mm/month).

Recently, in the Brookhaven Laboratory (USA), considerable interest has been directed towards the so-called nitrofluorine process. In this process, in order to dissolve the fuel elements anhydrous hydrogen fluoride with the addition of N_2O_4, N_2O_3, or NOF is used. This solution is capable of dissolving UC_2 and BeO, uranium-zirconium, uranium-aluminum fuel elements and stainless steel at room temperature, with the formation of uranium fluorides of highest valence ($NOUF_6$). This process is at an earlier stage of investigation than the others and its capabilities are still not sufficiently clear.

In the Argonne National Laboratory (USA), large-scale units are being tested which are designed for reprocessing ceramic fuels with low uranium enrichment. The development of this process received practical directive after methods had been found for removing the heat from the exothermic reaction between uranium dioxide and fluorine. Batch fluorinators were constructed for this purpose with a fluidized bed of particles of an inert material (e. g., Al_2O_3). The uranium dioxide, or other form of fuel is fluorinated by the direct action of gaseous fluorine. At a temperature of 500-550°C, not only uranium but also plutonium is converted into the gaseous hexafluoro-compound. It is proposed to purify them from fission product fluorides by distilling the mixture. The uranium and plutonium hexafluorides are not separated at the distillation stage, the mixture being routed directly by reduction to the dioxides ($UO_2 + PuO_2$). Technologically, this system is extremely simple. Thorough purification of the fuel can be accomplished by the fluoride rectification method.

At Fentenay-aux-Roses (France) preparations are also under way for a large-scale experiment to investigate dry methods of recovering nuclear fuel. France is constructing an experimental plant for reprocessing uranium-zirconium fuel elements and which is adaptable for operating with highly-active materials. Prior to fluorination of the uranium, it is proposed to remove the fuel element cladding with gaseous hydrogen chloride.

At Molle (Belgium) a plant being constructed will be used for investigating the behavior of fission products by fluorinating the mixed oxides from the core of a fast reactor with a high plutonium content.

It can thus be seen that many of the world's largest laboratories are occupied with the study of dry processes for recovering nuclear fuel. The scientific research front is not limited to the processes mentioned. It includes also the study of other physico-chemical methods for complete or partial separation of uranium and plutonium from neutron poisons.

During the course of the Conference it was stressed that the development of dry processes had attained the stage where prospects for their industrial application can be discerned. As a consequence of this, the question is now being discussed abroad for constructing small-scale dry chemical reprocessing plants in the immediate vicinity of reactors which are located at a large distance from the centralized wet-processing plants.

The increased requirement for isotope radiation sources has had a considerable influence on the improvement of methods for obtaining them from plutonium production waste products. Several reports were presented on this subject. In the USA report (252) there is a recommendation for producing Sr^{90}, Cs^{137}, Ce^{144}, Pm^{147}, etc., and also Kr^{85} and Tc^{99} on industrial scales. At the present time in the USA, all the old methods for producing isotopes

are being reviewed and replaced by more modern methods, largely extraction, using liquid ion-exchangers. It is interesting to note that Tc^{99} in the form of TcF_6 is separated and concentrated by a sorption method on magnesium fluoride from gaseous uranium hexafluoride. Its production in 1964 must have reached 70 kg.

In Sweden (609) investigations have been carried out into the separation of Cs, Sr, and Ce by the method of sorption on inorganic exchangers. In the Belgian paper (772) the use of solid inorganic ion-exchanger materials is also reported for extracting Cs and Sr from acid solutions. Cs and Sr can be concentrated by this method to a factor of 50-100 with good removal of accompanying elements.

In the USSR report (512), the extraction technology is discussed of a scheme for separating radioactive products contained in the concentrates from effluent solutions. The process includes an extraction process of four stages: extraction of Ce^{144} in the 4-valent state with di-2-ethylhexyl phosphoric acid, separation of Sr^{90} from an alkaline medium by a solution of salicylaldoxime in TBP, separation of the trivalent rare earths by TBP and, finally, separation of divalent europium.

In some reports, attention was drawn also to the problem of trapping radioactive A^{85} and Xe^{133}. The radioactive gases are finding a large application in technology. In the USA report (252, the possibility is shown for trapping A and Xe after dissolution of the fuel elements at low temperature by an adsorption-desorption method on carbon. Later a more efficient method was presented—low-temperature distillation of the liquefied gases. The Japanese report (437) is worthy of mention for trapping the radioactive inert gases by means of hydroquinone. It is shown that at 20-40 atm the mixture of A, Kr, and Xe, forms clanthrate compounds.

In a USA report (249, data are presented for separating Np^{237} which is a byproduct of uranium fission in thermal neutron reactors. By irradiating 10 kg of Pu^{239}, 900 g are obtained of a mixture of the isotopes Pu^{242}, Am^{243} and Am^{244}. The elements were subjected to separation and purification from fission products. It was proposed to produce in 1964 in the USA up to 7 kg of Pu^{238} and 20 g of Cm^{242}. In 1970 the production of Pu^{238} should reach 100 kg/annum, and of Cm^{244}—2-3 kg/annum. Methods for separating the transuranium elements Am and Cm by extraction with neutral organophosphorus compounds are described also in a USSR report (348) in which the extraction properties of about 20 compounds are described.

As already mentioned, information and data presented in the reports have been very successfully substantiated by the exhibitors at the Geneva Exhibition, in which 17 governments participated, and also by cine-films. To this must also be added the fact that the Soviet delegates took part in interesting and friendly discussions with their colleagues from foreign countries. This made it possible not only to exchange opinions and to discuss a number of technological problems but also to establish the contacts, which comprised one of the problems of the Third International Conference on the Peaceful Uses of Atomic Energy.

HOMOGENEOUS CRITICAL ASSEMBLY WITH A PROFILED FUEL CHARGE

(UDC 621.039.520.22)

A. K. Krasin and E. I. Inyutin

Translated from Atomnaya Énergiya, Vol. 18, No. 2,
pp. 175-177, February, 1965
Original article submitted July 15, 1964

Homogeneous critical assemblies conform most closely to the assumptions of the theory which forms the basis of the analytical methods for calculating reactors with profiled fuel charges [1-4].

A critical homogeneous assembly with an equalized thermal neutron flux was described in [5]; at approximately the samt time, the authors of the present article produced a homogeneous critical assembly with a profiled fuel charge for the purpose of equlizing the energy release in the core.

The critical assembly (see table and Fig. 1) constituted a six-zone cylindrical zero-power reactor. The reactor core 6 was divided into five coaxial zones; the sixth (external) zone, 7, acted as a physically infinite reflector. The zones were separated from each other by means of aluminum partitions, 3, which had a thickness of 1 mm. The aluminum vessel 4 of the core 6 was inserted in a stainless-steel vessel, 5; the space between them contained the lateral aqueous reflector, whose thickness was 15 cm. The wall thickness of the core vessel was 3 mm. A top reflector was not provided. The lower reflector was made of aluminum and stainless steel with thicknesses of 3 and 5 mm, respectively. The reactor was mounted at a height of 20 cm from the concrete floor.

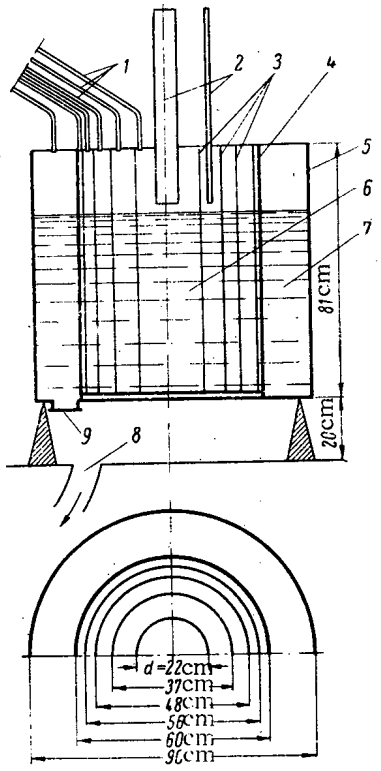

Fig. 1. Schematic diagram of the critical experiment. 1) Polyethylene pipes; 2) elements of the control and emergency protection system; 3) zone partitions; 4) core vessel; 5) critical assembly vessel; 6) core; 7) reflector; 8 and 9) emergency reflector drain.

The fissionable material (90%-enriched uranium) was used in the form of an aqueous solution of uranyl nitrate $UO_2(NO_3)_2$, acidified with nitric acid. Solutions with different fuel concentrations entered the corresponding reactor zones through polyethylene pipes, 1. The

Characteristics of the Critical Assembly

Experimental data		Calculation data
external radius of zone, cm	Fuel density, g U^{235}/liter of solutions	Fuel density, g U^{235}/liter of solutions,
11	22	23
18.5	23.5	
24	27.4	27.4
28	35.7	35.7
30	43	43
45	0	0

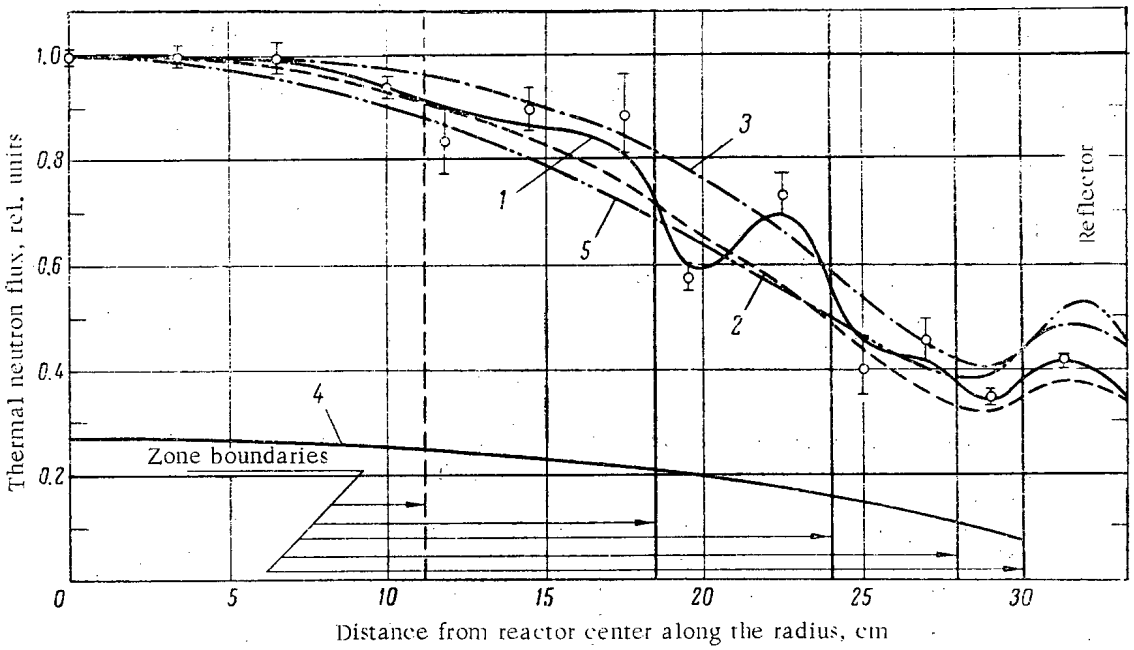

Fig. 2. Distribution of neutron fluxes. 1) Thermal neutron flux (experiment); 2) the same (calculation in the P_1–approximation); 3) the same (calculation based on the electric model); 4) epithermal neutron flux (calculation in the P_1–approximation); 5) thermal neutron flux in a reactor with uniform fuel distribution.

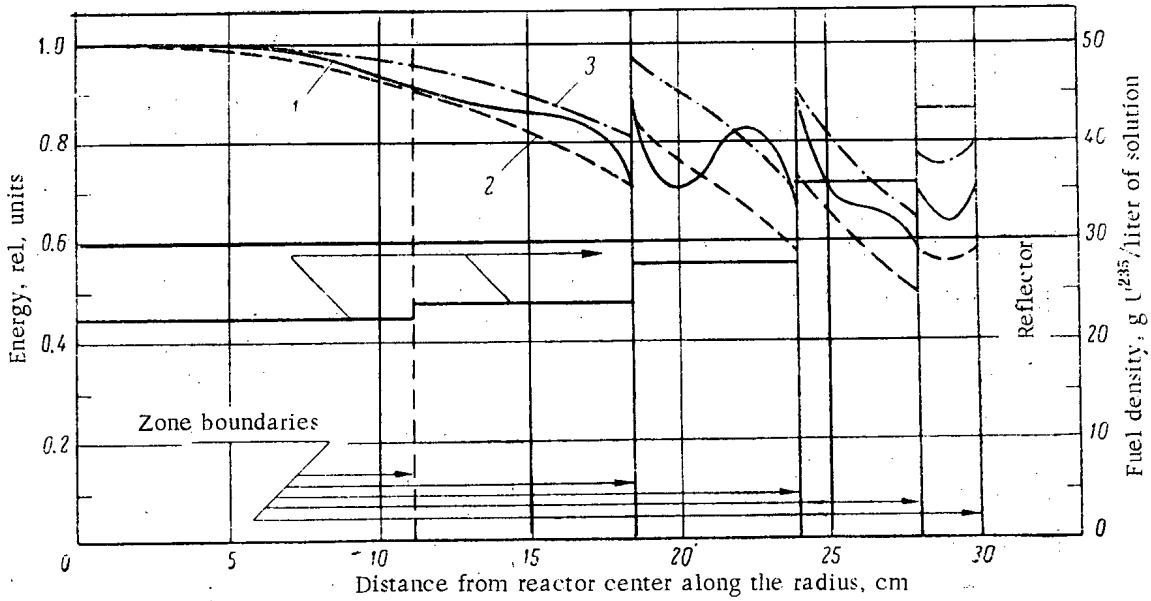

Fig. 3. Distribution of fuel and energy release. 1) Energy release (experiment); 2) the same (calculation in the P_1–approximation); 3) the same (calculation based on the electric model).

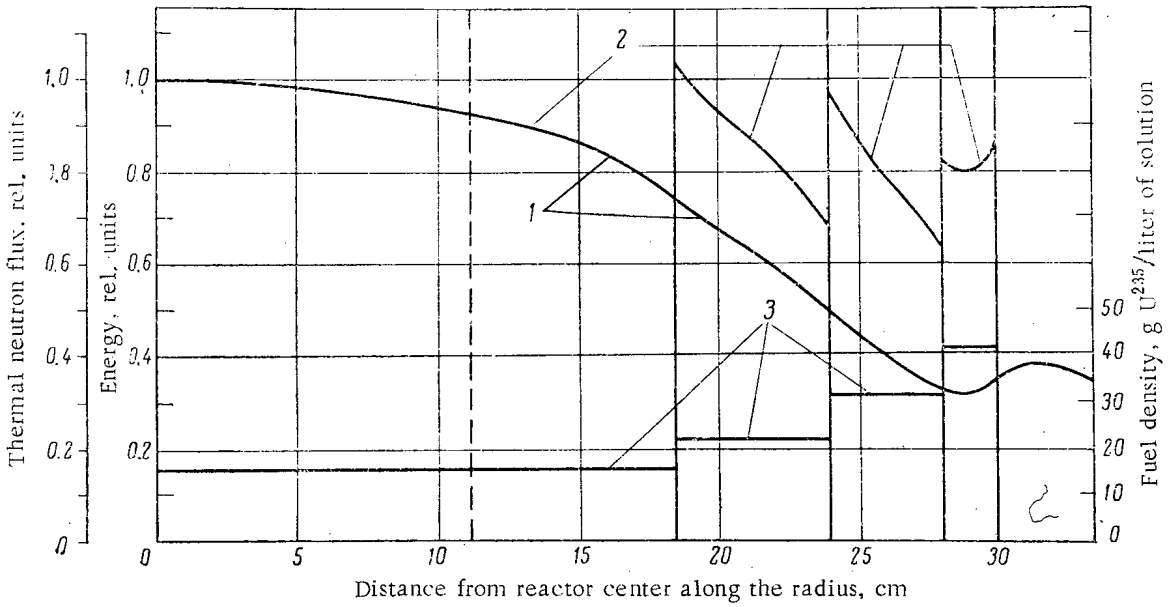

Fig. 4. Distributions of the thermal neutron flux (1), the energy release (2), and the fuel density (3) corresponding to a constant mean power released per unit volume of the core.

amount of solution poured into each zone was proportional to the area of the zone, due to which the solutions in all zones were maintained at the same level.

The radial distribution of neutron fluxes from the core center was measured by means of indium detectors. The arrangement of the detectors was such as to provide the best possibility of revealing the end effects at the boundaries between zones. In all zones of the critical assembly, the ratio of the concentration of hydrogen nuclei to the concentration of U^{235} nuclei had a high value, so that the relative energy release along the core radius was assumed to be equal to the product between the thermal neutron flux and the fuel concentration in the zone.

The experimental conditions made it possible to determine only the total activation of the indium detectors (by thermal and epicadmium neutrons). The correction for the activation by epicadmium neutrons was determined by calculation, for which data from [6] were used. The error in determining this correction was estimated to be ± 10%.

The reactor became critical when the height of the core reached a value of 39.6 ± 0.1 cm, which corresponded to a critical charge of 3250 ± 30 g U^{235}.

The results obtained in measuring the radial neutron flux are given in Fig. 2. "Splashes" in the distribution of thermal neutrons, which constitute a characteristic property of multizone systems, were detected in experiments. These splashes were observed in zones with a lower uranium concentration, which acted as peculiar reflectors with respect to zones with higher uranium concentrations.

The distribution of fissions (energy release) along the radius is shown in Fig. 3. The factor of energy release nonuniformity was equal to 1.19.

The profiling law which should secure a roughly constant mean energy release along the reactor radius was estimated on the basis of experimental data under the assumption of weak changes in the thermal neutron field. The estimates were confirmed by the results of calculations. Figure 4 shows the distributions of the thermal neutron flux and the energy release for the case under consideration.

The results of numerical and electric model calculations are compared with experimental data in Figs. 2 and 3. The 18-group calculations were performed in the P_1–approximation according to a five-zone program. In calculations, the reactor's first and second zones were combined into a single one, to which a certain mean fuel concentration was assigned. The disturbing effect of the aluminum partitions and the presence of nitrogen in the solution were not taken into account in calculations.

The calculations indicated a lesser degree of energy release equalization in comparison with experimental data. The calculated thermal neutron flux curves reflect the averaged character of the experimental curve, smoothing out local perturbations of the thermal neutron flux.

The authors are grateful to B. G. Dubovskii, A. P. Smirno-Averin, and A. V. Kamaev for their assitance in performing the experiments and also to I. I. Sidorova, V. P. Kochergin, and I. P. Markelov, who performed the calculations.

LITERATURE CITED

1. G. Goertzel and W. Loeb, Nucleonics, 12, No. 9 (1954).
2. F. Winterberg, Atomkernenergie, No. 11/12 (1957).
3. F. Winterberg, Report 1055, Submitted by the FRG at the Second International Conference on the Peaceful Uses of Atomic Energy, Geneva (1958).
4. N. N. Ponomarev-Stepnoi and E. S. Glushkov, Atomnaya énergiya, 11, 19 (1961).
5. Callihan, Morfitt, and Thomas, Report 834, Submitted by the USA at the First International Conference on the Peaceful Uses of Atomic Energy, Geneva (1955).
6. A. Dresner, Resonance Absorption in Nuclear Reactors [Russian translation], Moscow, Gosatomizdat (1962).

ANGULAR DISTRIBUTION OF COLLIMATED RADIATION

(UDC 539.121.8)

É. F. Fomushkin

Translated from Atomnaya Énergiya, Vol. 18, No. 2,
pp. 178-179, February, 1965
Original article submitted February 8, 1964; revision submitted March 19, 1964

A method based on the application of elements of the probability theory is used in this article for calculating the characteristics of radiation propagation. Such a method was used, for instance, in solving Buffon's problem [1]. The method consists in the following. The set of all values of the parameters determining the propagation of radiation (the coordinates of the trajectory origin and the orbital and the azimuthal emergence angles) constitutes the so-called field of events. The volume of the field of events can be calculated without difficulty in most cases. The effect of collimation leads to the fact that only a portion of the parameter values satisfy the condition of passage through the collimator. This portion forms a field of events which favor the phenomenon—the passage through the collimator in our case. The ratio of the volume of the field of events that favor the phenomenon to the total volume of the field of events is equal to the probability of the phenomenon in question. In this, the method whereby collimation is effected is of no consequence; for instance, collimation can be effected by the shapes and the mutual position of the source and the detector and also by the configuration of a collimator with absorbing walls.

A conical collimating system, which is shown in Fig. 1, is usually produced in recording the radiation from a flat round source whose radius is r by means of a detector whose radius is R; the centers of both circles lie on the same normal.

In this case, it can readily be shown that the field of events constitutes a circle whose radius is r, while the field of events that favor the falling of particles on the detector consists of the common part of two circles with the radii r and R.

In dependence on the angle θ, the probability that a particle will reach the detector is equal to

$$\text{for} \quad m=\frac{r}{R}<1, \quad n=\frac{L}{R}, \quad F(\theta)=1, \quad \text{if } 0\leqslant\theta\leqslant\operatorname{arctg}\left(\frac{1-m}{n}\right),$$

$$F(\theta)=\frac{1}{\pi}\left\{\alpha+\frac{\arcsin(m\sin\alpha)}{m^2}-\frac{n\operatorname{tg}\theta\sin\alpha}{m}\right\},$$

$$\operatorname{arctg}\left(\frac{1-m}{n}\right)\leqslant\theta\leqslant\theta_{\max}=\operatorname{arctg}\left(\frac{1+m}{n}\right),$$

where

$$\alpha=\arccos\frac{m^2-1+n^2\operatorname{tg}^2\theta}{2mn\operatorname{tg}\theta},$$

$$\text{for} \quad m=\frac{r}{R}\geqslant 1, \quad F(\theta)=m^{-2},$$

$$\text{if} \quad 0\leqslant\theta\leqslant\operatorname{arctg}\left(\frac{m-1}{n}\right),$$

$$F(\theta)=\frac{1}{\pi m^2}\left\{\beta+m^2\arcsin\left(\frac{\sin\beta}{m}\right)-n\operatorname{tg}\theta\sin\beta\right\},$$

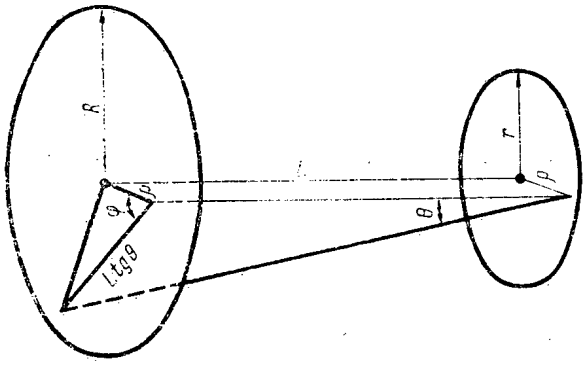

Fig. 1. Conical collimating system.

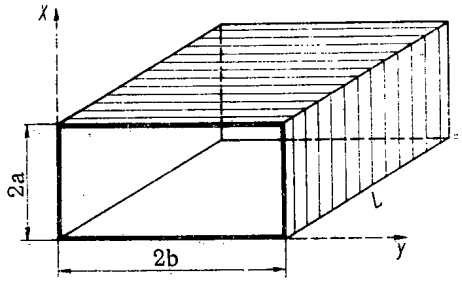

Fig. 2. Collimator with a rectangular cross section.

if

$$\operatorname{arctg}\left(\frac{m-1}{n}\right)\leqslant\theta\leqslant\theta_{\max}=\operatorname{arctg}\left(\frac{m+1}{n}\right),\tag{1}$$

where

$$\beta=\arccos\frac{1-m^2+n^2\operatorname{tg}^2\theta}{2n\operatorname{tg}\theta}.$$

A collimator with a rectangular cross section is shown in Fig. 2. The system may consist either of a single collimator or a set of identically shaped collimating cells. In both cases, the problem can be reduced to Buffon's problem with two mutually perpendicular systems of parallel straight lines [1]. The spacing between the straight lines of one system is equal to 2a, the spacing between the straight lines of the other system is 2b, and the pivot length is L tan θ, where θ is the orbital emergence angle of particles.

Omitting the consideration of the shape of the field of events for this case, we shall give the expression for the probability of the particle's passage through a collimating system with a rectangular cross section in dependence on the angle θ:

$$F(\theta)=1-\frac{\operatorname{tg}\theta}{2\pi}\left(q+p-\frac{qp\operatorname{tg}\theta}{2}\right),$$

$$\text{if}\quad 0\leqslant\theta\leqslant\operatorname{arctg}\left(\frac{1}{q}\right),$$

$$F(\theta)=1-\frac{2}{\pi}\left[q\operatorname{tg}\theta\left(1-\sqrt{1-(q\operatorname{tg}\theta)^{-2}}\right)+\arccos\left(\frac{1}{q\operatorname{tg}\theta}\right)-\frac{1}{2}qp\operatorname{tg}^2\theta+\frac{p}{q}\right],$$

$$\text{if}\quad \operatorname{arctg}\left(\frac{1}{q}\right)\leqslant\theta\leqslant\operatorname{arctg}\left(\frac{1}{p}\right),$$

$$F(\theta)=1-\frac{2}{\pi}\left[\arccos\left(\frac{1}{q\operatorname{tg}\theta}\right)+\arccos\left(\frac{1}{p\operatorname{tg}\theta}\right)-\sqrt{(q\operatorname{tg}\theta)^2-1}-\sqrt{(p\operatorname{tg}\theta)^2-1}+\frac{1}{2}qp\operatorname{tg}^2\theta+\frac{1}{2}\left(\frac{q}{p}+\frac{p}{q}\right)\right],\tag{2}$$

$$\text{if}\quad \operatorname{arctg}\left(\frac{1}{p}\right)\leqslant\theta\leqslant\theta_{\max}=\operatorname{arctg}\sqrt{q^{-2}+p^{-2}},$$

$$q=\frac{L}{2a}\geqslant p=\frac{L}{2b}.$$

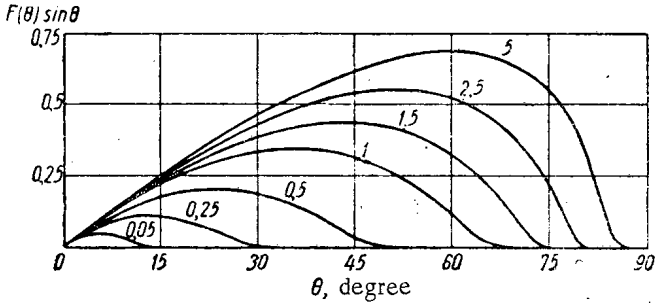

Fig. 3. Angular distribution of radiation at the exit from a collimator with a square cross section.

The angular distribution of radiation at the exit from the collimating system is determined by the expression

$$\Phi(\theta)\, d\theta = F(\theta)\, I(\theta)\, d\theta, \tag{3}$$

where $I(\theta)$ is the angular distribution of radiation at the entrance to the collimator; for an isotropic distribution, $I(\theta) \sim \sin\theta$.

Figure 3 shows the angular distributions of radiation at the exit from a collimator with a square cross section ($q = p$) for an isotropic distribution at the entrance for several q values.

The portion of radiation transmitted through the collimating system is calculated by using the equation

$$\Omega = \frac{\int_0^{\theta_{max}} F(\theta)\, I(\theta)\, d\theta}{\int_0^{\pi/2} I(\theta)\, d\theta}. \tag{4}$$

As a check of the method, we performed calculations using Eq. (4) for a conical collimating system. The calculation results are in good agreement with data from [2].

The proposed method can be applied in a wide range of problems. Its use considerably simplifies the calculations.

LITERATURE CITED

1. B. V. Gnedenko, Probability Theory Course [in Russian], Moscow, Fizmatgiz (1961).
2. K. A. Petrzhak and M. A. Bak, ZhTF, 24, 636 (1955).

DIFFUSION OF NEUTRONS IN SPIN-ORBIT INTERACTION

(UDC 539.125.523.33)

Yu. N. Kazachenkov and V. V. Orlov

Translated from Atomnaya Énergiya, Vol. 18, No. 2,
pp. 179-181, February, 1965
Original article submitted February 13, 1964; final version submitted May 21, 1964

Spin-orbit interaction leads to the polarization of fast neutrons in their scattering on nuclei. In many cases, experiments indicate a very high degree of polarization [1, 2]. The scattering of polarized neutrons is characterized by azimuthal asymmetry, which leads to the predominant scattering of neutrons in the direction opposite to that of the incident beam. A qualitative consideration of the polarization effect in the reflection of neutrons from different media was given in [3].

Multiple scattering of neutrons during diffusion in matter results in a certain mean polarization of neutrons, which, in turn, affects the diffusion process. In the first approximation, the polarization effect can be characterized by the change in the neutron diffusion factor.

Lepore has shown [4] that, while the neutron spin before scattering is described by the spinor $\chi_{m_s}^{1/2}$, the amplitude of the elastic scattering of such a neutron on a nucleus without spin is given by

$$f(\theta)=[A(\theta)+B(\theta)\,\mathbf{n}\sigma]\,\chi_{m_s}^{1/2}, \tag{1}$$

where σ is a vector whose components constitute Pauli matrices, $\mathbf{n}=[\Omega'\Omega]/|[\Omega'\Omega]|$, Ω' is the neutron's direction of motion before scattering, and Ω is the neutron's direction of motion after scattering; the values of A(θ) and B(θ) depend only on the scattering angle and can be expressed in terms of the phases which take into account the spin-orbit relationship.

If the neutron was polarized before scattering, the elastic scattering cross section will have the following form:

$$\frac{d\sigma}{d\Omega}=\frac{d\sigma_0}{d\Omega}\left[1+\frac{2ReA^*B}{AA^*+BB^*}\,\mathbf{n}\mathbf{p}_i\right], \tag{2}$$

where $\frac{d\sigma_0}{d\Omega}\equiv(AA^*+BB^*)$ is the microscopic cross section of the elastic scattering of unpolarized neutrons.

Let us consider the effect of polarization on the neutron distribution after the second impact. Assume that an unpolarized neutron flux is scattered from Ω' to Ω and then to Ω_1 to Ω_2 (see Fig. 1). Then (see [4]), the polarization $\mathbf{p}_1$ of the flux scattered from Ω' to Ω will be written thus:

$$\mathbf{p}_1=\frac{2ReA^*(\theta_0)\,B(\theta_0)}{A(\theta_0)\,A^*(\theta_0)+B(\theta_0)\,B^*(\theta_0)}\,\mathbf{n}=p(\theta_0)\,\mathbf{n}. \tag{3}$$

where

$$p(\theta_0)=\frac{2ReA^*(\theta_0)\,B(\theta_0)}{A(\theta_0)\,A^*(\theta_0)+B(\theta_0)\,B^*(\theta_0)}.$$

If Eq. (2) is used, the cross section of scattering from Ω to Ω_1 and Ω_2 can be written thus:

$$\frac{d\sigma_{12}}{d\Omega}=\frac{d\sigma_0}{d\Omega}\left[1\pm p(\theta)\,p(\theta_0)\,\mathbf{n}\mathbf{n}_1\right],$$

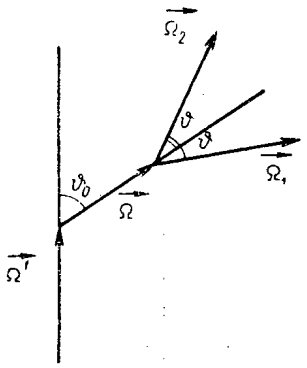

Fig. 1. Asymmetry of neutron scattering.

where $\mathbf{n}_1=\frac{[\Omega\Omega_1]}{|[\Omega\Omega_1]|}$. The upper sign pertains to scattering in the Ω_1 direction, while the lower sign pertains to scattering in the Ω_2 direction, i. e., it is found that more neutrons are deflected downward after the second scattering in this case than in the absence of polarization. It should be mentioned that this effect does not depend on the direction of polarization of unpolarized neutrons (along $\mathbf{n}$ or in the direction opposite to $\mathbf{n}$); however, in scattering at different angles, the polarization sign must be the same.

Let us introduce the functions $F(\mathbf{r}, \Omega, E)$ and $\mathbf{P}(\mathbf{r}, \Omega, E)$; $F(\mathbf{r}, \Omega, E)$ is the flux of neutrons at the point $\mathbf{r}$ with an energy E which move in the Ω direction; $\mathbf{P}(\mathbf{r}, \Omega, E)$ is the flux of neutrons multiplied by their mean polarization. Then, we can write the following system of equations for these functions:

$$\begin{aligned}(\Omega\nabla)\,F(\mathbf{r},\ \Omega,\ E)+F(\mathbf{r},\ \Omega,\ E)&=h\int dE'\int d\Omega' f(\mu_0,\ E')\,\{F(\mathbf{r},\ \Omega,\ E')+G_z(\theta_0,\ E')\,\mathbf{nP}(\mathbf{r},\ \Omega',\ E')\}\,\delta[\mu_0\\ &-g(E,\ E')]+\int d\mathbf{p}_i Q(\mathbf{r},\ E,\ \mathbf{p}_i,\ \Omega),\quad (\Omega\nabla)\,\mathbf{P}(\mathbf{r},\ \Omega,\ E)+\mathbf{P}(\mathbf{r},\ \Omega,\ E)\\ =h\int dE'\int d\Omega' f(\mu_0,\ E')\,\{&G_y(\theta_0,\ E')\,\mathbf{P}(\mathbf{r},\ \Omega',\ E')+G_z(\theta_0,\ E')\,F(\mathbf{r},\ \Omega',\ E')\,\mathbf{n}+G_x(\theta_0,\ E')\,[\mathbf{P}(\mathbf{r},\ \Omega',\ E')\mathbf{n}]\\ &+[1-G_y(\theta_0,\ E')]\,(\mathbf{nP}(\mathbf{r},\ \Omega',\ E'))\,\mathbf{n}\}\,\delta[\mu_0-g(E,\ E')]+\int d\mathbf{p}_i\mathbf{p}_i Q(\mathbf{r},\ E,\ \mathbf{p}_i,\ \Omega).\end{aligned}\tag{4}$$

We have assumed here that moderation occurs only as a result of elastic scattering; the δ-function takes into account the conservation of energy; $h=\Sigma_s/\Sigma$; $Q(\mathbf{r}, E, \mathbf{p}_i, \Omega)$ is the source of neutrons whose polarization is $\mathbf{p}_i$; the lengths are measured in Σ^{-1} units. The significance of the $G_i(\theta, E')$ functions is the following. Assume that a neutron flux with an energy E' which is completely polarized in the direction of the y axis (the z axis coincides with $\mathbf{n}=[\Omega'\Omega]/|[\Omega'\Omega]|$) is incident to the scatterer; then, $G_i(\theta, E')$ is the neutron polarization along the corresponding axis in scattering at the angle θ.

If we neglect the energy loss in elastic scattering and express $G_i(\theta)$ in terms of $A(\theta)$ and $B(\theta)$, we can write the following instead of system (4):

$$\left.\begin{aligned}(\Omega\nabla)\,F(\mathbf{r},\ \Omega)+F(\mathbf{r},\ \Omega)&=h\int d\Omega' f(\mu_0)\,\{F(\mathbf{r},\ \Omega')+\frac{2ReA^*B}{\sigma_s}\,\mathbf{nP}(\mathbf{r},\ \Omega')\}+\int d\mathbf{p}_i Q(\mathbf{r},\Omega,\ \mathbf{p}_i),\\ (\Omega\nabla)\,\mathbf{P}(\mathbf{r},\ \Omega)+\mathbf{P}(\mathbf{r},\ \Omega)&=h\int d\Omega'\Big\{\frac{AA^*-BB^*}{\sigma_s}\mathbf{P}(\mathbf{r},\ \Omega')+\frac{2ReA^*B}{\sigma_s}\,F(\mathbf{r},\ \Omega')\,\mathbf{n}+\frac{2ImA^*B}{\sigma_s}\,[\mathbf{P}(\mathbf{r},\ \Omega')\,\mathbf{n}]\\ &+\frac{2BB^*}{\sigma_s}\,(\mathbf{P}(\mathbf{r},\ \Omega')\,\mathbf{n})\,\mathbf{n}\Big\}+\int d\mathbf{p}_i\mathbf{p}_i Q(\mathbf{r},\ \Omega,\ \mathbf{p}_i).\end{aligned}\right\}\tag{5}$$

For a two-dimensional medium without sources in the diffusion approximation, Eqs. (5) will be reduced to the system

$$\left.\begin{aligned}\frac{dF_1(z)}{dz}+(1-h)\,F_0(z)&=0,\\ \frac{1}{3}\cdot\frac{dF_0(z)}{dz}+(1-hf_1)\,F_1(z)&=\frac{2h}{3}\,p_1(z)\,(\alpha_0-\alpha_2),\\ (1-hf_1)\,p_1(z)&=-\frac{hF_1(z)}{3}\,(\alpha_0-\alpha_2)\\ -\frac{hp_1(z)}{3}\,(\beta_0-\beta_2)&-\frac{h}{5}\,p_1(z)\,(b_1-b_3).\end{aligned}\right\}\tag{6}$$

Here,

$$\left.\begin{aligned}
&\frac{2ReA^*B}{\sigma_s}=\sin\theta\sum_{l=0}^{\infty}\frac{2l+1}{4\pi}\alpha_l P_l(\mu),\quad \frac{2ImA^*B}{\sigma_s}=\sin\theta\sum_{l=0}^{\infty}\frac{2l+1}{4\pi}\beta_l P_l(\mu),\\
&\frac{2BB^*}{\sigma_s}=\sin^2\theta\sum_{l=0}^{\infty}\frac{2l+1}{4\pi}b_l P_l(\mu),\quad F(z,\mu)=\sum_{l=0}^{\infty}\frac{2l+1}{4\pi}F_l(z)P_l(\mu),\\
&\mathbf{P}(z,\Omega)=\mathbf{e}_\varphi\sum_{l=1}^{\infty}\frac{2l+1}{4\pi}p_l(z)P_l^1(\mu);\quad \mathbf{e}_\varphi=\frac{[\mathbf{z}\Omega]}{|[\mathbf{z}\Omega]|}.
\end{aligned}\right\}\qquad(7)$$

The diffusion factor will be obtained from Eq. (6):

$$D=\frac{1}{3\Sigma_{tr}\left[1-hf_1+\frac{2}{9}h^2\frac{(\alpha_0-\alpha_2)^2}{1-hf_1+\frac{h}{3}(\beta_0-\beta_2)+\frac{h}{5}(b_1-b_3)}\right]}.\qquad(8)$$

If we calculate D by means of Eq. (8) using the experimental data from [1, 2] and then calculate $\Delta D/D$ (ΔD is the change in the diffusion factor due to polarization), we obtain the following values:

$$\text{for}\quad \text{Si},\ E_n=0.56\,\text{MeV}\quad \frac{\Delta D}{D}\approx-0.12,$$
$$\text{for}\quad \text{Mg},\ E_n=0.24\,\text{MeV}\quad \frac{\Delta D}{D}\approx-0.17.$$

Thus, polarization effects may exert a considerable influence on neutron diffusion. Estimates of the role played by these effects in different cases of practical interest require additional calculations, which, however, are rendered difficult by the lack of experimental data on polarization.

The authors are deeply grateful to I. I. Bondarenko[1] and P. S. Ot-stavnov for the useful discussion of the problem encountered in the work.

LITERATURE CITED

1. R. Lane and A. Elwyn, Phys. Rev., 126, 1105 (1962).
2. A. Elwyn and R. Lane, Nucl. Phys., 31, 78 (1962).
3. P. S. Ot-stavnov, Atomnaya énergiya, 14, 487 (1963).
4. I. Lepore, Phys. Rev., 79, 137 (1950).

[1]Deceased.

CHARACTERISTICS OF ASYMPTOTIC SPECTRUM OF NEUTRONS IN URANIUM

(UDC 539.125.52)

A. A. Malinkin, F. Nasyrov, and V. F. Kolesov

Translated from Atomnaya Énergiya, Vol. 18, No. 2,
pp. 181-183, February, 1965
Original article submitted February 8, 1964

The characteristics of the asymptotic spectrum of neutrons in natural uranium were investigated by the authors of [1, 2]. Some of their results are mutually inconsistent.

The present authors have attempted to clarify these characteristics. We measured the fission cross-section of U^{235}, U^{238} and other spectral indicators. Direct measurements were also made of the neutron spectrum in the region up to 0.95 MeV.

The apparatus consisted of a spherical critical assembly with a U^{235} core (90% enriched) in a uranium reflector of thickness 30 cm. The latter had a cylindrical extension of diameter 65 cm, which increased its thickness on one side to 100 cm. The critical assembly and extension were installed at the center of a room of size 8 × 7 × 4.5 m. To reduce the effect of background neutrons scattered from the walls of the room, the uranium extension was enclosed in a cadmium sheath.

The reaction cross sections were measured at the center of the extension, 65 cm from the core and not less than 32 cm from the outer surface. At the measuring point the neutron spectrum attained its equilibrium state; this was established from the constancy of the ratios $\sigma_f(U^{235})/\sigma_f(U^{238})$ and $\sigma_f(Pu^{239})/\sigma_f(U^{238})$. The cross sections were measured by means of small ionization chambers, and also by an activation method. The errors were mostly due to inaccuracy in calibrating the chambers or in the absolute β-count. The observed cross-section are given in Table 1.

The reaction cross sections were determined relative to the fission cross section of Pu^{239}, which is nearly constant in the fast-neutron region. The fission cross section $\sigma_f(Pu^{239})$ was determined by direct measurements on neutrons leaking from the critical assembly with uranium reflector thickness 30 cm. This value coincided within 1% with that obtained by averaging the $\sigma_f(E)$ curve [3] over the directly measured spectrum. From measurements of the radial intensity of Pu^{239} fission at 60-70 cm from the core surface, the diffusion length L_{ac} was found to be 9.5 ± 0.5 cm. Table 2 gives the L_{ac} values and cross-section ratios for various indicators, compared with data by other workers.

Direct measurements of the asymptotic neutron spectrum of natural uranium were made with a proportional helium counter like that described in [5]. This had inside diameter 52 mm and a working space of length 240 mm, and was filled with He^3 and xenon to 25 and 170 cm Hg, respectively. A small amount of CO_2 was added to ensure optimum electron collection. The spectrometer resolving power was checked for thermal and fast neutrons of energies 160 and 500 keV. In all cases it was 48-50 keV. The counter pulses were amplified and fed to a 100-channel amplitude analyser. The analyser channel width was determined on the energy scale (17 keV) from the known value of the pulse amplitude for thermal neutrons and the known analyser channel width.

The neutron spectrum measurements made with helium counters, like those made with spectral indicators, were carried out 65 cm from the core surface. The observed pulse amplitude distribution was corrected for the edge effect of the counter. This effect was determined both theoretically and by experiment in fluxes of thermal and fast neutrons. As the neutron energy increased from 0 to 0.95 MeV, the counter correction increased from 9 to 26%. An additional correction was made for the spectrometer's resolving power, and was appreciable in the neutron energy range up to 50 keV. The small correction for He^3 recoil nuclei was ignored. In calculating the neutron spectrum, use was made of the energy dependence of the reaction $He^3(n, p)T^3$, as given in [3].

TABLE 1. Reaction Cross Sections for Asymptotic Spectrum of Neutrons in Natural Uranium

Reaction	$Pu^{239}(n, f)$	$U^{233}(n, f)$	$U^{235}(n, f)$	$U^{238}(n, f)$	$Np^{237}(n, f)$	$Au^{197}(n, \gamma)$	$Pu^{240}(n, f)$	$Li^{6}(n, \alpha)$
Cross section, barn	1.78	2.98 ± 0.12	1.85 ± 0.07	0.0082 ± 0.0004	0.133 ± 0.0006	0.53 ± 0.04	0.24 ± 0.02	1.38 ± 0.12

TABLE 2. Characteristics of Asymptotic Spectrum of Neutrons in Natural Uranium

	Method of measurement	L_{ac}, cm	$\frac{\sigma_f(U^{235})}{\sigma_f(U^{238})}$	$\frac{\sigma_f(Np^{237})}{\sigma_f(U^{238})}$	$\frac{\sigma_f(Pu^{239})}{\sigma_f(U^{238})}$	$\frac{\sigma_f(U^{233})}{\sigma_f(U^{238})}$	$\frac{\sigma_f(Pu^{240})}{\sigma_f(U^{238})}$	$\frac{\sigma_{n\alpha}(Li^{6})}{\sigma_f(U^{238})}$	$\frac{\sigma_{n\gamma}(Au^{197})}{\sigma_f(U^{238})}$
Data from present work	Chambers	9.5 ± 0.5	227 ± 13	16.3 ± 0.9	218 ± 12	365 ± 19	29.4 ± 2.4	168 ± 16	–
	Activation	–	–	–	–	–	–	–	646 ± 6.0
Los Alamos Laboratory outside room [1]	Activation	9.17 ± 0.18	238 ± 6	15 ± 2	–	–	–	–	–
	Radio-chemical	–	240 ± 12	–	–	–	–	–	–
	Chambers	–	243 ± 15	14.5 ± 0.1	250 ± 16	–	–	–	–
	Chambers	–	241 ± 13	–	–	–	–	–	–
Los Alamos Laboratory, inside room[1]	Activation	13.18	220 ± 22	–	–	–	–	–	–
	Radio-chemical	10.35	200 ± 10	–	228 ± 12	–	–	–	–
	Chambers	–	210 ± 10	15.9 ± 0.8	–	–	–	–	–
Argonne Laboratory [1]	Chambers	10.0 ± 0.2	363 ± 40	–	–	–	–	–	–
Oak Ridge Laboratory [1]	Activation	9.6	336	–	–	–	–	–	–
USSR* [1]	Chambers	–	249 ± 20	–	230	–	–	–	–
Sakle [2]	Chambers	9.5 ± 0.5	230 ± 10	16.4 ± 1.2	256 ± 45	344	–	–	–

*Recalculation of results in [4] for depleted uranium.

Figure 1 shows the observed neutron spectrum. The hard region of the spectrum, for neutrons with energy > 0.95 MeV, is constructed in such a way that the fission cross sections of U^{238} and Np^{237}, obtained by averaging $\sigma_f(E)$ over the spectrum [3], show optimum agreement with the measured cross sections.

Direct measurement of the hard region of nearly asymptotic spectra [4, 6] showed that, in the energy region above 2 MeV, the shapes of these spectra remain the same as the fission spectra, though the fraction of fast neutrons in them is insignificant. For the spectrum shown in the diagram, the fraction of the neutrons with energies above the U^{238} fission threshold (1.1 MeV) is 1.7%. The measurement errors shown on the figure are mainly determined by corrections for the edge effect, and in the initial part of the spectrum by corrections for the spectrometer resolving power. The most probable energy is in the region of 50 keV; the mean neutron energy is 0.23 ± 0.02 MeV.

The data obtained by direct measurement agree with those obtained by means of spectral indicators. Thus, for all the spectral indicators, the cross sections obtained by averaging $\sigma(E)$ [3, 7] over the spectrum shown agree with the measured cross sections to within 10% (see Table 1).

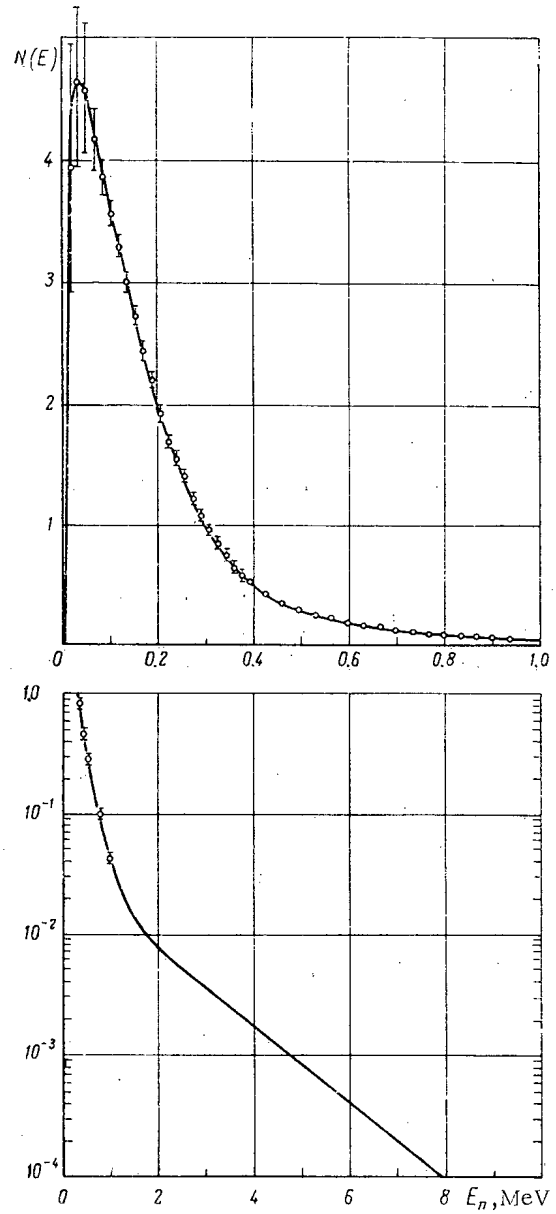

Fig. 1. Asymptotic spectrum of neutrons in natural uranium (normalized to $\int_0^\infty N(E)\,dE = 1$).

LITERATURE CITED

1. C. Chezem, Nucl. Sci. and Engng., 8, 652 (1960).
2. I. Campan, P. Clauzon, and C. Zaleski, Physics of Fast and Intermediate Reactors, Proceedings of a Seminar, Vienna, 3-11 (August, 1961), SM-18/29.
3. D. Hughes and I. Harwey, Neutron Cross Section, BNL-325 (1955).
4. A. I. Leipunskii et al., In book: "Proceedings of Second International Conference on the Peaceful Uses of Atomic Energy," Geneva (1958), Dokl. sovetskikh uchenykh (Reports of Soviet Workers), T. 2, Moscow, Atomizdat (1958), p. 377.
5. R. Batcheler, R. Aves, and T. Skyrme, Rev. Scient. Instrum., 26, 1037 (1955).
6. Report No. 404, Presented by Britain to the First International Conference on the Peaceful Uses of Atomic Energy, Geneva (1955).
7. D. Hyghes and R. Schwartz, Neutron Cross Section, Suppl., No. 1, BNL-325 (1957).

EXCITATION FUNCTION OF REACTION $Cu^{65}(d, 2n)Zn^{65}$ AND YIELD OF ISOTOPE Zn^{65}

(UDC 539.17.012)

P. P. Dmitriev and N. N. Krasnov

Translated from Atomnaya Énergiya, Vol. 18, No. 2,
pp. 184-185, February, 1965
Original article submitted February 20,

The reaction $Cu^{65}(d, 2n)Zn^{65}$ is widely employed for obtaining Zn^{65} without a carrier. In [1-5] the Zn^{65} yield was determined for cyclotron irradiation of copper targets by deuterons of various energies (see Fig. 1). It will be seen that these authors' results do not agree.

We therefore attempted to determine the excitation function of the reaction $Cu^{65}(d, 2n)Zn^{65}$ and the Zn^{65} yield at deuteron energy 20 MeV. The Zn^{65} yield was measured in two ways: (1) by irradiating a thick copper target; (2) by irradiating a stack of copper foils. In case (2) we also simultaneously determined the excitation function of the reaction $Cu^{65}(d, 2n)Zn^{65}$.

The Zn^{65} yield for a thick copper target at $E_d = 20$ MeV was found to be 16 ± 2 $\mu C/\mu a \cdot g$. We irradiated a rotating target, made of mark M-1 copper, with a hemispherical head. The head diameter was 90 mm. By intensive water cooling the irradiated surface was kept below 150°C. The current to the target was measured calorimetrically to within ±5%. The mean deuteron energy was measured by means of a separate target which simultaneously recorded the beam power (calorimetrically) and current (by a microammeter). The energies found did not differ by more than 2% from the values calculated from $H\rho$.

To determine the Zn^{65} yield, two targets were irradiated at beam currents of 300 and 600 μa. The observed yield values agreed to within 5%.

The Zn^{65} activities in the targets were measured by means of an ionization chamber with 4π geometry [6], calibrated with standard radium and Co^{60} sources. Measurements were made twice within ten days and once four months after irradiation. The activity was found to decay with half-life 240 days. The following values were used for the absolute γ-constants: for Zn^{65}, 2.83; Co^{60}, 13.2; Ra, 8.4 r/mC · cm · g). The accuracy of the target activity measurements, governed by that of the Ra and Co^{60} standards, was ±10%.

Since the isotope Co^{60} may be formed by the reaction $Cu^{63}(d\alpha p)Co^{60}$, zinc and cobalt were separated radiochemically from the irradiated copper. Measurements of the Co^{60} activity showed that its contribution to the total γ-activity did not exceed 2%, in agreement with [2]. No other long-lived γ-activity was detected in the residual solution. The accuracy of the observed Zn^{65} yield was chiefly determined by the accuracy of the ionization-chamber measurements of target activity and by the accuracy of measurement of the deuteron beam current. The overall error in our experiments was ±15%. The yield was found to be (16 ± 2) $\mu C/(\mu a \cdot g)$ or $(8.3 \pm 1.03) \cdot 10^{-4}$ atoms/deuteron.

The copper foils were irradiated in the internal beam of the cyclotron at deuteron energy 21 MeV and current 3 μa. A stack of 32 foils, each of thickness 15.5 mg/cm^2, was clamped to a cooled base by means of a copper plate with a hole. Using this target arrangement, we were able to determine the fraction of the beam going through the hole by comparing the activities of the foils and plate. In order to plot the excitation function, the relative activity of each foil was determined from the intensity of the 1120-keV line, using a scintillation γ-spectrometer.

For the foil with the greatest activity, corresponding to the maximum of the excitation function, an absolute activity measurement was made by comparison with a Zn^{65} standard, using a scintillation spectrometer. The cross section was found to be 920 mbarn. The path-energy curve for deuterons in copper was calculated from the formulae given in [8]. Two stacks of foil were irradiated. The two values for the cross section agree. The excitation function (mean for the two determinations) is shown in Fig. 1. The error, chiefly due to inaccuracies in measuring the beam current and the uncertainty of the Zn^{65} standard, is ±15%.

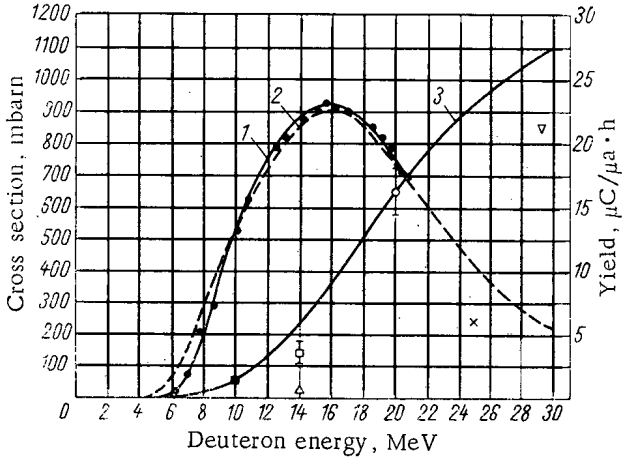

Fig. 1. Excitation function of reaction $Cu^{65}(d, 2n)Zn^{65}$ and yield of Zn^{65}, versus deuteron energy, for thick copper target. 1, 2) experimental and calculated excitation functions $\sigma = f(E_d)$, respectively; 3) Zn^{65} yield versus E_d. Yield values from: ○) present authors, □) [1]; ▽) [2]; ×) [3];) [14]; △) [5].

The Zn^{65} yield was plotted against dueteron energy up to E_d = 21 MeV by graphical integration of the excitation function. The yield for E_d = 20 MeV agreed with that given above, i.e., 16 μC/μa·h. The absolute activity of the stack of foils was also measured by means of an ionization chamber; the value obtained for the Zn^{65} yield also agreed with the results of the graphical integration.

The reaction (d, 2n) is known to take place chiefly via a compound nucleus. In such a case, the statistical theory affords comparatively simple methods of calculating the cross sections of a nuclear reaction, especially when neutrons are emitted. However, satisfactory agreement between the observed and theoretical cross sections can be obtained only by an appropriate choice of r_0 in the formula for the radius of deuteron-nucleus interaction:

$$R_d = (r_0 A^{1/3} + 1{,}2) \cdot 10^{-13} \text{ cm}.$$

The excitation function was calculated from the formula in [9] up to E_d = 30 MeV. In computing the cross section we used the relation

$$\sigma_{kn}(E_a) \approx \sigma_c(a)\,[P_{k-1}(y_k) - P_k(y_{k+1})].$$

In calculating $\sigma_c(a)$, the formation cross section of the compound nucleus, we took r_0 = 1.37. The calculated excitation function is shown in Fig. 1 (curve 2). The observed and theoretical curves practically coincide. This enables us to plot the Zn^{65} yield versus deuteron energy for a thick target up to E_d = 30 MeV (see curve 3). Up to 21 MeV, this curve agrees (within the experimental error) with that obtained by graphical integration of the experimental excitation function.

As seen from Fig. 1, the Zn^{65} yields found in [1-3, 5] lie below curve 3. These low values are probably due mainly to losses of Zn^{65}, caused by diffusion and evaporation of zinc during irradiation. The authors of [10] studied the way in which the achievable Zn^{65} yield depends on the thermal conditions of a copper target during irradiation by protons. On change of thermal conditions, the yield altered almost twofold.

The work was carried out on a 1½-meter cyclotron in the Fiziko-Énergeticheskii Institut (High-Energy Physics Institute). The authors wish to thank O. A. Sal'nikov for useful comments, Z. P. Dmitriev, who made the calculations, and Yu. G. Sevast'yanov and Yu. P. Pen'kov, who performed the radiochemical separation of zinc and cobalt.

LITERATURE CITED

1. E. Clarke and J. Irving, Phys. Rev., 69, 680; 70, 893 (1946); E. Clark, J. Chem. Soc. Suppl., No. 2, 356 (1949).
2. A. Aten, Philos. Tech. Rev., 16, No. 1 (1954).

3. H. Mocken, Production of Radioisotopes with Charged Particles, Amsterdam (1957).
4. P. P. Dmitriev et al., The Preparation of Isotopes: Transactions of Conference on the use of Isotopes [in Russian], Moscow (1957) p. 26; Moscow, Izd-vo AN SSSR (1957).
5. W. Carrison and I. Hamilton, Chem. Rev., 49, 237 (1951).
6. E. Trukhmahova and T. Afanas'eva, "Transactions of Conference on the Peaceful Uses of Atomic Energy (1959)" [in Russian], 2, Tashkent, Izd-vo UzSSR (1961).
7. P. Gusev, V. Mashkovich, and T. Obvintsev, Gamma-Radiation of Radioactive Isotopes and Fission Products [in Russian], Moscow, Fizmatgiz (1958).
8. M. Z. Maksimov, ZhÉTF, 38, 127 (1959).
9. M. Z. Maksimov, ZhÉTF, 33, 1411 (1957).
10. G. Glason, I. Gruverman, and I. Need, Internat. J. of Appl. Rad. and Isotopes, 13, 223 (1962).

USE OF AQUEOUS GLYCINE SOLUTION FOR γ-RAY AND FAST-NEUTRON DOSIMETRY

(UDC 539;12;04)

A. P. Ibragimov and A. V. Tuichiev

Translated from Atomnaya Énergiya, Vol. 18, No. 2,
pp. 185-187, February, 1965
Original article submitted February 13, 1964, final editing, April 13, 1964

Chemical dosimetry is concerned with the most widespread and convenient methods of determining energy absorption in various media. In particular, the ferrous sulfate dosimeter, which achieves accurate measurement for small doses in the range 1-100 rad, can be used to record x-, γ- and α-radiation, from low rates up to such high ones as 10^5 rad or 10^{18} eV/ml.

Transparent plastic and polystyrene are used for β- and γ-ray dosimetry. On irradiation, their UV absorption spectra are displaced towards longer wavelengths [1, 2]. Aqueous solutions of carbohydrates have been used to measure large doses and various dose rates of γ-rays and fast neutrons in a nuclear reactor [3, 4]. Solid α-alanine has been successfully used for the dosimetry of x- and γ-rays, and also of electrons and protons at doses up to 10^5 rad. The quantity of radicals formed, which is directly proportional to the radiation dose, is registered by electron paramagnetic resonance (EPR) [5].

However, no satisfactory method has been found of measuring energy absorption at very high doses (10^5-10^8 rad). In this connection we determined the yield of ammonia during the radiolysis of an aqueous solution of glycine. Ammonia determination is, of course, simple and easy.

Many investigators have studied the radiolysis of proteins and aminoacids [6-9]. The radiolysis of a 1 M aqueous solution of glycine, under the action of x-rays in vacuum or in the presence of oxygen, was studied in [8]. The

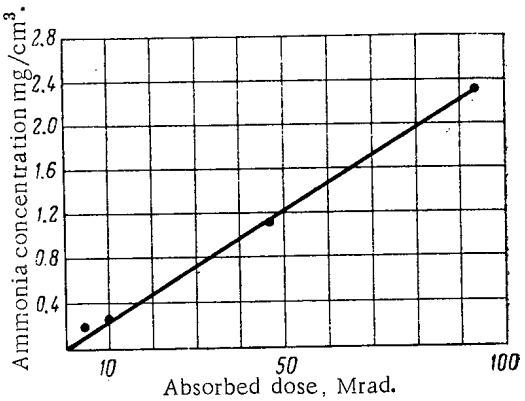

Fig. 1. Deamination of 1 M glycine solution irradiated with γ-quanta from Co^{60}.

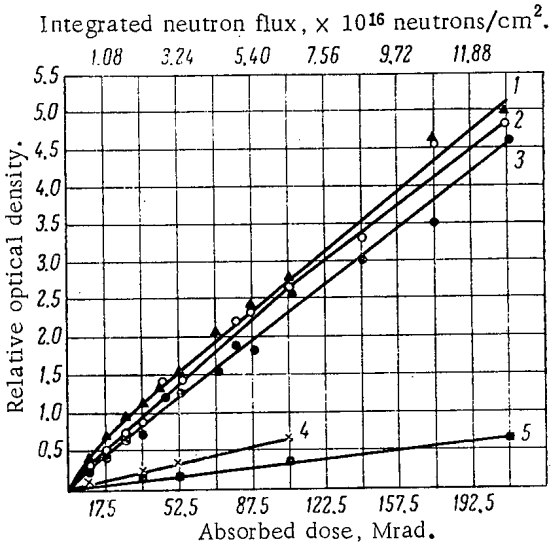

Fig. 2. Deamination of aqueous glycine solutions, irradiated in a reactor by a flux of fast neutrons of $1.8 \cdot 10^{13}$ neutrons/cm²·sec. Solution concentrations: ▲ (1), 2; ○ (2), 1.5; ● (3), 1; × (4), 0.1; (5), 0.01 M.

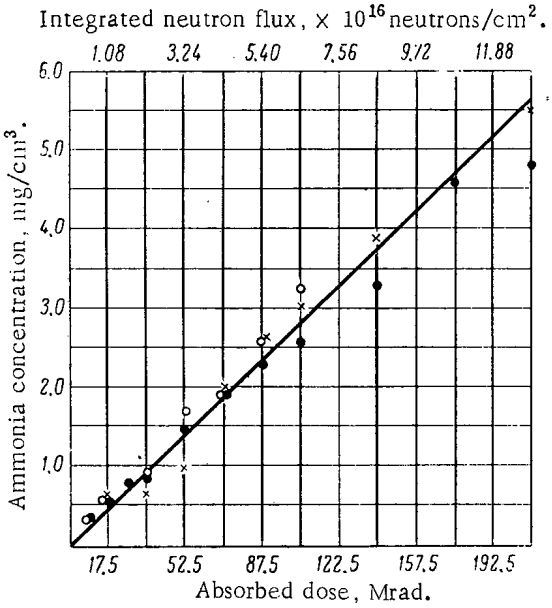

Fig. 3. Deamination of 15 M glycine solution, irradiated by γ-rays and fast neutrons at different dose rates and fluxes Φ: ⊕) 2000 kw, $\Phi = 1.8 \cdot 10^{13}$ neutrons/cm^2 · sec; ○) 1000 kw, $\Phi = 0.81 \cdot 10^{13}$ neutrons/cm^2 · sec. ×) 500 kw, $\Phi = 0.43 \cdot 10^{13}$ neutrons/cm^2 · sec.

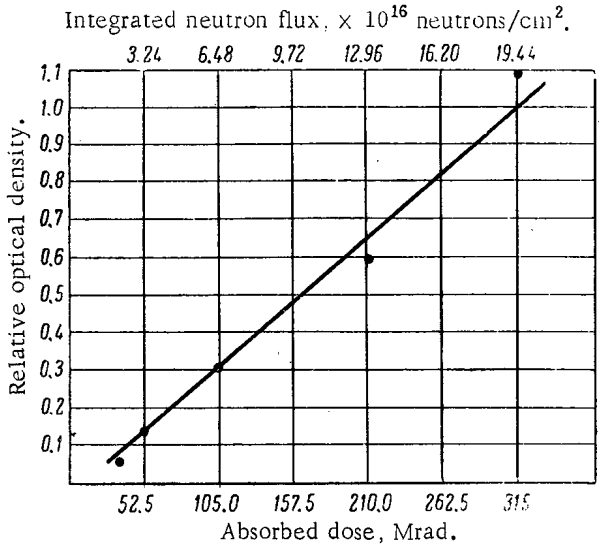

Fig. 4. Optical absorption of glycine versus absorbed dose and integrated neutron flux, wavelength 255 mμ.

following glycine decomposition products were identified and quantitatively determined: ammonia (radiation yield $G \approx 4.0$ at dose $\sim 10^{19}$ eV/ml), hydrogen ($G \approx 2.0$) formaldehyde ($G = 0.53$), acetic acid ($G \approx 1.2$), glyoxalic acid ($G = 2.10$), CO_2 ($G \approx 0.90$), etc.

On irradiation of glycine or its aqueous solutions by γ-rays or fast neutrons, the amount of ammonia formed and the optical density in the UV region were found to increase in direct proportion to the radiation dose [10].

Commercial glycine (pure grade) was twice recrystallized by the usual method, and its purity checked by paper chromatography. Aqueous solutions were prepared with bidistillate (i.e., double-distilled water). The glycine and solutions (of concentrations C = 0.01, 0.1, 1.0, 1.5 and 2 M) were irradiated in airtight double polythene bags, about 2 × 5 cm, and in cylindrical quartz ampoules, 1 cm diameter × 4 cm long, each containing 1 ml solution. The specimens were placed in vertical water-shielded channels of a nuclear reactor and subjected to a flux of fast neutrons at various power levels between 500 and 2000 kw. The channel temperature was 32-36°C. On irradiation for 1 h in the channel of a reactor working at 2000 kw ($1.8 \cdot 10^{13}$ neutrons/cm^2 · sec), the total absorption of γ-quanta and fast neutrons was ~ 105 Mrad, the error being 3-5% [3].

Pure γ-irradiation was carried out, using a Co^{60} source, at various absorbed doses (10^5-10^8 rad) and dose rates (17, 230 and 530 r/sec). The doses were measured by means of ferrous sulfate dosimetry; the Fe^{3+} yield was 15.5 ±0.5 [2]. Ammonia was determined by the method described in [11], using an SF-4 spectrophotometer and FÉK-2M photoelectric calorimeter and also by a microdiffusion method [12]. The accuracy of both methods was ± 2%.

Figures 1 and 2 show the deamination of aqueous glycine solution irradiated by γ-rays and a flux of fast neutrons. It is seen that the ammonia liberated is directly proportional to the absorbed dose of γ-rays or fast neutrons. The ammonia yield is slightly less at glycine concentration 0.1 M than at 1-2 M. The ammonia yields from the 1-2 M glycine solutions irradiated in the reactor were close together (G_{NH_3} = 1.50-1.65); those for γ-irradiation were also about the same (1.48-1.60). The ammonia yield is independent of temperature between 18 and 36°C. Figure 3 shows that the ammonia yield is independent of the dose rate within wide limits for solutions more concentrated than 1 M. The UV absorption of irradiated glycine and its aqueous solutions is directly proportional to the radiation dose (Fig. 4). The increase in optical density in the UV region is associated with the appearance of a yellow tint in the irradiated specimen; the color becomes more intense with increasing dose.

The deamination of concentrated aqueous solutions of glycine, measured by means of the ammonia formed, can thus be used for γ-ray and fast-neutron dosimetry in the dosage range 10^5-10^8 rad.

LITERATURE CITED

1. K. K. Aglintsev, Dosimetry of Ionizing Radiation [in Russian], Moscow, Gostekhteorizdat (1957).
2. K. K. Aglintsev et al., Applied Dosiemtry [in Russian], Moscow, Gosatomizdat (1962).
3. V. V. Generalova, Dissertation, Tashkent, IYaF AN UzSSR (1963).
4. S. V. Starodubtsev, Sh. A. Ablyaev, and V. V. Generalova, "Atomnaya Énergiya," 8, 264 (1960).
5. W. Bradshaw et al., Radiation Research, 17, 11 (1962).
6. G. Stein and J. Weiss, J. Chem. Soc., 3356 (1949).
7. W. Dale et al., Biochem. J., 45, 93 (1949).
8. Ch. Maxwell et al., Radiation Res., 1, 530 (1954).
9. M. A. Khenokh and E. M. Lepinskaya, In book, "Proceedings of First All-Union Conference on Radiation Chemistry" [in Russian], Moscow, Izd-vo AN SSSR (1958) p. 182.
10. A. P. Ibragimov and A. V. Tuichiev, In book, "Proceedings of Second All-Union Conference on Radiation Chemistry" [in Russian], Moscow, Izd-vo AN SSSR (1962) p. 263.
11. V. S. Asatiani, Biochemical Photometry [in Russian], Moscow, Izd-vo AN SSSR (1957) p. 421.
12. V. S. Asatiani, Methods of Biochemical Investigation [in Russian], Mowcow, Medgiz (1956) p. 149.

LIGHT OUTPUT AND AMPLITUDE RESOLUTION OF MONOCRYSTALS

(UDC 543.420.62+621.387.464)

G. V. Miroshnikov and A. I. Kirillov

Translated from Atomnaya Énergiya, Vol. 18, No. 2,
pp. 187-189, Feburary, 1965
Original article submitted February 15, 1964, final editing, May 7, 1964

[1-3] demonstrated the possibility of using lithium iodide monocrystals for fast-neutron spectrometry by means of the nuclear reaction

$$Li^6 + n \longrightarrow He^4 + T^3 + 4.78 MeV.$$

Interest thus attaches to the light output and amplitude resolution of LiI(Eu).

An FÉU-S photomultiplier was used: with an NaI(Tl) crystal its amplitude resolution for the Cs^{137} γ-line is 7%. LiI(Eu) monocrystals of diameter 30 mm were investigated. Their thicknesses were as follows: crystal 1, 10 mm (natural mixture of lithium isotopes); crystals 2 and 3, 10 and 11 mm respectively (90% enriched with Li^6). For thermal neutrons, the amplitude resolutions of crystals 1, 2 and 3 were 6.7, 8.2 and 8.8% respectively.

The light outputs of crystals 1, 2 and 3 for thermal neutrons were equal to those for β-particles with energies Q_β = 2.8 ± 0.3, 2.4 ± 0.1 and 3.5 ± 0.1 MeV, respectively.

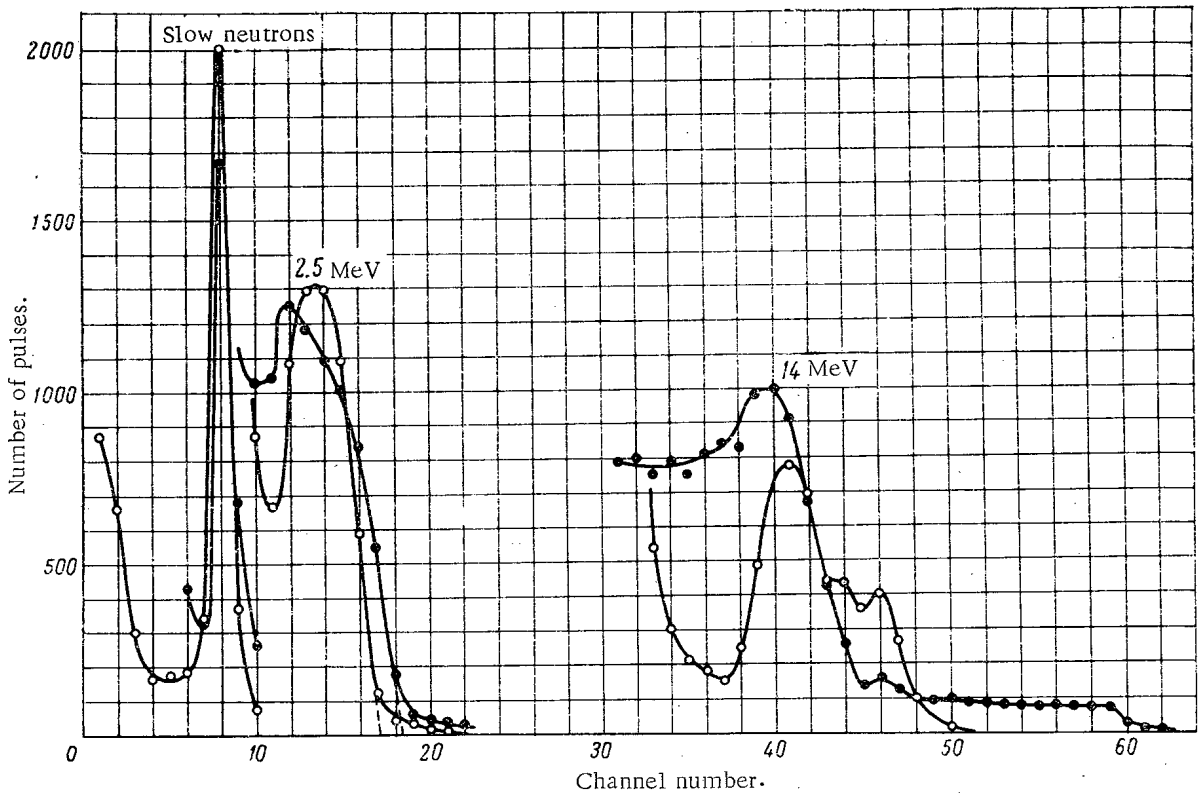

Fig. 1. Pulse amplitude distribution for neutrons of energies 2.5 and 14 MeV in LiI(Eu) crystal. ●) Crystal 2, Q_β = 2.4 MeV; ○) Crystal 3, Q_β = 3.5 MeV.

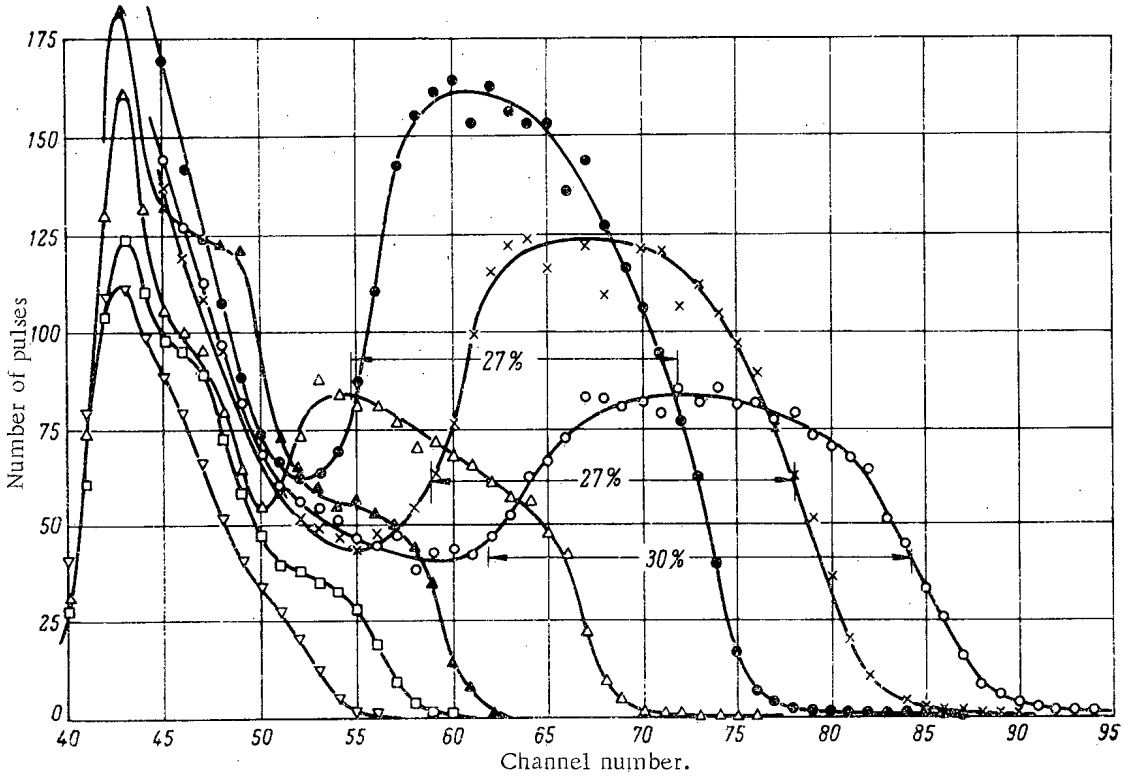

Fig. 2. Pulse amplitude distribution for monoenergetic neutrons in crystal 3. Neutron energies, MeV: ▽) 0.6; □) 0.8; ▲) 1; △) 1.5; ◉) 2; ×) 2.5; ○) 3.

Table 1. Energies of α-Particle and Tritium Nucleus in Reaction $Li^6 + n \rightarrow He^4 + T^3 + 4.78$ MeV, Versus Neutron Energy

E_n, MeV . .	0	0.5	1	1.5	2	2.5	3	6	10	14
E_α, MeV . .	2.05	1.95	1.68	1.63	1.61	1.6	1.68	1.93	2.28	2.88
E_T, MeV . .	2.73	3.33	4.1	4.65	5.17	5.7	6.1	8.85	12.5	15.9

In alkali halide crystals at normal temperatures, the light output varies markedly with the specific ionization dE/dx [4]. The light output reaches a maximum at proton energies of a few MeV; with further increase in specific ionization (e.g., for α-particles) it markedly declines. Consequently, the low Q_β values for these crystals are due to their weak light output for α-particles. In particular, in the registration of thermal neutrons the scintillation amplitude from α-particles is apparently negligible in crystals 1 and 2.

Owing to the indeterminate apportioning of the neutron energy between the α-particle and the tritium nucleus, crystals with low Q_β are unsuitable for fast-neutron spectrometry; this is confirmed by the pulse amplitude distribution for crystal 2 with neutrons of energies 2.5 and 14 MeV (Fig. 1).

We made a detailed study of the amplitude resolution of crystal 3 (Q_β = 3.5 MeV) for neutrons of energy 0.6, 0.8, 1, 1.5, 2, 2.5, 3 and 14 MeV, obtained from the reactions T(p, n)He^3 and T(d, n)He^4 which were carried out with an e.s. generator. The results are shown in Figs 1 and 2. The amplitude resolving power of the spectrometer was approximately constant up to neutron energy 3 MeV (27-30%); at E_n = 14 MeV it was 19%. The amplitude distribution curves show some departure from the Gaussian form, and the peaks for monoenergetic neutrons are broadened: this is due to the low light output of the crystal for α-particles. Figure 3 plots two curves for maximum light output V(E) versus total available energy, one curve being calculated from the amplitude distribution data and one from theory.

The maximum light output occurs when the α-particle is emitted in the opposite direction to the neutrons line of flight. For this case, the energy distribution between the α-particle and tritium nucleus, calculated from the

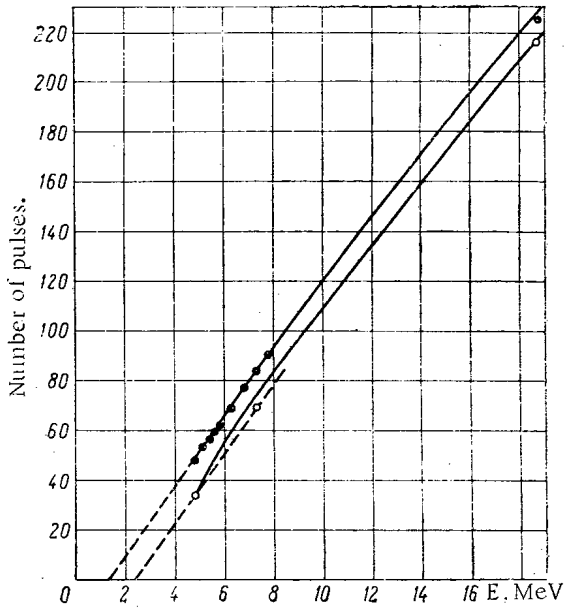

Fig. 3. Maximum light output V(E) versus total available energy E: ○, ●) experimental points for crystals 2 and 3, respectively; ———) theorectical curve (Eq. (2)); – – – –) linear interpolation (Eq. (1)).

laws of conservation of energy and momentum, is given in Table 1. This shows that, for neutrons from thermal energy up to 6 MeV, the α-particle energy is nearly constant, so that in this range V(E) is nearly linear. At E_n = 14 MeV the α-particle energy is nearly doubled, giving a marked deviation from linearity (see Fig. 3). The linear part of the light output curve agrees with the relation

$$V(E) = K(E - 4.78 + Q_\beta), \quad (1)$$

where E and Q_β are expressed in MeV, and K is the proportionality coefficient. The values of Q_β given by this relation are 2.5 ± 0.3 and 3.6 ±0.2 MeV for crystals 2 and 3 respectively, and agree with the values found from the β-particle energies.

The maximum light output is given approximately by the formula

$$V(E) = K(E - E_{\alpha 0} - E_{T0}). \quad (2)$$

Here $E = E_\alpha + E_T$, where E_α and E_T = energies of α-particle and tritium; $E_{\alpha 0}$ and E_{T0} are the energies of an α-particle and tritium nucleus which can be absorbed in the crystal without scintillation.

The calculation is performed on the assumption that when $Q_\beta \leq 2.73$ MeV the scintillations due to α-particles can be neglected, while the crystal's light output for tritium nuclei obeys the linear law $V(E_T) = K(E_T - E_{T0})$, where $E_{T0} = 2.73 - Q_\beta$; when $Q_\beta > 2.73$ MeV the light output for α-particles is $V(E_\alpha) = K(1-C)E_\alpha$, and for tritium nuclei $V(E_T) = KE_T$, where $C = \frac{4.78 - Q_\beta}{2.05}$ Q_β being expressed in MeV. As seen from Fig. 3, these theoretical expressions agree with experiment.

Thus the marked amplitude scatter for fast monoenergetic neutrons and the deviation from linearity, displayed by the light output of a LiI(Eu) crystal, are caused by the low light output for α-particles. Crystals with $Q_\beta \gtrsim 3.5$ MeV can be used for fast neutron spectrometry, being fast calibrated with monoenergetic neutrons. Crystals with $Q_\beta \lesssim 2.5$ MeV are unsuitable for fast neutron spectrometry.

The authors wish to thank V. P. Panovaya, N. I. Kuzin and A. A. Samakhov for preparing the crystals.

LITERATURE CITED

1. R. Murray, Nucl. Instrum., 2, 237 (1958).
2. K. Nicholson and I. Snelling, Brit. J. Appl. Phys., 6, 104 (1955).
3. V. V. Matveev et al., "Pribory i tekhnika éksperimenta," No. 4, 46 (1963).
4. T. Ophel, Nucl. Instrum., 3, 45 (1958).

SOME DATA ON EQUILIBRIA OF THE SYSTEMS $MeS(MeS_2) - UO_2SO_4 - H_2O$ AT ELEVATED TEMPERATURES AND PRESSURES

(UDC 550.41)

B. S. Osipov and R. P. Rafal'skii

Translated from Atomnaya Énergiya, Vol. 18, No. 2,
pp. 189-191, February, 1965
Original article submitted May 4, 1964

In the ore veins of many hydrothermal uranium deposits, the uranium minerals are closely associated with the sulfides of heavy metals. Pitchblende is often confined to earlier sulfide deposits, and uranium mineralization localized in sulfide-enriched rocks. These facts suggest that sulfides are important in the precipitation of uranium from hydrothermal solutions: interest therefore attaches to experimental study of the equilibria in the systems $MeS-UO_2^{2+}-H_2O$ at elevated temperatures and pressures.

The conditions and products of the reduction of hexavalent uranium by pyrite, galenite and other minerals were studied qualitatively in [1]. It was found that reduction could take place over a wide temperature range in acid or neutral solutions. Crystalline UO_2 and uranoso-uranic oxide were deposited in acid media. No quantitative data were obtained.

The present report gives the results of experiments to determine the equilibrium concentrations of uranium in the presence of sulfides at 200-360°C. 0.25 cc of natural sulfide, ground to $-0.6 \div 0.4$ mm, were freed from inclusions of extraneous minerals in heavy liquids and under a binocular magnifier, and placed in a quartz ampoule of diameter 8 mm. The ampoules were filled with UO_2SO_4 solution containing 10 g U per liter ($f = 0.5$), exhausted and sealed off. They were then placed in an autoclave and kept at the required temperatures. The temperatures were measured to within ± 7°C by means of a Chromel-Copel thermocouple and ÉPD-12 potentiometer.

The time required to reach equilibrium was determined by separate experiments with pyrite and galena. It was found that, with pyrite, equilibrium was reached in < 25 h at 200°C. The uranium concentration did not change (within the experimental error) after 50 or 95 h at this temperature. At 360°C (at which the heating time was varied from 11 to 48 h) equilibrium is attained in < 11 h. The uranium concentration at 360°C did not alter when the amount of pyrite in the ampoule was increased or its grain size altered.

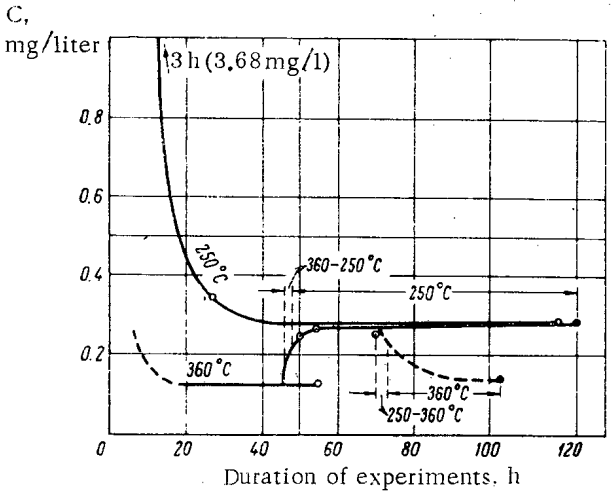

Fig. 1. Plot of uranium concentration in solution, in the presence of galena, versus temperature and heating time.

In experiments with galena at 250°C equilibrium was approached from both above and below. After preliminary heating at 360°C followed by a short period at 250°C, the uranium concentration in the solution increases to that attained by direct precipitation at 250°C (Fig. 1). If the temperature is then increased to 360°C, the uranium content in the deposit again falls. These results show that the concentrations obtained at 250 and 360°C are the equilibrium values and that the reaction is reversible in this system.

As the experiments on the influence of time were performed only with pyrite and galena, the times of retention at a given temperature with the other minerals were

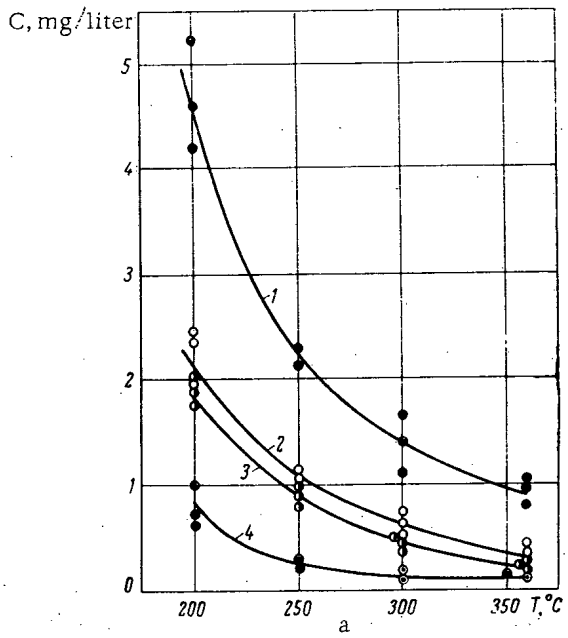

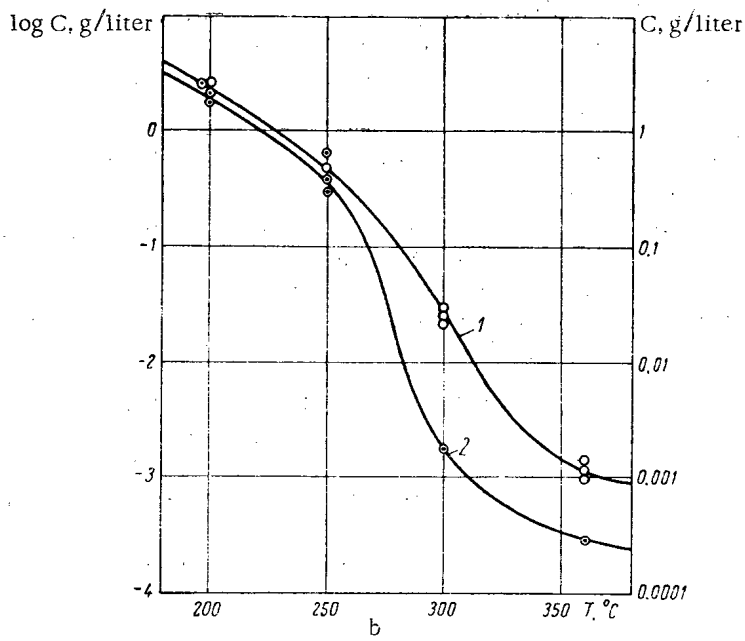

Fig. 2. Temperature-dependence of uranium concentration in solution in the presence of sulfides. a: 1) ZnS (0.4% Fe); 2) Zn(Fe)S (12.6% Fe); 3) $CuFeS_2$; 4) PbS; b: 1) MoS_2; 2) FeS_2.

given a large "safety margin"—120, 116, 78, and 54 h at 200, 250, 300, and 360°C, respectively. At the end of each experiment the autoclave with the ampoules was quickly cooled in water, the ampoules were broken open and the solid and liquid phases separated by filtration. We ruled out the possibility that the equilibrium uranium concentrations for the experimental temperatures might change appreciably during these operations, since crystalline UO_2 and U_3O_8 dissolve quite slowly. This had been established in previous experiments on the recovery of uranium by reduction with elementary sulfur.

The uranium concentration in the solution was determined by the fluorescence method. We used the method of addition and dilution [2, 3], into which we introduced certain corrections. The fluorescent intensities of the

NaF beads were measured with a fluorescence micro-photometer by the method of V. F. Grigor'ev. The uranium concentration in each sample was taken as the mean of 6-30 separate determinations. The relative analysis error was not more than ± 10%.

Fig. 2a, plots against temperature the uranium concentration in the solution in the presence of PbS, ZnS and $CuFeS_2$. With increase of temperature the equilibrium uranium concentrations decrease, becoming less than 1 mg/liter at 350°C. The amount of uranium is least in the presence of galena, and greatest in the presence of non-ferruginous sphalerite. However, even in the latter case about 5 mg/liter remains in solution at 200°C. In the presence of sphalerite, the uranium concentration depends on the divalent iron content.

The equilibrium uranium concentrations have quite different temperature-dependences in systems containing FeS_2 and MoS_2 (see Fig. 2b). At 200-250°C there are two to three orders higher than those for the other sulfides. However, with increasing temperature the uranium concentration in the solution falls sharply and at 360°C is 0.3-1 mg/liter.

The precipitation of uranium during reaction of the solution with sulfides is due to reduction of the uranyl ion by the sulfur in the sulfides. If the sulfide contains divalent iron, the latter also reduces the uranium. This is shown by similar experiments with magnetite, in the presence of which the uranium concentration at 200-300°C decreases to 1-0.1 m/liter. The equilibrium uranium concentration in the solution at a given temperature evidently depends both on the composition of the liquid phase and on the composition and properties of the minerals acting as reducing agents for the uranium. We calculated the lattice energies of PbS, ZnS, FeS_2, and MoS_2 (which were found to be 684.3, 833.9, 1201.4, and 1667.8 kcal/mole respectively), using A. F. Kapustinskii's formula [4] for the energy of a coordinate lattice:

$$U = 287.2 \frac{nW_a W_c}{r_a + r_c}\left(1 - \frac{0.345}{r_a + r_c}\right).$$

The metal-sulfide interatomic distances were taken from the reference book "Mineraly" [Minerals] (Vol. 1, Moscow, Izd-vo AN SSSR, 1960); for PbS, $r_a + r_c$ is 2.97 A, for ZnS 2.35 A, for FeS_2 2.26 A and for MoS_2 2.35 A. These values show that to break the interionic bonds requires most energy in the molybdenite lattice and least in the galenite lattice. Pyrite and sphalerite have intermediate values. On the whole, these calculated results agree with the experimental data, from which the sulfides can be arranged in the same order as that of their lattice energies. It is interesting that the equilibrium uranium concentrations in the solution do not seem to depend on the sulfur content of the sulfides. In fact, though galenite has the lowest sulfur content of all the sulfides, and this sulfur is the only reducing agent for U(VI), galenite causes the precipitation of the greatest quantity of uranium. The calculated sulfur content of molybdenite is 40%, i. e., less than in sphalerite and chalcopyrite. However, the equilibrium uranium concentration is much less in the presence of the two latter than in the presence of molybdenite.

The temperature-dependence of the uranium concentration in solution in the presence of sulfides is similar to that obtaining when U(VI) is reduced by elementary sulfur in the same conditions [5]. In the latter case it was shown that the U(IV) concentration in the liquid phase, determined by the solubility of crystalline UO_2, was approximately 0.02 mg/liter. The larger part of the dissolved uranium was hexavalent; the decrease in total uranium content with rise in temperature was caused by more complete reduction of U(VI) and a decrease in the U(VI) : U(IV) ratio. Since similar curves are found for uranium reduction by sulfur and sulfides, we can conclude that most of the dissolved uranium is hexavalent in the presence of sulfides also.

LITERATURE CITED

1. R. P. Rafal'skii, Physicochemical Investigation of the Conditions of Formation of Uranium Ores [in Russian], Moscow, Gosatomizdat (1963).
2. G. Price, R. Ferretti, and S. Schwartz, Analyt. Chem., 25, 2 (1953).
3. V. F. Grigor'ev, V. F. Luk'yanov, and E. P. Duderova, Zh. anal. khim., 15, 184 (1960).
4. A. F. Kapustinskii, Zh. obshch. khim., 13, 497 (1943).
5. R. P. Rafal'skii, A. D. Vlasov, and I. V. Nikol'skaya, Dokl. AN SSSR, 151 (1963).

SCIENCE AND ENGINEERING NEWS

INTERNATIONAL BETATRON COLLOQUIUM

A. A. Vorob'ev, V. A. Moskalev, M. F. Filippov,
and V. A. Vorob'ev

Translated from Atomnaya Énergiya, Vol. 18, No. 2,
pp. 192-193, February, 1965

In June 1964, the III International Colloquium on Betatrons was held at the Physics and Engineering Institute of the University of Jena (German Democratic Republic). Participating in the colloquium were delegations from the German Democratic Republic, Poland, Rumania, the USSR, West Germany, the Czechoslovak Socialist Republic, and Switzerland; 30 papers were heard.

Prof. R. Wideröe (Switzerland) and Prof. M. Steenbeck (East Germany) reported on the history of the development of betatrons.

K. Rytin (Institute of Plasma Physics, CSSR) reported on research and development work on betatrons in Czechoslovakia since 1954. The first betatron, 3.5 MeV, was operated at a frequency of 500 cps. A commercial betatron model accelerating to 17 MeV at intensities to 40 R/min · m has been successfully developed; 10 such machines have already been fabricated (seven for medicine and three for industrial flaw detection work). The betatron features a one-piece O-shaped electromagnet in which a single unit consisting of pole tips, central bearings, and the chamber is sealed in place with the aid of rubber fitted pads. Work has begun on the fabrication of a 18-MeV swinging betatron (swinging through an arc 60-240°) with extracted electron beam. After the electrons arrive in the region $n > 1$, they are extracted in 20-30 revolutions at up to 50% efficiency; the radiation dose rate is 300-400 R/min · m. A 100 kV external injector has been proposed for use in the industrial inspection betatron system.

M. Sajdl (Institute of Plasma Physics, CSSR) read a theoretical paper on the electron capture mechanism in betatron acceleration and reported on experimental research which confirms these theoretical conclusions. In his view, electrons are formed in bunches, and in the bunching process an appreciable portion of the electrons become lost with high-frequency oscillations resulting. Contraction of the instantaneous orbits ensues as a result, and the remainder of the electrons bypass the injector.

Prof. A. A. Vorob'ev (USSR) drew attention to the fact that this theory can possibly explain many experiments on electron acceptance in the acceleration mode.

C. C. Ilescu (Institute of Atomic Physics, Rumania) submitted an account of a 25-MeV Rumanian betatron. The equilibrium orbit radius of the betatron is 25 cm, the pole gap aperature is 6.74 by 7.8 cm^2, and $n = 0.75$. At an injection energy of 30 keV, the radiation dose rate is 42 R/min. The betatron is being employed in research on the interaction between nuclei and electrons, and in nondestructive testing.

L. Schmalz and E. Burger (Physics and Engineering Institute, East Germany) reported on the design of a 30-MeV betatron. Am improved Kerst injector is used in this machine. Conductors leading to the heating filament are enclosed in metal tubes fabricated together with a Wehnelt cylinder, in order to reduce the field intensity. The filament and the Wehnelt cylinder form a single replaceable unit. High-loss steel was used in fabricating the electromagnet, requiring a water-air cooling system to allow continuous betatron functioning for 6 h. Details in the center of the betatron poles are water-cooled.

Prof. S. Nowicki (Institute of Electronics, Poland) described the design of a 30-MeV betatron which has been in operation since 1956. The betatron generates radiation at dose rates up to 65 R/min · m. The energy of the accelerated electrons is stabilized and subject to smooth control. Cold-rolled steel with a maximum induction of 17,000 G in the rolling direction and 14,000 G transverse to the rolling direction is used for the electromagnet. The vacuum chambers are made of porcelain or of epoxy resin.

Prof. A. A. Vorob'ev (Tomsk Polytechnic Institute, USSR) reported on projects for developing miniaturized and high-current betatrons, and on betatrons for nondestructive inspection of thick-walled structures under industrial

conditions. The miniaturized betatrons (developed under the supervision of L. M. Anan'ev) and their use in practice are subjects of keen interest.

V. A. Moskalev (Nuclear Physics Research Institute, Tomsk Polytechnic Institute, USSR) reported on the development of high-current dual-chamber stereobetatrons and betatrons for physical research. As many as 10^{12} electrons are accelerated to 25 MeV in a pulsed stereobetatron by increasing the gap aperture of the electromagnet (220 by 290 mm) and by high-voltage external injection (350 kV). The intensity of the 25-MeV betatron now being manufactured, operating at 50 cps, is 780 R/min·m even at 15 MeV, and should be several times higher when the machine is brought up to its full energy rating.

A high-current bantam-size 3 MeV stereobetatron is designed to operate at frequencies to 1000 cps. Its magnet is wound from thin-sheet cold-rolled steel. It is suggested that its intensity will be about 10 R/min·m, with each accelerating system in the stereobetatron operating at the frequency 400 cps.

M. F. Filippov (Tomsk Polytechnic Institute, USSR) reported on engineering calculations procedures for designing a betatron electromagnet and for optimizing chamber dimensions in terms of a specified energy and specified dose rate.

V. A. Vorob'ev (Tomsk Polytechnic Institute, USSR) reported on applications of bantam-size 3-5 MeV betatrons for inspection of seam weldments under industrial conditions, and also reported on variations in absorption. The reporter suggested an approach for calculating the sensitivity of radiation flaw detection techniques in heterogeneous materials.

W. Polit (Institute of Biophysics, West Germany) reported on techniques for measuring the intensity and energy of γ-radiation. The design of calorimeters, flow-type and extrapolating ionization chambers facilitating absolute measurements of both intensity and energy of γ-radiation, was described.

A paper by F. Klapper (Physics and Engineering Institute, German Democratic Republic) was devoted to measurements of γ-radiation intensity at energies from 7 to 30 MeV, using a thick-walled chamber. The energy dependence of the chamber current over the 7 to 30 MeV energy range was shown to remain within 1% variation when the walls of the ionization chamber are 4.5 mm thick.

J. Slaba (Materials and Production Technology Research Institute, CSSR), I. Leibovici (Institute of Atomic Energy, Rumania), G. Nietzsche (Physics and Engineering Institute, German Democratic Republic), F. Klapper (Physics and Engineering Institute, German Democratic Republic) devoted their reports to betatron nondestructive inspection of thick-walled stuctures and parts. J. Slaba reported that on the development of contrast-enhancement screens of monolayer films of fluorescent material coated on metal to improve the productivity and sensitivity of betatron radiographic techniques. Because of the minute thickness of this screen, the sharpness of the resulting image is far greater than when screens on a cardboard substrate are used.

The report by G. Nietzsche told of the first work in the field of betatron radioscopic flaw detection undertaken at the Physics and Engineering Institute. The use of contrast-enhancing screens made of tantalum was found to be less expensive because of the long service life of the screens. When the betatron intensity was stepped up from 80 to 140 R/min, thick-walled parts could be inspected with acceptable exposures. The paper by I. Leibovici reported on the reduction in size of the focal spot when a protruding target was employed.

Prof. R. Wideröe reported that the Brown-Boveri Ltd. firm has delivered 31 medical betatrons to various countries throughout the world (USA, Japan, Italy, the Netherlands, West Germany, United Kingdom, etc.). These betatrons produce a beam of γ-radiation or an extracted electron beam; they are equipped with a 90-100 kV diagnostic x-ray tube. The firm delivered seven betatrons for industrial flaw inspection (the USSR was customer for one of these). Impregnated tungsten cathodes capable of generating emission currents of 250-300 A at a temperature of 1050-1080°C and capable of long service life are being used as a new feature in betatron injectors; some of the cathodes have already been through 23,000 h of operational service each.

Prof. P. Winderöe feels that radioactive radiation sources must be replaced by the miniaturized betatrons, since about 3000 isotopes have been used in West Germany alone during the past half decade.

W. Polit, in reporting some of the results of treatment of patients by betatron irradiation, noted an important psychological factor to be taken into account in the therapy, in addition to the high penetrating power of the betatron γ-radiation, the low scattering outside the collimating beam, etc. This psychological factor consists in the

freedom from radiation sickness symptoms (nausea, vomiting, headaches) which unfailingly accompany x-ray therapy, but which do not plague betatron irradiation therapy. The fact that the patients are readily willing to undergo treatment improves the chances for success. Polit reported that seven betatrons of energies randing from 10 to 50 MeV are in operation in various West German cities, in experiments following a single master plan. All of the laboratories share a common system of accident prevention and maintenance provided for by the supplier.

The colloquium revealed a high demand for betatrons; the main problem now is simplification of operating procedures and improvements in the intensity and reliability of the machines.

Mention was made of the unfeasability of raising the electron energy above 30 MeV. A decision was made to convoke the colloquium annually in one of the nations participating regularly in the Jena colloquium.

The colloquium demonstrated in life the creative contact of the socialist countries in the field of research and development work on induction accelerators.

Representatives of all the socialist countries engaged in work on betatrons, with the exeption of the USSR, were included on the staff of the organizing committee of the colloquium (as in the case of the two preceding colloquia). Our feeling is that an official participation by the USSR in this organizing work would have been desirable.

CONFERENCE ON THE PHYSICS AND TECHNOLOGY OF ALKALI HALIDE SCINTILLATORS

R. V. Bakradze and Yu. A. Tsirlin

Translated from Atomnaya Énergiya, Vol. 18, No. 2,
pp. 193-194, February, 1965

The April 1964 conference on the physics and technology of alkali halide scintillators was held at the All-Union Single Crystal Research Institute in Khar'kov. The purpose of the conference was to seek out ways to improve the scintillation efficiency and resolving power of alkali halide single crystals.

E. R. Il'mes et al., (Institute of Physics and Astronomy—Academy of Sciences of the Estonian SSR) submitted a report "Mechanism of photoluminescence and radioluminescence in ionic crystals" pointing out how the scintillation efficiencies achieved at present in the USSR and elsewhere fall below the theoretical estimates (see Table 1).

The reason for this appalingly low scintillation efficiency is said to be large inertial losses and partly migration losses.

A. B. Lyskovich (L'vov State University) reported on a study of the effect of etching quality in growing NaI(Tl) crystals by the Kiropoulos method. A correlation was established between the resolving power of the crystals and the slow component in scintillation quenching. The results confirmed the dual (exciton and electron-hole) mechanism of energy transfer in NaI(Tl).

A paper presented by K. K. Shvarts and E. D. Aluker (Institute of Physics of the Academy of Sciences of the Latvian SSR) cited data on the radioluminescence of thallium-activated KCl, KBr, KI, NaI, CsI crystals excited by γ-x-ray bombardment and in-pile radiation. The thermoluminescence spectra, the temperature dependence of the steady-state luminescence in excitation by x-radiation and γ-radiation, by α-particles and by pile radiation, were studied. The temperature dependence of the radioluminescence yield was found to deviate markedly from the temperature dependence of the yield of luminescence within the impurity centers. Differences were also found in the behavior of the yields for the fast and inertial components of radioluminescence. The variation of the luminescent yield with temperature differs substantially as dE/dx varies (e. g., in the case of α-radiation and γ-radiation). Even though the detailed mechanism underlying the temperature quenching process remains obscure, experimental data indicate that quenching of radioluminescence leads primarily to radiationless electron-hole recombination, i. e., to external quenching processes.

Findings of a study on thermal and thermo-optical de-excitation and on excited absorption of NaI(Tl) crystals exposed to x-rays were reported in a paper by Z. B. Baturicheva (Single Crystal Research Institute). Diminished absorption of paired thallium activator centers ($\lambda_{max} \sim 310$ mμ) following x-ray treatment was reported, with the absorption recovered exponentially with a period of 3 min. Redistribution of electrons over trapping levels (F centers and thallium centers) as a result of plastic flow and changes in thallium concentration was also considered. The reporter found a number of glow peaks due to breakdown of the trapping centers, which are associated with thermal microimperfections in the lattices. The proposition was advanced that the large light sums stored in certain crystals are due to the presence of impurities in those crystals, and particularly to the presence of anion impurities.

TABLE 1. Radioluminescent Efficiency of Alkali Halides

Substance	Radioluminescent efficiency, %	
	theoretical	experimental
KI(Tl)	31	3
CsI(Tl)	25	6
NaI(Tl)	33	15

A report by A. N. Panova (Single Cryatal Research Institute) was devoted to an investigation of the excitation spectra and kinetic behavior of NaI(Tl) single crystals containing both cationic and anionic

impurities. The presence of copper and of anionic impurities appearing in the crystal during the growth phase was found to lower the luminescent yield in the absorption region of the host material by recombination losses. Lead impurity introduced into the crystal, principally with the activator, was also found to reduce the luminescent yield, both by competition in the absorption of the exciting radiation and by reabsorption of thallium emission. The conclusion was reached that the inertial response and the ratio of the excitation in the lattice to the excitation in the long-wavelength activator band may be used to estimate the quality of the scintillator crystals (homogeneity throughout the volume, freedom from impurities).

A paper by Ya. A. Zakharin provided a review of the research conducted at the All-Union Single Crystal Research Institute on the development of a fabrication technology for variously dimensioned NaI(Tl) crystals of spectrometric purity. The significance of the quality of the raw material and of the preparation techniques prior to crystal growing was demonstrated. The best specimens of NaI(Tl) crystals 150 mm in diameter featured 10-11% resolution (over the Cs^{137} γ-ray photopeak).

A paper by T. A. Soovik, N. E. Lushchik, Ch. B. Lushchik contained the results of research by the Institute of Physics and Astronomy of the Academy of Sciences of the Estonian SSR on surface activation of alkali halides in order to produce scintillation detectors.

Problems related to the production of raw material for scintillators and to their fabrication technology were also discussed at the conference.

"ATOMIC ENERGY" PAVILION AT THE 1964 EXHIBIT OF ACHIEVEMENTS OF THE USSR NATIONAL ECONOMY

L. I. Petrenko

Translated from Atomnaya Énergiya, Vol. 18, No. 2,
pp. 194-197, February, 1965

The "Atomic Energy" pavilion at the exhibit of the achievements of the USSR national economy underwent substantial rearrangement and renovation in 1964, and was housed in a new building.

Approximately 130 research, design, and civil engineering organizations, industrial plants, educational institutions, and medical institutions demonstrated their achievements in the "Atomic Energy" pavilion, in over 550 exhibits.

The pavilion was opened to the public with a display of results achieved in the development of nuclear power and controlled fusion research. The public showed special interest in models of the I. V. Kurchatov nuclear power station at Belyi Yar and the nuclear power station at Novyi Voronezh, the OGRA, OREKH, TOKAMAK, and PR-5 thermonuclear machines, and the nuclear-powered icebreaker LENIN. Color film shorts on the work of Soviet research scientists in the promotion of nuclear power and plasma research, and film shorts on the navigation of the nuclear vessel LENIN were shown. Moving color displays presented the visting public with an opportunity to acquaint themselves with the operating principles of nuclear electric power stations, and exhibits of designs of fuel elements and various materials used in nuclear reactor construction and design provided a lucid picture of the complexity of the problems resolved by our scientists and engineers.

The adjoining hall showed the results of work in building unique accelerator facilities intended for the study of the structure of the atomic nucleus and for the production of new transuranium elements. Models of accelerators built at the Joint Institute for Nuclear Research are on display here (the 10-GeV proton synchrotron, the multiply-charged ion accelerator, and others), as well as machines in operation at other research centers. Excellent display stands give the public an idea of the scope of the construction work on the world's largest accelerator in the Serpukhov district—a 60-70 GeV strong-focusing proton synchrotron.

Here the public becomes acquainted with the principles for recording nuclear radiations, and with a wide variety of radiation detectors manufactured for that purpose by our industry. Gas discharge counters, scintillation crystals and plastics, photoelectric multiplier tubes on exhibit were indicative of the unyielding growth and advancement of this new field in scientific instrumentation. The accompanying table cited technical data on some of the photomultiplier tubes which the visitors displayed peak interest in.

A considerable portion of the exhibit in the pavilion was devoted to methods in the use of nuclear radiations, stable and radioactive isotopes in various branches of the national economy, and in the production of isotopes. This section took up about half the entire floor area of the pavilion, and was opended by a stand display showing the USSR isotope production picture.

Visitors manifested keen interest in models of research reactors such as the VVR, IRT, and SM-2 piles, and in exhibits demonstrating the possible uses of nuclear radiations in radiation processing of materials and in radiation chemical processes. Findings of research on radiation modification of cotton, radiation processing of polyethylene cable insulation, thermoradiation vulcanization of rubber tires, were presented to the public here. Industrial enterprises in such districts of the national economy as the Western Siberian, Donets basin, L'vov, Volgo-Vyatsk, Byelorussian, and others demonstrated their achivements on incorporating isotope techniques in industry.

Radioisotope studies of special aspects of the process of reduction of phosphorus pig iron melts and high-load-capacity tilting open hearth furnaces, and tracer studies of wear on the hearths, have been carried out at the Sergo Ordzhonikidze "Azovstal'" Zhdanovo metallurgical plant; these studies have resulted in a new improved technology for maintenance and overhaul of the furnace hearths.

TABLE 1. Engineering Data on Some Photomultiplier Tubes

Engineering characteristic	FEU-49-B	FEU-52	FEU-53	FEU-54	FEU-55	FEU-56
Design	Glass	Glass, baseless	Glass, baseless	Glass, baseless with hard or soft lead-in wires	Glass, baseless with hard or soft lead-in wires	Glass, baseless
Photocathode material	Antimony-potassium-sodium-cesium, semitransparent, on inner side of envelope		Antimony-cesium, semitransparent		Bismuth-silver-cesium, semitransparent	Antimony-cesium, semitransparent
Diameter of effective photocathode area, mm	150	70	45	16	16	70
Number of amplifying stages	12	12	14	14	14	12
Electron focusing	–	Electrostatic, alloyed louvers				
Spectral sensitivity range, Å	3000-8000	2000-8000	2500-6500	3300-6500	3300-7500	3000-6500
Wavelength corresponding to maximum spectral response, Å	–	4200 ± 500	4200 ± 200	4000-100 ± 200*	5000 ± 200	4000 ± 200
Peak height, mm	203	133.3	117	90	90	133.3
Peak diameter, mm	171	81	51	21.5	21.5	81
Largest weight, g	1000	180	120	25	25	180
Number of base pins	–	20	20	22	22	20
Minimum integrated sensitivity of photocathode, μA/lm	35	50	25	20	20	30
Dark current, 10^{-8} A	80	6	≤ 10	≤ 80	≤ 80	≤ 10
Cs^{137} peak amplitude resolution, %	–	≤ 14	≤ 12	≤ 13 ± 2	–	≤ 14
Time resolution (not inferior to), 10^{-9}	–	6	6	–	–	6
Peak supply voltage, V	3000	2500	2500	1800	1800	2500
Ambient temperature, °C	+ 70 ÷ − 60	+ 70 ÷ − 60	+ 70 ÷ − 60	+ 85 ÷ − 60	+ 85 ÷ − 60	+ 70 ÷ − 60

*As in Russian original—Publisher.

The Luga isotopes laboratory has carried out extensive work to promote the use of radioisotope devices and means in automatic process monitoring and control in that region. A γ-ray inspection method for monitoring joints in rubber conveyor belting buttressed by steel lines has been installed at the Novo-Druzheskii mine pits, thereby aiding in the organization of timely preventive maintenance and bringing about savings of 25 thousand rubles annually by eliminating tears in the belts. γ-ray electronic switches for monitoring fill levels in dumpcars, automation of skip hoist operation, automatic filling of wheelbarrows and automation of other processes in loading, unloading, and hauling of coal are being used at the Talovskaya-2, Artem No. 10, Krasnyi Partizan, and other mines, thereby freeing a certain number of miners from underground duties.

At the Angara oil refinery in the Eastern Siberian district of the national economy, the introduction of radioisotope instrumentation has meant significant improvements in production and working conditions at absorption plants, thermal cracking plants, and in apparatus where corrosive materials are used.

Annual savings not less than 40 thousand rubbles have been achieved at the State Razdol'skii ore chemical processing combine via improvements in sulfur technology resulting from the implementation or radioisotope instrument techniques.

A display sponsored by the Il'ich Zhdanovo metallurgical plant was quite popular; this stand showed the organization of radioisotope work for process monitoring and research. A special class II radiometric laboratory was set up, equipped for work with unsealed radioactive isotopes. Four teams are working in this laboratory on electronics and radiometry, on blast furnace and steelmaking production, on steel rolling and allied production, and on radiation safety. Staff members of the laboratory are principally engaged in the study of metallurgical production processes using radioactive tracers, and in the development and implementation of automatic control plans involving the use of commercial radioisotope instrumentation. The servicing and operation of radioisotope instruments installed in production premises are carried out by a special division of the instrument and measurement workshop. The radiation safety team is responsible for the systematic checking and supervision of the proper use and implementation of radioisotope techniques, for elaborating instructions on safe work practices, for indoctrinating servicing and maintenance personnel in the basics of work with radioactive materials. Radiation safety posts headed by leading laboratory technologists have been set up in those shops of the plant where radioisotopes are in general use (the blast furnace section, the steelmaking section, the rolling mill section). The electronics and radiometry team and the radiation safety team are headed by engineering physicists, while the team responsible for radioactive techniques in blast furnace, steelmaking, and rolling mill production are engineering technologists in the specialties involved.

Stands demonstrating the predominant use of radiation sources and isotopes in the prospecting, exploration, and development of mining ores are well designed and equipped; the work of the All-Union Institute of Nuclear Geophysics and Geochemistry and the "Tatneftegeofizika" petroleum geophysical trust, and others is represented in the display. Among the instruments on display is a variety of isotope equipment for process control and monitoring and special-function instruments. The IGN-1 pulsed borehole neutron generator designed to aid in the study of the actual composition of rocks encountered in prospecting and exploration work at ore deposits is an original design, and is used in pulsed neutron-neutron logging work in boreholes over 127 mm in diameter and down to 3000 meters in depth. This is a reliable instrument for tracking down displacements in water-oil and gas-liquid contacts in strata, and is a tremendously useful tool in monitoring the development of oil and gas fields, and in reducing loss of pay ores. A miniaturized ion accelerator in which fast 14 MeV neutrons are formed by bombarding a tritium target with up to 0.3 MeV deuterons, is employed as the neutron source; the average yield of fast neutrons is $5 \cdot 10^7$ neutrons/sec; the pulse rate is 200 Hz with pulse duration from 50 to 200 msec. Slow neutrons are recorded by means of proportional counters filled with boron trifluoride. The diameter of the well drilling rig is 102 mm, and the length is 2900 mm.

Visitors manifested special interest in the SDPU-1 smoke and fire alarm system; it is designed for remote detection of smoke from a conflagration, and may also be used as an alarm device for overheating or hot spots in electrical equipment and as a sensor for actuating fire-dousing equipment. The device operates on the basis of the difference in the ionization brought about by α-particles emitted by the isotope Pu^{239} in pure air and in smoke-filled air. The facility features 100 distinct sensors which may be stationed in different rooms, and serves to monitor an area of about 10,000 m^2. The facility is supplied from a 220 V ac supply, consuming 80 W power.

This section is completed with a display on applications of nuclear radiations and isotopes in construction, biology, agriculture, and medicine.

The Institute of Experimental Biology of the Academy of Sciences of the Uzbek SSR presented the results of the derivation of new strains of the cotton plant by radiation-induced selection experiments. Two new strains of cotton featuring distinct advantages over their precursors were obtained. One of these is distinguished by larger bolls weighing 9 to 9.5 g, and by an increase in the number of bolls, to 11 bolls on a single plant. The second strain produced had smaller bolls (0-7-1 g less than in the parent strain), but yielded a very slender silken fiber.

Substantial changes have been brought about in the outfitting of medical institutions in recent years, with the use of nuclear radiation and radioisotopes in the therapy and diagnostics of a variety of illnesses and malfunctions, and this was properly reflected in the exhibit at the pavilion. The Semashko Central Clinical Hospital demonstrated techniques for utilizing P^{32} in the treatment of erythremia, a blood disease. Small doses of radioactive phosphorus were introduced over a 5-7 day interval, to make up a total dosage of 8 mCi. Normalization of the state

NEW BOOKS

Translated from Atomnaya Énergiya, Vol. 18, No. 2,
pp. 198-200, February, 1965

A. M. Kabakchi, Ya. I. Lavrentovich, and V. V. Pen'kovskii. Khimicheskaya dozimetriya ioniziruyushchikh izluchenii [Chemical dosimetry of ionizing radiations]. Kiev, published by the Academy of Sciences of the Ukrainian SSR, 1964, 156 pages, 65 kopeks.

This compact item, written by prominent Soviet research scientists, consists of four chapters and a short introduction. The concise first chapter (16 pages) presents a clear outline of the field of applications of chemical dosimetry techniques. The next chapter (30 pages) carries a description of the fundamentals of chemical dosimetry. Radiation similitude of the medium investigation and of the dosimetric system, dependence of the radiation yield on various factors are presented in compact format, and a description is given of the techniques employed in recording chemical changes in dosimetric systems, with formulations of the basic requirements regarding radiation chemical reactions exploited in dosimetry. The highpoint of the book is chapter III (63 papers) which is devoted to chemical dosimetry techniques. Here the authors report information on the three basic types of radiation chemical systems: aqueous solutions and gels; polymers and organic compounds; glasses and ionic crystals. The electrochemical method for dose rate determinations is also described briefly in this chapter. The last chapter takes up dose determinations of several modes of radiation by chemical methods.

Each of the chapters features an extensive bibliography, and the total number of references runs to 435 titles.

The book is intended for a broad readership of specialists engaged in measurements of the absorbed energy of various types of ionizing radiations.

Directory of Nuclear Reactors. Volume 5, Research, Test and Experimental Reactors [in English]. Vienna, IAEA, 1964, 327 pages.

The International Atomic Energy Agency has now issued the scheduled fifth volume of the reference series on nuclear reactors, this one serving as a supplement to the second and third volumes. Volume 5 cites reference information on 78 research, testing, and experimental reactors in operation or under construction in 16 countries. As is the case in the preceding volumes, the reactors are grouped, principally by the type of moderator used.

Two such groups are formed by reactors using ordinary water as moderator. The first group includes pool type research reactors: OWR, SPR, WPIR, UWNP, HHLP, PRPR, Buffalo, TR-1, IRT (Sofiya), SPERT-4, TRR-1, Siloe, Siloetta, and the IISNR reactor. Of greatest interest in this group is the French 15 MW Siloe reactor, and the unique SPERT-4 reactor (USA) built for research on reactor kinetics and reactor stability.

The second group is formed by pressure-vessel type research reactors. These are mostly high-power modern reactors intended for nuclear engineering research: tests of fuel compositions, tests of fuel elements, controls, structural materials, and reactor parts. The reactors are also designed for isotope production and physics research. Worthy of mention in the reactors of this group are the improved test reactor ATR (250 MW power rating), the ETR engineering tests reactor (175 MW), the WTR (60 MeV), NASA-TR (60 MeV), and the Pegasus (30 MW) reactors. The ESADA nuclear superheat Vallecitos reactor and the HFIR high-flux reactor for isotope production, engineerin g and physics research are of enormous interest. This group also includes the NASA-MUR, Peggy, and SAFARI-1 (20 MW) reactors.

The next group is constituted by the now quite popular ARGONAUT family of reactors. In most cases these are low-power reactors (from 10 to 10 kW) with light water as both moderator and coolant. They are designed for training purposes and for nuclear physics research. Of the 17 reactors in this group, many are the property of universities and other educational bodies.

The fourth group combines two types of homogeneous research reactors. These include six pulsed TRIGA-2 in regular production, designed for prolonged operation at 200 kW power. Peak pulsed power is 250 MW. The second

of health of most patients so afflicted in the hospital was the result of this treatment, the blood composition being normalized for a 5-y period, after which the treatment is to be repeated. 209 patients have undergone this treatment in 12 y at the hospital, and the rate of recovery is 92%. The results of using Cr^{31} tracer to measure the volume of blood circulating through the organism as well as, the mass of circulating erythrocytes, and the use of Fe^{59} to estimate the activity of blood formation and to determine the causes of spleen enlargement were other applications displayed.

The Moscow municipal oncological hospital No. 62 had a display on the treatment of malignant tumors by radiative therapy combined with other familar techniques.

New equipment for use in the treatment of various malignancies was on display, including models of a medical accelerator, a medical betatron, and the γ-therapeutic ROKUS facility. The rotary-convergent γ-therapeutic ROKUS facility is built for convergent, pendulum type, rotary-convergent, tangential, and static γ-ray therapy of superficial and deeply embedded tumors. The radiation source employed is radioactive cobalt of up to 4000 Ci activity. The lesioned organs are treated by several fields of irradiation which are designed to minimize damage to unaffected tissues. The dose rate at one meter from the source is 60 R/min.

Other new pieces of equipment being introduced into our medical institutions are the diagnostic scintillation facility DSU-61 for making scans of the I^{131} in the human organism, and the general-purpose β-probe KOMETA radiometer for localizing malignant tumors by recording the P^{32} accumulated in them, and for intracavitary and skin examinations.

The pavilion displayed instruments and equipment used in radiation safety and health physics work, including remote-control devices, auxiliary equipment, instrument kits and materials for safe handling of radioactive isotopes and nuclear radiation sources. Visitors were familiarized with documents attesting to the international cooperation of the USSR in the field of peaceful uses of atomic energy, and with literature published by ATOMIZDAT.

Many of the organizations which put up displays in the "Atomic Energy" pavilion were awarded diplomas by the administration of the Exhibit. Among these were the I. V. Kurchatov Institute of Atomic Energy, the Power Physics Institute, the Institute of Theoretical and Experimental Physics, the D. V. Efremov Electronics and Physics Instruments Research Institute, the Moscow Design Institute, the Union Instrument Design Research Institute, the Joint Institute for Nuclear Research, the All-Union Institute of Nuclear Geophysica snd Geochemistry, the V. I. Lenin Nevskii Machine Tool Factory, the Shcherbakov Moscow Silk Combine, the Moscow Vacuum Tube Plant, the All-Union Research Institute for Medical Instruments and Equipment, the Radiological Division of the Moscow Municipal Clinical Hospital No. 40, the Moscow Research Institute for Safe Work Practices in the Coal Industry, and many others. The staff members of these institutions who took an active part in the development, design, and implementation of radiation techniques were awarded with medals and monetary prizes.

In addition to the main exhibit, the pavilion systematically organizes topical exhibits devoted to specific aspects of the use of atomic energy, which are accompanied by a discussion of the most important displays presented to the public and by an extensive exchange of experience.

NEW BOOKS

Translated from Atomnaya Énergiya, Vol. 18, No. 2,
pp. 198-200, February, 1965

A. M. Kabakchi, Ya. I. Lavrentovich, and V. V. Pen'kovskii. Khimicheskaya dozimetriya ioniziruyushchikh izluchenii [Chemical dosimetry of ionizing radiations]. Kiev, published by the Academy of Sciences of the Ukrainian SSR, 1964, 156 pages, 65 kopeks.

This compact item, written by prominent Soviet research scientists, consists of four chapters and a short introduction. The concise first chapter (16 pages) presents a clear outline of the field of applications of chemical dosimetry techniques. The next chapter (30 pages) carries a description of the fundamentals of chemical dosimetry. Radiation similitude of the medium investigation and of the dosimetric system, dependence of the radiation yield on various factors are presented in compact format, and a description is given of the techniques employed in recording chemical changes in dosimetric systems, with formulations of the basic requirements regarding radiation chemical reactions exploited in dosimetry. The highpoint of the book is chapter III (63 papers) which is devoted to chemical dosimetry techniques. Here the authors report information on the three basic types of radiation chemical systems: aqueous solutions and gels; polymers and organic compounds; glasses and ionic crystals. The electrochemical method for dose rate determinations is also described briefly in this chapter. The last chapter takes up dose determinations of several modes of radiation by chemical methods.

Each of the chapters features an extensive bibliography, and the total number of references runs to 435 titles.

The book is intended for a broad readership of specialists engaged in measurements of the absorbed energy of various types of ionizing radiations.

Directory of Nuclear Reactors. Volume 5, Research, Test and Experimental Reactors [in English]. Vienna, IAEA, 1964, 327 pages.

The International Atomic Energy Agency has now issued the scheduled fifth volume of the reference series on nuclear reactors, this one serving as a supplement to the second and third volumes. Volume 5 cites reference information on 78 research, testing, and experimental reactors in operation or under construction in 16 countries. As is the case in the preceding volumes, the reactors are grouped, principally by the type of moderator used.

Two such groups are formed by reactors using ordinary water as moderator. The first group includes pool type research reactors: OWR, SPR, WPIR, UWNP, HHLP, PRPR, Buffalo, TR-1, IRT (Sofiya), SPERT-4, TRR-1, Siloe, Siloetta, and the IISNR reactor. Of greatest interest in this group is the French 15 MW Siloe reactor, and the unique SPERT-4 reactor (USA) built for research on reactor kinetics and reactor stability.

The second group is formed by pressure-vessel type research reactors. These are mostly high-power modern reactors intended for nuclear engineering research: tests of fuel compositions, tests of fuel elements, controls, structural materials, and reactor parts. The reactors are also designed for isotope production and physics research. Worthy of mention in the reactors of this group are the improved test reactor ATR (250 MW power rating), the ETR engineering tests reactor (175 MW), the WTR (60 MeV), NASA-TR (60 MeV), and the Pegasus (30 MW) reactors. The ESADA nuclear superheat Vallecitos reactor and the HFIR high-flux reactor for isotope production, engineerin g and physics research are of enormous interest. This group also includes the NASA-MUR, Peggy, and SAFARI-1 (20 MW) reactors.

The next group is constituted by the now quite popular ARGONAUT family of reactors. In most cases these are low-power reactors (from 10 to 10 kW) with light water as both moderator and coolant. They are designed for training purposes and for nuclear physics research. Of the 17 reactors in this group, many are the property of universities and other educational bodies.

The fourth group combines two types of homogeneous research reactors. These include six pulsed TRIGA-2 in regular production, designed for prolonged operation at 200 kW power. Peak pulsed power is 250 MW. The second

type includes the very-low-power training reactors (0.1 W) manufactured by the West German Siemens-Schukkkert-werke firm, reactors which require no cooling. Both the TRIGA line of reactors and the four West German reactors belong to educational institutions. Aside from training of specialists, the TRIGA reactors were also designed for research on neutron physics, reactor physics, and for isotope production.

Of special interest in this group is the EBOR experimental high-temperature gas-cooled reactor using beryllia moderator. It is manufactured in the USA for engineering tests and for the study of the operating characteristics of its type.

The fifth group consists of 11 heavy-water-moderated research reactors. These are all pressure-vessel type reactors. The reactors NORA, ZED-2, DAPENE, and PDP, of several hundred watts power rating, are designed solely for physics research. The remaining reactors in this group feature power ratings from 5 to 60 MW and are designed for a broader range of applications. Especially interesting among these are the HWCTR (61 MW) reactor for comprehensive testing of fuel elements, materials, and parts; the HFBR reactor for neutron physics research and solid state physics studies, and the Hallén reactor built in Norway for the study of the dynamics and miscellaneous characteristics of boiling heavy-water reactors.

Characteristics of graphite-moderated research reactors are cited under the next heading: GLEEP, Zenith, Marius, RB-1, and HECTOR. The most interesting reactors in this group are however the experimental and testing reactors: the high-temperature gas-cooled Dragon reactor, 20 MW, the ultrahigh-temperature UHTREX reactor (1320°C helium temperature at the reactor exit) which has been in operation since October 1964, and the original-design MSRE reactor in which fluoride salt melts are used as nuclear fuel and coolant. These reactors are designed to verify engineering solutions, and for investigation and demonstration of the power capabilities of future reactors.

The concluding group encompasses seven fast research reactors: EBR-1, AFSR, LAMPRE, VERA, HPRR, Zebra, and Mazurka. Most of these reactors are being used for physics research associated with further development of fast reactors. The LAMPRE reactor burning liquid-metal plutonium fuel should be singled out here.

The following information is presented for each reactor in the handbook: the over-all characteristics and purpose of the reactor, data on reactor physics, core characteristics, fuel element specifications, data on the reactor control system, fuel element design, design of other important parts (pressure vessel, reflector, shielding, etc.), data on in-core heat transfer, costs, experimental reactor equipment.

This handbook will prove highly valuable to a broad range of specialists, the more so in that the last publication of a handbook on research reactors (Vol. 3 in this series) appeared as far back as 1960. In addition, one should not fail to note the unfortunate timing of the publication of this volume, i. e., on the eve of the third Geneva UN conference on the peaceful uses of atomic energy, a circumstance which prevented the compilers from supplementing the handbook with data on new research reactors and testing reactors made available at the Geneva conference.

Radiation Chemistry. Proceedings of the Tihany symposium. Budapest, published by Publishing House of the Hungarian Academy of Sciences, 1964 [in English], 482 pages.

A detailed report on the symposium may be found in this journal, Atomnaya énergiya 14, 595 (1963).

The book will be found useful by scientific workers engaged in research in the field of radiation chemistry.

Izv. AN SSSR O(td). Kh(im). N(auk)	Izvestiya Akademii Nauk SSSR: Otdelenie khimicheskikh nauk	Bulletin of the Academy of Sciences of the USSR: Division of Chemical Science	Consultants Bureau	16	1 1952
Izv. AN SSSR O(td). T(ekhn). N(auk): Metall). i top.	(see Met. i top)				
Izv. AN SSSR Ser. fiz(ich).	Izvestiya Akademii Nauk SSSR: Seriya fizicheskaya	Bulletin of the Academy of Sciences of the USSR: Physical Series	Columbia Technical Translations	18	3 1954
Izv. AN SSSR Ser. geofiz.	Izvestiya Akademii Nauk SSSR: Seriya geofizicheskaya	Bulletin of the Academy of Sciences of the USSR: Geophysics Series	American Geophysical Union	7	1 1957
Izv. AN SSSR Ser. geol.	Izvestiya Akademii Nauk SSSR: Seriya geologicheskaya	Bulletin of the Academy of Sciences of the USSR: Geologic Series	American Geological Institute	23	1 1958
Iz. Vyssh. Uch. Zav., Tekh. Teks. Prom.	Izvestiya Vysshikh Uchebnykh Zavedenii Tekhnologiya Tekstil'noi Promyshlennosti	Technology of the Textile Industry, USSR	The Textile Institute (Manchester)	4	1 1960
Kauch. i rez.	Kauchuk i rezina	Soviet Rubber Technology	Palmerton Publishing Company, Inc.	18	3 1959
	Kinetika i kataliz	Kinetics and Catalysis	Consultants Bureau	1	1 1960
	Koks i khimiya	Coke and Chemistry, USSR	Coal Tar Research Assn. (Leeds, England)		8 1959
Kolloidn. zh(urn).	Kolloidnyi zhurnal	Colloid Journal	Consultants Bureau	14	1 1952
	Kristallografiya	Soviet Physics – Crystallography	American Institute of Physics	2	1 1957
Metallov. i term.	Metallovedenie i termicheskaya obrabotka metallov	Metals Science and Heat Treatment of Metals	Acta Metallurgica	6	1 1958
	Metallurg	Metallurgist	Acta Metallurgica		1 1957
Met. i top.(gorn.)	Metallurgiya i toplivo (gornoye delo)	Russian Metallurgy and Fuels (mining)	Scientific Information Consultants, Ltd.		1 1960
Mikrobiol.	Mikrobiologiya	Microbiology	National Science Foundation*	26	1 1957
	Ogneupory	Refractories	Acta Metallurgica	25	1 1960
OS, Opt. i spektr.	Optika i spektroskopiya	Optics and Spectroscopy	American Institute of Physics	6	1 1959
Paleontol. Zh(urn)	Paleontologicheskii Zhurnal	Journal of Paleontology	American Geological Institute		1 1962
	Pochvovedenie	Soviet Soil Science	National Science Foundation**	53	1 1958
	Poroshkovaya Metallurgiya	Soviet Powder Metallury and Metal Ceramics	Consultants Bureau	2	1 1962
	Priborostroenie	Instrument Construction	Taylor and Francis, Ltd. (London)	4	1 1959
Pribory i tekhn. éks(perimenta)	Pribory i tekhnika éksperimenta	Instruments and Experimental Techniques	Instrument Society of America	3	1 1958
Prikl. matem. i mekh(an).	Prikladnaya matematika i mekhanika	Applied Mathematics and Mechanics	Am. Society of Mechanical Engineers	22	1 1958
PTE	(see Pribory i tekhn. éks.)				
	Problemy Severa	Problems of the North	National Research Council of Canada		1 1958
	Radiokhimiya	Radiochemistry	Consultants Bureau	4	1 1962
Radiotekh.	Radioteknika	Radio Engineering	Am. Institute of Electrical Engineers	16	1 1961
Radiotekhn. i élektron(ika)	Radiotekhnika i électronika	Radio Engineering and Electronic Physics	Am. Institute of Electrical Engineers	6	1 1961
	Stal'	Stal (in English)	Iron and Steel Institute	19	1 1959
	Stanki i instrument	Machines and Tooling	Production Engineering Research Assoc.	30	1 1959
Stek. i keram.	Steklo i keramika	Glass and Ceramics	Consultants Bureau	13	1 1956
Svaroch. proiz-vo	Svarochnoe proizvodstvo	Welding Production	Br. Welding Research Assn. (London)	5	4 1959
Teor. veroyat. i prim.	Teoriya veroyatnostei i ee primenenie	Theory of Probability and Its Application	Soc. for Industrial and Applied Math.	1	1 1956
Tsvet. metally	Tsvetnye metally	The Soviet Journal of Nonferrous Metals	Primary Sources	33	1 1960
UFN	Uspekhi fizicheskikh nauk	Soviet Physics – Uspekhi (partial translation)	American Institute of Physics	66	1 1958
UKh, Usp. khimi	Uspekhi khimii	Russian Chemical Reviews	Chemical Society (London)	29	1 1960
UMN	Uspekhi matematicheskaya nauk	Russian Mathematical Surveys	Cleaver-Hume Press, Ltd. (London)	15	1 1960
Vest. mashinostroeniya	Vestnik mashinostroeniya	Russian Engineering Journal	Production Engineering Research Assoc.	39	4 1959
Vop. onk(ol).	Voprosy onkologii	Problems of Oncology	National Institutes of Health**	7	1 1961
Zav(odsk). lab(oratoriya)	Zavodskaya laboratoriya	Industrial Laboratory	Instrument Society of America	24	1 1958
ZhAKh, Zh. anal(it). Khim(ii)	Zhurnal analiticheskoi khimii	Journal of Analytical Chemistry	Consultants Bureau	7	1 1952
ZhETF Zh. éksperim. i teor. fiz.	Zhurnal eksperimental'noi i teoreticheskoi fiziki	Soviet Physics – JETP	American Institute of Physics	28	1 1955
ZhFKh Zh. fiz. khimii	Zhurnal fizicheskoi khimii	Russian Journal of Physical Chemistry	Chemical Society (London)	33	7 1959
ZhNKh Zh. neorg(an). khim.	Zhurnal neorganicheskoi khimii	Journal of Inorganic Chemistry	Chemical Society (London)	4	1 1959
ZhOKh Zh. obshch. khim.	Zhurnal obshchei khimii	Journal of General Chemistry USSR	Consultants Bureau	19	1 1949
ZhPKh Zh. prikl. khim.	Zhurnal prikladnoi khimii	Journal of Applied Chemistry USSR	Consultants Bureau	23	1 1950
ZhSKh Zh. strukt(urnoi) khim.	Zhurnal strukturnoi khimii	Journal of Structural Chemistry	Consultants Bureau	1	1 1960
ZhTF	Zhurnal tekhnicheskoi fiziki	Soviet Physics – Technical Physics	American Institute of Physics	26	1 1956
Zh. tekhn. fiz.	Zhurnal vychislitel'noi matematika i matematicheskoi fiziki	U.S.S.R. Computational Mathematics and Mathematical Physics	Pergamon Press, Inc.	1	1 1962
Zh. vyssh. nervn. deyat. (im. Pavlova)	Zhurnal vysshei nervnoi deyatel'nosti (im I. P. Pavlova)	Pavlov Journal of Higher Nervous Activity	National Institutes of Health**	11	1 1961

*Sponsoring organization. Translation published by Consultants Bureau.
**Sponsoring organization. Translation published by Scripta Technica.

Declassified and Approved For Release 2013/09/24 : CIA-RDP10-02196R000700010002-5